Identification of autophagy-specific cargo and characterization of β-catenin as LC3/GABARAP interacting protein

Muhammed Kocak

April 2023

Primary Scientific Supervisor: Prof Sebastian Guettler & Dr Vladimir Kirkin

Associate Supervisor - Sharon Gowan

Number of pages: approximately 200

Word count: approximately 57,000

Acknowledgement

First and foremost, I would like to express my deep sense of gratitude to my research supervisors, Dr Vladimir Kirkin and Prof Sebastian Guettler. This thesis was accomplished with their assistance, motivation, inspiring discussions, and dedicated involvement in every step throughout the process. I would like to thank you very much for always being there with your leadership and, more importantly, with your friendship whenever I needed in the past four and half years.

I am also grateful to my CSPR and Structural Biology of Cell Signalling team lab mates for being such an amazing, helpful, warm, friendly, and cheerful team. They made me feel comfortable and safe in a foreign country, which helped me to adapt to a new life easily and quickly. I have learnt a lot from them both about life and academia. I was lucky to always feel their friendship during my Ph.D. endeavour.

My gratitude also extends to members of the ICR's microscopy, flow cytometry, and mass spectrometry facilities for their help in my experiments. I would also like to acknowledge all research collaborators that contributed to this study; Terje Johansen, Ian Ganley, Eeva-Liisa Eskelinen, Fulvio Regiorri, Robin Kettler, and Stephane Mouilleron.

Last but not least, I would like to thank the Institute of Cancer Research and ETN DRIVE which has received funding from the European Union's Horizon 2020 research and innovation program under grant agreement No: 765912 for supporting my Ph.D. programme.

Abstract

Autophagy is an evolutionarily conserved eukaryotic degradation system induced under cellular stress conditions in which cellular components, such as damaged organelles, and aggregated proteins sequestered through lysosomal fusion. Alterations in the process of autophagy can trigger several pathological conditions, such as neurodegeneration, infectious diseases, and cancer. Autophagy research is hampered mainly due to limited research tools and need for better understanding of its molecular mechanisms. Therefore, dissecting autophagy from a proteomics perspective has become a genuine interest of many studies for the characterization of the autophagy process. Nevertheless, whole-cell proteomics studies were not effective enough to selectively identify proteins targeted by autophagic degradation or regulate autophagy. Thus, the composition of autophagosomes is more selectively subjected to proteomic analysis using biochemical fractionation, affinity purification, and close-proximity labelling methods. These kinds of approaches can identify autophagy-specific substrates/regulators and provide significant insights on cellular functions that autophagy affects. **Here, this study aims to create the basis for understanding the functions of autophagy by studying the composition of autophagosomes isolated from tumour cells.** Consistent with this aim, a robust autophagosome purification technique combining fractionation and immune isolation methods was developed. This technique enabled purification of pure and intact autophagosomes from cancer cells at a sufficient amount to analyse their content by proteomics. Subsequent analysis of the autophagosome content revealed many novel potential candidates might be involved in the autophagy process. Biochemical analyses confirmed some of the candidates as autophagy substrates. EEAT1 protein was shown to be degraded by autophagy for the first time.

Maintaining cellular homeostasis requires a careful balance between many proliferative systems under physiological conditions and during cellular stress. Wnt/β-catenin signalling is an evolutionarily conserved regulatory pathway that governs numerous normal cellular and developmental processes, such as cell fate specification, stem cell maintenance, cell proliferation, and migration. However, aberrant Wnt/β-catenin signalling has also been identified as a critical mechanism in several types of cancer, with β-catenin accumulation and dysregulated β-catenin/TCF/LEF target gene expression as a major cancer driver. Recent evidence points toward autophagy as an alternative β-catenin degradation pathway. **Given the importance of Wnt/β-catenin signalling and autophagy, this study aims to investigate the role of autophagy in regulating Wnt/β-catenin signalling by identifying a link between these pathways.** For that purpose, a physical connection between LC3/GABARAP and β-catenin proteins was identified. An atypical LIR motif in the structure of β-catenin was shown to facilitate its binding to LC3/GABARAP proteins with a stronger binding to the GABARAP family. However, this interaction does not lead β-catenin to autophagic degradation. Instead, it was shown that LC3/GABARAP proteins enhance the transcriptional activity of β-catenin. In addition, β-catenin was found to regulate autophagy in a cell type-dependent manner.

Contents

Figure List

Table List

Abbreviations

3-MA	3-Methyladenine
APC	Adenomatous Polyposis Coli
ATG	Autophagy-Related Genes
$ATG4B^{DN}$	Atg4B-Dominant Negative Mutant
ATTEC	Autophagosome-Tethering Compound
AUTAC	Autophagy-Targeting Chimera
Baf A_1	Bafilomycin A1
BP	Biological Process
BSA	Bovine Serum Albumin
Ca^{2+}	Calcium
CALCOCO2	Coiled-Coil Domain-Containing Protein 2
CK1	Casein Kinase 1
CK2	Casein Kinase 2
CMA	Chaperone-Mediated Autophagy
Co-IP	Co-Immunoprecipitation
CoV	Coronavirus
CQ	Chloroquine
CRISPR	Clustered Regularly Interspaced Short Palindromic Repeats
CRY1	Cryptochrome Circadian Regulator 1
DMEM	Dulbecco'S Modified Eagle'S Medium
DUB	Deubiquitinating Enzyme
Dvl	Dishevelled
DVL2	Dishevelled Segment Polarity Protein 2
EBSS	Earl’S Balanced Salt Solution
EDTA	Ethylenediaminetetraacetic Acid
ER	Endoplasmic Reticulum
ERAD	ER-Associated Degradation
FAS1	Fatty Acid Synthase Subunit Beta
FBS	Fetal Bovine Serum
FIR	FIP200 Interacting Region
FP	Fluorescence Polarization
FSC	Forward Scatter
Fz	Frizzled
GABAAR	Gabaa(A) Receptor
GBM	Glioblastoma Multiforme
GEMM	Genetically Engineered Mouse Model
GO	Gene Ontology
h	Hour
HCQ	Hydroxychloroquine
HCV	Hepatitis C Virus
HeLa G120	Hela Atg4B Ko Gfp-Lc3B-G120
HeLa G120A	Hela Atg4B Ko Gfp-Lc3B-G120A

HP1	Hydrophobic Pocket 1
HP2	Hydrophobic Pocket 2
HSP	Heat-Shock Protein
HTT	Huntingtin Protein
IMDM	Iscove'S Modified Dulbecco'S Medium
JUBA	A-Helical J
Kd	Dissociation Constant
KO	Knock Out
LANDO	Lc3-Associated Endocytosis
LAP	Lc3-Associated Phagocytosis
Hexa KO	Lc3A/B/C And Gabarap/L1/L2 Ko
LC-MS	Liquid Chromatography-Mass Spectrometry
LDS	LIR-Docking Site
LEF	Lymphoid Enhancer Factor
LIR	LC3 Interacting Region
MEF	Mouse Embryonic Fibroblast
MM	Multiple Myeloma
MS	Mass Spectrometry
MS/MS	Tandem Mass Spectrometry
NBR1	Next To BRCA1 Gene 1 Protein
NCOR1	Nuclear Receptor Co-Repressor 1
NDD	Neurodegenerative Disease
NDP52	Nuclear Dot Protein 52 Kda
NEM	N-Ethylmaleimide
NES	Nuclear Export Signal
NLS	Nuclear Localization
NRF2	Nuclear Factor Erythroid 2-Related Factor 2
OPTN	Optineurin
p62/SQSTM1	Sequestosome 1
PBS	Phosphate Buffer Saline
PCP	Planar Cell Polarity
PDAC	Pancreatic Ductal Adeno Carcinoma
PE	Phosphatidylethanolamine
PI	Phosphoinositides
PI3P	Phosphatidylinositol 3-Phosphate
PMSF	Phenyl-Methyl-Sulfonyl Fluoride
POI	Protein Of Interest
PROTAC	Proteolysis-Targeting Chimera
RACK1	Receptor For Activated C Kinase 1
RPMI	Roswell Park Memorial Institute
SAR	Selective Autophagy Receptors
sgRNA	Single Guide RNA
shRNA	Short Hairpin RNA
SILAC	Stable Isotope Labelling by Amino Acids

siRNA	Short Interfering RNA
SSC	Size Scatter
STING	Stimulator Of Interferon Genes
TAX1BP1	Tax1-Binding Protein 1
TBK1	Tank Binding Kinase 1
TCEP	Tris-(2-Carboxyethyl) Phosphine Hydrochloride
TCF	T-Cell Factor
TEM	Transmission Electron Microscopy
TMT	Tandem Mass Tag
TPD	Targeted Protein Degradation
Tsc1	TSC Complex Subunit 1
Tx-00	Tirton-X100
UBA	Ubiquitin-Associated Domain
UBL	Ubiquitin-Like
UDS	Ubiquitin-Docking Site
UIM	Ubiquitin-Interacting Motif
UPR	Unfolded Protein Response
UPS	Ubiquitin-Proteasome System
UVRAG	UV Radiation Resistance-Associated Gene Protein
V-ATPase	Vacuolar-Type ATPase
WIPI2	Wd Repeat Domain, Phosphoinositide Interacting 2
WT	Wild-Type
Y2H	Yeast-Two-Hybrid
ZF	Zinc Finger
β-TrCP	Beta-Transducin Repeat-Containing Protein
ΔFP	Polarization Difference
LogFC	Logarithmic Fold Change

1. Introduction

1.1. Cancer and proteotoxic stress

Consolidated data from cancer genome sequencing projects indicate that cancer genomes contain many single-base mutations, translocations, deletions, and copy-number variations (e.g., see the Cosmic database)[1]. Cancer tends to arise from a single derailed cell and accumulate a number of mutations due to defective DNA repair. Following clonal selection (consistent with Darwinian principles), cancer cells develop random genetic and epigenetic alterations, such as unrestrained proliferation, avoidance of cell death cues, deregulated cellular energetics, and the ability to invade and metastasise. As a result, the readjusted cellular programmes and cell signalling progressively transform healthy cells into cancerous cells, which are able to survive and proliferate even under hostile conditions (e.g. continuous exposure to maintenance treatment, autologous anti-tumor immune response, and nonpermissive microenvironment)[2]. In cancer, frequent mutations in a number of proto-oncogenes and tumour suppressors, such as *PI3K*s, *KRAS*, *TP53*, *PTEN*, *RB1*, and *P16,* occur and contribute to oncogenesis[3]. In addition, multiple changes in the genome with low frequency, many of which will directly affect proteins, also play important roles in cancer formation and progression.

Even though 50% of human proteome is intrinsically disordered, proteins need to undergo correct folding and possess intrinsic stability to be functional. Often, to maintain native folding conformation, proteins are found in complexes with co-factors and/or other proteins that confer additional stability and provide the right functional context. Indeed, in addition to post-translational modifications, which may alter protein conformation, cells have developed sophisticated chaperone and quality control networks that can ensure correct protein folding during protein biogenesis (Fig 1.1)[4]. Nevertheless, point mutations in proteins can cause deviations from their native three-dimensional structure and alter or abrogate their function in the cell. Genomic alterations in cancer (e.g., translocations, amplifications, and large-scale deletions) will also affect protein abundance, composition of protein complexes and eventually the stability of individual proteins or protein complexes[4]. Together, these layered events will accumulate the appearance of misfolded proteins and result in protein aggregation inside cancer cells (e.g. p53[5]). Eventually, build-up of these aggregates will put an additional burden on protein degradation machineries and, if left unchecked, cause proteotoxic stress[6]. In addition, cancer cells typically synthesise proteins more rapidly due to higher rates of proliferation, to

escape from apoptotic death and to cope with metabolic stress, oxidative stress, and hypoxia. Consequently, basal proteasome load and cellular stress level may increase and result in proteotoxic stress in cancer cells[6].

In order to respond to proteotoxic stress and maintain homeostasis, cancer cells rely on stress response pathways to eliminate misfolded and aggregated proteins. Thus, cancer cells upregulate an interconnected network of protein quality control and proteostasis pathways, e.g. the ubiquitin-proteasome system (UPS), heat-shock protein (HSP) chaperone system, unfolded protein response (UPR), and autophagy[6] (Fig 1.1). During their short lifespan, misfolded proteins are prone to aggregate due to non-specific interactions via hydrophobic surfaces that are usually obscured and less accessible in fully folded proteins. Proteins of HSP superfamily, such as the HSP90, HSP70, HSP60, HSP40, and HSP27 families are upregulated during proteotoxic stress[7]. These molecular chaperones assist in protein refolding by masking misfolded regions. They are frequently highly expressed in a variety of cancer types and shown to be actively involved in tumour cell proliferation, invasion, differentiation, metastasis, and death[8]. Although HSP response confers partial rescue of protein aggregation events, there is often a requirement for the cells to degrade misfolded proteins.

The UPR pathway is a transcriptional and translational response to endoplasmic reticulum (ER) stress caused by accumulation of misfolded proteins. It is also triggered by altered Ca^{2+} levels, redox state, nutrient status, increases in the rate of protein synthesis, pathogens, or inflammatory stimuli, and aims to readjust ER folding capacity to restore protein homeostasis. Oncogenic signalling, hypoxia, and glucose deprivation are, on the other hand, thought to induce the ER stress in tumour cells[9, 10]. The UPR is triggered by interaction of misfolded proteins with the ER chaperone Grp78/BiP, which induces a number of events in the cells via three UPR activator proteins, IRE1, PERK, and ATF6: *i*, increase in expression of genes involved in protein folding, protein quality control and phospholipid synthesis; *ii*, phosphorylation and inhibition of translation initiation factor eIF2α to attenuate general protein synthesis; *iii*, upregulation of genes encoding ER-associated degradation (ERAD). ERAD plays an important role in the ER stress response/UPR (Fig 1.1). In this process, misfolded ER-resident proteins are retro-translocated across the ER membrane into the cytosol by luminal chaperones and associated factors, such as Hsp70, calnexin and calreticulin, and protein disulphide isomerases. This is aided by cytoplasmic Ubiquitin-binding protein complexes, thereby it is targeted for degradation via the 26S proteasome[10].

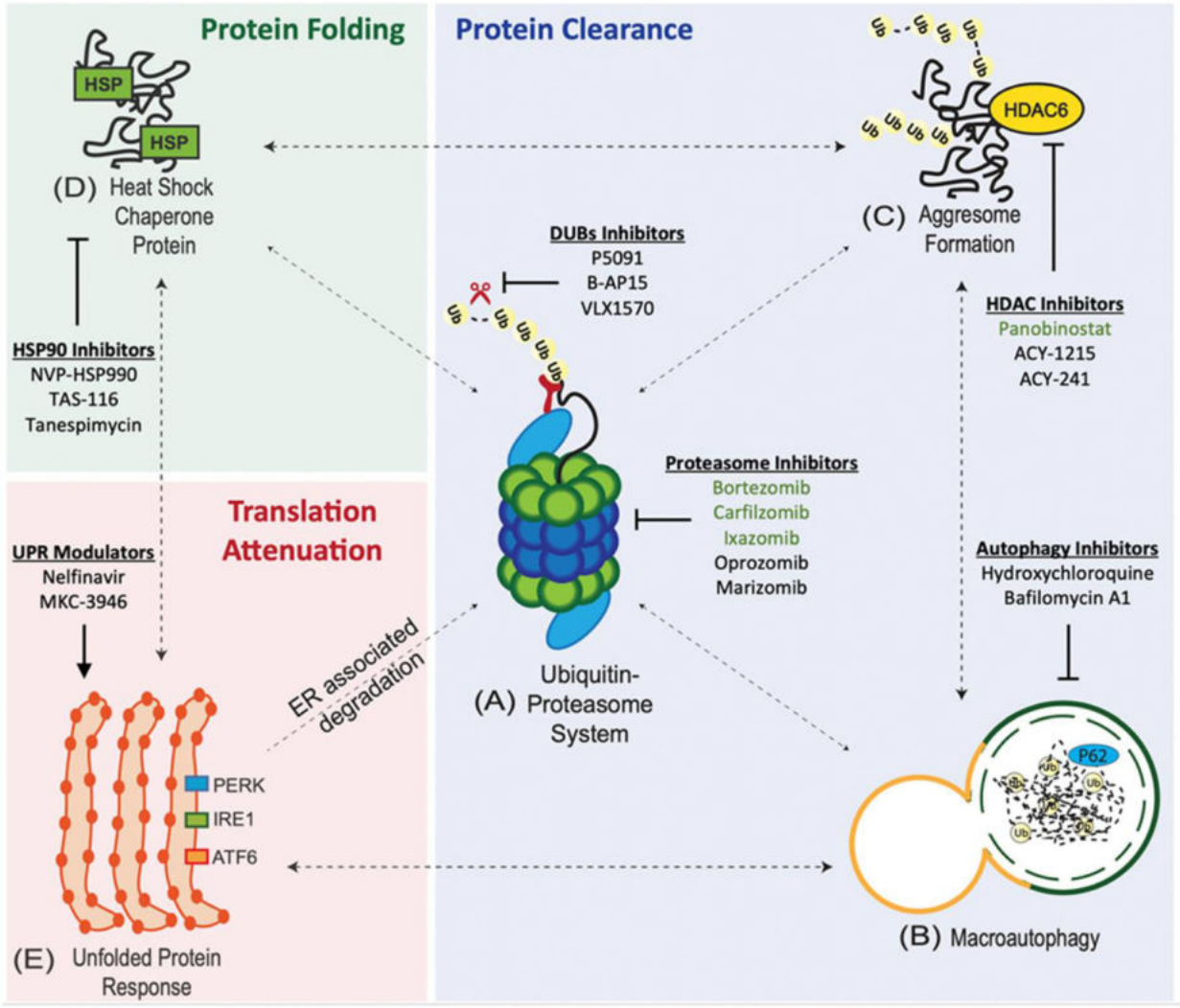

Figure 1.1 *Protein quality control systems (taken from[6]).* Proteins essentially degraded through UPS or lysosome systems, the two components of protein quality control. Cancer cells have to cope with the proteotoxic stress using tightly regulated network of protein quality control pathways such as (A) the UPS, (B) macroautophagy, (C) aggresome formation, (D) heat shock response, and (E) the UPR.

The UPS and autophagy are the main mechanisms involved in the elimination of both misfolded and aggregated proteins. The UPS involves a 3-staged ubiquitin conjugation cascade, consisting of E1 ubiquitin-activating, E2 conjugating and E3 ligating enzymes. By the activity of these enzymes, disordered proteins can be polyubiquitinated and then targeted to proteasomal degradation by ubiquitin-binding adaptor proteins or via proteasomal ubiquitin-receptor subunits. Inhibition of protein degradation in cells leads to accumulation of Ubiquitin-positive proteinaceous inclusions in cells subject to proteotoxic stress. Thus, drugs targeting the UPS to increase proteotoxic stress in cancer cells have emerged as anti-cancer treatment[11]. For example, proteasome inhibitors (Bortezomib, Calfilzomib, and Ixazomib) have been studied, and showed significant efficacy on Multiple Myeloma (MM) due to overactive

immunoglobulin synthesis-derived high levels of proteotoxic stress in this cancer[12]. In addition, as a way of overcoming treatment resistance, dual use of autophagy and UPS inhibitors, e.g., chloroquine (CQ), hydroxychloroquine (HCQ) and bortezomib, has also emerged recently[11]. Moreover, inhibitors targeting aggregation of misfolded proteins in the cells make them hypersensitive to the accumulation of protein aggregates and potentiate their use in cancer therapy. HDAC6, a microtubule-associated deacetylase, has the capacity to transport polyubiquitinated misfolded proteins[13]. Large ubiquitin-positive protein aggregates typically assembled at the microtubule organizing centre. This allows degradation of misfolded proteins by autophagy and UPS more effectively.

Autophagy, as a bulk degradation system, plays an important role in the removal of misfolded and aggregated proteins, and offers protection to cells. In this process, ubiquitinated protein aggregates are directed to lysosomal degradation via selective autophagy receptors, such as Sequestosome 1 (p62/SQSTM1, here after simply p62) and Next to BRCA1 gene 1 protein (NBR1), which may help cancer cells cope with their proteotoxic stress[14]. Reportedly, cancer cells use autophagy to maintain their metabolism. For example, genetic ablation of autophagy in KRAS-driven non-small cell lung cancer prevented tumour growth, which has made it a promising target for cancer treatment[15].

1.2. Autophagy

Autophagy mechanism was initially deciphered in yeast by the group of scientists around Yoshinori Ohsumi who was awarded a Nobel prize in 2016. Importantly, initial studies showed that the core yeast autophagy machinery is largely conserved throughout eukaryotes, including mammals[16]. Today, autophagy studies in yeast and other model organisms still contribute to our understanding of the autophagy mechanism and its possible involvement in the various human diseases. In this thesis chapter, I am going to focus on and discuss the current knowledge on mammalian autophagy.

1.2.1. Molecular mechanism of mammalian autophagy

Autophagy is an evolutionarily conserved eukaryotic degradation system induced under cellular stress conditions or by certain hormones (e.g., estrogen, glucagon, insulin)[16]. Autophagy pathways are classified into three different groups, namely macroautophagy, microautophagy, and chaperone-mediated autophagy (CMA)[17]. In microautophagy, a portion

of cytoplasm directly engulfed by lysosome. CMA does not require any membrane rearrangement; instead, unfolded, soluble proteins directly across the lysosome membrane.

Macroautophagy (hereafter referred to as simply "autophagy") is the main and most studied pathway, in which cellular components, such as damaged organelles, soluble and aggregated proteins (aberrant or dysfunctional proteins), as well as pathogenic invaders are sequestered into double-membrane vesicles (autophagosomes) and delivered to lysosomes by membrane fusion, thereby exposing autophagy substrates to the activity of lysosomal hydrolases[16]. Autophagosome biogenesis and degradation is controlled by more than 30 conserved autophagy-related genes (*ATGs*) (Fig 1.2) and implicated in the maintenance of cellular and tissue homeostasis[16]. Alterations in the process of autophagy can trigger several pathological conditions, such as neurodegeneration, infectious diseases, and cancer[16]. Since the first autophagy genes were discovered, the importance of this catabolic pathway in health and disease has been studied intensively, and an increasing body of evidence suggests that targeting autophagy could ameliorate neurodegeneration, cardio-metabolic diseases, and various forms of cancer[18]. The multi-step autophagy process can be divided into five discrete and consecutive steps controlled by specific sets of ATG proteins and other complexes: initiation, elongation of a primordial membrane (phagophore), maturation, fusion of the mature autophagosome with the endolysosomal compartment and as well as degradation and recycling[19]. Understanding of these steps are key to comprehend true nature of autophagy.

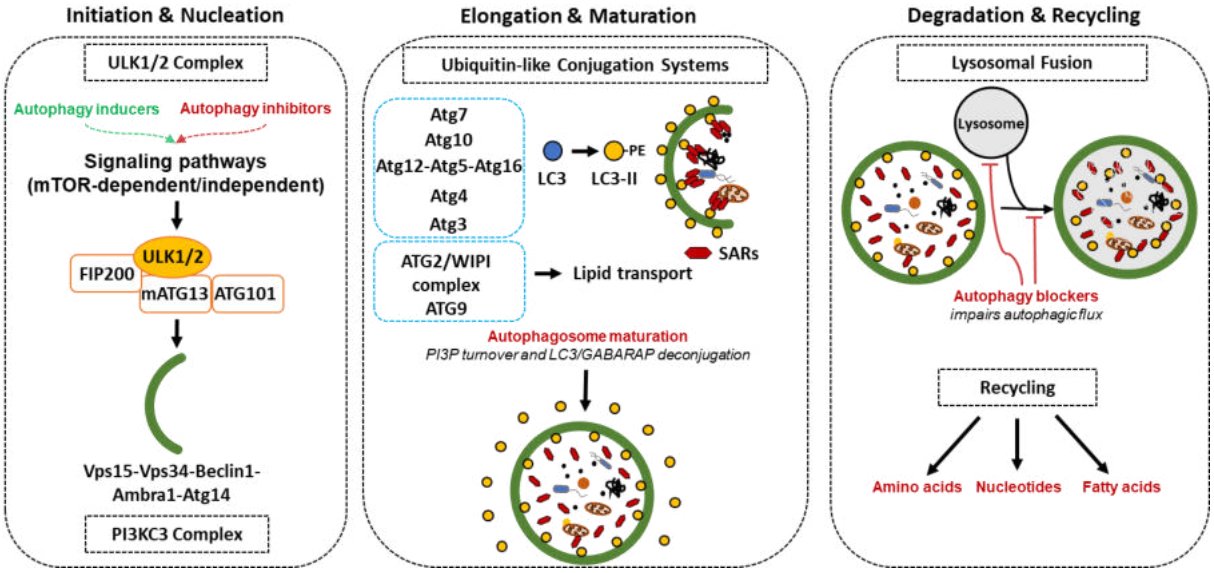

Figure 1.2 *Schematic representation of the autophagy pathway and core autophagy proteins.* The process of autophagy can be separated into five phases: Initiation and nucleation (left panel), elongation and maturation (middle panel), and degradation (right panel). Each step is

amenable to modulation at certain critical nodes of the process by different sets of ATG proteins.

1.2.1.1. Initiation

At the molecular level, induction of autophagy is triggered through the activation of AMPK and/or inhibition of mTOR kinase by diverse stress and physiological conditions, e.g., amino acid starvation, hyperthermia, hypoxia, and hormones. Also, mTOR-inhibiting drugs, e.g., Torin1 and Rapamycin, serve as autophagy inducers. Multiple signalling cascades regulating autophagy directly act on ULK1/2 kinase complex (Fig 1.2), an apical complex that initiates autophagy. Following the inducer signals, a series of phosphorylation events take place and activate the ULK1/2 kinase complex composed of ULK1/2, ATG13, ATG101, and FIP200 proteins[16]. In addition to phospho-regulation of ULK1/2 complex, its activation and stability is regulated by several ubiquitination events carried out by the E3-ligase TRAF6 bound to AMBRA1 (Lys-63), NEDD4 ligase (Lys-27, Lys-29) or CULLIN3 ligase (Lys-48)[20]. Supramolecular assembly and activation of this complex creates a scaffold for the formation of a precursor structure for the autophagosome (called phagophore), which initiates fusion of heterotypical membranes carried by ATG9-positive vesicles potentially derived from multiple membrane sources, including recycling endosomes, ER, mitochondria, Golgi complex, and the plasma membrane. Mammalian cells display formation of autophagosomes at multiple locations simultaneously; however, it is in general focused adjacent to the ER, which may point to a major role for the ER in providing membranes for autophagosomes[16]. For the nucleation of phagophores/autophagosomes, the ULK1/2 complex activates a second complex, the VPS34 lipid kinase complex, which contains the class III PI3KC3 lipid kinase VPS34, Beclin1, Atg14, and Vps15/p150 (Fig 1.2). The activity of the VPS34 complex is responsible for the catalysis and accumulation of phosphatidylinositol 3-phosphate (PI3P) on the nascent autophagosomal membrane that serves to recruit other phospholipid-binding ATG proteins involved in the membrane expansion[19].

1.2.1.2. Expansion

The expansion step relies on the association of the phagophore and the ATG machinery components, such as the ATG2-WIPI (WD Repeat Domain, Phosphoinositide Interacting 2) complex and ubiquitin-like conjugation systems[21] (Fig 1.2). ATG2 is a novel phospholipid transfer protein that mediates *de novo* autophagosome biogenesis. WIPI is a member of the PROPPIN protein family that binds to phosphoinositides (PIs) and recruits ATG2 to the site of

the autophagosome formation. Specific recruitment of the ATG2/WIPI complex to the phagophore is key for supplying part of the lipids required for phagophore expansion in conjunction with the ATG9A activity. It is thought that ATG2 transfers phospholipids from the ER to the phagophore during the process of autophagosome formation[21]. ATG2 also localises to lipid droplets, where it influences the size and distribution of those structures. ATG2's natural ability to bind membranes is consistent with its recruitment to developing autophagosomes and lipid droplets[21].

There are two ubiquitin-like conjugation systems involved in phagophore expansion, namely ATG5-ATG12 and LC3/GABARAP-phosphatidylethanolamine (PE) systems[16]. These proteins are ubiquitin-like (UBL) proteins that share the structural fold with ubiquitin, as well as ubiquitin's ability to be conjugated to protein/lipid substrates. ATG12 is conjugated to ATG5 via the action of the E1-like ATG7 and E2-like ATG10 enzymes. Next, the ATG5-ATG12 conjugate binds to ATG16L1 to generate a dimeric ATG12–ATG5–ATG16L1 complex. Of note, there is no need for an E3-like enzyme in the ATG12 conjugation system. The second ubiquitin like reaction covalently conjugates soluble LC3 and GABARAP proteins to the lipid PE enriched in the autophagosomal membrane. LC3/GABARAP proteins are expressed as cytosolic precursors and later conjugated to the autophagosome membrane. This process requires the activity of a cysteine protease ATG4 (ATG4A, ATG4B, ATG4C, and ATG4D homologs are known), which cleaves LC3/GABARAP proteins at the carboxy terminus. This produces LC3-I/GABARAP-I with an exposed glycine at C-terminus, capable of transient adenylation and permanent amide bond formation with the PE. E1-like ATG7 and E2-like ATG3 enzymes, as well as the E3-like ATG12–ATG5–ATG16L1 complex, catalyse formation of LC3/GABARAP-PE (also known as LC3-II/GABARAP-II) in the inner and outer sites of the double-membraned phagophore[16]. The conjugation of LC3/GABARAP on the autophagosome membrane is widely used to monitor autophagic activity in cells[22]. Alterations in the number of punctate LC3 foci and/or a shift in the size of LC3/GABARAP (i.e., LC3-II/GABARAP-II moves faster in SDS-PAGE gels) indicates a change in the activation of autophagy in cells. Together, this process allows LC3/GABARAP proteins to be anchored within/on the autophagosome membrane and mediate expansion and closure of the autophagic membrane by creating a membrane scaffold for core autophagy components. These proteins have additional roles in cargo recognition that will be mentioned below[23]. Closure and sealing of the autophagosome membrane require additional mechanisms, such as the recruitment of the filament-forming ESCRT-III complex[16].

In addition to its role in Golgi-related secretory pathways, in the initial stages of autophagosome production, Atg9 vesicles are also a crucial membrane source[24]. It has been challenging to determine the origin of the phagophore membrane and comprehend the dynamic events leading to phagophore elongation, bending, and closure, since autophagosomes typically lack any transmembrane proteins. The only known transmembrane ATG protein is ATG9, where ATG9-positive vesicles are implicated in phagophore elongation.

1.2.1.3. Maturation

Newly formed autophagosomes host almost all the ATG proteins on their surface. These proteins need to be recycled for building new autophagosomes. The maturation step is characterized by the removal of ATG proteins from the autophagosome surface and their release in the cytoplasm. This step is thought to be initiated just after the closure of the phagophore, for recycling of the components required for the autophagosome biogenesis[16] (Fig 1.2). Following that, motor proteins and microtubule tracks ensure that autophagosomes fuse with lysosomes. Two important aspects of this step are the PI3P turnover by myotubularin phosphatases and deconjugation of members of the LC3/GABARAP proteins by members of the ATG4 protease family. LC3/GABARAP deconjugation is also expected to avoid the premature fusion of incomplete/unclosed autophagosomes with lysosomes. It is thought that the fusion machinery must be acquired during this transition and activated only after the phagophore has closed[19]. Nevertheless, this is not necessarily the case. Interestingly, ATG conjugation-deficient cells were found to form incomplete/unclosed autophagosomes at a slower rate, and yet, these autophagosomes with ATG proteins and PI3P on their surface managed to fuse with lysosomes[25]. This let to speculate that either there might be some micro-domains enabling binding of fusion factors or maturation and fusion events might take place simultaneously. Although other scenarios, are also possible, it is fair to postulate that the crosstalk between all these factors still needs to be elucidated and dissected at the molecular level.

1.2.1.4. Fusion, degradation, and recycling

The completed and sealed autophagosome fuses with lysosomes (Fig 1.2) or late endosomes, which involves SNARE complexes (e.g., STX17, VAMP8), lysosomal membrane proteins (e.g., LAMP2), components of the protein sorting complex HOPS, as well as RAB GTPases (e.g., RAB5, RAB7). Dynein proteins are involved in the coordinated transport of these autophagosomes and lysosomes to the perinuclear area along microtubules[26]. Following

the fusion of the outer membrane of an autophagosome with the lysosome (called autolysosome) or endosome (called amphisome), the inner membrane may lose its integrity, and entrapped substrates become broken down by lysosomal acid hydrolases (e.g., cathepsins). The digestion products (e.g., amino acids, lipids, simple carbohydrates, and nucleosides) are recycled back to the cytosol to maintain a pool of metabolites required for cell metabolism[19]. The transport of degradation products to the cytosol is thought to be managed by numerous lysosomal membrane transporters (e.g., PQLC2, SLC30A1-4, CTNS, LIMP2)[26].

The lysosome is the degradative point in mammalian cells powered by the proton gradient created by the Vacuolar-type ATPase (V-ATPase) and orchestrated by more than 60 different hydrolases including lipases, proteases, and nucleases[26]. Moreover, the acidity of the lysosomes is found to be an important effector in their fusion with autophagosomes and endosomes[27]. Therefore, lysosomal lumen alkalizers, such as CQ and HCQ or the V-ATPase inhibitor Bafilomycin A_1 (Baf A_1), emerge as late-stage autophagy inhibitors. They act by neutralizing the acidic pH in the lumen of lysosomal vesicles, which is required for the activities of lysosomal hydrolases involved in autophagic degradation[28]. Thus, deacidification of lysosomal vesicles leads to the accumulation of autophagosomes which can be visualized by increase in the autophagic substrates, such as protein aggregates, damaged mitochondria, but also by amassing LC3-positive vesicles that have failed to fuse with and be cleared by lysosomes[22]. However, some studies have shown that these alkalizers block the autophagosome-lysosome fusion depending on the treatment time and dose. In these studies, extended treatments (12–24 h, 400 nM) with Baf A_1 decreased the percentage of vesicles that display colocalization with lysosomal (e.g., LAMP1) and autophagy (e.g., LC3B) markers. In contrast, in short-term treatments (1-2 h, 100 nM), undegraded autophagosomes accumulated in the cells did not result in an obvious separation between LC3-labelled vesicles and LAMP-1-stained vesicles[29]. This let to conclude that acidification of lysosomes might be dispensable for their fusion with autophagosomes. On the other hand, it is likely that the Baf A_1-mediated fusion-block activity might be an off-target result of the deacidification of lysosomes as genetic depletion of V-ATPase in *Drosophila* did not block the autophagosome-lysosome fusion[30].

1.2.2. Selective Autophagy

Historically, a non-selective bulk degradation of cytosolic molecules was ascribed to autophagy. However, the more recent identification of autophagy receptors that specifically bind various cargos revealed selectivity in the autophagic pathway. This phenomenon is

described as selective autophagy. The induction mechanism of selective and bulk autophagy differ as selective autophagosomes can form even under basal conditions, when nutrients are plentiful[31]. Bulk autophagy is induced by the activation of ULK kinase complex facilitated by multiple signalling cascades, such as mTOR, as discussed previously[16]. On the other hand, selective autophagy is involved in the regulated turn-over of portions of organelles; and, therefore, the autophagy machinery is assembled around these organelles by selective autophagy receptors (SARs) in order to confine the cargo inside of an autophagosome vesicle[32]. Activation and/or gathering of the SARs on the cargo molecules leads to the recruitment of FIP200, which later functions to recruit and concentrate ULK kinase complexes on the cargo. Activation of ULK kinase complexes and concomitant formation of a scaffold initiate the formation of an autophagosome membrane around the cargo molecule[32]. In addition, the very well-known, aggregation-prone huntingtin protein (HTT), associated with the Huntington disease, was also proposed to act as a FIP200 homolog[33]. It binds to ULK1, GABARAPs, and several SARs, and function as a scaffold for selective autophagy. Indeed, conditional knockout of HTT in the mouse brain leads to the accumulation of p62/SQSTM1, a hallmark of defective selective autophagy[33]. The interaction between the SARs and LC3 proteins on the surface of autophagosome membrane also ensures dramatic and exclusive entrapment of the cargo within autophagosomes[32]. Upon activation of the ULK kinase complex, the downstream events that takes place are identical to the bulk autophagy described above.

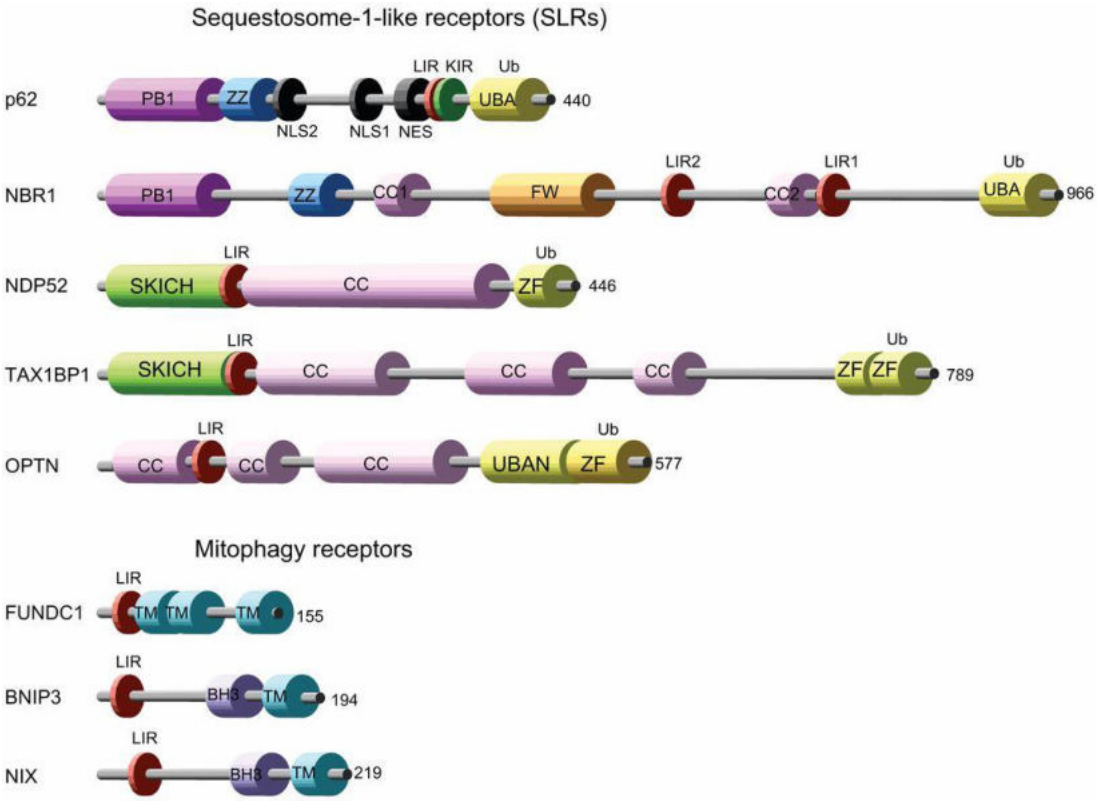

Figure 1.3 The domain architecture of five ubiquitin-binding SARs and three ubiquitin-independent mitophagy receptors in mammals. This includes the domains: PB1, Phox and Bem1 domain (dark pink); ZZ, ZZ-type zink finger domain (blue); CC, coiled-coil domain (light pink); NLS1 and NLS2, nuclear localization signals 1 and 2 (dark gray); NES, nuclear export signal (dark gray); LIR, LC3-interacting region (dark red); KIR, Keap interacting region (green); UBA, ubiquitin-associated domain (yellow); FW, four tryptophan domain (dark yellow); SKICH, SKIP carboxyl homology domain (light green); ZF, Zinc-finger domain (yellow); UBAN, ubiquitin binding in ABIN and NEMO domain (yellow); TM, transmembrane domain (light blue); BH3, Bcl-2 homology (BH) domain 3 (light purple). The image was adapted from[34].

1.2.2.1. Selective Autophagy Receptors

The selectivity to different cargo molecules, such as protein aggregates (aggrephagy), damaged mitochondria (mitophagy), cytoplasmic pathogens (xenophagy) or lipid droplets (lipophagy), is coordinated through different SARs, e.g., ubiquitin-binding: p62/SQSTM1, TAX1BP1, NDP52, NBR1, OPTN, and TOLLIP or ubiquitin-independent: NIX and BNIP3, FUNDC1, and Atg32[32] (Table 1). The research of the past two decades has led to the discovery of many SARs functioning in selective autophagy pathways and elucidated their mode of binding to cargo molecules. The common features among ubiquitin-binding SARs are as follows: (1) they share a sequence motif (LIR, LC3 interacting region or FIR, FIP200 interacting region) that allows them to bind core autophagy proteins (LC3/GABARAPs and FIP200), (2) they have a cargo-binding domain (e.g., ubiquitin-binding domains of the

aforementioned SARs), and (3) they possess the ability to oligomerize to create an efficient bridge between the autophagosome and the cargo as well as concentrate various autophagy factors, such as FIP200) at the cargo[32] (Fig 1.3). On the other hand, ubiquitin-independent (membrane-associated) SARs are specialized autophagy receptors that do not exhibit a ubiquitin binding domain in their structure and are able to interact with autophagy machinery[32] (Fig 1.3). These receptors are able to link intracellular cargo directly with autophagosomes through binding to LC3/GABARAP proteins, and they are in general intervening in the clearance or turn-over of organelles[35]. These receptors include NIX, BNIP3, and FUNDC1 for mitophagy; PEX14, and NBR1 for pexophagy; SMURF1 and TRIM5α for virophagy; FAM134B, RTN3, CCPG1, ATL3, and TEX264 for ERphagy; and NCOA4 for ferritinophagy (see Table 1 for more examples). Recruitment of the either ubiquitin-dependent or -independent SARs on the cargo surface enables activation of the ULK1/2 signalling and formation of autophagosome membrane[35]. In the literature, the list of SARs and proteins containing functional LIRs keeps growing, which casts light on the mechanistic regulation of autophagy and its involvement in cellular signalling.

Table 1: *Mammalian selective autophagy receptors*

Pathway	***Substrate***	***Mammalian autophagy receptors***	***Refs***
Aggrephagy	Protein aggregate	p62, NBR1, OPTN	36-39
Ubiquitin-dependent Mitophagy	Mitochondria	NDP52, OPTN, p62, TAX1BP1, AMBRA1	40-43
Ubiquitin-independent Mitophagy	Mitochondria	NIX, BNIP3, FUNDC1, Bcl2L13, FKBP8, PHB2, NLRX1, AMBRA1, cardiolipin, ceramide	43-51
Ubiquitin-dependent Pexophagy	Peroxisome	NBR1, p62, TNKS	52-54
Lysophagy	Lysosome	TRIM16, NDP52, TAX1BP1	55-57
Zymophagy	Secretory granule	p62	58
ERphagy	ER	FAM134B, SEC62, RTN3, CCPG1, ATL3, TEX264	59-64
Ferritinophagy	Ferritin	NCO4A	65
Glycophagy	Glycogen	Stbd1	66
Nuclear lamina autophagy	Nuclear lamina	Lamin B1	67
Xenophagy	Bacteria	NDP52, p62, OPTN, TAX1BP1	68-71

Virophagy	Viral capsids	TRIM5α, p62	[72, 73]
Ribophagy	Ribosomes	NUFIP1	[74]
Midbody autophagy	Midbody rings	p62, NBR1, TRIM17	[75-77]

For example, the protein p62 is the best known and first SAR discovered for its role in clearing protein aggregates via aggrephagy[37]. The discovery of the involvement of p62 in aggrephagy and characterization of its conserved domains that interact with polyubiquitin chains (UBA domain) and LC3 proteins (LIR motif) have paved the way for the elucidation of mechanisms of SAR-mediated selective autophagy in mammals. Overall, p62 delivers ubiquitinated cargo molecules bound to its UBA domain to the autophagosomes via its LIR motif bound to the LC3 proteins on the autophagosome membrane. The bridge formed between LC3, p62 and the protein aggregates ultimately leads to their joint sequestration in the autolysosomes[37]. Hence, accumulation of p62 along with LC3 proteins in cells are used as a marker for defects in the autophagic flux in the cells. In addition to the intermediate LIR and UBA domains, p62 contains multiple other conserved protein-interaction modules with diverse functions. These domains include a PB1 domain for homo- or hetero-dimerization with other PB1-containing proteins, which is crucial for its function capturing autophagy cargo; ZZ-type zinc finger (ZF) domain for binding to N-terminal arginine moieties and RNA; tumour necrosis factor receptor associated factor 6 (TRAF6)-binding domain for triggering TRAF6 polyubiquitination thereby activating the inflammatory NF-κB pathway; nuclear localization and nuclear export signal (NLS and NES) sequences[78]. More recently, p62 was also shown to interact with FIP200 protein via its dimeric Claw domain (also known as FIR domain)[79]. Recruitment of FIP200 to protein aggregates by p62 is mutually exclusive with its binding to LC3 and ubiquitin for selective degradation of protein aggregates[79]. In addition to its role in aggrephagy, p62 emerges as a crucial receptor for mitophagy and lipophagy (Table 1).

NBR1 is another SAR with a role in aggrephagy and displays a similar domain organization as p62. In addition to interacting with itself via a coiled-coil domain and p62 via its PB1 domain, NBR1 can bind to lipid membranes via its amphipathic α-helical J (JUBA) domain. This interaction has been shown to be an important regulator of turnover of peroxisomes via their selective autophagy (called pexophagy)[52]. On the other hand, selective autophagy of invading bacteria (xenophagy) requires another SAR, TBK1 adaptor nuclear dot protein 52 kDa (NDP52) (also known as calcium-binding and coiled-coil domain-containing protein 2 [CALCOCO2])[80]. In addition, Tax1-binding protein 1 (TAX1BP1) shares a structural

homology with NDP52, is also required for the autophagic clearance of *Salmonella*[68]. These proteins have also shown to function in aggrephagy and mitophagy (Table 1). Another SAR contributed to clearance of *Salmonella* is Optineurin (OPTN), which requires phosphorylation and activation of its LIR domain on Ser177 by the TANK binding kinase 1 (TBK1)[81]. In addition, OPTN was suggested as a major SAR in mitophagy and aggrephagy, which has been found to be enriched in various pathological aggregates such as Lewy bodies in Parkinson disease[82]. Comprehensive analysis of PINK1/Parkin-mediated mitophagy also revealed that ubiquitin binding domains of OPTN and NDP52 are also crucial for effective removal of depolarized mitochondria.

In addition to directing cargo to the autophagosomes, ubiquitination confers an essential post-translational modification in the regulation of bulk and selective autophagy[83]. E3 ubiquitin ligases and deubiquitinating enzymes (DUBs) have been shown to be fundamental players in the ubiquitination or de-ubiquitination of ATG proteins, and thereby regulation of their activity. For example, de-ubiquitination of Lys48 chains of ULK1 by USP20 prevents its proteasomal degradation, thus stabilizing ULK1 and activating autophagy[84]. However, USP1-mediated removal of Lys63 chains from ULK1 destabilizes the protein and thus supresses autophagy[85]. Likewise, ubiquitination of Lys29 and Lys48 chains of VPS34 by UBE3C promotes its degradation in the proteasomes, thus suppressing autophagy[86]. Many other components of the autophagic machinery, such as Beclin1, AMBRA1, WIPI2, and ATG16L1[83], are also subjected to regulation by a wide variety of E3s and DUBs. In a similar manner, engagement of membrane-bound or soluble autophagy receptors is often achieved through their phosphorylation. Various phosphorylation events are found to be essential in regulating SARs' activity, e.g., phosphorylation of the UBA domain of p62 (on Ser403) by Casein kinase 2 (CK2) enhances its affinity to ubiquitin chains; phosphorylation of NIX (on Ser34 and Ser35) enhances its interaction with LC3s; phosphorylation of FAM134B (on Ser151) by CAMK2B kinase facilitates its dimerization, thereby making it accessible for autophagosome sequestration[87-89]. Furthermore, acetylation is another mechanism implicated in the control of activity of various SARs. The acetylation of p62 at Lys420 by acetyltransferase is found enhance its binding to polyubiquitinated proteins[90]. Acetylation of ATG9A is also reported as a negative regulator of ERphagy[91].

1.2.2.2. LIR-LDS interaction

In mammals, there are 7 orthologues of yeast Atg8 protein: the LC3 proteins – LC3A, LC3B, LC3C, and LC3B2, and the GABARAP proteins – GABARAP, GABARAPL1, and GABARAPL2/GATE-16. LC3B is the most prevalent and well-established autophagosome marker[22]. All Atg8/LC3/GABARAP proteins share a conserved structural similarity. They contain a β-sheet wrapped around a central α-helix similar to ubiquitin in their C-terminus and two α-helices located N-terminally[32] (Fig 1.4A). Since they resemble ubiquitin structurally, they are also called ubiquitin-like protein (Fig 1.4B-C). The structure of the N-terminal subdomain varies among LC3/GABARAP subfamilies and determines their affinity for their interaction partners. LC3/GABARAP proteins also possess two characteristic hydrophobic pockets (Fig 1.4D). The first hydrophobic pocket (HP1) is located at the interface of the N-terminal α-helix and the ubiquitin-like core. The central α-helix and β-strand form another hydrophobic pocket (HP2). Combination of these two pockets constitutes a unique domain called the LIR-docking site (LDS), which enables LC3/GABARAP proteins to recognize and bind to a conserved structure commonly called LC3-interacting region (LIR)[32].

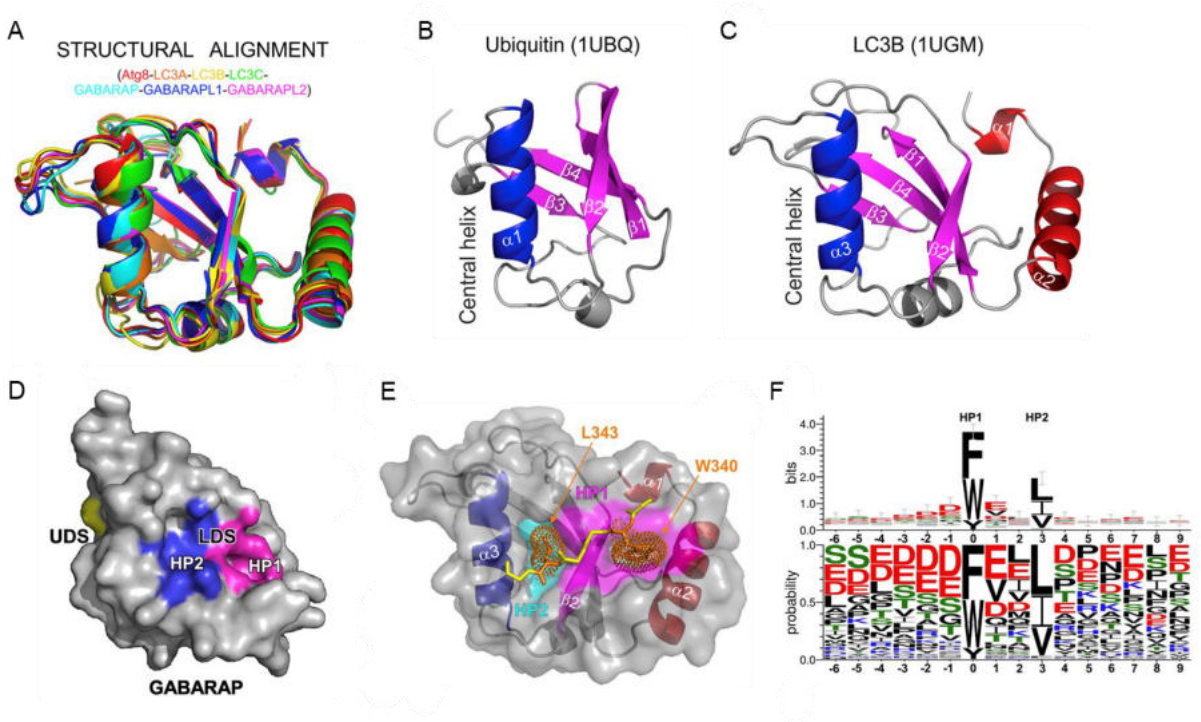

Figure 1.4 Structural similarity of LC3/GABARAP proteins, and sequence alignment of canonical LIR Motifs. **(A)** Structural alignment of LC3/GABARAP family and yeast Atg8 proteins are shown as ribbon diagrams. **(B-C)** Structures of ubiquitin (B), LC3B (C) are shown as ribbon diagrams with PDB accession codes in parentheses. **(D)** GABARAP surface structure with the location of the LDS (with HP1 and HP2) indicated relative to the ubiquitin-docking site (UDS) (PDB: 3WIM). **(E)** Structure of the p62/SQSTM1-LIR:LC3B complex (2ZJD).

LC3B is shown as a semi-transparent surface, and p62/SQSTM1-LIR is shown as a main chain (yellow). **(F)** Sequence logos of LIR motifs shown as information content in bits (upper panel) and residue probabilities at each position (lower panel). The images were adapted from[32, 92].

As a characteristic feature for the receptors of selective autophagy, p62 was the first protein identified to harbour a functional LIR motif facilitating its interaction with LC3B[37]. Detailed analysis of the p62 LIR motif with deletion mapping, point mutations, and structural analysis elucidated its binding determinants and binding mode to the LDS domain of LC3B. The consensus of the LIR motif is W-x-x-L (x means any amino acid), where two hydrophobic residues Trp (W) and Leu (L) docked deeply into HP1 and HP2 of LDS, respectively[37, 93]. In addition, alanine substitution of the three consecutive Asp (DDD) residues flanking the core motif at the N-terminus revealed their importance for LDS binding, and led to the definition of the core of p62's LIR motif as DDDWTHL[37].

Further structural studies revealed a consensus sequence of $[W/F/Y]_0$-X_1-X_2-$[I/L/V]_3$ for canonical LIR motifs[34]. Similar to the p62-LIR/LDS interaction, aromatic residues [W/F/Y] and aliphatic residues [I/L/V] are highly conserved and bind to two hydrophobic pockets (HP1 and HP2) within the LDS of any LC3/GABARAP protein[34]. Inspection of the amino acids at the X_0 position demonstrated that Tyr (Y) is the least frequent. In addition, Trp (W) is found to be energetically favoured over Tyr or Phe (F) (e.g., substitution of Y for W in the NBR1 LIR led to 7.5-fold higher binding affinity)[94]. Moreover, the residues documented at positions X_{-1} to X_{-3} seemed to be highly populated with acidic residues Asp (D) or Glu (E), or residues that can be phosphorylated Ser (S) or Thr (T)[95]. Acidic or hydrophobic residues are also found at positions X_1 and X_2, but basic residues, Arg (R) and Lys (K) as well as Pro (P) and Gly (G) residues are under-represented. The residues at X_1 and X_2 positions are also inhabited by acidic or hydrophobic residues and refrained from containing basic Arg (R) and Lys (K) residues as well as Pro (P) and Gly (G) residues. Indeed, Lys to Ile substitution at the X_2 position of PCM1 LIR motif enhanced its binding affinity and specificity to the LC3/GABARAP proteins[96]. The preference of the acidic residues at the flanking N- and C-terminus of the core motif can be explained by their favourable engagement with basic residues in the LDS pockets of LC3 and GABARAP proteins[95]. However, there is a focus on the core LIR signature, which results in a propensity to ignore the importance of flanking sequences of the core LIR motifs.

It is clear from the published literature that the majority of the LIR-containing proteins show higher affinity to GABARAP and GABARAPL1 as compared to GABARAPL2 and LC3 family proteins [92]. Some of them bind almost exclusively to GABARAP family proteins. Only a minority show preference for LC3 family proteins[45, 97-102]. It has been a long-standing goal to

elucidate the factors responsible for this binding preference. A recent study focused on screening 30 validated LIR sequences with a peptide-based assay proposed that Val (V) residing at the X_1 and X_3 positions confers enhanced interaction with endogenous GABARAP over LC3B[103]. However, many LIR peptides showing preference to the GABARAP binding do not contain Val residues at these positions. X-ray crystallography of LC3/GABARAP:LIR complexes showed that GABARAP specificity is determined by a combination of residues within and/or flanking the core LIR motif, and by GABARAP subfamily-specific residues within the LDS domain[104]. As exemplified with ULK1, ATG13, and PCM1 LIR motifs, hydrophobic residues within the positions X_4 to X_{10} interact with the HP2 pocket which is larger in the GABARAP subfamily protein compared to LC3 subfamily. In the HP2 pocket, GABARAP proteins exhibit more hydrophobic and aromatic residues ($L55^{GAB/GABL1}$/$I55^{GABL2}$ and $F62^{GAB/GABL1}$/$W62^{GABL2}$); however, there are fewer hydrophobic, even more charged residues in the corresponding positions for LC3 proteins ($V58^{LC3A/B}$/$L64^{LC3C}$ and $K65^{LC3A/B}$/$S71^{LC3C}$)[104].

The affinity of LC3/GABARAPs to the LIR peptides from various proteins can be determined by several biochemical assays, such as isothermal titration calorimetry, surface plasmon resonance and fluorescence polarization (FP) assays[105]. These assays measure various physicochemical changes over binding of the LIR peptide to the LC3/GABARAP proteins and extract binding curves enabling calculation of a dissociation constant (Kd) value for each interaction (i.e., a lower the Kd means binding affinity is higher). The binding affinity between LC3/GABARAP and LIR peptides ranges from approximately 0.1 to 100 μM, and is usually found on a low μM range (1-10 μM)[34]. However, the intracellular binding affinity of the LC3/GABARAP proteins to the LIR containing proteins might be more satisfying than its affinity measured with the aforementioned assays, due to some molecular interactions. First of all, homo- or hetero-oligomeric states of proteins (e.g., SARs) can result in the presentation of more than one LIR motif which can endow them with a higher binding avidity and selectivity for LC3/GABARAP proteins[106]. On the other hand, some proteins already identified with multiple LIR sequences in their structure. For example, some of the SARs, including NBR1, NDP52, and Tollip have multiple LIR motifs, each contributing to their interaction with LC3/GABARAP proteins[92]. More strikingly, the ERphagy receptor RTN3L has a total of six LIR sequences[61]. In some cases, phosphorylation regulates the affinity of the LIR motif. For example, TBK1-mediated phosphorylation of a Ser residue positioned at position X_{-1} of the OPTN LIR motif increased its affinity for LC3B 5-fold[107]. On the other hand, phosphorylation

of LIR motifs can be used by cells to control selective autophagy and to avoid unwanted degradation events. Phosphorylation of the LIR motifs of mitophagy receptors FUNDC1 (Tyr at X_0) and BNIP3 (Ser at X_{-1} and X_7) weakens or augments their LDS interaction respectively[108, 109]. It is also suggested that not only LIR motifs but also phosphorylation of the residues on the binding surface of LC3/GABARAP proteins might regulate their interaction with LIR motifs. For instance, PKA-mediated phosphorylation of a Ser residue adjacent to the LDS pocket negatively regulates autophagy; however, further studies are required to determine whether the Ser phosphorylation affects its binding to p62 or other SARs[110].

Proteins containing a functional LIR motif in their structure are likely subject to autophagic degradation. There is a growing list of LIR-containing proteins: dishevelled segment polarity protein 2 (DVL2)[111], β-catenin[112], fatty acid synthase subunit beta (FAS1)[113], lamin B1[67], paxillin[114], stimulator of interferon genes (STING)[115], cryptochrome circadian regulator 1 (CRY1)[116], and nuclear receptor co-repressor 1 (NCOR1)[117]. Given this plethora of cargo molecules demonstrated experimentally that interacting with LC3/GABARAP through their LIR motifs or adaptor proteins (SARs, ubiquitin), it is fair to postulate that autophagic degradation holds an extensive potential to regulate a broad range of cellular signalling pathways. Nevertheless, not all proteins interacting with LC3/GABARAP proteins through their LIR motif are targeted to autophagic degradation. The presence of functional LIR motifs in *bona fide* autophagy receptors demonstrates that autophagosome maturation and formation are also regulated by LIR-motif-mediated interactions. The LIRs of components of the core autophagy are found to be important for recruiting these proteins to the autophagosome membrane and regulating the activity of the autophagic machinery. These proteins include the LIRs in Beclin-1, ULK1/2, ATG13, FIP200, VPS34, ATG2A/B, ATG4A/B, ATG7, and ATG14[34].

Furthermore, a number of proteins have been found to contain a LIR but are not degraded by autophagy: e.g., TP53INP2[118], FYCO1[119], TBC1D5[120], TBC1D25[121], TECPR2[122], PLEKHM1[123], Ankyrin-3[124], PCM1[125], and BRUCE[126]. There are two possible explanations for the escape of these proteins from the autophagic degradation. One suggestion is that they might be recruited only to the outer membrane of the autophagosomes, not to the inner membrane, to perform a scaffolding/regulatory function. Another explanation might be that the suggested interactions might serve in autophagy-independent pathways. It should be mentioned that LC3/GABARAP family proteins also engage in interactions with LIR-containing proteins in non-autophagic processes[127]. Although all LC3/GABARAP family proteins seem to fulfil

specific roles within autophagy, several family members have been implicated in receptor trafficking; whereas others have been implicated in tumour-suppressive functions that appear to be autophagy-independent[127]. For example, LIR-mediated GABARAP binding of the adapter proteins KBTBD-6 and -7 is required for membrane targeting of the E3 ligase complex which enables regulation of RAC1 signalling via local regulation of the abundance of the guanine exchange factor TIAM1[101]. Another example is provided by the giant ankyrin-G protein which promotes GABAergic synapse stability through opposing endocytosis of GABAA receptors. This requires a super-strong LIR–GABARAP interaction of ankyrin-G with a K_d in the lower nanomolar range[124]. Furthermore, the GABARAP protein family was described in intracellular transport of the GABA (A) receptor (GABAAR)[128]. Further studies revealed that GABARAP and GABARAPL1 also mediate membrane expression of the angiotensin II receptors[129], the human κ opioid receptor (hKOR)[130] and the transient receptor potential cation channel subfamily V member (TRPV)-1[131]. Knockdown of either GABARAPL1 or GABARAP decreases the surface expression of KOR[130].

1.2.2.3. Atypical LIR motifs

Extensive research on the LIR-LDS interaction made a remarkable contribution to our understanding of the mechanistic assembly of the autophagy machinery, and led to the identification of new SARs[31]. However, detailed analysis of the LC3/GABARP binding proteins led to discovery of the alternative binding modes and sites on LC3/GABARAP surface. Exploitation of the LIR-LDS interaction has shown that not all SARs share the canonical LIR consensus. Some LIR sequences lack the aromatic residues ($W/F/Y_0$), whereas others do not have the hydrophobic residues ($L/V/I_3$)[97]. These are called atypical (or non-canonical) LIRs. Depending on which residues are present within the LIR, a different hydrophobic pocket on the LDS may be occupied. Although atypical LIR motifs do not show the canonical core consensus, they strongly and specifically bind to LC3/GABARAP proteins[92].

NDP52 was the first protein to be reported to contain an atypical LIR motif (so called c-type LIR, cLIR). The motif binds to LC3C proteins with a Kd of 1.6 μM[80]. The cLIR with the core sequence ILVV consists of three aliphatic residues (LVV) occupying the HP2, and lacks an aromatic residue typical for canonical LIRs; thereby HP1 stays unoccupied. Additional hydrophobic interactions between LVV and LDS and hydrogen bonds compensate for the absence of aromatic residues. Moreover, upon changing I in the cLIR to the best HP1-fitting

aromatic residue W, NDP52 shows no more LC3C specificity and begins to bind all LC3/GABARAP proteins. A similar pattern has also been found in TAX1BP1 protein where MLVV motif enables interaction with LC3B, LC3C, GABARAPL1, and GABARAPL2 proteins[68].

Likewise, there have also been reports of LIR-LDS interactions, where just the aromatic HP1 pocket is occupied. For instance, Bcl-2 directly binds to GABARAP proteins (K_d 25 µM) with an atypical LIR motif (EWD) in which W is protruding into the large hydrophobic pocket HP1 while HP2 is unoccupied[132]. *In silico* docking experiments revealed that the complex is stabilized by several hydrogen bonds and salt bridges. Furthermore, another similar "half LIR" motif (DWE) is projected from the α-helical coiled coil region of TRIM5α, which interacts with both LC3B and GABARAPL1 proteins with a high K_d of about 100 µM and 78 µM, respectively[133]. A crystal structure of the Trim5α coiled-coil region bound to LC3B revealed that W^{196} in the core LIR motif sits deeply in the HP1 pocket (Fig 1.5A). While the HP2 pocket is not filled due to the absence of the hydrophobic residue at position X_3. Substitutions of the adjacent acidic residues reduced or abolished LC3/GABARAP interaction of Trim5α, which provides crucial insight into the contribution of the general electrostatic interactions to LIR binding strength.

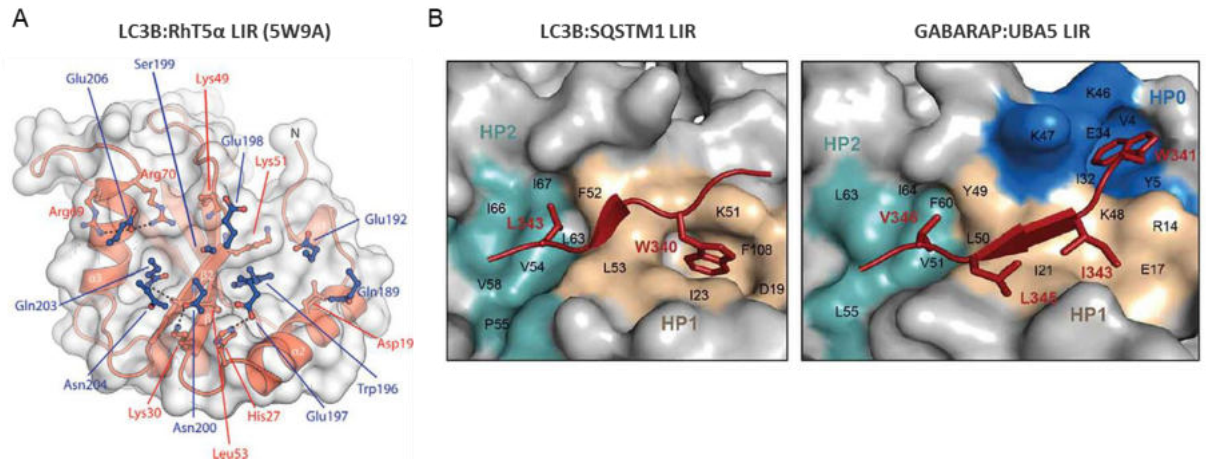

Figure 1.5 Interactions mediated by atypical LIR motifs. **(A)** A fold out of the LC3B:RhT5α (5W9A) interaction is shown (RhT5α in blue and LC3B in red). Trp^{196} of Trim5α occupies HP1 of LC3B. **(B)** Comparison of the typical (LC3B:SQSTM1, 2ZJD) and atypical (GABARAP:UBA5, 6HB9) binding mechanisms. The images were adapted from[133, 134]

In addition to the atypical LIR motifs occupying only one of the two hydrophobic pockets in the LDS, a third and novel binding mode has been revealed in the structure of UBA5 (ubiquitin like modifier activating enzyme 5) binding to GABARAP protein[134]. In this motif, WGIELV, Ile and Val residues were shown to occupy HP1 and HP2 pockets, like a canonical

LIR. However, the conserved Trp at X_{-2} position causes structural rearrangements in the side chains of key GABARAPs residues which creates a new hydrophobic pocket (called HP0) and a suitable docking surface for Trp residue of UBA5 LIR (Fig 1.5). Structural studies (X-ray crystallography and NMR), a peptide array assays, and swapping mutations have shown that W_{-2} binding to HP0 is crucial for the binding of the core UBA5 LIR motif to GABARAP proteins. The conformational changes on the side chain geometry and subsequent formation of HP0 pocket is so far unique to UBA5-GABARAP/L1 interaction.

1.2.2.4. Ubiquitin docking site (UDS)

In parallel, the studies of alternative binding sites on the LC3/GABARAP surfaces led to the identification of an alternative (LIR-LDS independent) binding mode: an evolutionary conserved hydrophobic patch called UDS. The UDS pocket lies on the opposite surface of LDS pocket (Fig 1.4D). This pocket allows binding of LC3/GABARAP to amphiphilic α-helical ubiquitin-interacting motif (UIM) with an affinity in the lower micromolar range[135]. The UIM form an about 20-amino-acid-long and fold into amphipathic α helix that binds to the hydrophobic I^{44} patch of ubiquitin. The conceptually new mechanism of UDS-UIM was tested using 28 UIM-containing proteins, and only 6 of them (EPN1, EPN2, EPN3, Rabenosyn, ATXN3, and ATXN3L) bound to LC3/GABARAP subfamilies, showing that only a subset of UIM-containing proteins may bind ATG8 proteins[136]. Even though it is too early to approach UIM as a predictive sequence for LC3/GABARAP binding, structural studies of UIM-UDS docking are needed to reveal the mode of binding. Besides that, UIM-like α-helical substructures might be found to interact with LC3/GABARAP proteins in an UDS-dependent way. Thus, future studies focusing on UDS-mediated interactions of LC3/GABARAP proteins will help characterize this binding mode and lead to identification of new SARs, adaptors, and scaffolding proteins.

1.2.2.5. FIP200 interacting region (FIR) motif

FIP200 (homologue of yeast Atg17) is a subunit of the ULK1 complex in more complex eukaryotes, which is indispensable for initiation of autophagy under stress conditions. However, the ULK1 complex participates in selective autophagy regardless of stress conditions[16]. FIP200 plays important roles in the recruitment of the autophagy machinery on protein condensates or ERphagy sites[79]. Specifically, the FIP200 Claw domain (RB1CC1 Claw) was shown to recognize a short FIP200-interacting region (FIR) in TBK1-binding adaptors(NAP1 and SINTBAD), the ER-resident autophagy receptor CCPG1, core autophagy

protein ATG16L1, and the cytosolic autophagy receptors p62 and NDP52[59, 137-140] (Fig 1.6). Even though there is not a well-defined consensus FIR motif, a sequence alignment analysis of the currently known FIP200-binding regions revealed a consensus core sequence reminiscent of the LIR motif with two extra acidic residues at the N-terminus[141]. Furthermore, recent studies showed that p62 and CCPG1 can directly bind to the Claw domain of FIP200 through their FIR motifs; this recruits the ULK complex and induces phagophore formation *in situ* [141]. Of note, FIR-mediated binding of autophagy receptors to the FIP200 Claw domain is reported to comprise a phosphoregulatable binding mode, as phoshomimetic mutations increased its binding affinity[138, 141]. Overall, these results imply that FIR-mediated molecular assembly of autophagy machinery at the cargo might be independent of LC3/GABARAP proteins. FIR-motif dependent assembly may facilitate the formation and maturation of autophagosomes even in the absence of LC3/GABARAP proteins. However, due to the lack of related complex structures and mechanistic explanation of FIR-mediated interactions, it is presently difficult to ascertain its true role in selective autophagy. Nonetheless, FIR motifs open a new field for exploration of autophagy regulation and new FIP200 interactors.

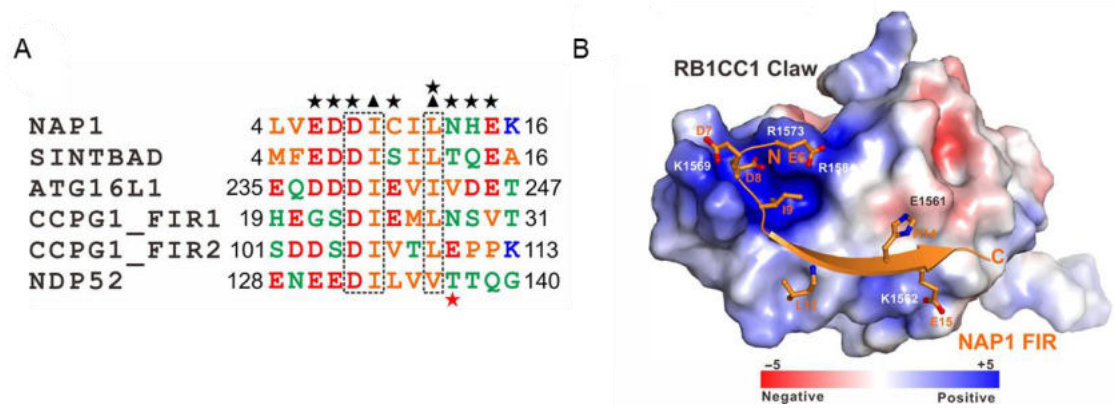

Figure 1.6 Sequence alignment of FIR motifs, and structural analyses of the interactions of RB1CC1 Claw with NAP1 FIR. **(A)** Sequence alignment analyses of the FIR motifs (NAP1, SINTBAD, ATG16L1, and CCPG1 and the LIR region of NDP52). In this alignment, the highly conserved residues are boxed, and the residues involved in NAP1:RB1CC1 Claw are highlighted with black stars (polar interactions) and black triangles (hydrophobic interactions). **(B)** Surface charge potential representation and between RB1CC1 Claw surface and NAP1 FIR (ribbon-stick model). The images were adapted from[140].

1.3. *In vitro* platforms for identification of autophagy receptor and cargo

Autophagy plays pivotal roles in many human diseases, including cancer and neurodegenerative disorders. Thus, it is naturally of interest to decipher underlying molecular mechanisms of autophagy and autophagy cargo molecules as well as to identify small

molecules regulating autophagy for their exploitation as therapeutics. The success of genetic approaches to map *Atg* genes in *Saccharomyces cerevisiae* has encouraged genetic screening studies in mammalian cells to reveal proteins involved in autophagy regulation[142]. Many alternative approaches for loss-of-function screens in mammalian cells have been used to pinpoint the genes regulating autophagic activity. Initially, several arrayed RNAi high content screens and 'pooled' short hairpin (sh)RNA screens were employed to discover new regulators of LC3, p62, and selective autophagy substrates[143-147]. Later, introduction of the clustered regularly interspaced short palindromic repeats (CRISPR)-mediated gene knockout technology became a more robust approach to interrogate proteins involved in autophagy, as it confers lower false negative/positive rates compared with RNAi and shRNA approaches[148]. For instance, CRISPR-mediated screens exerted new mechanistic understanding for the regulation of LC3, p62, NDP52, NBR1, TAX1BP1, and PARKIN[149-151]. Moreover, many high-throughput screening platforms were developed for the genetic screening of autophagy regulators or the identification of autophagy-regulating small molecule compounds[152]. The commonly used autophagy reporters in screening platforms are either based on the autophagy marker LC3 (GFP-LC3, mCherry-GFP-LC3, GFP-LC3-RFP-LC3ΔG), selective autophagy receptor p62 (GFP-p62, mCherry-GFP-p62, p62-fLuc), or autophagy substrates (EGFP-HD^{Q74}, HA-α-syn(A53T))[153]. In the same context, clearance of dysregulated mitochondria is also assessed as a key interest to identify mitophagy regulators. This allowed the development of fluorescence-based imaging methods to measure *in vitro* and *in vivo* mitophagy using pH-sensitive mitochondrial proteins, such as mt-Keima and mito-QC (mCherry-GFP-FIS$^{1101-152}$)[154, 155]. In the genetic screens, candidate genes whose loss of function deregulates the autophagic flux in one of these platforms are considered as autophagy regulators. Data arising from primary genetic screens can be further evaluated and characterized using stringent secondary autophagy assays including immunofluorescence, immunoblotting, or electron microscopy.

1.3.1. Identification of selective autophagy receptors

In addition to genetic screening studies, modern bioinformatics can also predict autophagy-associated proteins using autophagy-specific motifs, such as LIR motif. A web-based tool, iLIR, is designed to forecast whether a protein carries a potential functional LIR motif based on its amino acid sequence[156]. While iLIR-based searches can predict LIRs and hence LIR-containing proteins, the findings require experimental validation. Also, LC3/GABARAP interactions facilitated by atypical LIR motifs or the UDS domain cannot be

assessed by using the iLIR tool so far. Therefore, unbiased interaction assays such as yeast-two-hybrid (Y2H) assay, GST pulldown, and peptide array assays can be applied to either discover or validate LC3/GABARAP interactors. The Y2H assay is a powerful tool to identify LC3/GABARAP interactors by exploiting the modular nature of the yeast Gal4 transcription factor[105]. In this assay, a physical interaction between two proteins fused to either the DNA binding or activation domain of Gal4, respectively, is scored by transcription of a reporter gene. This system has been successfully applied to identify many LC3/GABARAP interactors, such as NBR1, NIX, and FAM134B[38, 44, 62]. Yet, the Y2H method requires direct interaction of two proteins in yeast cells *in vivo*, which may not perfectly represent the outcome in different species. Another limitation of the standard Y2H system is that it is unsuitable for membrane-bound proteins; it thus needs an additional strategy, e.g., the split-Ubiquitin-based Y2H method[157].

Another powerful and commonly used method to identify/validate LC3/GABARAP interactors is the affinity pulldown assays. For example, GST-tagged recombinant LC3/GABARAP proteins are used to pulldown interacting proteins in solution[105]. The target protein can be either a recombinant protein or a protein as a component of a cell lysate. The bound proteins can be analysed by immunoblotting, or the assay can be coupled with MALDI or LC-MS/MS analysis[38, 119, 158]. Following the confirmation of a protein-protein interaction, peptide array assays are a reliable method to identify binding peptide of the protein of interest, especially LIR peptides[105]. The minimal size of each found LIR motif can be determined using peptide arrays, which also make it possible to identify interaction sites in a protein of interest. Two-dimensional peptide arrays are also suitable for probing each position of the LIR with different amino acid changes. The sequential binding of LC3/GABARAP proteins to the overlapping peptides on the array is strong evidence for the presence of a LIR motif inside that sequence[105, 159]. Yet, the peptide array results should be interpreted with care due to extensive hydrophobic regions, like WD40 or KELCH repeats, where many aromatic and hydrophobic residues increase the chance of detecting false-positive interactions[159]. Therefore, peptide array results should always be verified by other interaction studies, like GST pulldown assays with introducing mutations in the putative LIR sequence of the protein of interest. To conclude, studying proteins involved in autophagy requires combination of more than one discipline at a time.

1.3.2. Proteomics insights into autophagy

Given the key functional role that proteins play in almost every aspect of cell biology, dissecting autophagy from a proteomics perspective has become a natural interest of many studies. For this purpose, proteomics based on mass spectrometry (MS) have proven to be an effective method for the proteome-wide, unbiased characterisation of autophagy. Over the last two decades, at an accelerating pace, numerous studies have been published that used proteomics to investigate autophagic machinery and cargo [160, 161]. Technical advancements in tandem mass spectrometry (MS/MS) and liquid chromatography-mass spectrometry (LC-MS) have made it possible to detect and identify proteins from complex mixtures, such as cell lysates and body fluids, with high throughput and high sensitivity. Advancements in chemical-labelling and detection techniques also conferred additional specificity and versatility to the process. Beyond qualitative analysis, comparative quantitative studies facilitated investigation of global proteome changes, post-translational modifications, spatio-temporal protein dynamics, enzyme activity and protein-protein interactions in autophagy[160]. These studies show great variations in terms of technical implementations (e.g., on-label vs. label-free, instrumentation, sample processing, and quantification) and can be conceptually subdivided into main three experimental approaches.

In the first approach, changes in the total cellular proteome are examined by proteomics in the setting of genetic or pharmacological modulation of autophagy. To cite some examples, a SILAC (stable isotope labelling by amino acids)-based proteomics approach has been used to examine global protein dynamics during amino acid starvation-induced autophagy at different time periods[162]. Analysis of recorded proteins revealed an orderly processing of substrates during amino acid starvation-induced autophagy: i.e., cytosolic proteins were degraded rapidly, followed by mitochondria and other organellar proteins. Thus, starvation-induced autophagy appears to degrade proteins in a selective and ordered fashion, in contrast to the anticipated non-selective bulk degradation[162]. Another study has been conducted to identify upregulated and downregulated proteins in Atg7-/- MEFs compared to WT cells[163]. The results led to identification of F-actin as an active autophagy regulator in both basal and starvation-induced autophagy. This kind of comparative whole-cell analysis delivers a general picture of how autophagy affects cellular proteostasis. Nevertheless, the whole-cell proteomics studies do not distinguish between proteins that are selectively targeted by autophagy and proteins whose expression is affected independently of autophagy.

In the second approach, composition of autophagosomes or autolysosomes are more selectively subjected to proteomics analysis using biochemical fractionation, affinity purification, and proximity labelling methods. These approaches can identify autophagy-specific substrates/regulators and can provide insights into cellular functions of autophagy. As an example, Behrends and colleagues carried out an extensive proteomics analysis of the autophagy interaction landscape under basal conditions[164]. In this study, 32 human autophagy proteins were overexpressed in HEK293 cells and used as a prey in immuno-precipitations to reveal their interaction network via MS. Hierarchical clustering of the interactions revealed total of 751 interactions among 409 candidate interacting proteins showing extensive sub-network connectivity. Later, the study focussed on LC3/GABARAP interaction partners, and 34 of them were tested via *in vitro* GST-pulldown assays for their binding to WT or LDS mutant LC3B and GABARAP proteins. In total, up to 60% of proteins tested showed reduced or no biding to LDS-mutant LC3B (F52A/L53A) and GABARAP (Y49A/L50A) proteins, indicating that the majority of LC3/GABARAP-interacting proteins employs the LDS/LIR interaction for assembly. Many other studies have been done in which proteins from LC3/GABARAP immunoprecipitates and GST pulldowns were subjected to MS analysis to identify functional elements of the autophagy network[65, 119, 158, 164, 165].

In addition, proximity-proteomics-based strategies have been employed to examine the interaction network of autophagy proteins. Behrends and colleagues used genetically engineered APEX2 fused with LC3/GABARAP proteins to label and capture the contents of autophagosomes in living cells[166]. This is a chemical labelling approach enabling biotinylation of the proteins in close proximity with LC3/GABARAP proteins and subsequent purification of the autophagosome protein inventory using streptavidin resin. By combining this strategy with MS-based proteomics, 1,147 potential autophagosomal substrate proteins were identified with considerable overlap across LC3/GABARAP subfamily proteins. This approach also led to the identification of a novel Parkin-independent mechanism for mitophagy in which the mitochondrial protein MTX1 is targeted in an LC3C- and p62-dependent manner. The Behrends's group used the same strategy to address the contribution of each of the selective autophagy receptor to protein turnover by selective autophagy under basal and proteostasis-disturbing conditions[167]. They fused APEX2 with p62, NBR1, NDP52, OPTN, TAX1BP1, and TOLLIP separately, and screened for autophagy cargo molecules. Overall, this study led to identification of *bona fide* autophagy cargo molecules, and implication of the aggrephagy receptor TOLLIP, which is implicated in endosomal microautophagy. Many other studies have

employed proximity labelling with quantitative proteomics to systematically map autophagy-related proteins[64, 168-171]. Even though these approaches provide more specific insights into autophagy compared to whole-cell proteomics studies, the involvement of autophagy proteins, labelled with APEX2 or used as a bait, in other non-autophagy pathways gives rise to many false-positive results.

Proteins associated with autophagosomes were also identified from isolated autophagosomes (Table 2). Several protocols for isolation of autophagosomes have been published[172-176]. They typically involve use of density gradients or, alternatively, immunoprecipitations using GFP-LC3 anchored in the autophagic membranes. Special treatments, such as vinblastine to block microtubular movement and thus fusion between the autophagosomes and the lysosomes can be an additional modification to the protocols aiming to enrich the autophagosomal fraction. Early purification studies aimed to analyse lipid content and morphologicalal features of autophagosomes isolated from the rat liver using a density gradient[175-177]. Later, protocols established in the early studies were used in many other laboratories for various purposes[172, 178-180]. In 2010, autophagosomes and lysosomes isolated *in vitro* or *in vivo* were used to establish an *in vitro* fusion assay[181]. This study revealed that altered lipid content of autophagosomes and lysosomes inhibits autolysosomal fusion. Another study showed that autophagosome enriched fractions from a density gradient activate dendritic cells, suggesting an involvement of autophagy in cross-presentation[182]. Furthermore, Dengjel and colleagues used a label-free proteomics to analyse biochemically fractionated or immune-isolated autophagosomes from GFP-LC3-expressing MCF7 breast cancer cells subjected to amino acid starvation or treatment with the mTOR activator rapamycin or the lysosomal inhibitor concanamycin A[172]. A total of 728 putative autophagosome-associated proteins were identified in this study, however only 94 of the proteins were common to all stimuli, and a few of them had previously been identified in other autophagosome-proteomics studies[174, 183]. The possible explanation for the poor overlap between these studies might be due to the differences in cell types, stimuli, and methods used for purification and MS analysis. In another study, proteomics analysis of density gradient or immune-isolated autophagosomes from GFP-LC3 expressing pancreatic cancer cell lines led to identification of the NCOA4 protein as a ferritinophagy receptor that regulate intracellular iron homeostasis by recruiting ferritin for autophagic degradation[65]. Overall, the density gradient and immune isolation methods provide a holistic picture of proteins residing inside and outside the autophagosomes. However, it should be noted that density gradient separation methods can only provide an enrichment of

autophagosomes in certain fractions, which still includes many other organellar pieces and protein complexes. In addition, proteomics analysis of LC3 protein-based immune isolations should be interpreted cautiously due to involvement of LC3 proteins in the ER and Golgi compartments. In this regard, a combinatorial approach (density + immune isolation) might help reducing unwanted impurities in the final autophagosome fraction. Recently, Kim et.al., and colleagues combined membrane flotation and affinity isolation approaches for the purification of autophagosomes from GFP-LC3-expressing cells that harbour a Hepatitis C Virus (HCV) subgenomic RNA replicon[184]. In this approach, the autophagosome-enriched fractions from density-gradient separation were subjected to immune isolation using anti-GFP resin. Later, proteomics analysis of these autophagosomes revealed that HCV-induced autophagy directs lipid raft proteins caveolin-1, caveolin-2, and annexin A2 to autophagosomes. Of note, in Kim's study, the complete list of proteins that were identified in proteomics included only 132 proteins without any known autophagy substrate or regulator proteins. The reason for the low yield of total proteins identified and absence of autophagy proteins might be due to interference of large HCV-induced lipid rafts with the immune isolation step as they might destabilize the membrane structure of autophagosomes that results in loss of autophagosome content. Also, the study did not use any lysosomal blockers to enrich autophagosomes in the cells, which might be another reason for the low yield in the proteomics. Consequently, this combinatorial approach might help isolating pure autophagosomes, but still needs to be improved.

Table 2: *List of autophagosome purification studies*

Method	*Source*	*Material*	*Autophagy stimulation*	*Proteomics technique*	*Outcome*	*Ref*
Density-gradient	Mouse liver and mouse fibroblasts (NIH3T3)	Metrizamide	High-fat diet or starvation	-	In vitro autophagosome-lysosome fusion assay revealed that altered lipid contents of autophagosomes inhibits fusion.	[181]
	HeLa cells	Metrizamide and Nycodenz	-	-	Htt103Q inclusion were visualized in the autophagosomes	[185]
	Rat liver	Metrizamide	Vinblastine sulphate	-	Phospholipids are degraded more slowly than proteins	[176]
	Rat liver	Nycodenz, percoll, iodixanol, sucrose	Vinblastine sulphate	-	Amphisomes (autophagosome/endome fusion) seem to be capable of receiving	[183]

					inputs both from early and late endosomes	
	Saccharomyces cerevisiae	Optiprep (iodixanol)	Starvation	Label-free LC-MS/MS	Pfk1/2 complex, a key enzyme of glycolysis, was selectively transported vacuole by autophagy	[186]
Immune isolation	661W cells and mouse retina	Anti-GFP µMACS™ microbeads	Starvation, Baf A_1 or CQ	-	The visual transduction proteins transducin and ARR/arrestin are associated with autophagosome-specific proteins	[187]
	Retina, lung, liver and brain tissues from GFP-*Lc3b* mice	Anti-GFP µMACS™ microbeads	Starvation and Leupeptin	-	An immune isolation method from mice tissue were established	[188]
Density-gradient and immune isolation	MCF7, PANC1 and 8988T	Nycodenz and anti-GFP µMACS™ microbeads	Wortmannin and CQ	SILAC LC-MS/MS	Identification of NCOA4 as a Ferritinophagy receptor	[65]
	HEK293T cells	Percoll and anti-GFP coupled Dynabeads	NH_4Cl	-	Purified autophagosomes were found to be efficient antigen carriers for cross-presentation	[182]
	MCF7	Iodixanol and Anti-GFP µMACS™ microbeads	Starvation or Concanamycin A	SILAC LC-MS/MS	Autophagosome composition is influenced by the nature and timing of the stress stimulus	[172]
	HeLa	Optiprep and Anti-FLAG magnetic beads	-	-	STX17 overexpression inhibits the fusion between autophagosomes and lysosomes	[189]
Density gradient followed by immune isolation	Huh7 hepatoma and GLR glial cells	Sucrose and anti-GFP monoclonal antibody-conjugated magnetic beads (MBL)	-	Label-free LC-MS/MS	HCV polyprotein, Annexin A2, Caveolin-1, Caveolin-2 proteins were associated with autophagosomes	[184]

In the third approach, proteomics is applied to measure autophagic flux in a quantitative or semi-quantitative manner. In this approach, the cellular autophagic activity and changes in the composition of the autophagy substrate are examined simultaneously using proteomics. For example, SILAC was employed to carry out a pulse-chase experiment in human fibroblasts to calculate protein half-lives under basal conditions[190]. Comparison of autophagy-incompetent cells (bearing *ATG5* or *ATG7* deletion) with wild-type cells enabled the calculation of

autophagy-mediated degradation rates of hundreds of proteins simultaneously. Another study used a label-free approach to study circadian variations in autophagic flux in mouse liver[191].

To conclude, the sensitivity of proteomics techniques and labelling methods was greatly improved in the last two decades which favoured its use in many autophagy studies. However, the results showed that the autophagy studies still need to be improved in terms of yield and purity of samples submitted for proteomics analysis. This can be overcome by analysing pure autophagosome fractions rather than whole-cell homogenates. Further improvements in the autophagosome isolation techniques will provide more reliable and reproducible results.

1.4. Alternative and non-canonical autophagy

Autophagosome formation is a complex and multi-step process in which the hierarchical recruitment of ATG proteins seal the fate of cargo molecules destined for the lysosomal degradation. Even though the core mechanism of the autophagy is well-defined, autophagy researchers must be aware of two issues colouring outside the lines of canonical autophagy, named as alternative autophagy and non-canonical autophagy.

1.4.1. Alternative autophagy

Initially, analysis of *ATG* gene knockout studies revealed an essential and unique role for each *ATG* gene in the regulation of the autophagic machinery, as well as in the autophagic flux in the cells. Although more than 30 *ATG* genes have been identified so far, some genes silenced more commonly by the researchers to stop autophagic degradation in the cells, e.g., Beclin1, ULK1, FIP200 in the initiation complex and ATG4, ATG5, ATG7, LC3/GABARAP proteins in the lipidation complex. However, these studies led to discovery of the fact that autophagosomes can also be formed by using only a subset of ATGs, which is called alternative autophagy[192]. Several lines of evidence confirmed the existence of alternative autophagy in cells that lack ATG proteins: (1) lysosomal proteins containing autophagosomes (autolysosomes) were observed under fluorescent or electron microscopy assays, (2) lysosomal inhibitors (e.g., Baf A_1) increased the number of autophagosomes and decreased autolysosomal proteolysis.

The ULK1/2 kinase complex is the apical complex that initiates the autophagy cascade. However, mouse embryonic fibroblasts (MEFs) that lack ULK1/2 proteins still underwent hypoxia- or ammonia-induced autophagy[193, 194]. Similarly, knocking out two other components of ULK complex, ATG13, or FIP200, did not block the hypoxia-induced formation of

autophagosomes, suggesting ULK complex-independent mechanism for autophagy induction under certain stress conditions[194]. In line with these observations, Coxsackievirus and Poliovirus infections were found to reduce levels of ULK complex proteins, whilst increasing the autophagy signalling[195, 196]. This viral hijacking of the ULK complex can be used to investigate the ULK-independent induction of autophagy. On the other hand, members of VPS34 complex responsible for PI3P production on the autophagosome membrane were also found to be dispensible for autophagy under certain circumstances. For example, Beclin1-independent autophagosome formation and autophagy-mediated protein degradation has been reported in various cells under certain stressors, such as pro-apoptotic compounds (neurotoxin 1-methyl-4-phenylpyridinium, resveratrol, Z18, MK801)[197-199]. Furthermore, some recent studies suggest that autophagy can be independent of Vps34 in that *Vps34−/−* sensory neurons and T-lymphocytes showed autophagosome formation and LC3-II production[200]. In addition, under sheer stress (i.e., mechanical force induced by the friction of liquid against the cell membrane), absence of *VPS34* can be compensated for by the activity of another enzyme responsible for PI3P synthesis, PI3KC2α[201].

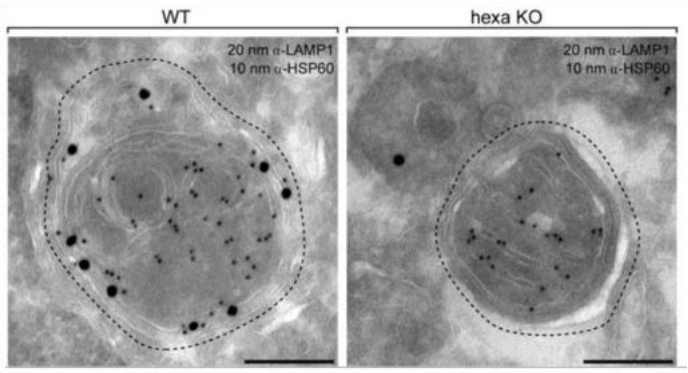

Figure 1.7 LC3/GABARAP proteins are dispensable for autophagosome formation, but essential for lysosomal fusion. Representative immunogold TEM images of WT and LC3/GABARAP family KO cells (Hexa KO), double labelled for LAMP1 (20 nm gold) and HSP60 (10 nm gold) (compartment perimeters indicated by offset dashed line) shows smaller autophagosomes. Absence of bigger dots (LAMP1) inside the autophagosome on the left panel (Hexa KO cells) suggest that LC3/GABARAP proteins are required for lysosomal fusion. The image was adapted from[202].

Lipidation of LC3/GABARAP proteins on the autophagosome membrane is generally considered to be a good indicator of autophagy. However, it does not occur during the ATG5/ATG7-independent, alternative process of autophagy[203]. The presence of phagophores and autophagosomes was confirmed in various *Atg5−/−* and /or *Atg7−/−* cells[203-205]. Indeed, they generated smaller autophagosomes, albeit at a drastically reduced rate compared to WT cells. Unlike conventional autophagy, the autophagosomes in *ATG5*-depleted cells seemed to

be Rab9-dependent and formed by the fusion of phagophore membranes with vesicles derived from the trans-Golgi and late endosomes[206]. Similarly, ATG7- and ATG3-deficient HeLa cells could form Syntaxin 17-positive autophagosomes, which could be explained by delayed degradation of the inner autophagosomal membrane[205]. The purported critical role of ATG5 and ATG7 proteins in autophagosome formation was challenged in a range of cells including fibroblasts, pancreatic β-cells, and as well as in various cancer cell lines, such as prostate DU145, erythroleukemia K562 cells, adenocarcinoma H1650 cells, and lung carcinoma A549 cells[203, 207-211]. Of interest, also lack of LC3/GABARAPs was shown to still be compatible with generation of autophagic vacuoles under some conditions (Fig 1.7). Similar to ATG5/7-deficiency, loss of all LC3/GABARAP family proteins yields smaller autophagosomes forming at a lower rate in HeLa cells[202]. However, the autophagosome–lysosome fusion was defective in these HeLa cells. Reconstitution experiments also identified GABARAP subfamily members as primary contributors of autophagosome–lysosome fusion in PINK1/Parkin-mediated mitophagy and starvation-induced autophagy[202].

In conclusion, a considerable body of evidence suggests that an alternative process of autophagy occurs even in the absence of some of core ATG machinery[192]. As it is a relatively new area of research, the current knowledge about the biological roles of alternative autophagy is limited, and its elucidation may help expand the role of autophagy in various illnesses including neurogenerative, metabolic, and neoplastic diseases. This may lead to the design of new and more effective autophagy targeting drugs.

1.4.2. Autophagy-independent roles of ATG proteins

Components of the autophagic machinery were also found to participate in cellular reprogramming that does not involve delivery of cytosolic constituents to lysosomes. Such non-canonical functions of the *ATG* genes comprise various cellular processes[212, 213]. The non-autophagic roles of ATG proteins draw attention to the fact that some of the metabolic outcomes of autophagy research might be independent of the main function of autophagic degradation machinery (Table 3).

LC3/GABARAP proteins play crucial roles outside autophagy: e.g., coordination of cellular membrane trafficking events; AKAP-Lbc-mediated actin cytoskeleton remodelling; regulation of viral replication such as Coronaviruses (CoVs), and mouse hepatitis virus[214-216]. In addition, there are some well-defined pathways in which autophagy proteins play a central role, such as LC3-associated phagocytosis (LAP) and LC3-associated endocytosis

(LANDO)[217, 218]. During LAP and LANDO, some parts of autophagy components are used to conjugate LC3 proteins to the phagosome and endosome membranes, respectively. The LAP pathway is regulated by the activity of a PI3KC3 complex similar to VPS34 complex involved in autophagy, including VPS34, VPS15, and Beclin1, but instead of ATG14, it contains UV radiation resistance-associated gene protein (UVRAG) and Rubicon[217]. Even though Rubicon is known as a negative regulator of canonical autophagy, during LAP, it is indispensable for conjugation of LC3 to PE on the phagosomal membrane due to its involvement in PI3P generation and NOX2 association with the phagosome. Notably, the LAP pathway does not require all mechanistic components of the autophagy machinery, such as WIPI2, but strictly requires the activity of the LC3 conjugation machinery(i.e. ATG12-ATG5-ATG16L1, ATG3, and ATG7) for LAPosome formation where the engulfed extracellular cargos can be digested through the endosomal pathway[217]. Another difference from autophagosomes, is that LC3 conjugation takes place after single-membrane LAPosome formation, while it occurs in parallel with the autophagosome membrane formation. So far LAP has mainly been studied in macrophages, which helps engulfment of dead cells and several pathogens, and subsequent promotion of anti-inflammatory signals or presentation of antigens on the MHCII molecules, respectively[219]. For instance, impaired phagocytosis of dead cells in LAP-deficient mice is accompanied by an increase in proinflammatory cytokines[220]. In addition, inhibition of the LAP pathway was reported to compromise antigen presentation in human macrophages[219, 221]. Another pathway requiring LC3 conjugation is LANDO in which LC3 proteins are conjugated onto clathrin- and Rab5-positive endosomes instead of phagophores or autophagosomes[212, 218]. The conjugation process relies on BECN1, Vps34, ATG5, ATG7, and RUBCN, just like LAP. However, the loss of LC3 conjugation leads to impaired receptor recycling rather than defects in cargo sequestration. So far, the recycling of the putative Aβ receptors including TREM2, CD36, and TLR4 in microglia has been linked to LANDO[218].

Autophagy has also been proposed as a novel mechanism of unconventional secretion[222]. This pathway is used by proteins lacking leader peptide sequences and/or transmembrane domain, with IL-1β being the model substrate[223]. Secretion of IL-1β is enhanced by starvation and can be inhibited by ATG5 depletion[224, 225]. In WM793 melanoma cells, secretion of IL-1β, CXCL8, LIF, FAM3C, and DKK3 correlated with the increased autophagic activity[226]. Secretion of misfolded α-synuclein was autophagy-dependent[227]. Interestingly, autophagy was also implicated in secretion of alanine by pancreatic stellate cells required for optimal growth of pancreatic ductal adeno carcinoma (PDAC) tumours *in vivo*[228]. Of interest, a novel

unconventional secretion pathway was recently published[229]. During the so-called misfolding-associated protein secretion, the ER-associated deubiquitylase USP19 deubiquitylates the cargo and assist in its encapsulation into ER-associated late endosomes, which secrete misfolded proteins to the exterior of the cells. As this process was LC3-independent and not modulated by starvation, the role of autophagy was ruled out[229]. Further work (e.g., using CRISPR/Cas9 *ATG* gene knockout) is required to confirm (the lack of) the connection between autophagy and this secretion pathway.

Table 3: *Non-autophagic roles of autophagy proteins*

ATG proteins	**Non-autophagic role**	**Ref**
LC3/GABARAP	Interaction with GTPases and GAPs: signalling platforms, redirection of endosomal components to autophagosomes, recruitment of autophagy regulators, replication of certain viruses	119, 120, 214, 230, 231
ATG5 or ATG12–ATG5	Regulation of siRNA-generated type I IFN production through interactions with RIG1 and MDA5, calpain-cleaved ATG5-mediated activation of apoptosis, IFNγ-mediated host defense against murine norovirus replication	232, 233
Atg16L	Hormone secretion in PC12 neuroendocrine cells and granule exocytosis in intestinal Paneth cells	234-236
Atg5, Atg7, Atg4B and LC3	Required for cathepsin K secretion in bone osteoclasts, and needed for adipogenesis in mice	237
Atg4, beclin 1	Their caspase-mediate cleavage suppresses autophagy and induces apoptosis	238-240

1.5. Autophagy-modulating compounds

The use of autophagy for therapeutic purposes has been discussed concurrently with the analysis of its various functions in human diseases. A strong push to the investment in drug discovery in the autophagy field came from awarding the Nobel Prize in Physiology or Medicine to Yoshinori Ohsumi in 2016 for his discovery of mechanisms for autophagy. Early compounds with abilities to modulate autophagy were found by serendipity, such as mTOR inhibitors (e.g., rapamycin) or lysosomal inhibitors (e.g., CQ). Below, several of these compounds targeting autophagy will be discussed.

1.5.1. Autophagy activators

MTOR, a serine/threonine kinase, is a well-known regulator of cell metabolism and autophagy [19]. Inhibition of the growth factor signalling pathway PI3K/Akt/TSC/mTOR signalling and activation of the ATP-depletion-activated AMPK, lead to inhibition of mTOR which induces autophagy by enhancing the kinase activity of ULK1 [19]. To date, a plethora of small-molecule activators of autophagy acting via different mechanisms have been reported (reviewed by Kocak et al.). Some of them include rapamycin and rapalogs (e.g., temsirolimus, everolimus) which are amongst the most potent autophagy enhancers. They stabilize the association of mTOR with regulatory-associated protein of mTOR (Raptor), thus inhibiting mTOR activity [241]. Inactivation of mTOR can also be achieved with selective ATP-competitive inhibitors torin1 and dactolisib, or AMPK activators, such as metformin, trehalose or resveratrol, which trigger AMPK-dependent mTOR inhibition [241]. In addition, many studies suggest that the ubiquitous intracellular messenger calcium (Ca^{2+}) has a rather complicated and controversial modulatory impact on autophagy [242]. Nevertheless, several Ca^{2+} antagonist (e.g., fluspirilene, verapamil, nicardipine) were reported to induce autophagic flux in cells by various mechanisms. In addition, different lipid species (e.g. sphingolipids, sterols, and phospholipids) play important roles in the various steps of autophagosome membrane formation [243]. In particular, accumulating evidence suggests that activation of phosphoinositol signalling pathways increases the levels of free inositol and myo-inositol-1,4,5-triphosphate levels, which in turn negatively regulates autophagy [244]. Lithium, which interferes with the phosphoinositol cycle, leads to depletion of free inositol, and thereby enhances autophagosome formation in the cells [245]. However, none of these compounds are selective autophagy activators because they also interfere with many other metabolic processes. To date, the closest candidate designed as a specific autophagy activator is TAT-beclin peptides. These cell-penetrating peptides induce autophagy by interacting with the autophagy suppressor proteins GAPR-1/GLIPR2. These proteins are Golgi-localized, and under basal conditions, they bind to the Beclin1 proteins and block their movement across the cytosol to participate in autophagosome formation. TAT-beclin peptides mimic the binding groove of Beclin1 protein (residues 267-284) to GAPR-1/GLIPR2 proteins, release Beclin1 and induce autophagy.

1.5.2. Autophagy inhibitors

Over the past decades, chemotherapy- as well as radiotherapy-induced autophagy emerged as a pro-oncogenic factor contributing to malignant progression and drug resistance

of cancer [246]. Therefore, studies on autophagy inhibition have drawn considerable interest as a potential new strategy for cancer therapy. Several attractive druggable key nodes exists to modulate autophagy. However, only a few inhibitory compounds that can directly target the autophagy machinery have been identified so far and are discussed below.

Lysosomal lumen alkalizers are molecules that inhibit autophagy in the later steps of the process, when lysosomal fusion facilitates degradation of the autophagosome content. They act by neutralizing the acidic pH in the lumen of lysosomal vesicles, which is required for the activities of lysosomal hydrolases involved in autophagic degradation. Thus, alkylation of lysosomal vesicles leads to the accumulation of autophagosomes by blocking lysosomal degradation [247]. Two main examples of lysosomal lumen alkalizers are CQ and HCQ, which are drugs used for the treatment of various diseases, such as malaria and, more recently, cancer [248]. They are the first and only autophagy inhibitors approved for clinical use so far. Although short-term CQ/HCQ treatment has been considered safe, some toxicity, such as retinopathy and cardiotoxicity, has been reported depending on dosage and duration of exposure [249]. In addition, some autophagy-independent activities of these agents have been reported. HCQ-treated mice show an autophagy-independent severe disorganization of the Golgi and endo-lysosomal systems in renal and intestinal tissues [28]. On the other hand, HCQ has been reported to activate lysosome-initiated cell death by causing release of cathepsins from lysosomes [250]. Recent reports raised a major concern that CQ/HCQ-mediated sensitization of cancer cells to anti-cancer drugs might be due to autophagy-independent toxicity in the cells[251-253]. For example, Thorburn *et al*. showed that CQ sensitized cancer cells against anti-cancer drugs even in the absence of Atg12, whereas the same sensitization was not mimicked by Atg12 and Beclin1 knockdown or another lysosome inhibitor, Baf A_1 [254]. These toxicity-associated and autophagy-independent issues of CQ/HCQ have led to development of other lysosomal inhibitors, such as: CQ-derivates Lys01 and Lys05, HCQ and lucanthone derivative ROC325, [255], the ionophore monensin [256], the antibiotic azithromycin [257], the V-ATPase inhibitor Baf A_1 [258], as well as lysosomal protease inhibitors E64D, Pepstatin A, and leupeptin [259]. However, these compounds have not yet reached clinical trials yet due to issues including low solubility, high toxicity or lack of knowledge about their mechanism.

In addition to lysosomal alkalizers, a plethora of small molecules interfering with the autophagosome biogenesis have been discovered, and their mechanism of action and clinical status are listed and reviewed by Kocak *et al.* in detail[260]. Some of these inhibitors include compounds that target components of the core autophagy machinery proteins, such as the

ULK1 (SBI-0206965 and MRT68921) and PIK3C3 kinases (3-methyladenine (3-MA), wortmannin and LY294002, SAR405, VPS34-IN1, SB02024), as well as the enzymes involved in LC3/GABARAP–PE conjugation pathway, the ATG4 proteases (NSC185058), and the E1-like enzyme ATG7 (derivatives of pyrazolopyrimidine sulfamates). However, these drugs produce many other autophagy-independent activities and severe cytotoxicity.

To conclude, a number of compounds modifying autophagy were discovered so far. For many of those compounds, efficacy has been demonstrated using *in vivo* models. However, many of the compounds identified *in vitro* did not reach clinical testing because they failed to predict their specificity or showed detrimental toxicities. Moreover, one of the main issues encountered in clinical application of autophagy modulators is the unintended consequences on patients, that affecting other biological functions[260]. The ultimate goal of drug discovery programs in this context is to find the right therapeutic index and an autophagy-specific druggable node to minimise unacceptable side-effects.

1.5.3. Rational drug design approaches and LIR peptides

Selective autophagy offers the potential to control the quantity of numerous signalling proteins. Therefore, exploitation of the LC3/GABARAP interaction with cargo molecules could represent an entry point for drug desing. Several studies demonstrated that engineered LIR peptides or small molecules harnessing affinities to the LC3/GABARAP proteins higher than naturally occurring LIRs, could lead to effective inhibition of selective autophagy of the cell. Identification of ultra-high-affinity LIR peptides (K_d: 2-20 nM) derived from ankyrins have recently been used to disrupt selective autophagy in *C. elegans*, causing accumulation of the SQST-1 (p62 homolog), delayed development and shortened life span[261]. This provides an *in vivo* proof of principle for the LIR peptide-based approach which can be used in some disease settings, such as some forms of cancer, to block autophagy could lead to cell death. Similar studies have been done by using synthetic cyclic peptides derived from AnkB LIR. The cyclic peptides showed high affinity against GABARAP and strong antiproliferative effects against prostatic adenocarcinoma PC-3 cells[262]. Likewise, macrocyclic peptides targeting the autophagy protein LC3A and LC3B, inhibited autophagy in mouse models of metastatic ovarian cancer and increased sensitivity to chemotherapy agent carboplatin[263]. Another example of autophagy inhibiting peptides comes from structure-based design of stapled peptides that bind GABARAP family proteins with nanomolar affinities[264]. These peptides displayed remarkable cytosolic penetration as well as resistance to biological degradation.

They reduced autophagic flux in ovarian cancer cells and sensitized them towards cisplatin, which may justify their development as novel cancer therapeutics. These peptide-derived approaches can be considered as a template offering rational design of new small molecules interfering with the LIR:LDS interaction in cells. Indeed, a screening study has identified a small molecule (DC-LC3in-D5) that compromises LC3B lipidation *in vitro* and in HeLa cells, leading to the deficiency in the autophagosome formation and degradation of autophagy substrates, such as p62/SQSTM1. Of note, FIR motifs can also offer an entry point for autophagy manipulation. In this regard, directing an ATG16L1-derived engineered FIR peptide to mitochondria has shown to induce clearance of mitochondria through mitophagy[265]. These experiments using a synthetic FIR peptide offers another druggable node for autophagy researchers.

Recently, targeted protein degradation (TPD) strategies have emerged as an innovative approach to target autophagy[266]. This milestone was inspired by the class of pharmacological agents called proteolysis-targeting chimeras (PROTACs). In the PROTAC approach, there are two covalently linked protein-binding molecules: one binds to E3 ubiquitin ligases and the other binds to the target protein [267] (Fig 1.8). This system enables ubiquitination of targeted proteins and thereby facilitates their selective clearance by proteosomes. However, PROTAC can only target soluble proteins in a ubiquitin-dependent manner. It is not suitable for non-proteasomal targets, such as protein aggregates and damaged organelles. There, autophagy-targeted approaches come into play. For example, recently, autophagy-targeting chimeras (AUTACs) have been developed for the clearance of intracellular disease-related debris through selective autophagy[268] (Fig 1.8). Similar to PROTACs, AUTACs comprise two subunits: a guanine degradation tag that binds to autophagosomal membranes, and a warhead that can target specific intracellular components. By this way, selective autophagy mechanism relying on LIR:LDS interactions and SARs can be highjacked by small molecules, and potentially any target protein can be directed to autophagic degradation. A pioneer AUTAC study has shown to successfully target fragmented mitochondria in a Down Syndrome model and led to their clearance though autophagic degradation[269]. This proof-of-concept was further evaluated by the authors who proposed a similar concept called autophagosome-tethering compound (ATTEC)[270] (Fig 1.8). In this approach, compounds that can interact simultaneously with both LC3 and mutant HTT proteins were identified in a screening study. These compounds showed considerable success at targeting mutant HTT proteins, not native HTT proteins, to

autophagic degradation which rescued disease-relevant phenotypes in cellular and animal models of Huntington.

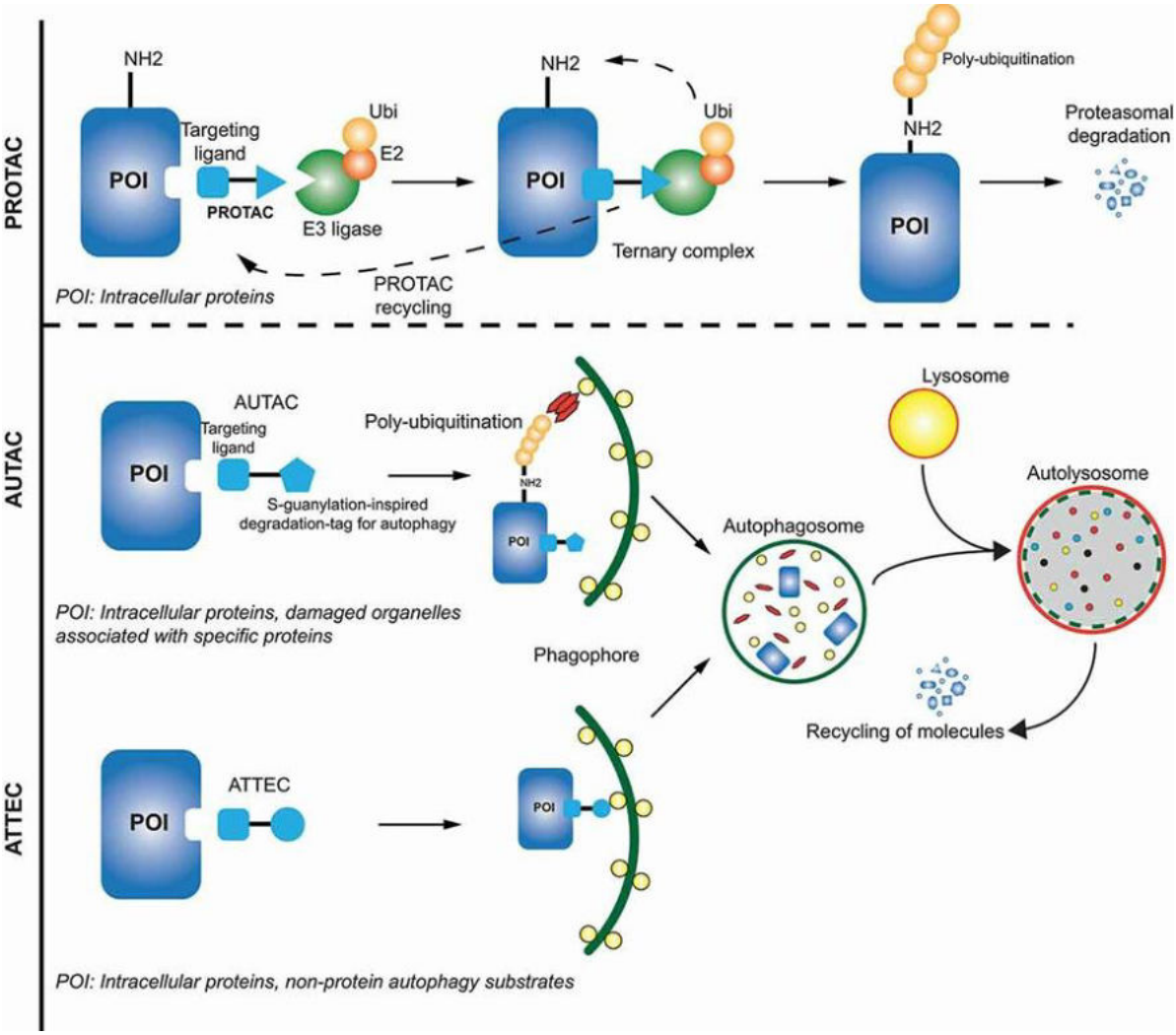

Figure 1.8 Targeted protein degradation strategies. Visual summary of current proteasome (PROTAC) and autophagosome (AUTAC and ATTEC) targeting degradation systems. Each approach is designed to deliver a protein of interest (POI) to the responsible degradation machinery. PROTAC and AUTAC systems requires ubiquitination machinery, where ATTEC does not require ubiquitination of POI. The image was adapted from[260].

In conclusion, PROTACs provide new modalities for directing proteins/organelles to autophagic degradation. The lessons learned from LIR peptide-based autophagy inhibition approaches may help develop small-molecules which can strongly and selectively bind to LDS pocket of LC3/GABARAP proteins. Later, combination of such small molecules with target-specific other small molecules may expand the landscape of applications for autophagy-mediated targeted protein degradation systems. Nevertheless, the above studies have shown a great potential of LIR:LDS interaction as a druggable node and it will spark great clinical interest.

1.6. Autophagy in human diseases

Targeting autophagy has been explored as a promising therapeutic approach due to its role in various pathologies[271]. In many studies, inducers of autophagy have been shown to clean toxic protein aggregates in the cytosol and promote cell survival under stress conditions. Thus, autophagy activators are considered to potentiate therapeutic benefit in certain cardio-metabolic and neurodegenerative diseases[272]. On the other hand, there are also diseases in which autophagic activation emerges as an important driver of disease progression. For example, therapeutic inhibition of autophagy could eliminate chemo-resistant cancer cells, hence improving anti-cancer therapy[249]. Accordingly, either activating or inhibiting autophagy might have the potential to confer therapeutic benefit for human diseases.

1.6.1. Autophagy in cancer.

The role of autophagy in cancer has been studied and identified predominantly in genetically engineered mouse models (GEMMs) and xenograft models through systemic or organ/tumour-specific loss of *Atg* genes, such as *Becn1*, *Atg5* or *Atg7*, or by pharmacologically targeting autophagy[273]. The recurring theme from autophagy inhibition in GEMMs is that autophagy is involved in elimination of oxidative stress, limiting DNA damage, induction of the immune response and regulation of a number of signalling pathways, such as mTOR and nuclear factor erythroid 2-related factor 2 (NRF2)[274]. Autophagy inhibition is known to cause genomic instability and sustained oncogenic signalling, which is consistent with the notion that autophagy acts as a tumour suppressor mechanism. However, once the tumour is established, cancer cells use autophagy to evade apoptosis and to cope with cancer-associated stress conditions [275]. Observations in established tumours have indicated that autophagy is upregulated in hypoxic tumour regions and promotes cell survival[276]. Also, autophagy enables cancer cells to suppress tumour-induced inflammation[275]. Therefore, the present consensus is that autophagy is an early tumour suppressor but, perhaps somewhat paradoxically, also a late tumour promoter. These concepts thus suggest that the autophagic activity might be one of the mechanisms underlying the ability of cancer cells to survive under hostile conditions.

Autophagy as a tumor suppressor. The involvement of autophagy genes in individual cancers have been systemically questioned by several groups. A large-scale cross-cancer profiling of somatic mutations within the human autophagy interaction network revealed that the core autophagy machinery was not targeted by mutations in almost all solid cancers[277].

Thus, it is conceivable that core autophagy machinery is more likely to have its own way to escape from molecular alterations, as it is vital to protect genomic and mitochondrial stability.

Despite the predominant absence of *ATG* genes in human cancers, the loss of *BECN1* is a frequent event in many cancers including breast, prostate, and ovarian cancers. Biallelic loss of *Becn1* gene in GEMMs caused neonatal death, however *Becn1-/+* mice survived and evidenced *Becn1* as a haploinsufficient tumour suppressor gene[274]. *Becn1* heterozygous mice are prone to develop spontaneous carcinomas of liver, lung, and mammary hyperplasia late in life[273]. In a hepatitis B virus-induced model of hepatocellular carcinoma, Qu et al also demonstrated that heterozygous disruption of *Becn1* increased premalignant liver lesions[278]. In another study, Atg9A protein level positively correlates with the survival of HBV-associated HCC tumors[279]. However, expression level of tumour suppressor gene *p53* showed significant reduction in *Becn1-/+* tumours suggesting an autophagy-independent tumour suppressor role for *Becn1*[278]. Yet, it is important to note that these tumours retained second allele of *Becn1* and showed functional autophagy. Indeed, absence of biallelic *BECN1* mutations in human cancers, as it is lethal in mice, might reflect the fact that autophagy is an essential process, and its complete elimination would result in prevention of malignant transformation in cancer.

Furthermore, the allelic loss of Beclin1-interacting proteins UVRAG and Bax-interacting factor-1 (Bif-1) has also found in breast, gastric, colon and prostate cancer[280]. Bif-1 null mice developed normally but had an enlarged spleen. Similar to *Becn1, Bif-1* deletion impaired autophagy and showed a higher incidence of spontaneous tumor formation such as lymphoma[281]. Moreover, in a study with gastric and colorectal cancers with microstatellite instability, it was shown that over 25% of these cancers harbour frameshift mutations in *ATG2B, ATG5, ATG9B*, and *ATG12*, suggesting a role for deregulated autophagy in tumour formation[282]. Recently, it was reported in multiple tumour types that *ATG5* somatic mutations and alternative mRNA splicing specifically disrupt ATG12 conjugation by disrupting ATG5-ATG16L1 interactions, which results in autophagy inhibition[283].

Autophagy is a vital mechanism during development. Different from biallelic *Becn1* loss, mice without either one of the core autophagy proteins Atg5 or Atg7 born alive but died after the first day of delivery[284, 285]. Intriguingly, these mice showed neuronal dysfunction which seemed to be responsible from their death, and neuronal transgenic Atg5 expression rescued them form neonatal death.[286] Therefore, conditional knockout mice models were generated to study their role in cancer progression. Kuma et. al. showed that mice with liver-specific biallelic or systemic heterozygous loss of Atg5 indicated benign liver adenomas[284]. Similarly,

organ specific *Atg7* deletion in the liver of adult mice resulted in increased incidence of hepatomegaly, abnormal organelle accumulation and ubiquitin-positive aggregates in the liver[285].

Moreover, chronic p62 elevation in HCC tumours has been proposed to contribute to tumour growth by enhancing the Nrf-2 signalling, which is a major defence mechanism against oxidative stress and can activate oncogenic signalling pathways[287, 288]. Accordingly, mice harbouring systemic mosaic deletion of *Atg5* or hepatocyte-specific disruption of *Atg7* reportedly developed benign liver adenomas that reduced partially in size after simultaneous deletion of *p62*[289]. Furthermore, deletion of autophagy genes (*Atg5* or *Atg7*) in *Kras*-driven *p53*-mutant murine model of pancreatic adenocarcinoma showed that autophagy inactivation in these mice stimulated the formation of premalignant pancreatic lesions (PanIN) but simultaneously impaired their malignant transformation to PDAC[290]. Similarly, deletion of *Atg7* in *K-ras* induced lung cancer models reported to limit tumour pathology from carcinomas to benign oncocytomas[15, 291]. On the other hand, these tissue-specific knockouts abrogated autophagy irreversibly which precludes us to mimic human aetiology or therapeutic modulation of autophagy. Regarding this, Liam et al developed a doxycycline (dox)-inducible shRNA mouse model targeting *Atg5*, enabling inhibition and restoration of systemic autophagy *in vivo*[292]. In response to autophagy suppression by a dox-infused diet for 6-weeks, these mice recapitulated key phenotypes, such as hepatomegaly, reduced adipose tissue, and pancreatic degeneration, described previously in tissue-specific knockouts[284, 285, 292]. Moreover, restoration of Atg5 (absence of dox for further 6 weeks) recovered tissues' autophagy and pathological features of autophagy deficiency. Autophagy restoration reversed the ageing-like phenotype and extended life span of mice. Intriguingly, autophagy restored mice showed spontaneous tumour formation earlier and with higher incidence than mice with continuing autophagy inhibition, which was predominant cause of death[293]. These findings suggest that transient inhibition of autophagy may be enough to induce irreversible cellular damage (e.g., genomic instability), which might enable tumour initiation, and cooperative restoration of autophagy might promote tumour development. Thus again, autophagy can play both tumour suppressive and oncogenic roles depending on the context.

In summary, these studies suggest that autophagy might play a tumour suppressive role and limit tumour formation. It is also important to note that loss of different *ATGs* resulted in diverse phenotypes implying that the observed effects might be related with autophagy-independent roles of those genes[275]. The exact mechanism of how autophagy inhibition leads

to tumour formation is largely unknown. However, loss of autophagy causes oxidative stress, chronic inflammation, and tissue damage; those are well-known factors making cells vulnerable to mutations and oncogenic transformations[274]. Even though loss of *ATG* genes as in the mice models have not been identified in human cancers, autophagy inhibition might come into play by different mechanisms like mTOR inhibition. In the later stages, increasing stress conditions in cancer cells might exert a need for autophagy to provide energy and protect cells from stress induced damages.

Autophagy as a tumour promoter. Although autophagy has been shown to have tumour suppressive roles in cancer formation, once tumour has been established, cancer cells can exploit autophagy that switches its role paradoxically to tumour promoter in order to support survival[275]. Observations have indicated that autophagy is upregulated in hypoxic tumour regions and promotes cell survival. Also, autophagy contributes cancer cells to suppress tumour-induced inflammation[275].

Previous studies on different cancers have suggested that mutations in Ras proteins enhance autophagy that elicit a selective dependency of tumors on autophagy for maintaining cellular homeostasis[294]. In this regard, lung-specific deletion of essential autophagy genes *Atg5* or *Atg7* in mice with *Kras*- or *BrafV600E*-driven lung cancer inhibited autophagy and remarkably suppressed tumour growth compared to mice with tumours in which autophagy was intact[15, 291, 295, 296]. However, this effect was shown to be *Trp53* dependent, and concomitant deletion of the tumour suppressor *Trp53* restored tumour progression in autophagy-deficient mice and abolished the survival advantage[296]. In addition, *Atg7* deletion in Kras-activated lungs caused inflammation, and those mice died from inflammatory pneumonia while *Atg7*+/+ mice died from cancer[15]. Likewise, genetic knockdown of autophagy (either through *Atg5* or *Atg7*) has been shown to block the progression of PanINs to invasive adeno carcinomas in the presence of both *Trp53* allele[297]. Moreover, monoallelic deletion of *Trp53* allowed the formation of invasive pancreatic adeno carcinoma formation even in the absence of Atg5, however, their growth is retained compared to *Atg5* WT tumors[290]. Strikingly, tumour suppressive effect of autophagy inhibition was lost in *Trp53 -/-* tumours, suggesting that the tumour suppressive role of autophagy might be stated depending on genetic background (presence of *Trp53*)[290].

From a pharmacological perspective, complete autophagy inhibition in mouse tissues comes with the problem of inflammation and histological tissue damage. In a recent study, Yang et al. generated a PDAC mouse model (*Atg4B*$^{CA+}$, *Trp53*$^{lox/+}$, *LSL-Kras*^{G12D}, *Rosa-*

rtTALSL, p48^{Cre+}), which allows the acute and reversible inhibition of autophagy without complete blockage[298]. In this model, intermittent expression of dominant negative form of Atg4B decreases growth in fully-formed tumours with a tolerable toxicity in mice. Further, inhibition of autophagy in these tumours showed prominent tumour regression and extended overall survival of mice[298]. The validity of this model has been challenged by Pfizer and Novartis[252].-Inhibition of tumour autophagy using *Atg4BCA+* expression, *Atg7* depletion or CQ treatment did not abrogate tumour growth. However, these observations have been done in immunodeficient mice, suggesting tumour growth does not reliant on autophagy in the absence of immune signalling. Therefore, if we consider the inducible models as a genetic drug, it suggests that intermittent interventions of autophagy inhibitors might be a promising approach in cancer treatment.

Furthermore, the impact of autophagy deficiency investigated in BrafV600E-driven melanoma mouse model with and without *Pten* codeletion[299, 300]. *Pten* is a commonly deleted gene in melanoma, and *BrafV600E*-activation alone in mouse models was insufficient to induce melanoma formation regardless of autophagy status. Further, biallelic or monoallelic *Pten* loss in mice has allowed the formation of *BrafV600E*-driven cutaneous melanoma resembling the human disease. In this model, tumour specific deletion of *Atg5* or *Atg7* impaired autophagy, prevented tumour growth and prolonged survival of mice[299, 300]. Intriguingly, in the same model, heterozygous *Atg5+/-* deletion (compared to *Atg5-/-* or *Atg5+/+*) had increased tumour growth and compromised the response to BRAFi dabrafenib[300]. Similarly, castrate-naïve prostate cancer model driven by *Pten* deficiency showed tumour regression and extension of life span of mice in response to Atg7 deficiency[301]. Moreover, monoallelic loss of *Becn1* prevents *Palb2*-associated mammary tumorigenesis only in the presence of wild type *Trp53*[302]. This might indicate that autophagy facilitates formation of hereditary (Pten-/Palb2-driven) tumour formation by promoting Trp53 signalling.

Another cancer in which elevated levels of autophagy draws attention is colorectal carcinoma (CRC). Development and progression of CRC is promoted by an initial loss of the *adenomatous polyposis coli (APC)* gene and followed by sequential mutations in *tumour protein p53 (p53)*, and mutations in *KRAS*[303]. Autophagy has been documented as one of the molecular mechanisms that demonstrates pro-tumorigenic functions in CRC[304]. Autophagosomal marker, LC3-II protein, was found highly expressed in CRC tumours compared to surrounding non-cancerous tissue, and associated with aggressiveness of CRC, suggesting involvement of autophagy in colorectal pathology[305, 306]. Loss of tumour suppressor

APC gene enhances autophagy in intestinal epithelium in murine and human colorectal cancers [307]. The conditional inactivation of *Atg7* in the intestinal epithelial cells of *Apc+/-* mice prevents tumour initiation and progression. In these tumours, inhibition of autophagy led to activation of anti-tumour innate immune response, and depletion of CD8(+) T cells abolished the anti-tumoral responses mediated by *Atg7* deficiency[307]. Likewise, deletion of another essential autophagy gene *Fip200* in polyoma middle T antigen (PyMT)-driven mammary cancer blocked tumour growth and prolonged lifespan of mice[308]. Mechanistically, ablation of Fip200 in mammary epithelial cells caused decrease in cyclin D1 expression, reduced glycolysis, and increased immune surveillance. A deeper understanding of tumour suppressive role of autophagy inhibition came from an avian retrovirus (RCAS)-based endogenous mouse model of *Kras*-driven glioblastoma mouse model that also expresses shRNAs against *Atg7*, *Atg13*, or *Ulk1*[309]. This model allows development of glioblastoma in mice resembling histological features of human disease. The authors found that knockdown of *Atg7* impaired tumour growth while knockdown of *Atg13* and *Ulk1* completely blocked tumour formation. Further analysis revealed that tumours arose in the Atg7 knockout settings had escaped from *Atg7* disruption and showed functional autophagy[309]. Collectively, these data showed involvement of autophagy in tumour development and growth, which presented a rationale for autophagy targeted-adjuvant therapy.

1.6.2. Autophagy in neurodegenerative diseases (NDDs), infectious diseases, and metabolic diseases

Autophagy is an essential quality-control/homeostasis mechanism inside the cells that has been linked to ageing and neurodegeneration[310]. As molecular and cellular damage builds up over time, cellular repair processes gradually fail, causing a decline in the function of the cell. Age-related reductions in the cell's capacity for autophagic degradation have been linked to a loss of the homeostatic function and may contribute to ageing process[310]. Consequently, failure of the autophagic capacity has been associated with a wide variety of ageing-related diseases, including neurodegeneration and cardiovascular diseases[311, 312].

Genetically inherited NDDs, such as Parkinson's disease or Huntington's disease, present mutations that affect the autophagy machinery, for example, during vesicle formation, leading to accumulation of undesired proteins in the cytoplasm[312]. Defective mitochondrial accumulation or aberrant protein aggregation in neurons are hallmarks of NDDs[313]. Removal

of these pathogenic molecules to maintain neuronal homeostasis is highly facilitated by autophagy[314, 315].

Autophagy fulfils immunomodulatory functions; thus, autophagy activation may serve as an anti-microbial strategy. Autophagic activity regulates the development and differentiation of innate immunity and adaptive immunity cells and promotes production of pro-inflammatory cytokines (e.g., TNF, tumour-necrosis factor and IL-6, interleukin-6)[316, 317]. In addition, autophagy-mediated removal of dysfunctional mitochondria can regulate innate immune responses by limiting the release of mitochondrial ROS and mtDNA into cytosol[318]. Moreover, autophagy can target and eliminate cytosolic pathogen such as bacteria, viruses, and intracellular protozoa by xenophagy[319, 320].

Emerging evidence suggests that autophagy can play a central role in the maintenance of homeostasis in a wide variety of tissues[321]. Metabolites produced through autophagic activity, such as carbohydrates, amino acids, nucleosides, and fatty acids, are essential for the maintenance of tissue homeostasis. Accordingly, dysregulation of autophagy has been associated with metabolic diseases, such as obesity, diabetes, and myopathies[322].

1.7. Wnt/β-catenin signalling and autophagy

Autophagy and Wnt/β-catenin signalling both play important roles in development, tissue homeostasis, and tumorigenesis[323].Recent studies described a reciprocal relationship between Wnt/β-catenin pathway and autophagy[323]. For example, a negative feedback loop between autophagy and Wnt pathway was suggested to regulate metastasis of melanoma cells[324]. High autophagic activity also implicated in the activation of Wnt signalling in colon cancer cells[111]. Uncovering the interconnection between autophagy and Wnt/β-catenin pathways may therefore suggest important implications for cancers driven by an aberrant Wnt signalling.

1.7.1. Wnt/β-catenin signalling

The Wnt/β-catenin pathway (shortly Wnt pathway) is essential during development, regeneration, and cellular homeostasis[325]. For example, the Wnt signalling pathway is associated with the development and regeneration of small intestinal epithelial tissue and promotes Paneth cell differentiation at the base of crypts[326]. In addition, Wnt signalling is closely associated with liver and lung tissue metabolism and repair, hair follicle regeneration, hematopoietic development, and osteoblast maturation and activity[325].

Wnt signalling in human diseases. Wnt signalling plays a complex and important role in human disorders[325]. Wnt signalling is a multifaceted mechanism that is essential for cell proliferation, tissue homeostasis, and embryonic development. Nevertheless, disruption of this system has been linked to the onset and development of a number of illnesses[325].

Cancer is a well-known area where WNT signalling is active[327]. Uncontrolled cell growth and tumour development can result from the Wnt pathway being activated in an abnormal way. Many malignancies, including colorectal cancer, breast cancer, and melanoma, show dysregulation of Wnt signalling[327]. The Wnt activation frequently results from changes or mutations in crucial pathway elements including Wnt ligands, receptors (Frizzled), or downstream effectors (Axin or β-catenin)[328]. A crucial pathway mediator, β-catenin, accumulates and translocate to the nucleus as a result of abnormal Wnt signalling, activating the transcription of target genes involved in cell survival and proliferation[329]. The dysregulated Wnt signalling system in cancer can boost invasion and metastasis, encourage unchecked cell proliferation, and prevent apoptosis[330]. It helps keep cancer stem cells, which are capable of self-renewal and differentiation, survival. Additionally, Wnt signaling can interact with other signaling pathways, such as Notch, Hedgehog, and EGFR, to further enhance cancer progression[328]. The investigation of therapeutic approaches targeting this system has resulted from knowledge of the function of Wnt signalling in cancer[331]. Numerous strategies are being looked into, such as the creation of tiny compounds that block essential Wnt pathway elements or disrupt the connection between β-catenin and its transcriptional partners. Researchers are also investigating the potential of gene and immunotherapies to modify Wnt signalling in the treatment of cancer[331].

Additionally, Wnt signalling is important in neurological diseases[332]. Parkinson's and Alzheimer's are two neurodegenerative illnesses that have been linked to changes in the Wnt route. Dysregulated Wnt signalling in Alzheimer's disease impacts the processing of β-amyloid[333]. Moreover, Wnt signalling affects synaptic plasticity and neuronal survival in Parkinson's disease[334].

Wnt signalling mechanism. There are two major pathways referred to as canonical and noncanonical Wnt pathways. The canonical Wnt/β-catenin signalling mainly regulates cell proliferation, whereas the noncanonical Wnt pathways regulate cell polarity and migration[325]. The canonical Wnt signalling is the most-studied and best-understood pathway, which regulates the amount of the β-catenin protein and its transcriptional role. Cellular functions of β-catenin are strictly regulated by many kinases (Table 4, Fig 1.9). Under basal conditions (i.e.,

absence of a Wnt stimulus generated by Wnt ligands such as Wnt1, 2, 3, 8a, 8b, 10a and 10b), β-catenin constantly phosphorylated by a destruction complex that consists of AXIN, adenomatous polyposis coli (APC), GSK3β, and Casein kinase 1 (CK1)[335]. Phosphorylation of Ser45 by CK1 primes other sites (Ser33/37/41) to be phosphorylated by GSK3β, and facilitates phosphorylation-dependent binding of E3 ligase β-TrCP (Beta-transducin repeat-containing protein) to β-catenin, which promotes its ubiquitylation and subsequent degradation[336].

Wnt/β-catenin signalling is activated by secreted Wnt ligands, which bind to the seven-pass transmembrane receptor Frizzled (Fz) and the single-pass low-density lipoprotein receptor-related protein (LRP)[325]. The signalling molecule Dishevelled (Dvl) is recruited to the receptor complex. Dvl interaction with AXIN is critical to the inactivation of β-catenin destruction complex (Fig 1.9). These events result in accumulation of β-catenin in the cytosol and its subsequent accumulation in the nucleus. Nuclear β-catenin forms a complex with two other transcriptional factors, T-cell factor (TCF) and lymphoid enhancer factor (LEF), and activates transcription of Wnt target genes including *cyclin D1*, *c-jun*, and *c-myc*[329]. In addition to its transcriptional role, most of the β-catenin is found at the intracellular junctions in complex with cadherin molecules, where it is thought to link the cadherins to actin filaments[325]. β-catenin interacts with E-cadherin and translocate to cell membrane together (Fig 1.9). This event is thought to be independent from canonical and non-canonical Wnt signalling pathways and contributes to cell-cell communication and cell adhesion[337]. The switch between its transcriptional and adhesive functions regulated by several post-translational modifications[338]. For example, β-catenin (Y142 and Y654) can be phosphorylated by multiple kinases, leading to its release from cell membrane interactors (α-catenin and E-cadherin)[338].

Table 4: *Post-translational modifications (PTMs) of β-catenin protein*

PTMs	***Sites***	***Domains***	***Involved enzymes***	***Function***	***Ref***
Phosphorylation	S45	-	CK1	Primes phosphorylation by GSK3	339
	S33/S37/T41	-	GSK3	Required for β-TrCP recognition	339, 340
	Y64	-	PTK6	May regulate for β-catenin nuclear localization	341

	T120	-	PKD1	May suppress β-catenin transcription activity	[342]
	Y142, Y654	Armadillo repeats domain	FAK	Promotes β-catenin disassociation from cell-cell contact	[343]
	S191/S605	Armadillo repeats domain	JNK2	Critical for β-catenin nuclear localization	[344]
	S552	Armadillo repeats domain	AKT	Promotes β-catenin disassociation from cell-cell contact and accumulation in both the cytosol and nucleus	[345]
	S675	-	PKA	Increases stability	[346]
Ubiquitylation	K19/K49 (K48-linked chain)	-	β-TrCP	Targets for degradation	[347]
	- (K11/K29-linked chain)	-	EDD	Increases stability	[348]
	K394 (K63-linked chain)	-	Rad6B (ubiquitin conjugating enzyme)	Increases stability	[349]
	- (K11/K63-linked chain)	-	FANCL	May increase β-catenin expression and activity	[350]
	-	-	Jade-1	Targets for degradation	[351]
Acetylation	K49	-	CBP	Inhibits β-catenin ability to activate c-myc gene	[352]
	K345	Armadillo repeats domain	P300	Enhances β-catenin interaction with TCF-4	[353]
	K19/K49	-	PCAF	Increases stability	[354]

Wnt proteins (Wnt4, 5a, 5b, 6, 7a, 7b and 11) have been classified into non-canonical based upon β-catenin-independent downstream signalling[355]. Non-canonical Wnt ligands bind to Fz receptor as well as a variety of co-receptors (such as receptor tyrosine kinase, tyrosine-protein kinase transmembrane receptor 1 or 2 and collagen triple helix repeat containing protein 1) on the cell membrane[355]. The non-canonical Wnt signalling is highly context specific, depending on cell type and receptor availability. Unique combinations of the receptor/ligand

complexes define the downstream effects of the Wnt signalling[355]. Non-canonical Wnt signalling can be divided into two groups: Planar cell polarity (PCP) pathway and Wnt/Ca^{2+} pathway. In PCP signalling, Fz receptors on the cell membrane activate JNK kinase and stimulate the transcriptional activity of ATF2 and c-JUN proteins, which leads to coordinated polarisation of cells[336]. In the Wnt/Ca^{+2} pathway, activated Fz receptors trigger a different signalling cascade, including activation of PKC and PLC kinases, which results in the release of intracellular Ca^{2+} [336]. Later, elevated cytosolic Ca^{2+} molecules can activate the phosphatase Calcineurin which dephosphorylates the transcription factor NFAT. These events lead to accumulation of NFAT in the nucleus and regulate cell fate and migration[336].

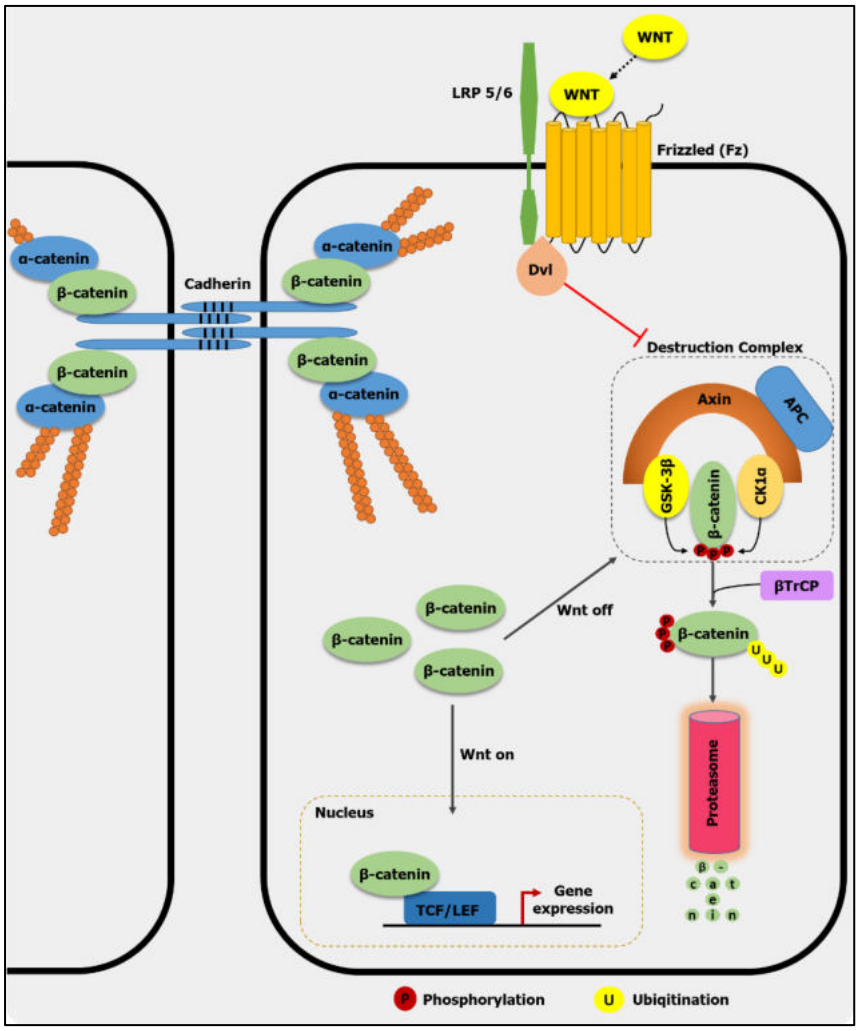

Figure 1.9 Canonical Wnt/β-catenin pathway and the role of β-catenin in the cell junctions. In the absence of Wnt (Wnt off), cytoplasmic β-catenin is phosphorylated by a destruction complex (Axin, APC, GSK3 and CK1), and subsequently recognized by the E3 ubiquitin ligase β-Trcp, which ubiquitylates and targets β-catenin for proteasomal degradation. In the presence of Wnt ligand (Wnt on), a receptor complex forms between LRP5/6 and Fz on the cell membrane. Dvl recruitment by Fz disrupts the formation of the destruction complex. This allows β-catenin to accumulate in the nucleus where it serves as a co-activator for the transcription factors TCF/LEF to transcribe Wnt responsive genes. In addition, β-Catenin binds to Cadherins at the internal site of the plasma membrane and connects them to the actin filaments (orange filaments) together with α-catenin.

Aberrant Wnt signalling is associated with several types of cancer. The tumour suppressor *APC* gene is mutated in almost 80% of sporadic colorectal cancers[356]. Mutational

inactivation of APC results in an elevated amount of nuclear β-catenin and dysregulated β-catenin target gene transcription. In addition, mutational inactivation of Wnt signalling molecules has been observed in over 50% of breast tumours and associated with a decrease in overall survival[330]. Moreover, high expression of Wnt receptors and ligands was found in several breast cancer subtypes[330]. Mounting evidence also suggests that dysregulation of the Wnt pathway is linked to tumorigenesis in most leukaemia and melanoma cancers[330]. For example, in leukaemia, Wnt/β-catenin signalling is found to be dysregulated through increased expression of Frizzled-4, a receptor of WNT ligands. To conclude, the driver mutations in the Wnt pathway favour constitutive activation of the Wnt/β-catenin signalling, leading to up-regulation of genes involved in cell proliferation and cell-cycle progression. Thus, this pathway is an attractive target in cancer therapy. Several drugs targeting the Wnt/β-catenin pathway (e.g., Porcupine inhibitors, PRI-724) targeting Wnt pathway are currently being investigated[331]. Moreover, monoclonal antibodies for secreted Wnt molecules preventing activation of Wnt signalling emerge as another potential therapeutic strategy[331].

1.7.2. Molecular crosstalk between Wnt/β-catenin signalling and autophagy

Interaction between autophagy and Wnt/β-catenin has been reported at different molecular levels and various cellular processes[323]. Several reports have suggested an inverse correlation between Wnt/β-catenin signalling and autophagy. Thao *et al.,* reported that activation of Wnt/β-catenin inhibited Beclin1 expression in the MG63 human osteosarcoma cell line[357]. In the same way, both basal and stress-induced autophagy are negatively regulated by Wnt/β-catenin signalling in Glioblastoma Multiforme (GBM) cells[358]. Moreover, mRNA and protein levels of p62 are found to be elevated upon silencing TCF4 or β-catenin in GBM cells[359].

Conversely, autophagy activation was also reported to be able to downregulate Wnt/β-catenin signalling. Enhanced autophagy was shown to inhibit Wnt/β-catenin signalling at an early phase of cardiac differentiation in an *in vitro* cardiomyocyte differentiation system (PC19CL6 cells)[360]. In the same study, blocking autophagy by silencing *Atg5* and *Atg7* genes promoted formation of a complex of LC3 with β-catenin[360]. In another study, autophagy was found to inhibit Wnt/β-catenin signalling through β-catenin relocalisation in glioblastoma cells[361]. More strikingly, several proteins in Wnt signalling pathway have been found to exhibit functional LIR motifs and be regulated by autophagy[323]. A canonical (WxxI) LIR motif was

suggested in the C-terminus of β-catenin, enabling its interaction with LC3 proteins under both basal and stress-induced conditions[112]. In the same study, starvation-induced autophagy was shown to degrade β-catenin. Also, accumulation of β-catenin in the nucleus suppressed the *p62* promoter leading to autophagy inhibition[112]. Moreover, a recent study showed that elevated autophagy deregulates Wnt signalling by degrading Dvl2 protein that binds to p62 and LC3 via a canonical LIR motif (W-XX-I)[111]. In addition, Receptor for activated C kinase 1 (RACK1) deregulates Wnt signalling by directing Dvl protein to lysosomal degradation, which is enhanced by autophagy induction[362]. Also, several other mechanisms including ULK1-mediated Dvl phosphorylation and FIP200-mediated β-catenin ubiquitylation were suggested to impair Wnt/β-catenin signalling[363, 364]. These findings illustrate an integration between Wnt/β-catenin signalling and autophagy in which they regulate each other inversely.

There are also some reports suggesting a positive correlation between autophagy and Wnt/β-catenin signalling. For instance, Wnt5a is upregulated in melanoma, and it acts as an intrinsic inhibitor of canonical Wnt signalling by diverting the signal to the noncanonical pathway[365]. Overexpression of Wnt5a is linked to reduction in basal autophagy in melanoma cells and increased invasion[365]. Moreover, Wnt3a ligand, an activator of Wnt/β-catenin (canonical) signalling, enhances autophagy in hippocampal neurons[366]. Autophagy activation in HCC cells increased β-catenin levels and promoted glycolysis, whilst the same effect was reversed by autophagy inhibition[367]. Furthermore, repression of TSC complex subunit 1 (Tsc1) *in vivo* was shown to inhibit autophagy which was correlated with a GSK3β-independent β-catenin degradation, suggesting an autophagy-mediated positive feedback mechanism[368].

Regarding the studies above, the interconnection between Wnt/β-catenin and autophagy pathways is still controversial and needs further investigations.

1.8. Aims of the thesis

The implication of autophagy in a broad range of cellular activities (as mentioned above) has gathered great interest in deciphering its molecular mechanism to understand the functions of autophagy. However, our understanding of how specific cargo including organelles, proteins, or intracellular pathogens are targeted for selective autophagy is limited. In addition, the question of how autophagy regulates proliferative signals to maintain cellular homeostasis have not been properly addressed to date. Resolution of cargo targeted by autophagy and interconnections between proliferative signals such as Wnt/β-catenin signalling and autophagy can help to better understand its mechanism and physiological roles. Therefore, this project aims:

1- to create the basis for understanding the functions of autophagy through studying the composition of autophagosomes isolated from tumour cells (Chapter I)
2- to study the role of autophagy in Wnt/β-catenin signalling (Chapter II)

It is expected that this thesis will reveal novel autophagy-substrates and deliver integration points for analysing the impact of autophagy on the regulation of Wnt/β-catenin signalling.

2. Materials and Methods

2.1. Plasmids, antibodies, and cell lines

Plasmids: GFP-β-catenin (addgene, # 71367), HA-β-catenin and HA-β-catenin W504A, I507A (kind gift from Alexander Greenhougha), GST-LC3/GABARAP (backbone: pGEX-4T1) plasmids (kind gift from Terje Johansen and Vladimir Rogov). pCMV-hATG7wt (addgene, #87867), pCMV-hATG7CS (addgene, # 87868), CMV-hEAAT1 (addgene, #32813), pSpCas9(BB)-2A-GFP (PX458) (addgene, #48138), pCW57.1-EGFP and pCW57.1-EGFP-ATG4B^{DN} (produced by Owen Conway using Gateway cloning), *Plasmids from Cancer Pharmacology and Stress Response (CPSR) Team's plasmid bank:* mcherry-LC3B, EGFP-LC3B and EGFP-GABARAP, viral packaging vectors (psPAX2, pMD2.G). *Plasmids from Structural Biology of Cell Signalling Team's plasmid bank:* pKLV2-U6gRNA5(BbsI)-PGKpuro2ABFP-W (addgene, #67974), Bacmid plasmids, pLIP-2xStrepII-TEV-β-Catenin, luciferase reporter assay constructs (ptkRL and TOP/FOPflash).

Table 5: *Plasmids produced with restriction enzyme cloning.*

Produced Plasmid	***Source***	***Restriction cut***	***Cloning***
pGEX-4T1 empty plasmid, expresses GST in bacteria	pGEX-4T1-GABARAP	BamHI-XhoI	After restriction cut, the backbone was purified using a gel extraction kit (NEB, # T1020S) and incubated with two filling primers (F: AATTCCCGGGTCGAC, R: TCGAGTCGACCCGGG) in the presence of 1 unit quick ligase (NEB, #M2200S) for 10 minutes (min).
mCherry-GABARAP	mCherry-LC3B (backbone) and EGFP-GABARAP (insert)	XhoI-BamHI	After restriction and gel purify, cloning was done using 1 unit quick ligase (NEB, #M2200S) for 10 min.
HA-EAAT1	hEAAT1 (insert) and HA-β-catenin (backbone)	NotI-BamHI	After restriction and gel purify, cloning was done using 1 unit quick ligase (NEB, #M2200S) for 10 min.

Table 6: *Plasmids produced using site-directed mutagenesis kit (NEB # E0554S) according to the manufacturer's instructions.*

Produced Plasmid	***Source***	***Primers (F: Forward, R: Reverse primers)***
HA-β-catenin (W/A)	HA-β-catenin	F: CCTGTATGAGGCGGAACAGGGATTTTC R: ACTTGGGAGGTATCCACA
HA-β-catenin (LW/AA)	HA-β-catenin	F: GAGGCGGAACAGGGATTTTCTCAGTC R: ATACGCGACTTGGGAGGTATCCAC

HA-β-catenin (ΔLIR: YEWE/AAAA)	HA-β-catenin	F: ATGTGGATACCTCCCAAGTCCTGGCTGCGGCGGCACAGGGATTTTCTCAGTCCTTCACTC R: CCTCTTCCTCAGGATTGCCTTTACC
HA-β-catenin (ΔLIR+ W504A, I507A)	HA-β-catenin W504A, I507A	
GFP-β-catenin (Y64A)	GFP-β-catenin	F: CCAAGTCCTGGCTGAGTGGGAAC R: GAGGTATCCACATCCTCTTC
GFP-β-catenin (Y64F)	GFP-β-catenin	F: CAAGTCCTGTTTGAGTGGGAAC R: GGAGGTATCCACATCCTC
GST-GABARAP ΔLDS (Y49A)	GST-GABARAP	F: CAAAAAGAAAGCCCTGGTGCCTTCTGATCTCACAG R: TCCAGGTCTCCTATCCGA
GST-GABARAP ΔLDS (Y49A, L50A)	GST-GABARAP	F: CAAAAAGAAAGCCGCGGTGCCTTCTGATCTCACAG R: TCCAGGTCTCCTATCCGA
GST-GABARAP ΔUDS (L76A, F77A, F78A)	GST-GABARAP	F: TGAGGATGCCGCGGCTGCCTTTGTCAACAATGTCATTC R: GCTCGGAGATGAATTCGC
pLIP-2xStrepII-TEV-β-Catenin (ΔLIR)	pLIP-2xStrepII-TEV-β-Catenin	F: GCGGCGCAGGGTTTCAGCCAGAGC R: TGCGGCCAGAACTTGGCTGGTGTC
pLIP-2xStrepII-TEV-β-Catenin (ΔNT: 141-781)		F: TACCAGGACGATGCGGAGC R: GCCCTGAAAATACAGGTTTTCAG
pLIP-2xStrepII-TEV-β-Catenin (ΔCT: 1-664)		F: TAAGCTTGTCGAGAAGTACTAGA R: TTCGCTCATACGGAACAGAACC
pLIP-2xStrepII-TEV-β-Catenin (Arm: 141-664)	pLIP-2xStrepII-TEV-β-Catenin (ΔNT: 141-781)	F: TAAGCTTGTCGAGAAGTACTAGA R: TTCGCTCATACGGAACAGAACC

Table 7: *Plasmids produced with 1C cloning.*

His6-MBP-LC3B	LICv1 (Backbone), GST-LC3B (insert)	F: TACTTCCAATCCAATGCAAAGTTCGTGTACAAAGAAGAGCA R: TTATCCACTTCCAATGTTATTAGTAGACACTTTCGTCACTGTAGG

His6-MBP-GABARAP	LICv1 (Backbone), GST-GABARAP (insert)	F: TACTTCCAATCCAATGCACCGTCGGAGAAGACCTTCAA R: TTATCCACTTCCAATGTTATTAGAACGTCTCCTGGGAGGCATA

1C Cloning: The inserts (LC3B and GABARAP) were amplified by Polymerase Chain Reaction (PCR) using the forward and reverse primers above. The PCR products were gel purified and treated with T4 DNA polymerase (NEB, # M0203L) in the presence of 10 mM dGTP (NEB, N0442S). The mixture incubated at room temperature for 30 minutes (min). and cleaned up using PCR purification kit (NEB, T1030S). LICv1 vector was digested with SspI and gel purified. The prepared inserts and vector were combined (approximately equimolar; 5 µl) in a total volume of 20 µl (rest volume is filled with ddH2O); incubated at room temperature for 10 min, and immediately performed transformation thereafter.

CRISPR cloning: CRISPR plasmids were engineered using the Zhang's lab protocol[369] to silence *CTNNB1* gene. Briefly, single guide RNA (sgRNA) was designed using DeepBaseEditor tool: TTCCCACTCATACAGGACTT, then the sgRNA sequence were modified for cloning (Forward: CACCGTTCCCACTCATACAGGACTT, Reverse: CAAGTCCTGTATGAGTGGGAACAAA). To clone these two oligos into the CRISPR vector (pKLV2-U6gRNA5(BbsI)-PGKpuro2ABFP-W), the vector was restriction digested with BbsI (NEB, #R0539), and the digested plasmid were gel purified (NEB, # T1020S). In parallel, two oligos were phosphorylated using T4 Polynucleotide Kinase (NEB, #M0201S) and annealed in a thermocycler (temperature gradually ramped down from 95 °C to 25 °C within 70 min). Then, the ligation reaction was carried out between digested plasmid (50 ng) and phosphorylated/annealed oligo duplex (1:200 dilution) using 1 unit quick ligase (NEB, #M2200S) for 10 min. The same protocol was followed to clone sgRNAs targeting *ATG4A* and *ATG4B* genes into another CRISPR vector.

Table 8: *CRISPR plasmids*

Target	**CRISPR plasmid**	**sgRNA sequence**	**Cloned oligos**
ATG4A	pSpCas9(BB)-2A-GFP (PX458)	ACCGGGGAGAATGGAGTCAG	F: CACCGGGGAGAATGGAGTCAGGTAC R: CCCCTCTTACCTCAGTCCATGCAAA

ATG4B	pSpCas9(BB)-2A-GFP (PX458)	ACCGGCTGCGGAAAGACCGA	F: CACCGGCTGCGGAAAGACCGACCCC R: CCGACGCCTTTCTGGCTGGGGCAAA

Correct assembly of all plasmids produced above was verified by restriction digest and sequencing of the open reading frames.

Antibodies: LC3B (Cell Signalling #3868), GABARAP (CST, #13733S), p62 (MBL #PM045), Phospho-p62 (Ser403) (Cell signalling #39786), GAPDH (Cell Signalling #2118), β-Actin (Cell signalling #4970), E-Cadherin (Cell signalling #3195), Bcl-2 (Cell signalling #2870), Strep Tag (ThermoFisher, #MA5-37747), β-catenin (BD Bioscience, #610153), Non-phospho (Active) β-Catenin (Cell signalling #8814), Phospho-β-Catenin (Ser33/37/Thr41) (Cell signalling #9561), ATG7 (R&D, #MAB6608), EEA1 (CST, #3288), Lamin B1 (CST, #12586), Golgin97 (CST, #13192S), TOMM20 (CST, #42406S), LAMP2 (Thermo Fisher, #PA1-655), ATG5 (R&D, #MAB5294), Calreticulin (CST, #12238S), EAAT1 (CST, #5684), DAB2 (Scbt, #sc-13982), HGS (Abcam, ab62447), WBP2 (Scbt, #sc-514247), PAICS (St John's, #STJ195870), ITM2B (Scbt, #sc-374362), FAM174A (Sigma, #HPA019539), PRKAR1B (Sigma, #HPA026719), ILK1 (Scbt, #sc-20019), EpHa2 (Scbt, #sc-924), CCN1 (Scbt, #sc-374129), RuvBL2 (Scbt, #sc-374135), PRDX1 (Proteintech,#15816-1-AP), BST2 (Scbt, #sc-390719), SDCBP (Scbt, #sc-515538), SAR1a (Scbt, #sc-130463), LITAF (Scbt, #sc-166719), IFITM3 (IFITM3, #59212T), PPIA (Scbt, #sc-134310), GLG1 (R&D, #MAB78791), GFP (Abcam, #ab290), ATG4A (CST, #7613), ATG4B (CST, #5299).

Cell lines: HeLa WT, HeLa *ATG7* KO, HeLa *LC3* TKO (triple KO), HeLa *GABARAP* TKO, HeLa Hexa KO are kind gift from Michael Lazarou. HeLa *ATG4B* KO GFP-LC3-G120/G120A (kind gift from Robin Kettler), HEK293T, HCT116, HCT116 Bax-/- GFP-LC3B, Ls174T, HT29, Colo320, Colo205, SW480 (CPSR cell stocks). U2OS WT and mutant U2OS (ATG7 KO, ATG9A KO, ATG13 KO, ATG14 KO, ATG16L1 KO, WIPI2 KO) cells are kind gift from Fulvio Regorri. HEK293T WT, HEK293T *ATG7* KO, HepG2 WT, HepG2 *ATG7* KO cells are kind gift from Masaaki Komatsu. HAP1 cells are taken from Structural Biology of Cell Signalling Team's cell bank.

- **Production of HeLa *ATG4 A/B* KO cells**

HeLa *ATG4 A/B* KO cells were produced with transiently transfecting HeLa WT cells with pSpCas9(BB)-2A-GFP (PX458) containing an sgRNA targeting *ATG4A* gene. After 48 hours (h) of the transfection, the cells were treated with puromycin (1 mg/ml). After two passages,

the cells were transiently transfected again with pSpCas9(BB)-2A-GFP (PX458) containing an sgRNA targeting *ATG4B.* After 48 h of the second transfection, the cells were selected against puromycin. Simultaneous deletion of *ATG4A* and *ATG4B* genes were confirmed by western blotting against ATG4A/B antibody.

- **Production of inducible ATG4B^{DN} HeLa cells**

HeLa WT cells were genetically engineered with the lentiviral vector pCW57.1 to inducibly express EGFP alone or EGFP-tagged mutated ATG4B (C74A point mutation, shortly ATG4^{DN}). To obtain lentiviruses, HEK293 cells were transfected with either pCW57.1-EGFP or pCW57.1-EGFP-ATG4B^{DN} plasmids along with viral packaging vectors (psPAX2, pMD2.G). After 2 days of transfection the media was collected as a source of lentivirus. The presence of lentiviruses was confirmed using Lenti-X GoStix (Takara, #631280). To transduce HeLa cells, they were treated with 200 µl of the virus in the presence of 8 µg/ml polybrene (Sigma, # TR-1003). After 48 h of the transduction, the cells were selected against puromycin (1 mg/ml). After the antibiotic selection, engineered HeLa cells were grown in Tetracycline-free medium. Doxycycline inducible EGFP or EGFP-ATG4B^{DN} expressions were determined by western blotting using GFP antibody.

- **Production of β-catenin KO HAP1 cells**

HAP1 cells were genetically engineered with the pKLV2-U6gRNA5(BbsI)-PGKpuro2ABFP-W vector containing an sgRNA targeting *CTNNB1* gene. Lentiviruses were produced as explained above. The cells were transduced with the lentiviruses and selected against puromycin (1 mg/ml). After 48 h, single clones were produced by serial dilutions in a 96-well plate. Mutation in the *CTNNB1* gene and depletion of β-catenin expression were determined using sanger sequencing and western blotting respectively.

- **Production of GFP-reporter HEK293 cells**

To assess β-catenin transcription activity, HEK293 and HEK293 ATG7 KO cells were transduced with lentiviruses (produced by Ben Broadway using pLenti-FNLS-P2A-Puro lentiviral vector and packaging vectors: psPAX2, pMD2.G). The transduced cells were selected against Puromycin (1 mg/ml) and used in further analysis.

2.2. Cell culture and transfection

For standard cell culture, cells were grown in a specific growth medium (see Table 9) supplemented with either 10% FBS (Fetal Bovine Serum, Pan Biotech, #P30-3702) or

tetracycline free FBS (Pan Biotech, #P30-3602), the latter for Dox inducible cell lines at 37 °C, 5% CO_2. A polymerase chain reaction (PCR)-based assay was used regularly to screen for mycoplasma for each cell line.

Table 9: *Cell culture mediums*

Cell lines	**Growth medium**
HeLa, HCT116, HEK293 cells and their mutants	Dulbecco's Modified Eagle's Medium (DMEM) (Gibco, #10566016)
Ls174T, HepG2, HT29, Colo320, Colo205, SW480, U2OS	
HAP1	Iscove's Modified Dulbecco's Medium (IMDM) (Gibco, # 31980030)

To induce autophagy, Earl's Balanced Salt Solution (EBSS, Sigma #E2888) or Torin-1 (250 nM, Bio-Techne #4247), were used for 4 h. To inhibit autophagy, Baf A_1 (200 nM, TOCRIS #1334) was used for 2-4 h. To inhibit the UPS, Velcade/Bortezomib (100 nM, Selleckchem #S1013) was used for 4 h. To inhibit GSK-3β, CHIR-99021 (Sigma #SML1046) was used.

Transfections of cells with plasmid constructs were done using Lipofectamine 3000 reagent (Thermo Fisher #L3000008) according to manufacturer's instructions. Short interfering RNA (siRNA) oligonucleotides for β-catenin and EAAT1 were purchased from Dharmacon in the ON-TARGETplus™ design format for high specificity and high potency (siCTNNB1: #L-003482-00-0005, siEAAT1: #L-007391-01-0005). For mock transfections, ON-TARGETplus Non-targeting Control Pool (Dharmacon, # D-001810-10-05) siRNAs were used. SiRNA transfections were done using DharmaFECT 1 Transfection Reagent (#T-2001-01) according to manufacturer's instructions. SiRNAs were used in the range of 12.5 to 50 nM for 24 or 48 h.

Primary PDAC and fibroblast cell line were produced from autophagy reporter *KPC* mice which were generated by crossing BL6 *KPC* mice (*K-ras*$^{LSL.G12D/+}$*; p53*$^{LSL.R172H/+}$*; pdx-cre, k*indly provided by Anguraj Sadanandam) and autophagy reporter mice (*Rosa26*; mCherry-GFP-LC3B, kindly provided by Ian Ganley). To produce fibroblast cells, pancreatic tissues were collected from autophagy reporter *KPC* mice. These tissues are then processed to release the fibroblast. After initial dissection the tissue is finely minced and digested in 'liberase

blendzyme' for 30- 90 min. After neutralising and thoroughly washing the liberase away tiny tissue fragments are plated onto 100 mm tissue culture plates and allowed to attach. Fibroblasts were seen to 'crawl' out of the tissue for up to 10 days. Initially the fibroblasts divided and replicated but soon they stopped, and the population number then stayed the same or possibly gradually decreased until they overcome this 'crisis' and begun to grow again as spontaneously immortalized cells. To produce PDAC cells, all the cells from the PDAC solid tumours separated out by 4 mg/ml collagenase (dissolved in a 1mg/ml PluriSTEM Dispase solution). This was then used to digest a finely minced tumour sample. Digestion took 30-90 min at 37 °C with frequent mixing. Digestion was completed when no tumour fragments were visible in the supernatant, and the mixture appeared cloudy/turbid. This cell suspension was then passed through a series of progressively finer cell strainers. Then, cells were centrifuged (500 g, 5 min) and the pellet was incubated with red blood cell lysis buffer. The cells were then once again passed through the finest cell strainer and then centrifuged (500 g, 5 min) and banked. Primary PDAC cells were grown in Roswell Park Memorial Institute (RPMI) 1640 (Gibco, #11530586) media supplemented with 10 %FBS at 37 °C, 5% CO_2.

2.3. Autophagosome isolation

A previously published autophagosome isolation protocol[188] was used with some modifications. Briefly, confluent and Baf A_1-treated GFP-LC3B expressing cells grown in 3x 15 cm tissue culture plates were collected into homogenization buffer (250 mM Sucrose, 10 mM HEPES, and 1 mM ethylenediaminetetraacetic acid (EDTA; Thermo Fisher Scientific, AM9262) including protease inhibitors: 1 mM PMSF (Phenyl-Methyl-Sulfonyl Fluoride), Roche protease cocktail (Sigma cat#04693159001, at 1 tablet/10 ml), and NEM (N-ethylmaleimide) (1 mM, Sigma #04259)) for each isolation, and disrupted by Nitrogen cavitation (Parr Instrument, 4639; 800 psi, 10 min, 4 °C) followed by 10 strokes with Dounce homogenizer. Next, the homogenate was centrifuged at 1,000*g* for 10 min to obtain a post-nuclear fraction. Another centrifugation at 17,000*g* for 12 min was applied to pellet whole organellar structures (Organellar fraction) including autophagosomes from the post-nuclear fraction. The pellet was washed twice with homogenization buffer to remove residual cytoplasmic proteins.

To immune-isolate autophagosomes, the organellar fraction was resuspended in the homogenization buffer and incubated with 100 µl of µMACS anti-GFP magnetic microbeads (Miltenyi Biotec, #130-091-125) at 4 °C with rotation at 100 rpm. After an hour of incubation,

the bead-homogenate mix was applied to µMACs LS column (Miltenyi Biotec, #130-091-125) and separated magnetically from the rest of the homogenate. After 3 consecutive washing steps with the homogenization buffer (10 ml each) under a magnetic field, autophagosome-bead complexes were eluted by separating LS columns from the magnetic field and running homogenization buffer through the column. The preparation was used for further analysis. The success of two other magnetic beads (MBL #D153-11, and GFP-Trap, ChromoTek #gta-20) were also tested.

To fractionate the autophagosomes, organellar fraction was resuspended in 1.2 ml homogenization buffer and diluted with an equal volume of 60% OptiPrep (Sigma-Aldrich, D1556). A discontinuous OptiPrep gradient was generated in a SW41 tube for ultracentrifuge rotors (Beckman Coulter, 344059) by overlaying the following OptiPrep solutions all in homogenization buffer: 2.4 ml of the diluted organellar fraction in 30% OptiPrep, 2 ml 20% OptiPrep, 2 ml 15% OptiPrep, 2 ml 10% OptiPrep, 2 ml 5% OptiPrep, and 2 ml 0% OptiPrep. The gradient was centrifuged at 150,200 g in a SW41Ti rotor (Beckman Coulter) using an Optima XE-90 ultracentrifuge (Beckman Coulter) for 3 h, and subsequently 14 fractions (0.85 ml each) were collected from the top to bottom. The fractions were used for further analysis.

To fractionate the autophagosomes from mouse tissue, tissues of interest from the autophagy-reporter *KPC* mouse (produced by Melanie Valentie) were collected freshly, dissected into small pieces, and homogenized using a Dounce homogenizer, which was followed by Nitrogen cavitation (800 psi, 10 min, 4 °C). After preparation of a tissue homogenate, it was passed through a cell strainer to eliminate components of connective tissue. Then, cells from each tissue were subjected to density gradient separation as explained above, to fractionate autophagosomes from the rest of the organelles.

For the combined autophagosome isolation approach, fractions 3-6 from the density gradient were combined and diluted with an equal volume of homogenization buffer and incubated with 100 µl of µMACS anti-GFP magnetic microbeads (Miltenyi Biotec, #130-091-125) at 4 °C with rotating for 1 h. Later, the same steps for immune isolation protocol were followed.

2.4. Mass Spectrometry

For the whole-cell proteomics analysis (TritonX-soluble), HeLa cell lysates were prepared in cell lysis buffer (50 mM TRIS-HCl pH7.4, 1 mM EDTA, 1% TritonX-100 (Tx-100), 150 mM NaCl, 1 mM sodium vanadate, 1 mM PMSF, 0.1 % of protease cocktail (Sigma,

P8849), 0.1% of phosphatase inhibitor 2 and 3 (Sigma, # P5726, # P0044), 1mM NEM (N-ethylmaleimide, Sigma, #E3876)). Then, proteins were reduced using 5 mM TCEP (Tris (2-carboxyethyl) phosphine hydrochloride, Sigma, #C4706) (10 min. shaking at 650 rpm at 60 °C), and cysteines were blocked with 10 mM of Iodoacetamide (Sigma, I1149-56) at room temperature in dark for 30 min. Next, samples were trypsin digested (5 µg/sample, prepared in 0.1% formic acid (Fisher chemicals, A117-50)). After trypsin digestion overnight at room temperature, 0.5% formic acid added on the samples to precipitate the detergent (Tx-100, or any other detergent). The samples were centrifuged at 17,000 g and the supernatant was collected as detergent-free peptides. Next, samples were dried, and protein pellets were dissolved in 100 µl of TEAB buffer (Sigma, #T7408). 40 µl of TMT (Tandem Mass Tag) labels were added to the samples and incubated at room temperature for 1 h. TMT labels were quenched by adding 2 µl of 5% Hydroxylamine (prepared in water) on the samples for 15 min at room temperature. All the samples were pooled and dried. Later, they were dissolved in 20 µl of 0.1% formic acid and run for MS analysis.

For the proteomics analysis of the autophagosome preparations, autophagosomes were isolated as indicated above. The autophagosomes eluted in homogenization buffer were centrifuged and precipitated at 17,000 g for 30 min at 4 °C. Later, the autophagosome pellets were dissolved in 100 µl of MS buffer (1% w/v sodium deoxycholate, 100 mM triethylammonium bicarbonate, 10% isopropanol, 50 mM NaCl). Later, reduction, blocking cysteines, trypsin digestion, and detergent precipitation steps from above were followed. Before proceeding to TMT labelling, samples were cleaned up with Pierce High pH Reversed-Phase peptide fractionation kit (Thermo, #84868) to remove residual Optiprep from the peptides which can interfere with TMT labelling. After that TMT labelling followed as mentioned above and samples were analysed in the MS machine.

2.5. Mass Spectrometry Analysis

LC-MS analysis was performed on a Dionex UltiMate 3000 UHPLC system coupled with the Orbitrap Lumos Mass Spectrometer (Thermo Scientific). Peptides were loaded onto the Acclaim PepMap 100 (100 µm × 2 cm C18, 5 µm) trapping column at flow rate 10 µL/min and analysed with an Acclaim PepMap (75 µm × 50 cm, 2 µm, 100 Å) C18 capillary column. Mobile phase A was 0.1% formic acid and mobile phase B was 80% acetonitrile, 0.1% formic acid. The separation method was: for 95 min gradient 5%-38% B, for 5 min up to 95% B, for 5 min isocratic at 95% B, re-equilibration to 5% B in 5 min, for 10 min isocratic at 5% B at a

flow rate of 300 nL/min. MS scans were acquired in the range of 375-1,500 m/z with mass resolution of 120k, AGC 4×105 and max IT 50 ms. Precursors were selected with the top speed mode in 3 sec cycles and isolated for HCD fragmentation with quadrupole isolation width 0.7 Th. Collision energy was 38% with AGC 1×105 and max IT 50 ms at 30k resolution. Targeted precursors were dynamically excluded for further fragmentation for 45 seconds with 7 ppm mass tolerance.

For peptide identification and quantification, the mass spectra were processed in Proteome Discoverer 2.4 (Thermo Scientific) with the SequestHT search engine. The precursor and fragment ion mass tolerances were 20 ppm and 0.02 Da respectively. Spectra were searched for fully tryptic peptides with maximum 2 missed-cleavages. TMT6plex at N-terminus/K and Carbamidomethyl at C were selected as static modifications. Oxidation of M and Deamidation of N/Q were selected as dynamic modifications. Spectra were searched against reviewed UniProt Homo sapiens protein entries, peptide confidence was estimated with the Percolator node and peptides were filtered at q-value<0.01 based on target-decoy database search. The reporter ion quantifier node included a TMT11plex quantification method with an integration window tolerance of 15 ppm. Only peptides with average reporter signal-to-noise>3 were used.

2.6. Immunoblotting

For immunoblotting, cells were collected into a lysis buffer containing 50 mM Tris-HCl, pH7.4, 1 mM EDTA, Tx-100 (1%, v/v), 150 mM NaCl, freshly supplemented with 1 mM sodium vanadate, 1 mM PMSF, Roche protease cocktail (Sigma, #04693159001, at 1 tablet/10ml), phosphatase inhibitor 2 (Sigma, #P5726), phosphatase inhibitor 3 (Sigma, #P0044), and NEM (1 mM, Sigma, #04259). Soluble proteins were collected after a centrifuge at 17,000 g for 15 min at 4 °C. The pellet were considered as cell debris and insoluble proteins. Protein concentration was determined by the BCA assay kit (Thermo Fisher Scientific, #23228). Protein samples were resolved on 4-12% NuPAGE Bis-Tris Protein Gels (Thermo Fisher Scientific, #NP0336BOX), then transferred onto polyvinylidene difluoride membrane (Merck Millipore, #IPVH00010) For visualizing proteins of interest, membranes with immobilized proteins were blocked in 5% Bovine serum albumin (BSA, sigma, # A3294) prepared in Tris Buffered Saline with 1% Tween-20 (TBST), then incubated with primary and HRP-linked secondary antibodies (anti-rabbit (Cell Signalling #7074S), anti-mouse (Cell Signalling #7076S). Signal was detected with BioRad Chemidoc machine using ClarityMax ECL substrate (BioRad #1705060).

To solubilize insoluble proteins, the pellet from above remained after the soluble protein isolation was solubilized in RIPA buffer (Thermo, #89900) and sonicated (Amp: %20, 1 sec on, 1 sec off) for 1 min on ice. Then, the solubilized pellet was centrifuged for 10 min at 17,000 g, 4 °C. The supernatant was analysed in the western blotting as insoluble protein fraction.

2.7. Fluorescence microscopy

Cells were fixed using methanol at -20 °C for 20 min, then blocked with 10% FBS in Phosphate Buffer Saline (PBS). For indirect staining, fixed samples were incubated with primary (overnight, 4 °C) and secondary antibodies (1 h, room temperature; Alexa Fluor 568 goat anti-rabbit IgG, Life Technologies #A-11011 and Alexa Fluor 488 goat anti-mouse IgG, Life Technologies #A-10680) in PBS containing 0.3% Tx-100 and 0.2% BSA. After washing with PBS, DAPI (4',6-diamidino-2-phenylindole)-containing mounting medium (Sigma, #DUO82040) was added onto the cells. Zeiss LSM700 confocal laser scanning microscope (LSM) was used for imaging.

2.8. Electron microscopy (EM)

To visualize autophagosome preparations under EM, autophagosomes preparations (either after immune isolation or fractionation) were pelleted at 17,000g and were fixed with 0.2 M HEPES solution containing 2% Glutaraldehyde (Sigma # G5882), pH: 7.4 at 4 °C for 2 h. After that a previously published protocol was used[370]. Briefly, the pre-fixed samples were transferred into beem embedding capsules (Laborimpex, #70010) and centrifuged for 5 min at 12,000 g at room temperature. Then, the pellet collected at the bottom washed with water. For post-fixation of the samples, the pellet were incubated with 2% OsO4 (Merck, #20816-12-0) and 3% K-ferrosyanide (Merck, #144-59-95-1) for 2 h at room temperature. Then, the pellet washed with water. To remove, all the water from the pellet, it was washed with sequentially 70%, 95% and 100% Ethanol at 4 °C for 1 min each. Then, the pellet was washed in acetone and incubated in acetone+ DMP (Fluka chemical, #45348)+ Epon at a ratio of 10: 0.15: 10. To prepare Epon solution, 2 ml Epon A (62 ml Epon 812 (Fluka chemical, #45345) and 100 ml DDSA (Fluka chemical, #45346) mixed for 3 h at 4 °C while stirring) and 3 ml Epon B (100 ml Epon 812 and 89 ml MNA (Fluka chemical, #45347) mixed for 3 h at 4 °C while stirring) were mixed at 4 °C while stirring. After 2 h of incubation, the pellet was incubated in Epon + DMP (10:0.15) mix for 12 h at room temperature and 36 h at 60 °C. Then, the sections were

cut on an ultramicrotome at 70 nm thickness and applied on grid. TEM (transmission electron microscopy) pictures were taken in Eeva-Liisa Eskelinen's Lab in Turku University, Finland.

2.9. Recombinant protein expression and GST-pulldown assays

GST- and His-MBP-tagged proteins (plasmids used: pGEX-4T1, GST-LC3/GABARAP, His-MBP-LC3B/GABARAP) were expressed in *E. coli* BL21 (DE3) (NEB, #C2530H) strain according to a previously published protocol[38]. Briefly, production of recombinant proteins was induced (OD: 0.5-1.0) by 1 mM IPTG (Sigma # 367-93-1) for 4 h at 37 °C or overnight at 18 °C. Then, bacteria were pelleted at 5,000 g for 30 min. Bacterial pellets were lysed after resuspension in lysis buffer (50 mM Tris-HCl (pH 7.5), 500 mM NaCl, 10 mM β-mercaptoethanol and protease inhibitors (1 mM PMSF, 1 EDTA-free Roche protease inh) +5 mM imidazole (pH 7.5, only for His-MBP tagged proteins)) by sonication (5 min, 1 min on/1 min off Amp: 40%). The lysate was centrifuged at 5,000 g for 50 min and filtered through a 0.45 µm filter. Production of the recombinant proteins were confirmed in the SDS-PAGE gel by InstantBlue Coomassie Protein Stain (Abcam, #ab119211).

- **GST and GST fusion protein purification**

Recombinant GST and GST fusion proteins were purified using Glutathione-Sepharose resin (GE Healthcare, #17-0756-01) which were incubated with bacterial protein lysate for 2 h at 4 °C. Unbound proteins were removed by washing the resins five times with the lysis buffer. Protein coated resins were used for further GST pulldown assays.

- **Recombinant LC3B and GABARAP protein purification**

The His-MBP-tagged LC3B and GABARAP proteins were purified using 5 ml Ni HisTrap HP affinity columns (GE Healthcare, #GE17-5248-02) according to manufacturer's instructions. His-MBP fusion proteins were eluted with a linear imidazole gradient (5 to 250 mM imidazole, pH 7.5) in a buffer also containing 50 mM Tris-HCl (pH 7.5), 100 mM NaCl and 10 mM β-mercaptoethanol. High protein content fractions were combined and the His-MBP tag was removed using TEV protease (4 mg/ml) overnight while dialyzing (cut-off: 3500 MW) against 50 mM Tris-HCl (pH 7.5), 100 mM NaCl, 10 mM β-mercaptoethanol. The His-MBP tag was removed by another Ni affinity chromatography step using a 5 ml Ni HisTrap HP affinity column. The flow-through was concentrated using ultrafiltration tubes (Sartorius, #VS2092, cut-off: 3000 MW). Purity of LC3B and GABARAP proteins were confirmed in

SDS-PAGE gel by InstantBlue Coomassie Protein Staining. The purified protein latter used in fluorescent polarization assay.

- **Recombinant β-catenin protein purification**

Multi-protein expression constructs were assembled using the biGBac system (Weissmann et al., 2016) to generate single baculoviruses with full-length and truncated β-catenin variants. Viral bacmids were generated using Tn7 transposition in DH10 MultiBacTurbo E. coli competent cells[371] for the expression of individual β-catenin constructs (from pLIB vectors, Table 2.3). Later, recombinant baculoviruses were generated by transfecting purified bacmids into Sf9 cells (Thermo Scientific, #11496015) using Cellfectin II reagent (Thermo Scientific, #10362100). Insect cells were cultured in Insect-Express media (Lonza, #BELN12-730Q) supplemented with 1% Penicillin-Streptomycin (Thermo Scientific, #15070063). After 72 h of incubation at 27 °C, the media of the Sf9 cells (P1 virus) was harvested infect a fresh and bigger (25 ml) culture of Sf9 cells for a second round of viral production at 27 °C while shaking at 130 rpm. When the Sf9 cell's viability dropped around 80% (approximately 72 h later), the virus containing media (P2 virus) were harvested. The amplified P2 viruses were used to infect High-Five cells (Thermo Scientific, #B85502) to express full-length and truncated β-catenin variants. The infected cells were grown in Insect-Express media at 27 °C, 130 rpm. After 72 h, the cell pellets were collected by centrifugation (250 g for 10 min at 4 °C).

To purify β-catenin and its variants, the High-Five cell pellets were resuspended in a lysis buffer (50 mM HEPES-NaOH (pH 7.5), 500 mM NaCl, 10 mM β-mercaptoethanol and protease inhibitors (1 mM PMSF, 1 EDTA-free Roche protease inh)). The lysates were sonicated for 5 min (2 sec on 2 sec off) at 40% amplitude on ice. The resulting homogenate were cleared by centrifugation at 5,000g for 50 min, and filtered through a 0.45 µm filter. The Strep-tagged β-catenin and its variants were purified using 5 ml StrepTrap column (GE Healthcare, #28907547) according to manufacturer's instructions. Strep-tagged protein fractions were eluted with an elution buffer containing 50 mM HEPES, pH: 7.5, 500 mM NaCl, 10 mM β-mercaptoethanol, 2 mM d-Desthiobiotin (Sigma, #D1411-1G). The eluted fractions were pooled and dialysed overnight at 4 °C against 50 mM HEPES-NaOH pH 7.5, 150 mM NaCl, 2 mM TCEP.

- **GST pulldown assay**

GST pulldown assays were performed by incubating GST or GST-LC3/GABARAP immobilized Sepharose resin either with HEK293 cell lysate (400 µg per 100 ml resin) or with recombinant β-catenin proteins (0.5 µg per 100 ml resin) or with fluorescently labelled LIR peptides (1 µM) for 2 h at 4 °C with gentle agitation. Unbound proteins and peptides were removed by washing the resins five times with a buffer containing 50 mM Tris-HCl (pH 7.5), 150 mM NaCl and 10 mM β-mercaptoethanol. The proteins were then eluted by boiling the beads for 5 min in SDS gel loading buffer and separated by SDS-PAGE. Pulled down proteins were detected by Western blotting. Binding of fluorescent peptides were detected by visualising the beads under confocal microscopy.

2.10. Protease Protection Assay

Integrity of immune-isolated autophagosomes was tested using a protease protection assay. 10 µl of autophagosome preparation was incubated on ice with and without 100 µg/ml proteinase K (NEB, P8107S) for 15 min in the presence or absence of 1% Tx-100. After incubation, 1 mM PMSF was added to the samples. Then the samples were immediately boiled at 95 °C for 10 min and subjected to immunoblotting or fluorescent microscopy. Untreated and Tx-100 treated samples were used as control.

2.11. Peptide overlay assay

The peptide overlay assay was done by Terje Johansen (University of Tromsø, Finland) as previously described[159]. Briefly, synthesis of β-catenin peptide arrays on cellulose membranes were performed using a MultiPep automated peptide synthesizer (INTAVIS Bioanalytical Instruments AG). The cellulose membrane with the peptides were blocked in TBST with 5% nonfat dry milk. Peptide interactions with GST-GABARAP proteins were tested by overlaying the membrane with recombinant GST-GABARAP (1 µg/ml) for 2 h at room temperature. After washing the membrane with TBST, bound proteins were detected with HRP-conjugated anti-GST antibody (GE Healthcare, #RPN1236).

2.12. Fluorescence polarization assay

This assay measures the direct binding of a fluorescently labelled β-catenin and Bcl-2 peptides to LC3B and GABARAP proteins. Fluorescently labelled (5-FAM) peptides were synthesized by GeneScript over 90% purity. The lyophilized peptides were dissolved in FP buffer (25 mM HEPES–NaOH pH 7.5, 100 mM NaCl, 1 mM TCEP, 0.05% w/v 3-[(3-

Cholamidopropyl) dimethylammonio]-1-propanesulfonate hydrate). Their concentration was determined spectrophotometrically (492 nm). The optimal probe concentration was determined by plating out the probes (0-200 nM, titrated in FP buffer) in technical triplicates. Opaque, black, 96-well, non-binding, flat-bottom plates (Greiner Bio-One, #781,900) were used. Readings were done using PheraStar plate reader (BMG Labtech), which automatically calculates FP values. 5 nM free fluorescein were used to adjust the FP values to 35 mP. 50 flashes per well were done. Each reading was blank corrected (i.e. FP reading from FP buffer only wells were subtracted from other values: ΔFP). The average FP vs. [probe concentration] was plotted using GraphPad Prism, and 12.5 nM probe concentration were chosen to be used in further analysis with the LC3/GABARAP proteins.

Binding experiment for Kd determination were set up mixing 12.5 nM probe with recombinant LC3B and GABARAP proteins (0-200 μM) in technical triplicates. Expression and purification of LC3B and GABARAP proteins were explained above. The plate was centrifuged at 500 g for 10 seconds and incubated in the dark at room temperature to reach an binding equilibrium before FP measurement. Then, the ΔFP values were calculated as above and plotted against protein concentration. Kd values were calculated by performing a nonlinear regression analysis (one-site total binding model) using GraphPad.

2.13. Co-immunoprecipitation (Co-IP) experiments

GFP–Trap (ChromoTek, #gta-20) was used to pull-down tagged GFP–tagged proteins. HA-tagged magnetic Dynabeads (Thermo Scientific, #88837) were used to pull-down HA-β-catenin proteins. A quantity of 400 μg of whole cell lysate was used per condition and treated according to manufacturer's instructions. Bound and unbound protein was assessed by western blotting.

2.14. TOP/FOPflash luciferase and GFP-reporter assays

All luciferase assays were carried out in flat bottom 96-well plates with technical duplicates. HEK293 WT or ATG7 KO cells were used for this analysis. Luciferase reporter assay constructs (2 ng ptkRL, 10 ng TOP/FOPflash topped up to 50 ng with a vector lacking a mammalian promoter) were co-transfected with or without another plasmid (10 ng) shown in the figure legends using Lipofectamine 3000. After 24 h of the transfections, cells were treated as depicted in the figure legends. Luciferase activity was determined using a dual-luciferase

reporter system (Promega, #E1910) according to manufacturer's instructions. Luciferase signals were measured into Beckman Paradigm Multi-Mode SpectraMax Microplate Reader.

GFP-reporter assay was carried out using the GFP-reporter HEK293 cells which are generated as explained above. These cells were seeded in 12-well plates. After 24 h, they were treated and/or transfected with mCherry-LC3B/GABARAP plasmids (0.1 µg/well) as depicted in the figure legends. To measure the fluorescence signal produced, the cells were trypsinized and analysed using a BD Symphony A5 and FlowJo™ v10.8 software (BD Biosciences). GFP fluorescence was excited by the blue laser and measured through a 530/30-nm band pass filter. MCherry signal was excited by the green laser and measured through a 582/30-nm pass filter. A FSC (forward scatter) versus SSC (size scatter) gate was used to discriminate single cells and the median GFP-A value. At least 10,000 events per condition was measured and quantified for fluorescence signal.

2.15. Statistical analysis and significance

Where indicated, Prism (v 8.0.2) was used for statistical analysis of student t-test, or ANOVA test with experimental values post-hoc. Data values are all biological distinct replicates, unless specified. As indicated; (*** = $p>0.001$, ** = $p>0.01$, * = $p>0.05$, or n.s. = not significant). Error bars represent standard error of the mean (SEM) of the indicated number of biological replicates. In general, the SEM represent a minimum of three biological replicates unless otherwise stated. The formula for z-score calculation is $z = (x-\mu)/\sigma$, where x is the raw score, μ is the population mean, and σ is the population standard deviation. For all experiments, the number of biological replicates (n) is stated clearly in the figure legend of each figure.

3. Results: Identification of new autophagy substrates by proteomics

Dissecting autophagy from proteomics perspective has become a natural interest in many studies. This chapter mainly aims to create the basis for understanding the functions of autophagy through studying the composition of autophagosomes. Therefore, it is aimed to establish a robust method to purify autophagosomes from cancer cells and analyse their composition using proteomics as a proof-of-principle study. The methodology described in this chapter has the potential to identify novel autophagy receptors in addition to cancer-specific substrate proteins and suggest vulnerabilities that could be exploited therapeutically in follow-up studies. The four main objectives were:

1- To analyse whole-cell proteome of autophagy-competent and -incompetent cells to create a comparative panel for the isolated autophagosomes

2- To establish a robust method for isolating autophagosomes

3- To profile autophagosomal constituents using proteomics

4- To study candidate proteins as an autophagy substrate/regulator from the proteomics analysis

5- To study applicability of the established method to mice tissue samples

3.1. Whole-cell proteome of autophagy-competent and -incompetent cells

Whole-cell proteomics analysis in the settings of autophagy inhibition can provide a holistic picture of how autophagy affects cellular proteostasis. This approach can allow identification of proteins targeted to autophagic degradation as their level will be increased in the cells with defective autophagy. For that purpose, wild-type (WT) and autophagy-incompetent HeLa cells were used to identify the autophagy substrates in a comparative manner (Fig 3.1). Additionally, the UPS and autophagy are interconnected, and inhibition of one system was shown to affect the other[372], which could hinder detection of autophagy targets. Therefore, to prevent compensation for the absent autophagic degradation by the UPS, all cells, including WT HeLa cells, were treated with a proteasome inhibitor (Velcade; 100 nM for 4 h) (Fig 3.1A). Accumulation of β-catenin, a known substrate of proteasomal degradation, in the cells confirmed inhibition of the proteasome upon Velcade treatment (Fig 3.1A). Staining for

endogenous β-catenin (red) was increased in all the cells at a similar level with the inhibition of the proteasomal pathway. In addition, autophagic activity of the cells was tested using the lysosomal V-ATPase inhibitor, Baf A_1 (Fig 3.1A). Only the WT HeLa cells have shown accumulation of autophagosomes (LC3B dots, green) in their cytoplasm, which suggests presence of an ongoing basal autophagy in these cells but not in any of the other *ATG*-KO cells (Fig 1A). Moreover, decrease in the p62 level and increase in the LC3B turnover (the second lower MW size band building in the LC3B blot) upon amino acid starvation (autophagy inducer) showed active autophagy ongoing in the WT HeLa cells, while there was no change in the autophagy deficient cells (Fig 3.1B and 3.1C). Also, the absence of the ATG proteins was confirmed by immunoblotting (Fig 3.1B and 3.1C). Of note, absence of all six isoforms of the *ATG8* genes (*LC3A/B/C* and *GABARAP/L1/L2*) in Hexa KO cells were previously confirmed by Nguyen *et. al.,*[202] and in this study only the absence of LC3B and GABARAP was shown (Fig 3.1A and 3.1B).

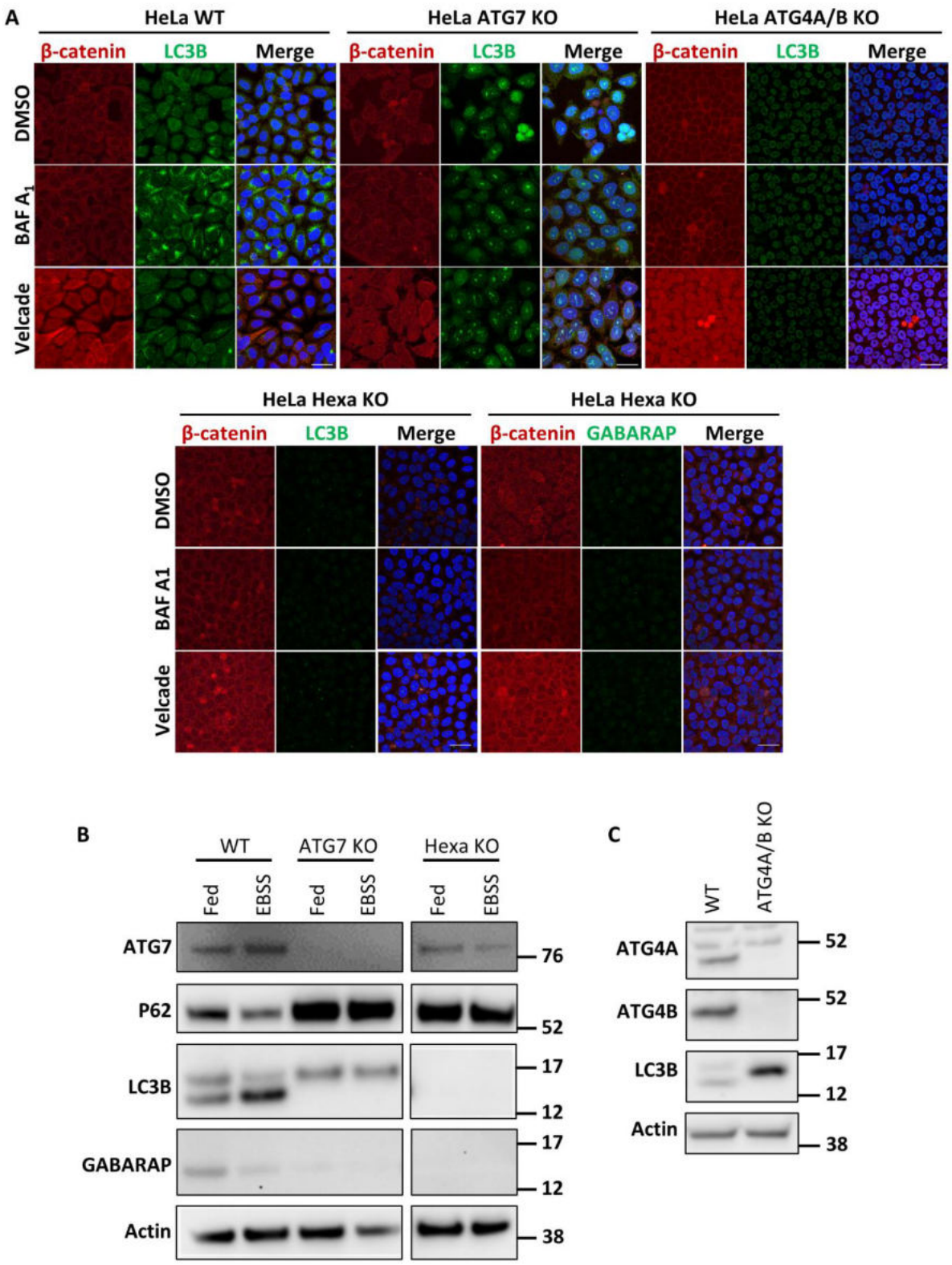

Figure 3.1 Validation of autophagy-incompetent cells and proteasome inhibition. **(A)** Indirect immunofluorescence analysis of HeLa WT, *ATG7* KO, *ATG4A/B* KO, and Hexa KO (*LC3A/B/C*, *GABARAP/L1/L2*) cells under confocal microscopy. HeLa cells were treated with Baf A_1 (200nM, 4 h) or Velcade (100 nM, 4 h) and co-stained with antibodies against β-catenin (red) and LC3B (green) or GABARAP (green). DMSO treatment (4 h) was used as a vehicle control. DAPI staining was used to mark the nuclei (blue), scale bar = 25 μm. Single-channel

DAPI staining was not shown. **(B)** Immunoblots for ATG7, p62, LC3B, and GABARAP from HeLa WT, *ATG7* KO, and Hexa KO cells in the presence of serum (Fed), or amino acid starved (EBSS, 4 h). **(C)** Immunoblots for ATG4A, ATG4B, and LC3B from HeLa WT and ATG4A/B KO cells. Actin was used as a loading control in immunoblot analysis.

To facilitate quantitative identification of autophagy substrates, proteome content of the cell lysates from HeLa cells treated with Velcade were analysed using TMT-based proteomics (Fig 3.2A). The TMT profiling of the cell lysates resulted in the quantification of >8000 proteins. The identified proteins were then visualized with a heat map and clustered using the k-means algorithm, which allows to find meaningful groups in the data (Fig 3.2B). The heatmap clustering showed that each *ATG* KO cell lines had their own set of proteins specifically increased in their cell lysate. According to k-means clustering, group 1 represents *ATG7* KO-specific increase, group 2 represents Hexa KO-specific increase, and group 4 represents *ATG4A/B* KO-specific increase (Fig 3.2B). In addition, proteins in KO cells commonly decreased or increased compared to WT cells were clustered in group 3 and group 5, respectively.

To systematically examine the autophagy proteins in this hit list, the average change in the protein abundance in the KO cells was plotted against WT cells; then the autophagy receptors (SQSTM1, TAX1BP1, NBR1, CALCOCO2, OPTN, and Tollip) were located in the graph (Fig 3.2C). Almost all of the receptors (with the exception of OPTN) were increased in the KO cells commonly. Also, all of the increased receptors were clustered in the group 5, which suggests that group 5 provides a better image of autophagy target proteins. To gain greater insight into the proteins in the group 5, gene annotation analysis was used. It showed that RNA-binding proteins, involved in translation, gene expression, mRNA processing, and ribosome biogenesis, were enriched in this group (Fig 3.2D). In addition, many genes were annotated for autophagy-related processes with significant p-values such as regulation of autophagy (number of genes: 67, p values: 7.82E-07), macroautophagy (number of genes: 38, p values: 1.23E-04), and selective autophagy (number of genes: 17, p values: 0.0109). On the other hand, all of the identified proteins were grouped into three categories (1. ATG8 proteins, 2. SARs, and 3. autophagy regulators) in order to observe their change in the autophagy gene KO cells (Fig 3.2E). As expected, LC3/GABARAP, ATG4, and ATG7 proteins were absent in the respective KO cells, and all of the SARs were commonly increased in these cells. Surprisingly, only GAPARAPL2 was increased in *ATG7* and *ATG4A/B* KO cells, but LC3B, GABARAP, and GABARAPL1 levels showed no change or decrease compared to WT cells. This might suggest that GABARAPL2 is the main driver of the autophagosome formation in

HeLa cells amongst other LC3/GABARAP proteins. Moreover, autophagy regulators (ATG proteins) did not show a dramatic change in general, except for ATG4C, which was elevated in all KO cells studied.

Overall, these results suggest that whole-cell comparative proteomics cannot distinguish proteins those levels changed with autophagy inhibition from proteins those levels that may be changed due to autophagy-independent roles of each ATG proteins. Even though comparing more than one *ATG* KO cells allowed clustering into subgroups, such as group 5, representing a better image of autophagy-related proteins, the whole-cell analysis may not be enough to distinguish proteins directly targeted by autophagy. Therefore, in this study, I aimed to identify autophagy target proteins by analysing autophagosomes purified from the rest of the cell lysate.

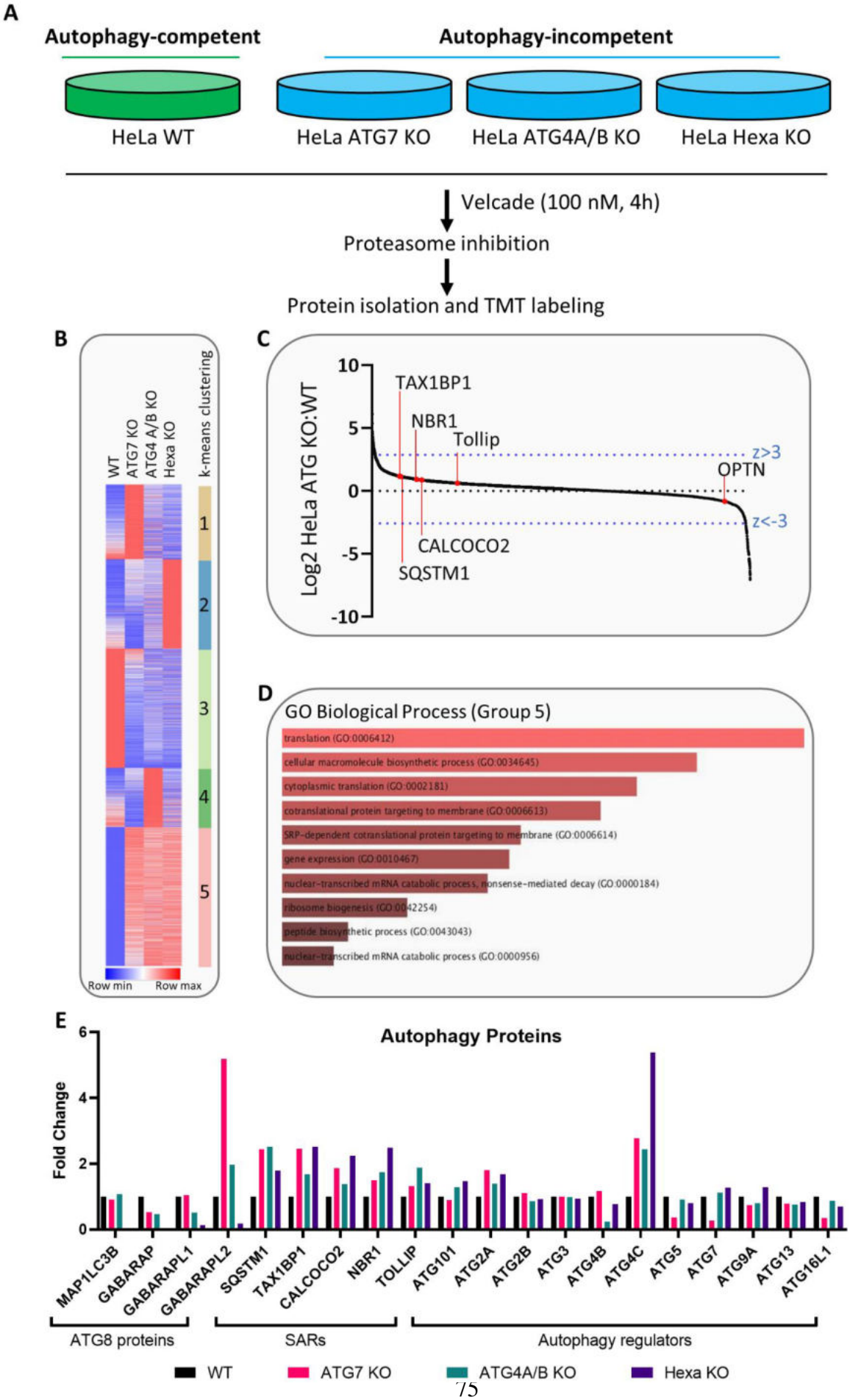
A
Autophagy-competent
Autophagy-incompetent
HeLa WT
HeLa ATG7 KO
HeLa ATG4A/B KO
HeLa Hexa KO
Velcade (100 nM, 4h)
Proteasome inhibition
Protein isolation and TMT labeling
B
WT
ATG7 KO
ATG4 A/B KO
Hexa KO
k-means clustering
1
2
3
4
5
Row min
Row max
C
Log2 HeLa ATG KO:WT
10
5
0
-5
-10
TAX1BP1
NBR1
Tollip
z>3
OPTN
z<-3
CALCOCO2
SQSTM1
D
GO Biological Process (Group 5)
translation (GO:0006412)
cellular macromolecule biosynthetic process (GO:0034645)
cytoplasmic translation (GO:0002181)
cotranslational protein targeting to membrane (GO:0006613)
SRP-dependent cotranslational protein targeting to membrane (GO:0006614)
gene expression (GO:0010467)
nuclear-transcribed mRNA catabolic process, nonsense-mediated decay (GO:0000184)
ribosome biogenesis (GO:0042254)
peptide biosynthetic process (GO:0043043)
nuclear-transcribed mRNA catabolic process (GO:0000956)
E
Autophagy Proteins
Fold Change
6
4
2
0
MAP1LC3B
GABARAP
GABARAPL1
GABARAPL2
SQSTM1
TAX1BP1
CALCOCO2
NBR1
TOLLIP
ATG101
ATG2A
ATG2B
ATG3
ATG4B
ATG4C
ATG5
ATG7
ATG9A
ATG13
ATG16L1
ATG8 proteins
SARs
Autophagy regulators
WT
ATG7 KO
ATG4A/B KO
Hexa KO

Figure 3.2 Quantitative analysis of the autophagy substrates. **(A)** Scheme for tandem mass tagging (TMT)-based proteomics of cell extracts from HeLa WT, *ATG7* KO, *ATG4A/B* KO, and Hexa KO treated with 100 nM Velcade for 4 h. **(B)** Heat map showing the log(fold-changes) of cellular proteome after 4 h exposure to Velcade treatment of HeLa cells. Fold changes (FC) in HeLa *ATG7* KO, *ATG4A/B* KO, and Hexa KO cells were calculated versus the HeLa WT. The data were clustered into 5 groups based on the k-means clustering algorithm. Group 5 represents proteins enriched commonly in all the *ATG* KO cells. The heat map analysis and k-means clustering were done using the web-based Phantasus tool (version 1.17.4). The color scale ranges from red to blue which respectively denotes the up-or down-regulated of the genes. The data shown are representative of n=1, with no biological replicates. **(C)** Plot of means of Log2 FC for proteins identified in the proteomics analysis. Means were calculated from the average FC in the HeLa ATG KO cells for each gene. Selective autophagy receptors were marked on the plot. Calculated z-score lines for the data set above and under 3 were shown as blue dashed lines **(D)** Bar chart showing the proteins from the group 5 cluster for Gene Ontology (GO) terms for Biological Process (BP). **(E)** Bar chart showing FC from proteomics analysis for ATG proteins and SARs in each HeLa cell.

3.2. Establishing an autophagosome isolation method

Having a robust technique for purifying autophagosomes was key to the success of this project. Autophagosomes were purified from cultured cancer cells, such as HCT-116 and HeLa, under conditions fostering formation and retention of autophagosomes (e.g., Baf A_1). Purification was performed by immune isolation using anti-GFP antibodies and density gradients. Purified material was assessed using microscopy (GFP signal, electron microscopy) as well as biochemically (the presence of LC3 and p62). Finally, successful isolation of high quality autophagosomes enabled analysis of their constituents using comparative proteomics.

3.2.1. Immune isolation approach

Autophagosomes are double-membraned vesicles with LC3/GABARAP proteins anchored at their surface. The principle of the immune isolation method consists in capturing these organelles using the LC3B proteins. To show the proof of principle, I decided to focus on capturing substrates of basal, steady-state autophagy. However, to enrich for autophagosomes, cells were supplemented with Baf A_1 which prevents lysosomal fusion of autophagosomes and results in their accumulation. This accumulation (GFP-LC3B dots as autophagosomes) was validated using confocal microscopy in HCT116 GFP-LC3B cells (Fig 3.3A), and by immunoblotting (data not shown). The number of GFP-LC3B dots in the cells was quantified using an image analysis tool Definiens (see methods for analysis parameters). This analysis showed that Baf A_1 treatment facilitated accumulation of significant numbers of autophagosomes in the cells after 2 h; however, one-hour Baf A_1 treatment did not result in a

dramatic change in the number of GFP-LC3B puncta (Fig 3.3B). In the same way, 4 h of Baf A_1 treatment even further increased the number of autophagosomes; however, it also started increasing the size of GFP-LC3B dots observed in the cells (Fig 3.3C). Since this study was set out to determine substrates of basal autophagy, the longer exposure to Baf A_1 might cause some lysosomal damage and change the autophagosomal cargo sequestered. In addition, the size increase could compromise with the density-gradient separation methods which will be practised later in this study. Therefore, it is decided to avoid longer Baf A_1 treatments, and for its coherence 2 h treatment used in the rest of the study.

For the immune isolation of autophagosomes, HCT116 GFP-LC3B cells treated with Baf A_1 were initially used as a source of autophagosomes, and the protocol is described in Figure 3.4A (see methods for detailed protocol). Briefly, cell homogenate was prepared in an isotonic sucrose buffer which allows organelles to preserve their integrity. Later, the nuclear fraction of the homogenate was removed by centrifugation. Next, the post-nuclear homogenate was centrifuged again. The resulting pellet (organelle fraction) was then resuspended in the same isotonic sucrose buffer and incubated with anti-GFP antibody coated magnetic microbeads (µMACS). The mixture of organelle-bead was then run through a column under magnetic field to separate autophagosomes from other organelles. After several washes, the autophagosome fraction was eluted from the column together with the beads for morphological and protein analysis. The sequential centrifugal preparation of post-nuclear and post-cytoplasmic fractions was monitored using Lamin B1 (nuclear marker) and GAPDH (cytosolic marker). Both Lamin B1 and GAPDH levels were reduced in the organelle fraction (Fig 3.4B). In addition, the presence of autophagosomal proteins GFP-LC3B, endogenous LC3B, and p62/SQSTM1 was assessed in each fraction. It is important to note that only the processed and lipidated form of LC3 proteins (LC3-II) incorporates onto the autophagosomal membrane. Therefore, LC3-II proteins, not LC3-I, in the organelle fraction could be mainly observed, which suggests the presence of autophagosomes (Fig 3.3B). Moreover, the efficiency of the µMACS magnetic microbeads used to capture autophagosomes was assessed in comparison to other commercial magnetic beads (Fig 3.3C). For comparison, autophagosomes were enriched in the same number of cells using BAF A_1 (Fig 3.3C). And then, the organelle fraction was prepared, as mentioned earlier, and incubated with the same volume of the µMACS, MBL, or GFP-trap magnetic beads. Results showed that the µMACS microbeads captured the autophagosome proteins (GFP-LC3B, LC3B, and p62) more efficiently than other magnetic beads, and therefore it was chosen to be used for the rest of the study (Fig 3.3C).

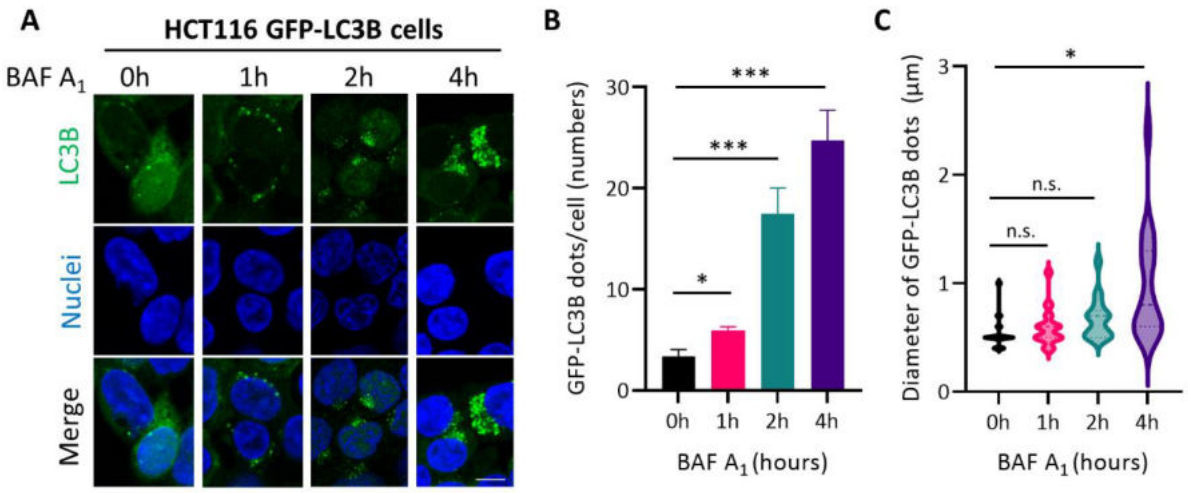

Figure 3.3 Characterization of autophagosome formation in response to Baf A1 treatment. **(A)** Immunofluorescence analysis of GFP-LC3B expressing HCT116 cells. The cells were either mock-treated (0 h) or treated with 200 nM Baf A_1 for 1-4 h before fixation. DAPI staining was used to mark the nuclei (blue), scale bar = 10 µm. **(B, C)** Quantification by image analysis of the number and diameter of GFP-LC3B dots per cell of HCT116 GFP-LC3B cells mock-treated or Baf A_1 treated for 1-4 h. The number and diameter of the GFP-LC3B dots were analyzed using Definiens Tissue Studio. At least 200 cells were analyzed for each data point corresponding to >3 independent experiments. Data in B are mean ± SD from >3 independent experiments. Statistical significance was assessed using ANOVA (with Post Hoc) analysis (*p<0.05, and ***p < 0.001 as compared to cells at 0 h, non-significant (n.s.)).

This study aimed to examine substrates inside the autophagosomes along with the proteins on the autophagosome membrane. Therefore, it was intended to isolate completely sealed, nascent autophagosomes. For that purpose, presence of intact autophagosomes in the immune isolation eluate was interrogated using the protease protection assay (Fig 3.4D). In this assay, proteins enclosed in membranous organelles will be protected from the degradation caused by protease (*i.e.,* proteinase K) treatment, as the protease cannot penetrate thorough biological membranes. However, upon addition of a detergent, such as Tx-100, all of the proteins will be exposed to protease and undergo degradation (Fig 3.4D). In the same experimental context, the protease protection of GFP-LC3B (inside and on the membrane of autophagosomes) and p62 (inside the autophagosomes) in the immune-eluates from DMSO- or Baf A_1-treated cells were assessed. Even though the amount of p62 and GFP-LC3B proteins were enriched in the Baf A_1 eluate compared to DMSO samples, contrary to expectations, there was no protease protection of these proteins, suggesting that the immune-eluates consisted of compromised autophagosomes (Fig 3.5E).

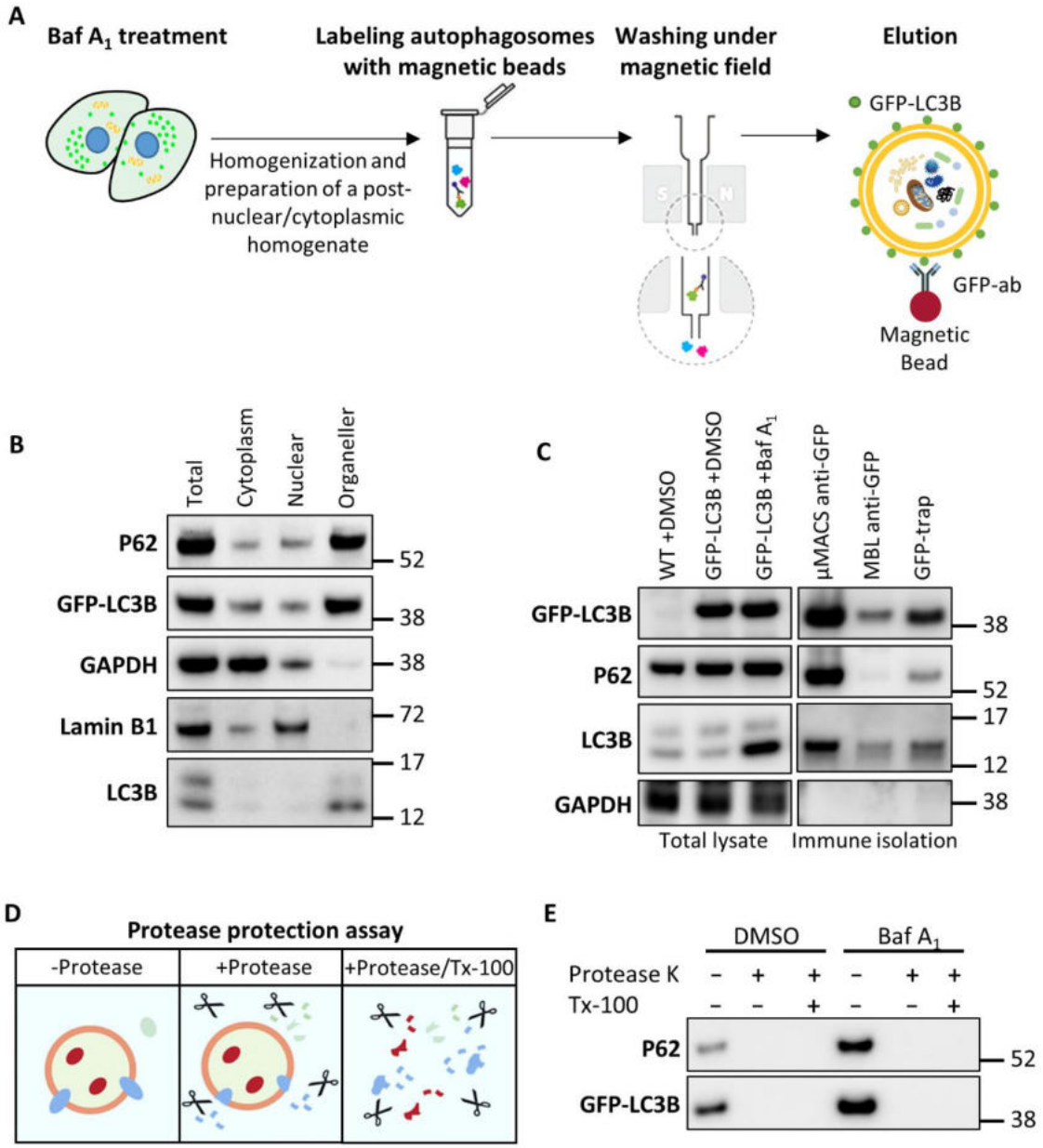

Figure 3.4 Immune isolation of autophagosomes from HCT116 GFP-LC3B cells. **(A)** Scheme depicting major steps in the immune isolation approach employed to purify autophagosomes from cell homogenate using GFP antibody-conjugated (GFP ab) magnetic beads. **(B)** Centrifugal separation of cytoplasm, nuclear, and organellar fractions from the total homogenate. Immunoblots for GFP-LC3B, p62, and LC3B represent the organellar fraction, including autophagosomes. GAPDH represents the cytoplasmic fraction, and Lamin B1 represents a nuclear fraction from HCT116 GFP-LC3B cells. The organellar fraction was later subjected to immune isolation of autophagosomes. **(C)** Immune-isolation efficiency of different GFP antibody-conjugated magnetic beads. Immunoblots on the left represent changes in the GFP-LC3B, p62, LC3B, and GAPDH in the total lysates of HCT116 WT and HCT116 GFP-LC3B cells treated with DMSO or 200 nM Baf A_1 for 2 h. Immunoblots on the right represent the immune efficiency of three different magnetic beads. The organelle fraction from HCT116 GFP-LC3B cells treated with Baf A_1 for 2 h was subjected to immune isolation with three different magnetic bead preparations. Of note, only µMACS beads were run through an LS column as shown in A. The rest of the beads was collected using a magnetic separator in a

tube. The data shown are representative of n=1, with no biological replicates. **(D)** An illustration for protease protection assay. The proteins inside a membrane-enclosed organelle are protected from degradation by the protease as shown in the middle panel. A detailed protocol can be found in methods **(E)** Immunoblots for the protease protection assay were done with immune-isolated autophagosomes (eluates) from HCT116 GFP-LC3B cells treated with DMSO or 200 nM Baf A_1 for 2 h. The data shown are representative of n=2 independent experiments.

ATG4 is a cysteine protease with an essential function in autophagosome formation. It cleaves the C-terminus of the nascent LC3/GABARAP proteins to expose their conserved glycine residue (G120 for LC3B), which further facilitates their conjugation onto the autophagosome membrane as a result of series of ubiquitin-like reactions[373]. On the other hand, ATG4 also functions as a deconjugating enzyme that catalyses breakage of the amide-bond between LC3/GABARAP proteins and PE once the autophagosome is fully sealed[373]. This deconjugating activity of ATG4 releases LC3/GABARAP proteins from the surface of autophagosomes and allows their recycling. This dual function of ATG4 is shown in Figure 3.5A. Of note, ATG4B is the main isoform of ATG4 proteins in HeLa cells[373].

To produce autophagosomes with more GFP-LC3B on their surface with an intent of enhancing their affinity against GFP-magnetic beads, ATG4-deconjugation activity should be avoided. For that purpose, *ATG4B* KO HeLa cells expressing a pre-cleaved GFP-LC3B (GFP-LC3B-G120, as it does not require ATG4 cleavage activity) were used for immune isolation of autophagosomes (Fig 3.5B). In addition, *ATG4B* KO HeLa cells with conjugation-deficient GFP-LC3B-G120A expression, which cannot produce autophagosomes, were used as a negative control for the isolation (Fig 3.5C). First, the accumulation of autophagosomes with Baf A_1 was confirmed in HeLa *ATG4B* KO GFP-LC3B-G120 cells (hereafter simply HeLa G120) under confocal microscopy (Fig 3.5D). Similar to HCT116 cells, 2 h of Baf A_1 treatment caused accumulation of a large number of autophagosomes in the cells and stimulated an increase in the size of GFP-LC3B dots with the 4^{th} h of Baf A_1 exposure (Fig 3.5E and 3.5F). Moreover, HeLa *ATG4B* KO GFP-LC3B-G120A cells (hereafter simply HeLa G120A) has shown no response to Baf A_1 treatment, which confirms lack of autophagosome formation in these cells (Fig 3.5G). Following these validations, HeLa G120 cells treated with DMSO or Baf A_1 for 2 h along with HeLa G120A cells, as a negative control, were used to immune isolate autophagosomes as explained previously (Fig 3.4A). Subsequently, the immune-eluates were subjected to the protease protection assay (Fig 3.5H). Immune-eluate from HeLa G120 cells treated with Baf A_1 showed protection for GFP-LC3B and p62 proteins, which was

abrogated by Tx-100 addition. This result gives evidence for the presence of some membrane-enclosed organelles in the isolation, which are likely to be autophagosomes. However, there was no detectable protection in the eluate obtained from DMSO-treated HeLa G120 cells, suggesting Baf A_1 treatment is required for efficient autophagosome isolation. Also, the immune-eluate from HeLa G120A cells showed only a trace amount of GFP-LC3B binding, which did not bring along p62 or LC3B proteins (Fig 3.5H). These results suggest that inactivating ATG4B-mediated deconjugation system in the cells increases the chances of capturing intact autophagosomes by GFP-magnetic beads.

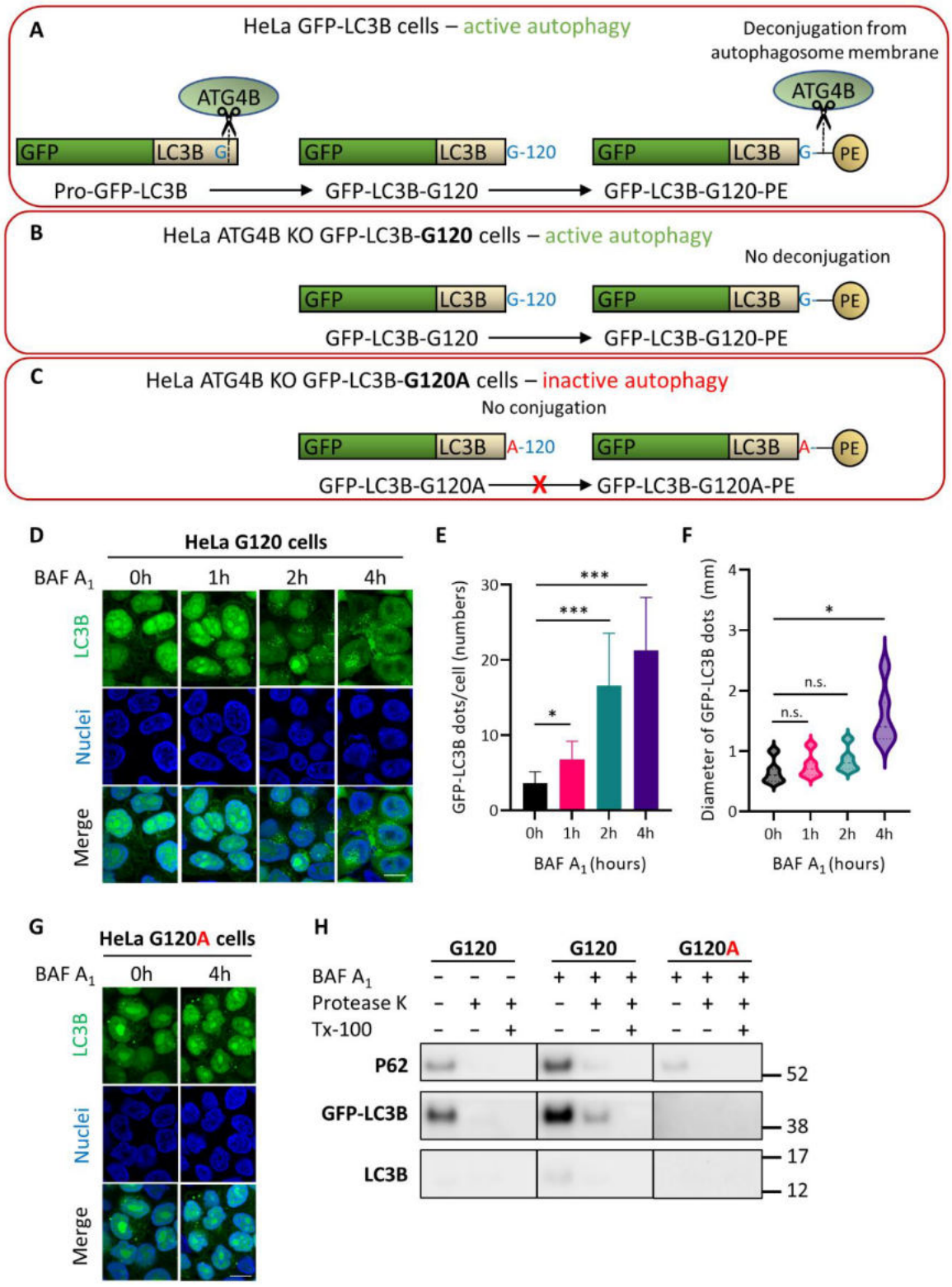

Figure 3.5 Immune isolation of autophagosomes from HeLa ATG4B KO GFP-LC3B-G120 cells. **(A)** A scheme depicting LC3 processing in the HeLa GFP-LC3B cells. Endogenous ATG4 proteins cleave GFP-LC3B from its C-terminus, and later the membrane-conjugated GFP-LC3B proteins were trimmed off from the outer surface of autophagosomes through the action of ATG4 proteases. **(B)** A scheme depicting LC3 processing in the HeLa ATG4B KO GFP-LC3B-G120 cells. GFP-LC3B-G120 proteins are pre-cleaved, thus do not require ATG4

cleavage activity, and allow autophagosome formation in these cells. Of note, since there is no ATG4B in these cells, deconjugation of GFP-LC3B-G120 proteins from the outer autophagosome membrane is halted. **(C)** A scheme depicting LC3 processing in the HeLa ATG4B KO GFP-LC3B-G120A cells. These cells cannot perform autophagy, as GFP-LC3-G120A cannot be conjugated to the autophagosomal membranes. **(D)** Immunofluorescence analysis of HeLa ATG4B KO GFP-LC3B-G120 cells (simply HeLa G120). The cells were either mock-treated (0 h) or treated with 200 nM Baf A_1 for 1-4 h before fixation. DAPI staining was used to mark the nuclei (blue), scale bar = 10 μm. **(E, F)** Quantification by image analysis of the number and diameter of GFP-LC3B dots per cell of mock-treated or 200 nM Baf A_1 treated for 1-4 h. The number and diameter of the GFP-LC3B dots were analyzed using Definiens Tissue Studio. At least 200 cells were analyzed for each data point corresponding to >3 independent experiments. Data in E are mean ± SD from >3 independent experiments. Statistical significance was assessed using ANOVA (with Post Hoc) analysis (*$p<0.05$, and ***$p < 0.001$ as compared to cells at 0 h, non-significant (n.s.)). **(G)** Immunofluorescence analysis of HeLa ATG4B KO GFP-LC3B-G120A cells (simply HeLa G120A). The cells were either mock-treated (0h) or treated with 200 nM Baf A_1 for 4 h before fixation. DAPI staining was used to mark the nuclei (blue), scale bar = 10 μm. **(H)** Immunoblots for the protease protection assay were prepared with immune-isolated autophagosomes (eluates) from HeLa G120 and G120A cells treated with DMSO or 200 nM Baf A_1 for 2 h. HeLa G120A cells treated with Baf A_1 were used as a negative control for the immune isolation of autophagosomes. The data shown are representative of $n<3$ independent experiment.

In addition to the protease protection assay, another way to check the presence of intact autophagosomes in the isolation is Electron Microscopy (EM), which remains the gold standard for the characterisation of morphology of intracellular organelles. Immune-eluates obtained from Baf A_1 treated HCT116 (Fig 3.6A) and HeLa cells (Fig 3.6B) were visualized under TEM. The results, as shown in Figure 3.6, indicate that there are many autophagosome-like double membranes (arrows) in both HCT116 GFP-LC3B and HeLa G120 isolations. However, majority of these membranes were ruptured. There were only a few intact autophagosome-like vesicles detected in these isolations. Moreover, the observed membranes could also be derived from other organelles. However, the HCT116 WT cells showed no membrane in the TEM images but the magnetic beads (small black dots, Fig 3.6A). Also, HeLa G120A cells showed a very limited number of membrane (Fig 3.6B). These results can be inferred as the membranes appeared in the HCT116 GFP-LC3B and HeLa G120 isolations should be presenting GFP-LC3B proteins on them, thereby they may belong to autophagosomes.

Even though inhibiting the ATG4 deconjugation activity seems to bring more autophagosome-like membranes in the HeLa G120 isolation compared to HCT116 GFP-LC3B isolation (Fig 3.6), it did not provide a sufficient improvement to the analysis of autophagosomal contents, as it was probably compromised due to disintegrated membranes. It is important to note that the physical (mechanical) forms of cell disruption methodologies, such

as Nitrogen cavitation and Dounce homogenizer used in this study, can generate many broken membranes along with intact organelles. Regarding that the GFP-magnetic beads might have captured broken autophagosome membranes in the organelle fraction more than intact autophagosomes. Therefore, it can be hypothesized that removal of broken membranes and submitting an intact-autophagosome enriched fraction to purification with the GFP-magnetic beads could improve the outcome of the immune isolation. In this regard, a membrane flotation assay (density gradient separation method) was established to separate autophagosomes from other organelles as well as broken membranes.

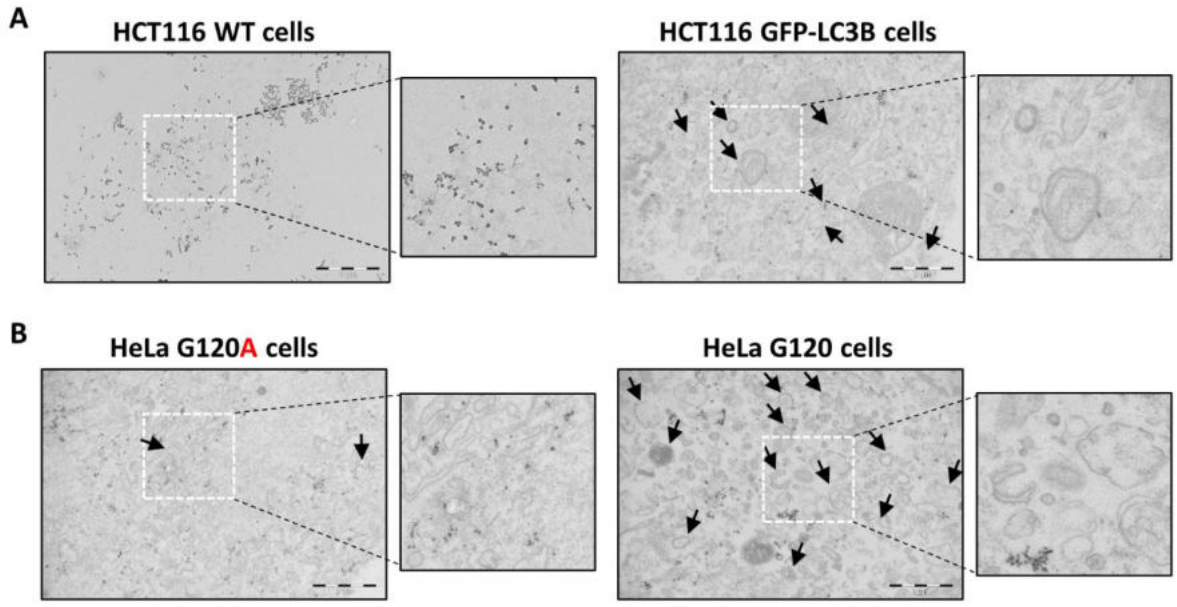

Figure 3.6 Morphology of autophagosome preparations from HCT116 GFP-LC3B and HeLa G120 cells. **(A, B)** Immunoisolated autophagosomes from Baf A_1 treated cells were stained and sectioned for TEM analysis (see methods). HCT116 WT and HeLa G120A cells were used as negative controls. Lower and higher magnification TEM images confirmed the presence of ruptured autophagosome-like double membranes. Arrows in the lower magnification panels point to these double membranes. Scale bar: 1 µm.

3.2.2. Density-gradient separation approach

Density gradient centrifugation (also known as membrane floatation) is a common method for sorting intracellular organelles and large macromolecules. In this technique, organelles float and distribute through a density gradient matrix according to their density, which depends on their content, size, shape, and the lipid:protein ratio[374].

In order to separate autophagosomes from other organelles, organelle fractions were prepared from the HeLa G120 cells treated with DMSO or Baf A_1 and Torin 1 (Tor). Of note,

Baf A_1 plus Tor treatment conferred a better assay gap (*i.e.,* separation from control) than Baf A_1 alone treatment in comparison to DMSO treated samples (data not shown), thus Torin was included in further analysis. Then, the organelle fractions were subjected to flotation analysis using OptiPrep density gradients (see methods for more detail). After ultracentrifugation of the gradients, fractions were collected from the top to the bottom of the gradient and then checked against GFP-LC3B and p62 immunoblot to determine which fractions were enriched in terms of autophagosomes (Fig 3.7A). In addition, the same analysis was also carried out using autophagy-incompetent HeLa G120A cells (Fig 3.7A). Comparative analysis of fractions revealed that autophagy marker proteins GFP-LC3B and p62 accumulate in the factions between 3-6 upon Baf A_1 +Torin treatment (Fig 3.7A and 3.7B). Moreover, these accumulations were not observed in HeLa G120A samples (Fig 3.7A) or HeLa *ATG7* KO cells (data not shown). It is important to note that the denser fractions (11-14) also contained a small amount of GFP-LC3B proteins (Fig 3.7A), which can be considered as unconjugated GFP-LC3B proteins or broken autophagosome membranes. In addition, the same separation was observed in the HCT116 GFP-LC3B cells (Fig 3.7C).

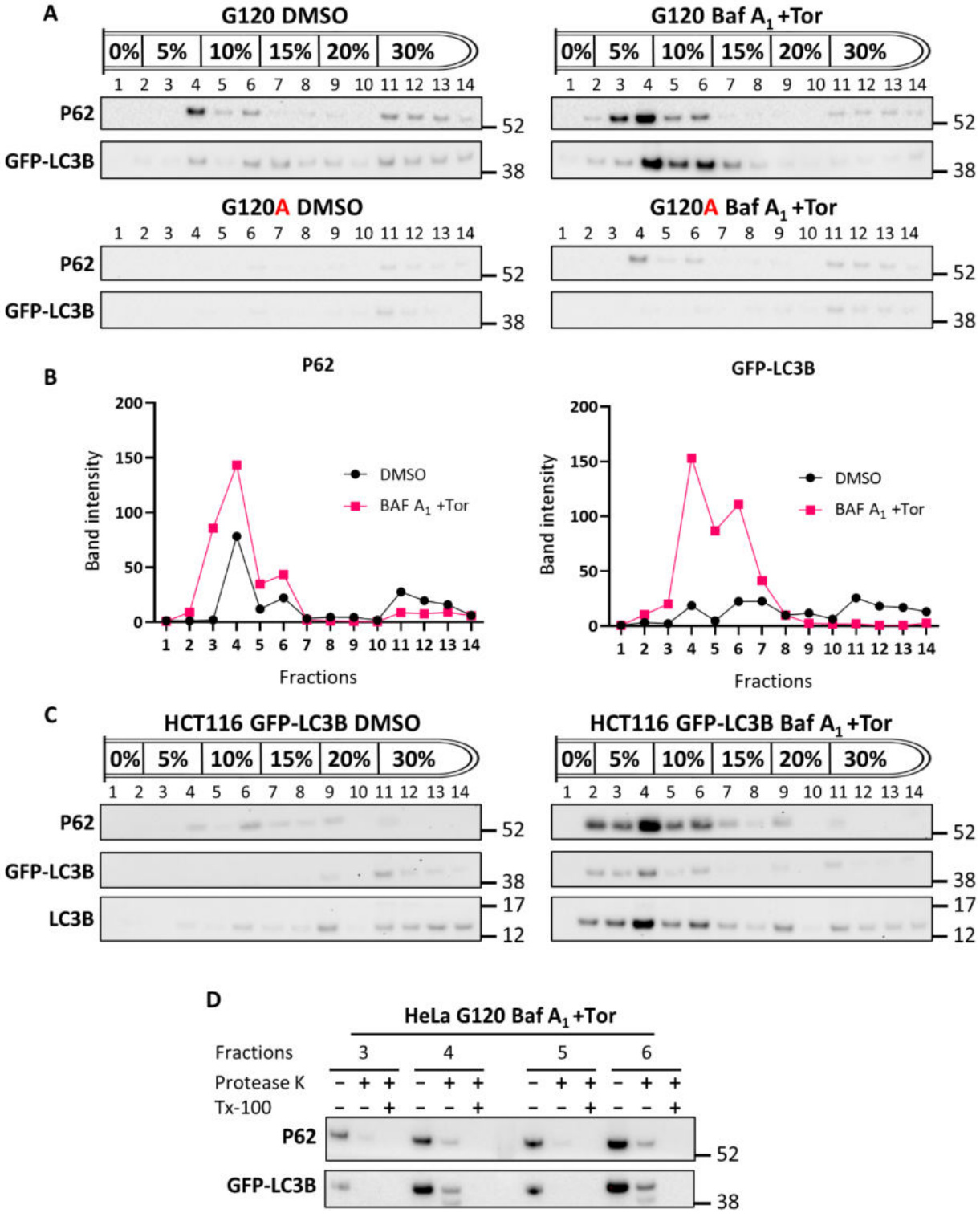

Figure 3.7 Density-gradient fractionation of autophagosomes. **(A)** Organellar fraction from G120 and G120A cells treated with DMSO or co-treated with Baf A_1 (200 nM, 2 h) and Torin 1 (Tor, 250 µM, 2 h) were separately loaded at the bottom of a discontinuous Optiprep density gradient matrix (Optiprep concentrations as indicated). After ultracentrifugation of the gradient, each fraction (14 in total) was collected from the top to the bottom of the gradient. Later, each fraction was analyzed by immunoblotting, representative of n>3 independent experiment. Distribution of the p62 and GFP-LC3B proteins along the fractions was used to determine where the autophagosomes were enriched. **(B)** Graph depicting quantification of

GFP-LC3B and p62 band intensities for 14 fractions from DMSO or Baf A_1 +Torin treated HeLa G120 cells. Quantification of the band intensities was done using Image J. (C) Immunoblots for the fractions from density gradient separation of the organellar fraction of DMSO treated and Baf A_1 +Torin treated HCT116 GFP-LC3B cells. **(D)** Immunoblots for the protease protection assay were done with autophagosome enriched fractions (F3-F6) from Baf A_1 +Torin treated HeLa G120 cells. The data shown are representative of n=2 independent experiments.

Distribution of GFP-LC3B, LC3B, and p62 proteins revealed that flotation profiles of autophagosomes isolated from different cell lines in the density gradient matrix was rather similar. The flotations of autophagosomes from HeLa and HCT116 cells showed only small differences, such as higher accumulation in the fraction 2 in HCT116 cells than in the HeLa cells. In summary, these results indicate that autophagosomes can be enriched in fractions 3-6 using the Optiprep density gradient floatation assay. Next, the integrity of the autophagosomes in these fractions was interrogated via the protease protection assay (Fig 3.7D). The results showed that each fraction consists of various amount of intact autophagosomes, as p62 and GFP-LC3B proteins were protected from degradation.

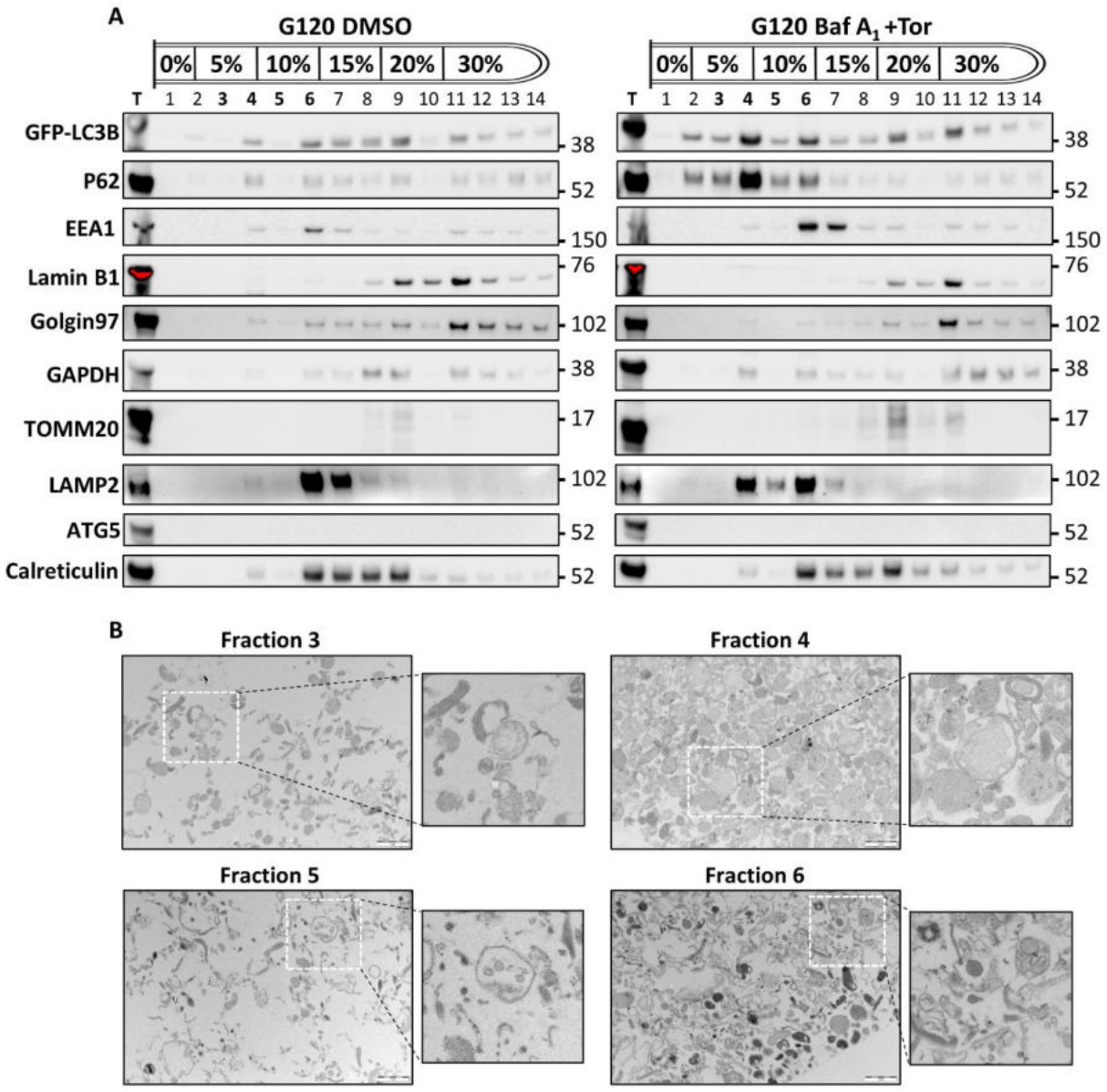

Figure 3.8 Purification of autophagosomes. **(A)** Fractions from density gradient separation were immunoblotted against organelle marker proteins to observe the overall distribution of the intracellular organelles along the fractions. Comparative analysis of DMSO and Baf A_1 +Torin samples was allowed to detect other organelles moving together with autophagosomes in the gradient matrix. **(B)** Autophagosome enriched fractions (F3-F6) from Baf A_1 +Torin treated HeLa G120 cells were stained and sectioned for TEM analysis. Lower and higher magnification TEM images confirmed the presence of many double membraned autophagosomes and single-membraned vesicles in each fraction. Fraction 4 had the highest number of autophagosomes. In fraction 6, some lysosomes (dark vesicles) were observed. Scale bar: 1 μm.

In addition to enrichment of autophagosomes in certain fractions, another aim of the membrane flotation assay was to separate the autophagosomes from other intracellular organelles and macromolecules. To test whether the Optiprep gradient provides a good separation, fractions from DMSO and Baf A_1 +Torin treated samples were blotted against

intracellular organelle marker proteins (Fig 3.8A). Comparison of the distribution of these proteins revealed that EEA1 (endosome marker) and LAMP2 (lysosome marker) were also enriched in the fractions 3-6 along with GFP-LC3B and p62 upon Baf A_1 +Torin treatment. Strikingly, LAMP2 proteins move towards lighter fractions upon Baf A_1 treatment suggesting lysosomal fusion of the autophagosomes. As it was shown previously, short-term Baf A_1 treatment does not completely block lysosomal fusion of autophagosomes but effectively prevents degradation of autophagosome content by changing pH of the lysosomes.

In order to better separate and analyse physical contents of the resulting autophagosome enriched fractions, they were visualised under EM (Fig 3.8B). The double-membrane configuration of the isolated autophagosomes was validated using a rapid fixation negative staining process. However, the density and purity of the autophagosomes varied greatly amongst the fractions. It seemed liked the fraction 4 contained the most abundant and the purist autophagosome portion (Fig 3.8B). In fraction 3 and 5, there was relatively less autophagosomes appearing, which was in accordance with GFP-LC3B and p62 levels as assayed by immunoblotting (Fig 3.7A, 3.8A, and 3.8B). Moreover, fraction 6 contained lysosomes (dark vesicles) in addition to autophagosomes (Fig 3.8B). Even though many of the vesicles observed in these fractions showed the typical *in situ* ultrastructures of autophagic organelles, a morphological heterogeneity among these vesicles was observed. These results showed that, although the preparation was essentially enriched for autophagosomes and free of rigid organelles, such as mitochondria and nucleus, it was clear that an additional purification step was required to separate the autophagosomes from other vesicular/membranous elements.

3.2.3. Combined approach

Combination of the density gradient approach with an immune isolation method can provide several key advantages over using these approaches on their own. From an immune isolation perspective, subjecting the autophagosome-enriched fractions to the immune isolation instead of the total organelle fraction could improve final purity as well as generate a preparation free of broken membranes. From a density gradient fractionation perspective, an additional purification step such as immune isolation could improve purity and help separate autophagosomes from other non-autophagic vesicles. In addition, the Optiprep gradient matrix used in the fractionation approach was found to interfere with the efficiency of proteomics sample preparation protocol (i.e., reducing efficiency of trypsin cleavage and TMT labelling).

Thus, proteomics analysis of the autophagosomes can favour removal of Optiprep matrix with an additional immune isolation step.

To achieve a combinatorial approach, organelle fractions were prepared again from HeLa G120 cells and processed by density gradient separation. Next, fractions enriched in autophagosomes (3 to 6) were combined and mixed with the GFP-magnetic beads. Then, autophagosomes were immune-isolated from this mixture (see material methods). To assess isolation efficiency of this approach, GFP-LC3B and p62 proteins were tracked in each step of the purification protocol (Fig 3.9A). The results showed that majority of the GFP-LC3B and p62 proteins was captured in the column, and thus there were only scarce amounts of them in the flow-through (Fig 3.9A). To interrogate the presence of intact autophagosomes in this combined approach, the protease protection assay was used. Protection of GFP-LC3B and p62 showed the presence of intact autophagosomes in the combined preparation (Fig 3.9B, 9C, 9D). In addition, the autophagosome preparation was observed under confocal microscopy in the setting of protease protection assay (Fig 3.9E). Under microscopy, the preparation showed a GFP background and green dots, which are assumed to be autophagosomes. Upon treatment of the preparation with the Proteinase K, the green background disappeared, green dots, however, were protected from degradation which shows that they were protected from degradation. As expected, addition of Tx-100 to the Proteinase K abolished almost all the green signal in the preparation. Together with these results, it is concluded that the combined approach has achieved isolation of intact autophagosomes. Furthermore, the preparation was visualized under EM (Fig 3.9F). The EM images showed that preparation from HeLa G120A cells contain no membranous structure or vesicles, but the magnetic beads (black dots). However, preparation from HeLa G120 cells shows many vesicles specifically surrounded by the magnetic beads (black dots). Even though many of these vesicles showed the known double-membrane configuration of the autophagosomes, some of them were observed to contain single membranes. Nevertheless, each of these vesicles was surrounded by the GFP-magnetic beads, which confirms the presence of GFP-LC3B on their surface as a proof of being autophagosome. All these results led suggest that the combined approach facilitates highly pure and selective isolation of autophagic vesicles from HeLa G120 cells. Therefore, these results sufficient to proceed with analysis of the proteome content of the isolated autophagosomes with mass spectrometry.

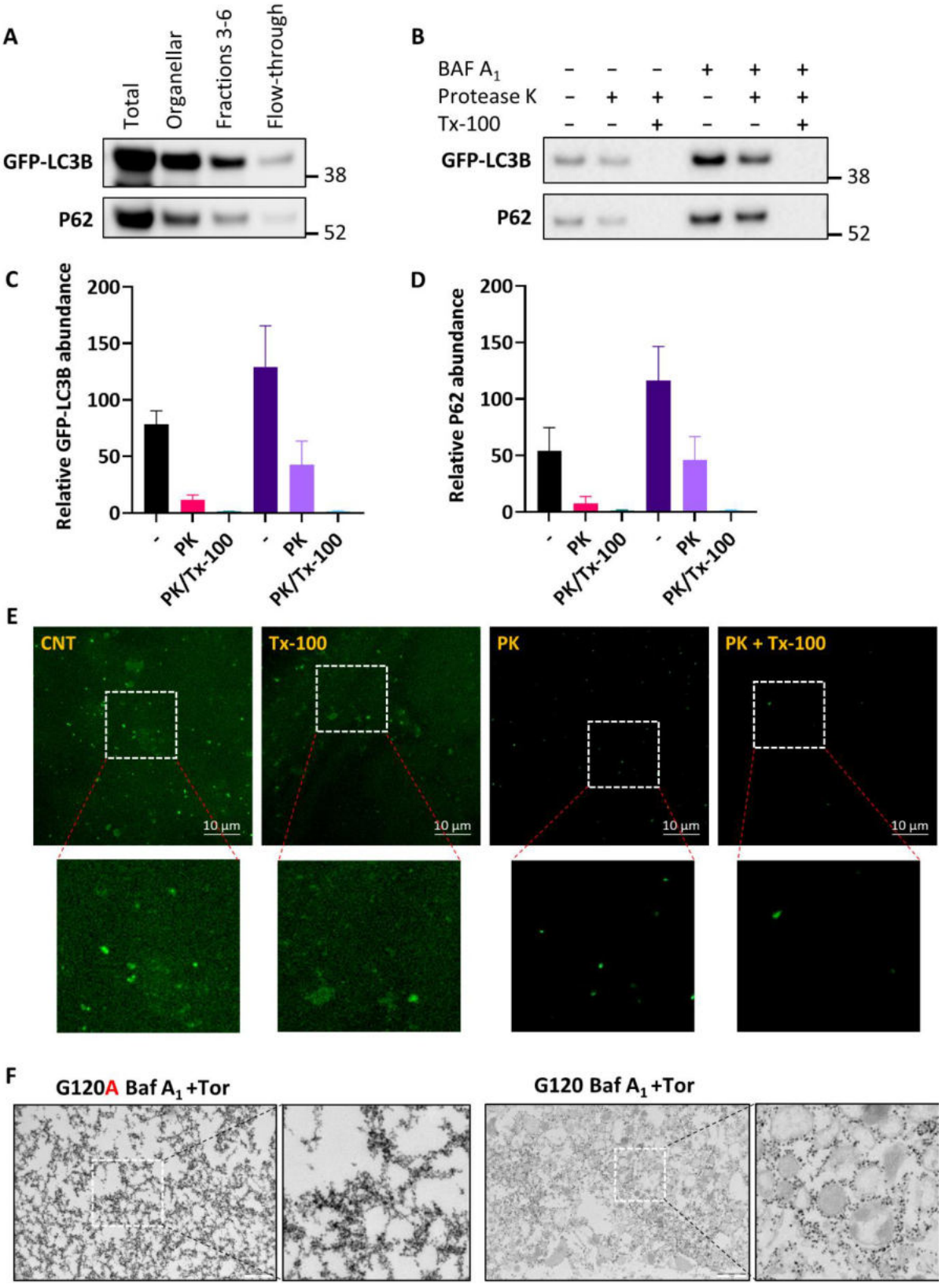

Figure 3.9 Isolation of autophagosomes using an approach combining density gradient and immune isolation. **(A)** In the combined approach, autophagosomes were first enriched in fractions 3-6 using density gradient separation. Then, these fractions were combined and subjected to the immune isolation protocol. Immunoblots for GFP-LC3B and p62 for the total

homogenate (Total), organellar fraction, and combined fractions 3-6 (from density gradient) from Baf A_1 +Torin treated HeLa G120 cells were represented. The flow-through from immune isolation of autophagosomes from fractions 3-6 shows that the majority of the autophagosomes/magnetic bead mixture was captured in the LS column under the magnetic field. **(B)** Immunoblots for the protease protection assay were done with autophagosomes isolated using the combined approach from DMSO or Baf A_1 +Torin treated HeLa G120 cells. **(C, D)** Quantification of the protection of GFP-LC3B (C) and p62 (D) proteins in the autophagosome preparations from DMSO or Baf A_1 +Torin treated HeLa G120 cells using the combined approach. The data shown are representative of n>3 independent experiment. **(E)** Autophagosome preparation from HeLa Baf A_1 +Torin treated HeLa G120 cells using the combined approach visualized under fluorescence microscopy under the settings of protease protection assay. The green dots that appeared in the images are considered autophagosomes. **(F)** Autophagosomes isolated using the combined approach from Baf A_1 +Torin treated HeLa G120 and G120A cells were stained and sectioned for TEM analysis. There are many vesicles (presumably autophagosomes) surrounded by magnetic beads (small black dark dots) detected in the preparation from G120 cells. G120A preparation shows nothing but magnetic beads. Scale bar: 1 μm.

3.3. Profiling proteome constituents of the isolated autophagosomes

To identify a cohort of novel and known autophagosome-enriched proteins, including cargo receptors, a quantitative proteomics analysis of the autophagosomes that were isolated using the combined approach was employed. In this analysis, proteome contents of the isolated autophagosomes from DMSO or Baf A_1 +Torin treated HeLa G120 cells were labelled with a different TMT tag, and the resulting peptides were quantified using MS/MS analysis (Fig 3.10A). Of note, autophagosome-enriched fractions from Baf A_1 +Torin treated samples were applied to an LS column without GFP-magnetic beads, and then proteins enriched on the column subjected to MS analysis in order to assess specificity of the beads and catchment capacity of these columns. The proteomics analysis resulted in the quantification of >2000 proteins. The average peptide abundance detected by MS analysis showed that the samples prepared without the magnetic beads (No bead control) detected almost no protein, which represents GFP-magnetic beads specificity of the peptides detected in other samples (Fig 3.10B). On the other hand, it is conceivable that the number of proteins (autophagosomes) subjected to MS analysis in the Baf A_1 +Torin samples was higher than the DMSO samples, therefore it resulted in a dramatic difference in the peptide amount detected in the MS analysis between these samples (Fig 3.10B). According to the raw data (non-normalized), almost every single protein detected in the MS analysis enriched in the Baf A_1 +Torin samples compared to DMSO samples. To fix the initial difference in the protein amount subjected to MS analysis,

the peptide counts in the DMSO samples were normalized against the average peptide count in the Baf A_1 +Torin samples, which equalised the total peptide count in each sample (Fig 3.10B). This normalization enables detection of proteins enriched upon Baf A_1 +Tor treatment more specifically, which presumably represents autophagosome-related proteins. After this normalization, all the proteins detected (2460 in total) were subjected to gene annotation analysis (Fig 3.10C), and a volcano plot was produced, which shows fold change (Baf A_1 +Tor:DMSO) versus statistical significance (Fig 3.10D). The total proteins were annotated to a broad range of organelles; however, the average fold change (green line, Fig 3.10C) was the highest for autophagosome proteins, which represents enrichment of the autophagosome proteins in the total hit list. The presence of organelle proteins in the list is consistent with intermixing of the membrane sources during autophagosome maturation or lysosomal fusion.

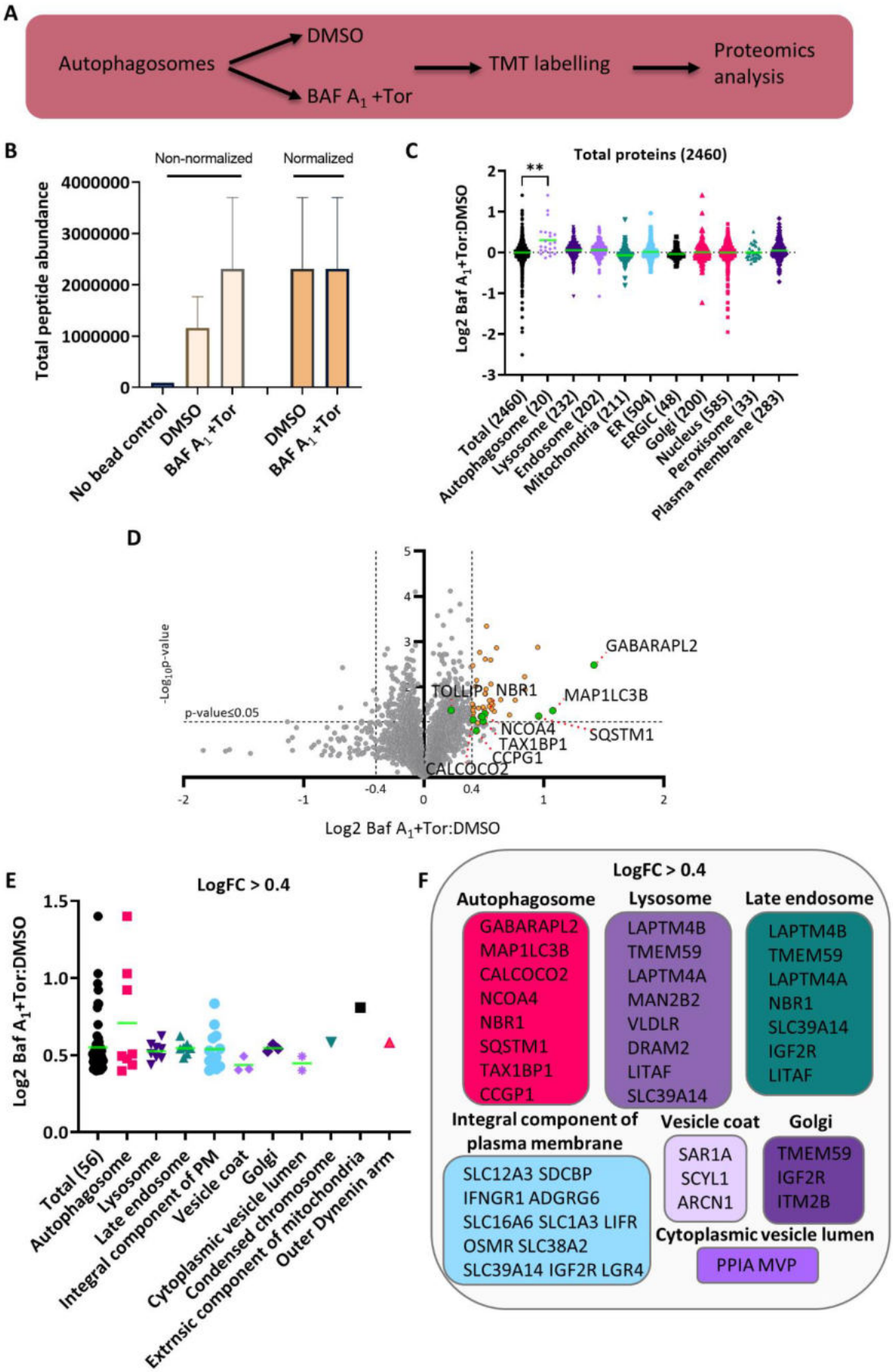
A
Autophagosomes
DMSO
BAF A1 +Tor
TMT labelling
Proteomics analysis
B
Non-normalized
Normalized
Total peptide abundance
4000000
3000000
2000000
1000000
0
No bead control
DMSO
BAF A1 +Tor
DMSO
BAF A1 +Tor
C
Total proteins (2460)
**
Log2 Baf A1+Tor:DMSO
Total (2460)
Autophagosome (20)
Lysosome (232)
Endosome (202)
Mitochondria (211)
ER (504)
ERGIC (48)
Golgi (200)
Nucleus (585)
Peroxisome (33)
Plasma membrane (283)
D
-Log10p-value
p-value≤0.05
GABARAPL2
MAP1LC3B
SQSTM1
TOLLIP
NBR1
NCOA4
TAX1BP1
CCPG1
CALCOCO2
Log2 Baf A1+Tor:DMSO
E
LogFC > 0.4
Log2 Baf A1+Tor:DMSO
Total (56)
Autophagosome
Lysosome
Late endosome
Integral component of PM
Vesicle coat
Golgi
Cytoplasmic vesicle lumen
Condensed chromosome
Extrnsic component of mitochondria
Outer Dynenin arm
F
LogFC > 0.4
Autophagosome
GABARAPL2
MAP1LC3B
CALCOCO2
NCOA4
NBR1
SQSTM1
TAX1BP1
CCGP1
Lysosome
LAPTM4B
TMEM59
LAPTM4A
MAN2B2
VLDLR
DRAM2
LITAF
SLC39A14
Late endosome
LAPTM4B
TMEM59
LAPTM4A
NBR1
SLC39A14
IGF2R
LITAF
Integral component of plasma membrane
SLC12A3 SDCBP
IFNGR1 ADGRG6
SLC16A6 SLC1A3 LIFR
OSMR SLC38A2
SLC39A14 IGF2R LGR4
Vesicle coat
SAR1A
SCYL1
ARCN1
Golgi
TMEM59
IGF2R
ITM2B
Cytoplasmic vesicle lumen
PPIA MVP

Figure 3.10 Quantitative analysis of autophagosomal proteins isolated in the combined approach **(A)** Scheme for TMT-based proteomics of autophagosomes isolated from DMSO and Baf A_1 +Torin treated HeLa G120 cells. In total, n=5 biological replicates from each sample (except No beads control, n=1) were submitted to MS analysis. **(B)** Graph showing average peptide abundance detected in each sample submitted to proteomics analysis. No bead control represents the full course application of the combined approach without the magnetic beads. To normalize the peptide counts, protein counts in the DMSO sample were multiplied by the normalization constant (total peptide count of Baf A_1 +Tor samples/total peptide count of DMSO samples). **(C)** Violin plots for individual organelles, showing enrichment of proteins identified in the proteomics analysis. Proteins were annotated in GO enrichment (component) analysis. The average LogFC was shown with a green line for each organelle. Statistical analysis was done using Welch's t-test (0.001<**p<0.05). **(D)** Volcano plot for Baf A_1 +Tor versus DMSO (Log2 FC versus −Log10 p-value) for the proteomics analysis. P-value calculations were done using the student-paired t-test. Significantly (p<0.05) increased proteins over Log2FC=0.4 were marked orange on the plot. The SARs and ATG proteins were also marked green on the plot. **(E)** Proteins with Log2FC>0.4 were annotated in GO enrichment (component) analysis. **(F)** Summary of proteins enriched in the indicated subcellular compartments (LogFc >0.4).

The significantly increased proteins in the proteomics analysis were determined as those levels (LogFC) increased more than at least 1.8-fold of the standard deviation (0.22) with a p-value less than 0.05. Within significantly increased 46 proteins (LogFc>0.4 and p<0.05, shown in Fig. 3.10D and Appendix Table 2), 2 ATG8 paralogs (GABARAPL2, LC3B), 4 known autophagy cargo receptors (SQSTM1/p62, CALCOCO2/NDP52, NBR1, TAX1BP1), 2 proteins previously reported as selective autophagy receptors (NCOA4, GORASP2), and 15 proteins previously reported to regulate autophagy (LAPTM4B, TMEM59, DRAM2, SDCBP, OSMR, IGF2R, LGR4, SAR1A, MVP, NCAPD2, TAMM41, CCN1, PRKAR1A, LITAF, LGR4) were identified. Moreover, gene annotation analysis (proteins LogFc>0.4) clustered many proteins for autophagosome, lysosome and late endosome (Fig 3.10E), which are listed in Figure 3.10F.

As further validation, the total proteins identified in our study were compared with 3 previous studies described the use of MS to identify proteins in autophagosomal preparations through density gradient separation (Iodixanol)[172], immune isolation[65], or close-proximity labelling of ATG8 proteins[166] (Fig 3.11A). Many proteins that significantly associated with autophagosomes in these studies overlapped with the proteins increased in our study at various levels. It is understandable that there would be variations between datasets depending on cell type, autophagy stimulus, and purification technique. Moreover, the proteins significantly enriched in our study were also compared with the proteins increased (LogFc>0.4) in the whole cell analysis of each *ATG* KO HeLa cells in Figure 3.2 (Fig 3.11B). This analysis showed that

the 29/46 of the proteins increased in the isolated autophagosomes did not overlap with the proteins enriched in any of the *ATG* KO cells. It is important to note that 10 (TMEM59[375], OSMR[376], IGF2R[377], LGR4[378], SAR1A[379], MVP[380], NCAPD2[381], CCN1[382], LITAF[383], GORASP2[384]) of these non-overlapping proteins were previously identified as autophagy regulators. There was only 3 shared autophagy regulating proteins, except SARs and ATG8s, (SDCBP[385], TAMM41[386], PRKAR1A) between isolated autophagosomes and *ATG* KO cells (Fig 3.11C). On the other hand, focusing on the shared proteins between *ATG* KO cells and isolated autophagosomes, 13 out of 16 proteins were commonly shared by all. SARs (SQSTM1/p62, TAX1BP1, CALCOCO2/NDP52 and NBR1) commonly shared by all of the *ATG* KO cells and the isolated autophagosomes. This could also suggest that the shared proteins might represent proteins targeted by autophagic degradation. In the light of these comparative analysis, I moved on questioning involvement of some of the hits from the proteomics list in the autophagy pathway.

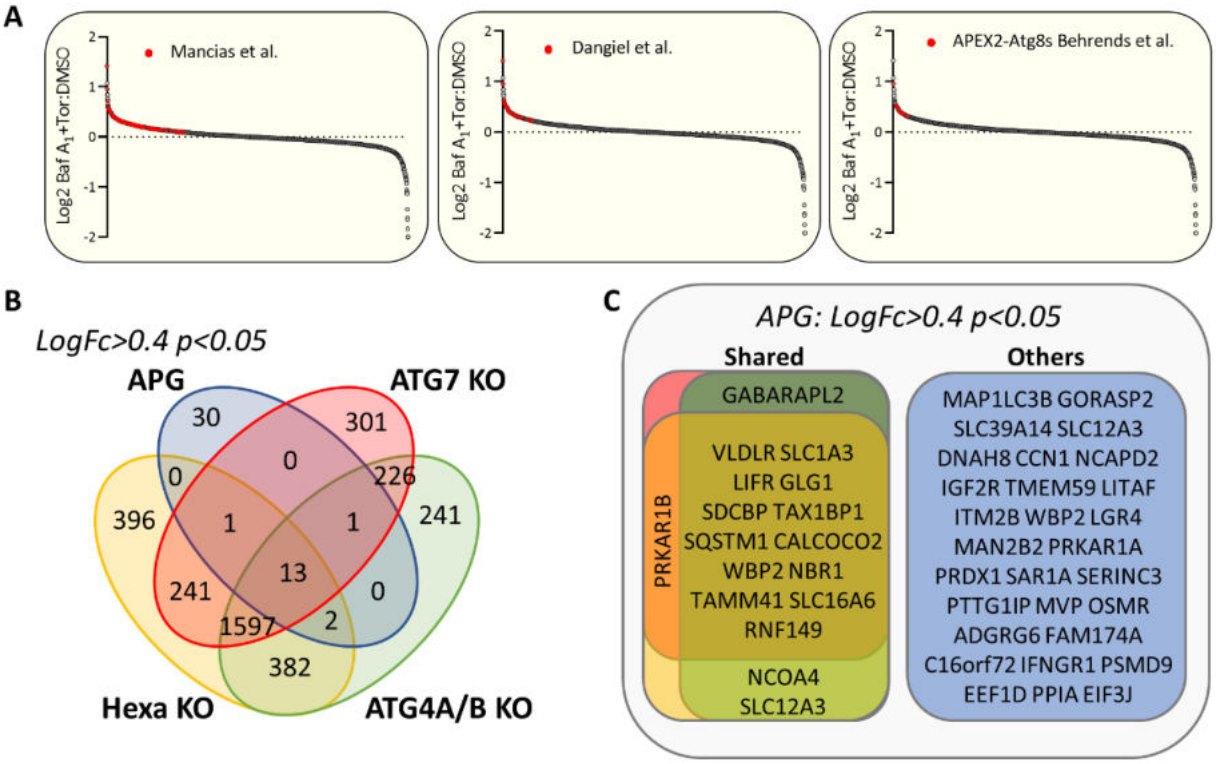

Figure 3.11 Comparative analysis of autophagosome proteome **(A)** Plot of LogFC means for proteins (Baf A_1 +Tor/DMSO) identified in proteomics analysis of isolated autophagosomes. Proteins that are significantly increased in three independent studies analysed the protein content of autophagosomes are shown in red on the plots. (B) Venn diagram showing the number of proteins shared between proteomics analysis of isolated autophagosomes (APG, LogFc >0.4, p <0.05) and *ATG* KO HeLa cells from Figure 3.2 (LogFC >0.4 compared to HeLa WT). (C) Summary of proteins represented on the Venn diagram.

3.4. Characterization of the identified proteins

As further validation of the proteins identified in the proteomics analysis of the autophagosomes, autophagy competent (HeLa G120) and incompetent (HeLa G120A) cells were used in the settings of DMSO or Baf A_1 treatments. A compilation of proteins was defined either based on their levels significantly increased in the proteomics analysis or antibody resources in the house. Initially, to identify autophagy substrates, changes in the protein levels were evaluated based on the changes in the abundance of the p62 protein, which is a well-known autophagy substrate. In HeLa G120 cells, blocking of autophagic degradation using Baf A_1 treatment stimulated an accumulation of p62 in these cells (Fig 3.12A). On the other hand, HeLa G120A cells have already shown high p62 level since they are autophagy incompetent. Moreover, p62 level was irresponsive to Baf A_1 treatment in the HeLa G120A cells as a proof of no autophagic flux in these cells. In return, the expression levels of the proteins (β-catenin and GAPDH), which are known to be not targeted by autophagic degradation, have shown no changes upon Baf A_1 treatment, or corresponding to autophagy competence (Fig 3.12A).

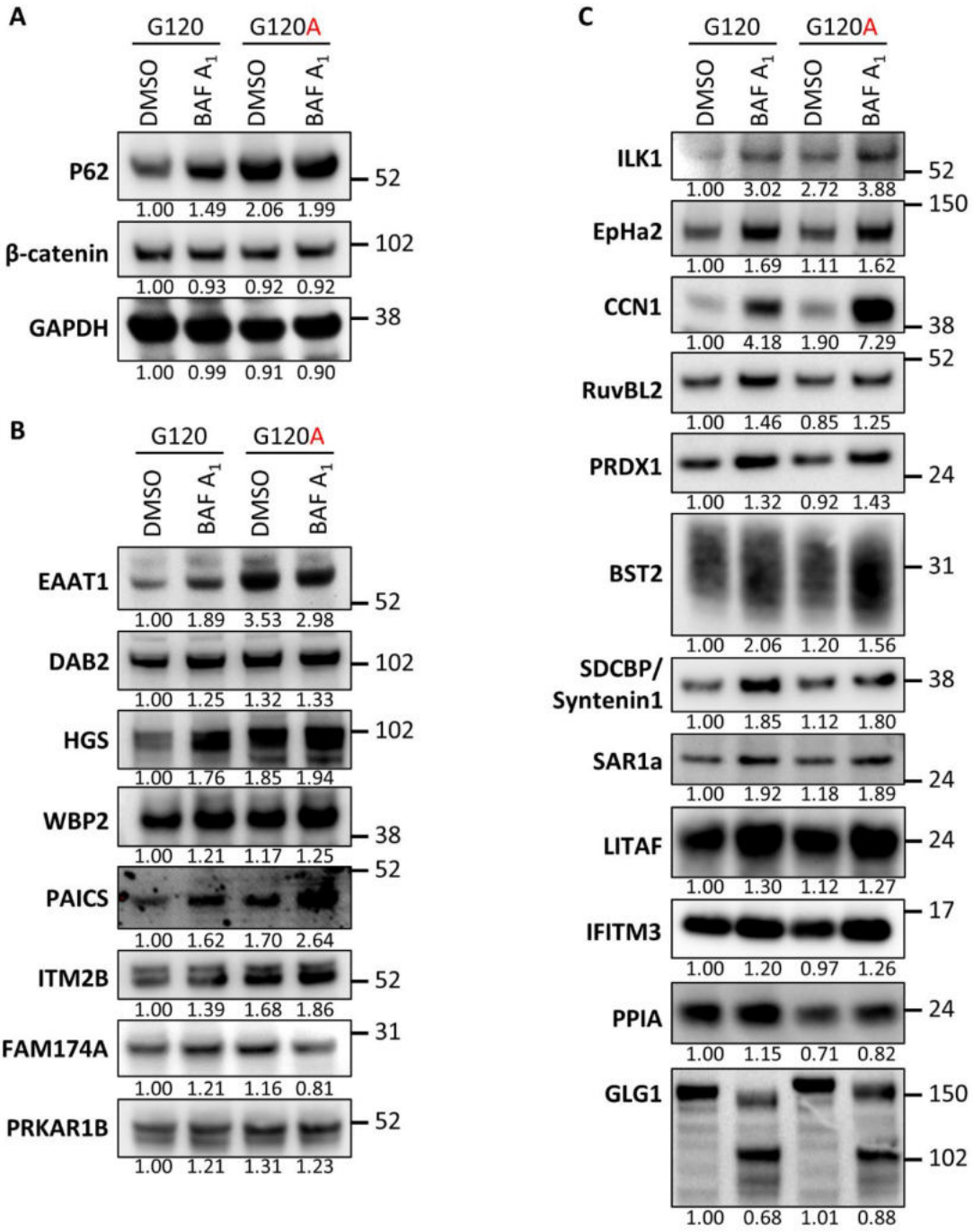

Figure 3.12 Validation of candidates from autophagosome proteomics analysis. **(A)** Immunoblots for p62, β-catenin, and GAPDH (loading control) of cell extracts from HeLa G120 and G120A cells treated with DMSO or 200 nM Baf A_1 for 2 h. **(B)** Immunoblots for proteins with a similar expression profile with p62 in HeLa G120 and G120A cells. **(C)** Immunoblots for proteins showed sensitivity against Baf A_1 treatment independent of autophagy competence. Densitometric analysis of the corresponding bands for each protein was done using ImageJ and indicated below each blot. Each blot represents at least n=2 biological replicate.

A panel of protein was then screened under the same settings, and it was hypothesized that proteins that show similar profiles with p62 might be targeted to autophagic degradation.

In this experimental context, 8 proteins were found to show a similar pattern to p62 protein, which potentiate them to be a target of autophagic degradation (Fig 3.12B). In addition, in this screening, another group of proteins with a sensitivity against Baf A_1 treatment in both autophagy competent and incompetent HeLa cells was identified (Fig 3.12C). Two of these proteins IFITM3[387] and LITAF[383] were previously identified as autophagy regulator proteins as well as colocalizing with GFP-LC3B dots in cells. Of note, GLG1, Golgi complex-localized glycoprotein 1, protein level decreased upon Baf A_1 treatment. However, it is also observed that Baf A_1 treatment stimulated a shift in the size of GLG1 protein possibly due to induction of some post-translational modifications. The fold changes of the proteins represented in Figure 3.12 were shown in Appendix Table 2.

Following the immunoblot analysis, an image-based approach was also employed to identify proteins localizing in/on the autophagosomes. For that purpose, HeLa G120 cells were immunostained against the proteins from Figure 3.12 in the presence or absence of Baf A_1 treatment. The results showed that p62 completely colocalize with GFP-LC3B dots in the cells as expected (Fig 3.13A). Similarly, putative autophagy regulators IFITM3 and LITAF also showed great (not complete) colocalization with GFP-LC3B dots under Baf A_1 treated conditions (Fig 3.13A). Of note, Baf A_1 treatment increased the amount of IFITM3 and LITAF protein levels around the perinuclear area. This is where autophagosomes (GFP-LC3B dots) also accumulate[388]. In this analysis, β-catenin staining was used as a negative control for proteins not targeted by autophagy.

In line with these results, many other proteins have shown partial colocalization with GFP-LC3B dots, similar to IFITM3 and LITAF. These proteins include BST-2, FAM174A, ITM2B, EAAT1 (shown in Fig 3.13B), PAICS, Syntenin1, DAB2, and EpHa2 (not shown). It should be noted that most of the antibodies used to stain proteins in the cells have not conferred an efficient signal to visualize them under microscopy.

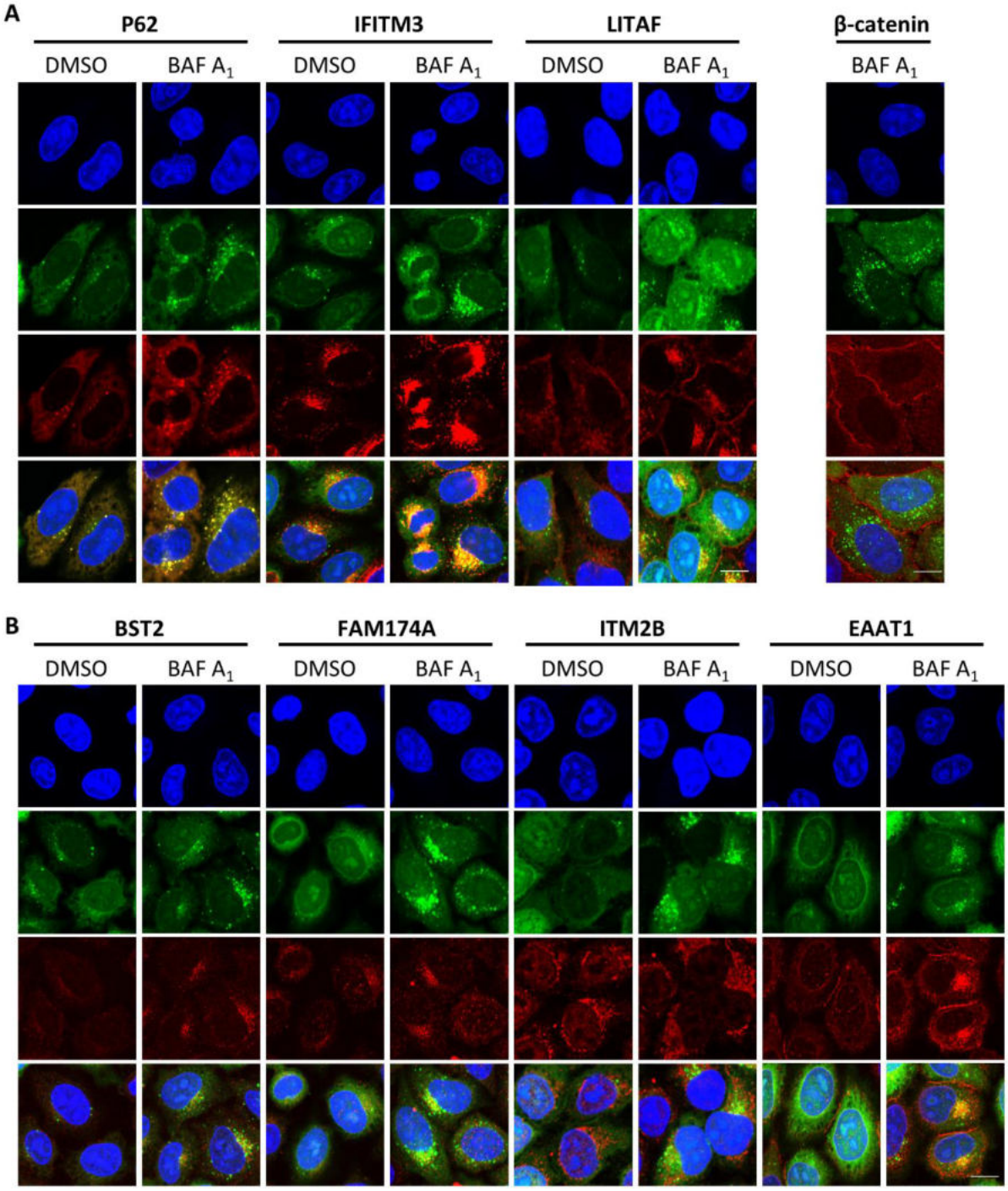

Figure 3.13 Localization of candidates from autophagosome proteomics analysis. Proteins from the autophagosome proteomics study were visualized under confocal microscopy in HeLa G120 cells treated with DMSO or 200 nM Baf A_1 for 2 h. **(A)** Indirect immunofluorescence analysis of putative autophagy substrates p62, IFITM3, and LITAF shown in red, and GFP-LC3B is green. **(B)** Indirect immunofluorescence analysis of candidates from autophagosome isolation shown in red. DAPI staining was used to mark the nuclei (blue), scale bar = 10 μm.

Among these candidate proteins, I decided to study EAAT1 (the excitatory amino acid transporter 1, also known as SLC1A3) as a target of autophagy as it shows a similar pattern to p62 in immunoblot analysis and a good degree of colocalization with autophagosomes under microscopy (Fig 3.12B and 3.13B). It was also one of the most highly and consistently enriched proteins in the proteomics analysis (Appendix Table 2). Moreover, EAAT1 protein level increased commonly in the *ATG* KO cells in the whole-cell proteomics analysis (Appendix Table 3). EAAT1 (a 58 kDa protein) undergoes glycosylation which produces a shift in molecular weight and mediates its cell surface expression[389]. EAAT1 is also known to exist in the plasma membrane as a homomultimer[389]. Expression patterns of EAAT1 in HeLa cells were indicated in Figure 3.14A. The results indicated glycosylated EAAT1 and non-glycosylated EAAT1 (shown with**). There are also two higher molecular weight bands appearing in the immunoblots which might be non-specific binding of the EAAT1 antibody or EAAT1 dimer (shown with *). Baf A_1 treatment increased both glycosylated and non-glycosylated forms of EAAT1 in HeLa G120 cells (Fig 3.14A). Moreover, EAAT1 glycosylation is halted in autophagy-incompetent G120A cells, which suggest a role for autophagy in EAAT1 glycosylation (Fig 3.14A).

To better observe the effect of autophagy on EAAT1 regulation, HeLa G120 and G120A cells were transfected with human EAAT1 gene (Fig 3.14B). Results showed that transfection of EAAT1 increased bot glycosylated and non-glycosylated EAAT1 levels. In autophagy incompetent HeLa G120A cells, monomeric EAAT1 expression was higher than HeLa G120 cells. However, the same accumulation was not observed in HeLa G120 cells with Baf A_1 treatment, which may suggest involvement of autophagy-independent mechanisms in the regulation of EAAT1 level in the cells (Fig 3.14B). Nevertheless, a small increase was observed in the amount of non-glycosylated EAAT1 upon Baf A_1 treatment in HeLa G120 cells compared to untreated cells. Moreover, amino acid starvation (EBSS) has shown to be decreasing EAAT1 levels in HeLa G120 cells while increasing glycosylated EAAT1 it in HeLa G120A cells compared to untreated cells (Fig 3.14B). All these data suggest that the post-translational modifications of EAAT1, such as glycosylation, could be an important factor on targeting EAAT1 to autophagic degradation.

Finally, the effect of EAAT1 on autophagy was interrogated by overexpressing HA-EAAT1 or silencing endogenous EAAT in HeLa WT cells (Appendix Fig 1). EAAT1 overexpression increased LC3-II level (lower band), which suggest a change in autophagy.

However, this effect was lost upon Baf A_1 treatment. Moreover, a slight increase in the p62 level was observed upon EAAT1 overexpression, which is even further incresed by Baf A_1 treatment. On the other hand, silencing EAAT1 did affect neither LC3B nor p62 level compared to cells transfected with non-targeting siRNAs. These results may suggest that EAAT1 is not a key autophagy regulator, but it needs further investigation to elucidate its true potential on autophagy regulation. Because, silencing EAAT1 in HeLa G120 cells produced bigger GFP-LC3B dots, presumably protein aggregates (Appendix Fig 1). This might suggest a role for EAAT1 in directing protein aggregates to autophagic degradation.

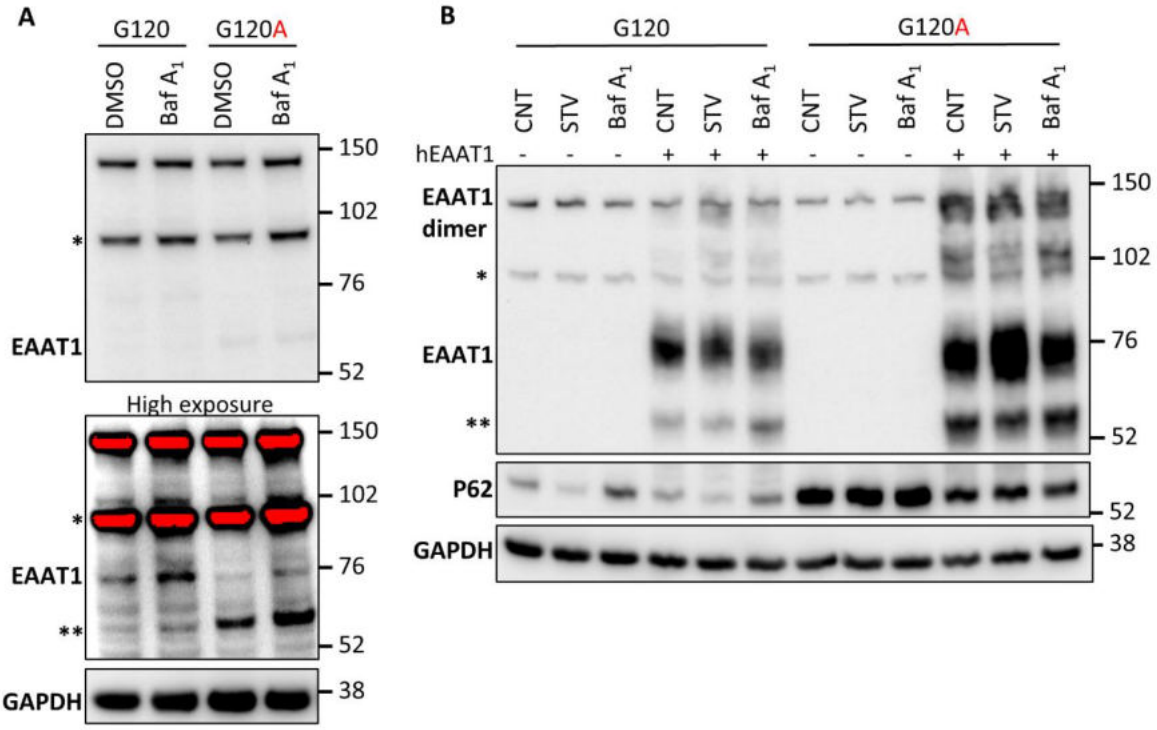

Figure 3.14 Analysis of EAAT1 as a target of autophagic degradation. **(A)** Expression patterns of EAAT1 in HeLa G120 and G120A cells treated with DMSO or 200 nM Baf A_1 for 2 h. EAAT1 dimer was obvious in the upper panel. Monomer EAAT1 proteins were observed under high exposure (lower panel). GAPDH is used as a loading control. An asterisk (*) represents a non-specific band. **(B)** Overexpression of EAAT1 in HeLa G120 and G120A cells treated with DMSO, amino acid starvation (EBSS, 2 h), or Baf A_1 (200 nM, 2 h). A double asterisk (**) indicates deglycosylated EEAT1 proteins.

3.5. Isolation of autophagosomes *in vivo*

To test the applicability of the established autophagosome isolation protocol to tissue samples, transgenic mice (autophagy reporter mice) with mCherry-EGFP-LC3B expression were used. Moreover, it was initially aimed to identify differential autophagy targets in

cancerous and non-cancerous tissues. Therefore, PDAC prone *KPC* mice were crossed with the autophagy reporter mice, which led us to generate a PDAC-prone mCherry-EGFP-LC3B expressing mice (Fig 3.15A). This work has been done by Melnaie Vanlentie. These mice have shown to form small lesions called pancreatic intraepitheliel neoplasia within 4 weeks, which later grow into PDAC within the next 12-20 weeks.

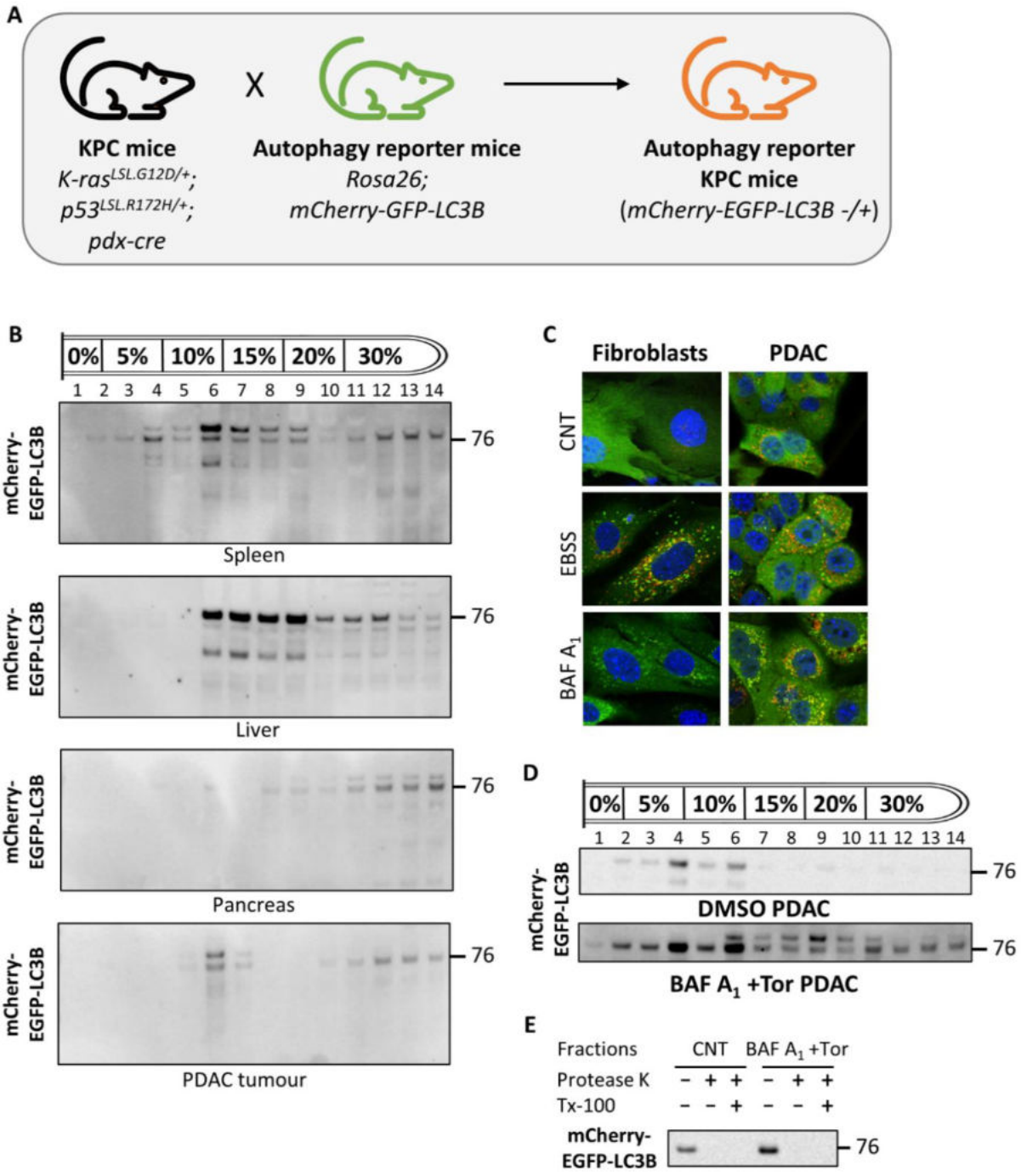

Figure 3.15 Isolation of autophagosomes from mouse tissue. **(A)** A scheme showing the generation of an autophagy reporter *KPC* mouse model, which produces PDAC tumours expressing mCherry-GFP-LC3B. **(B)** Density-gradient separation of organelle fraction obtained from mouse tissues. Anti-GFP immunoblots are shown. **(C)** Confocal images of primary tumour and fibroblast cells generated from the murine pancreatic tissue expressing mCherry-GFP-LC3B. Their response to starvation (EBSS, 4 h) and Baf A_1 (200 nM, 4 h) is shown. **(D)** Density gradient separation of organellar fraction from DMSO or Baf A_1 (200 nM, 2 h) treated primary PDAC cells. **(E)** The autophagosomes isolated from primary PDAC cells were subjected to protease protection assay.

Autophagosomal preparation was produced from tissues as described in methods and used to study contents. Density gradient separation revealed a different profile for each tissue, which is most probably caused by different composition of each tissue (Fig 3.15B). These results showed the established protocol requires further optimization to enable isolation of autophagosomes from tissue samples.

On the other hand, to eliminate drawbacks of tissue samples, primary PDAC and pancreatic fibroblast cell lines from the autophagy reporter *KPC* mice were created (see methods) to be later used for autophagosome isolation. The response of these cells to autophagy stimulus was determined under confocal microscopy (Fig 3.15C). Results showed that these cells form autophagosomes under amino acid starvation, and Baf A_1 treatment can cause a dramatic accumulation of autophagosomes. Later PDAC cells were used for autophagosome isolation. The density gradient separation showed a similar accumulation of autophagosomes (mCherry-EGFP-LC3B protein) in the factions 2-6, similar to HeLa G120 cells (Fig 3.15D). Later, the immune isolation of autophagosomes from these fractions was carried out, and the eluates were subjected to protease protection assay (Fig 3.15E). However, there was no protection against protease degradation, suggesting that there is need for further optimization.

4. Results Chapter II: Identification of β-catenin as an LC3/GABARAP interacting protein

Maintaining cellular homeostasis requires a careful balance between many proliferative and cell death systems under physiological conditions as well as during cellular stress[260]. Given the function of the Wnt/β-catenin signalling and autophagy pathways in cell homeostasis, it is important to study the interplay between these two pathways. This chapter describes studying the potential role of autophagy in the regulation of the Wnt/β-catenin signalling by identifying and elucidating the link between these pathways. The interaction model described in this chapter provides new insights in the regulation of both pathways. The three main objectives were:

1- To identify a physical link between autophagy proteins and those implicated in the Wnt/β-catenin pathway
2- To study autophagy as a regulator of the Wnt/β-catenin pathway
3- To study β-catenin as a regulator of autophagy

4.1. Identification of a linear LIR motif in β-catenin

The LC3/GABARAP proteins are the best-studied proteins of the core autophagy machinery. In autophagy, LC3/GABARAP proteins play dual roles in the formation of autophagosome and recruitment of autophagy cargo (e.g. SARs)[32]. The role of LC3/GABARAP protein is generally dependent on the LIR motif present on the autophagy regulators or substrates[34]. Given the published interaction between β-catenin & autophagy pathway as well as suggested LIR motif, I decided to confirm the published LIR and identify any new ones. In this regard, we performed a peptide array analysis in collaboration with Dr. Terje Johansen (Tromso University, Norway) (Fig 4.1A). In this assay, the binding of GST-GABARAP to a set of consecutive β-catenin peptides revealed a putative non-canonical (atypical) LIR motif in β-catenin (Fig 4.1A). This atypical LIR motif contains only one hydrophobic residue ($W66^{\beta\text{-catenin}}$) in contrast to typical LIR motifs (W/F/YxxI/L/V) with two hydrophobic residues. The abbreviated, atypical LIR (63-YEWE-68) in β-catenin is found adjacent to the known phosphodegron motif, amino acids 25-47, which is frequently mutated in cancers[330]. The putative LIR motif locates at the unstructured N-terminus of β-catenin and is conserved among the animal kingdom (Appendix Fig 2A and 2B). Initial analysis of

COSMIC data did not identify any mutations in cancer in the LIR motif. Moreover, the β-catenin LIR motif shows similarities with other atypical LIR motifs, such as those in Bcl-2 and TRIM5α (Fig 4.1B). The Trp residue in these motifs is surrounded by acidic residues (Glu or Asp). The conserved acidic residues may be further contributing to the interaction with LC3/GABARAP proteins.

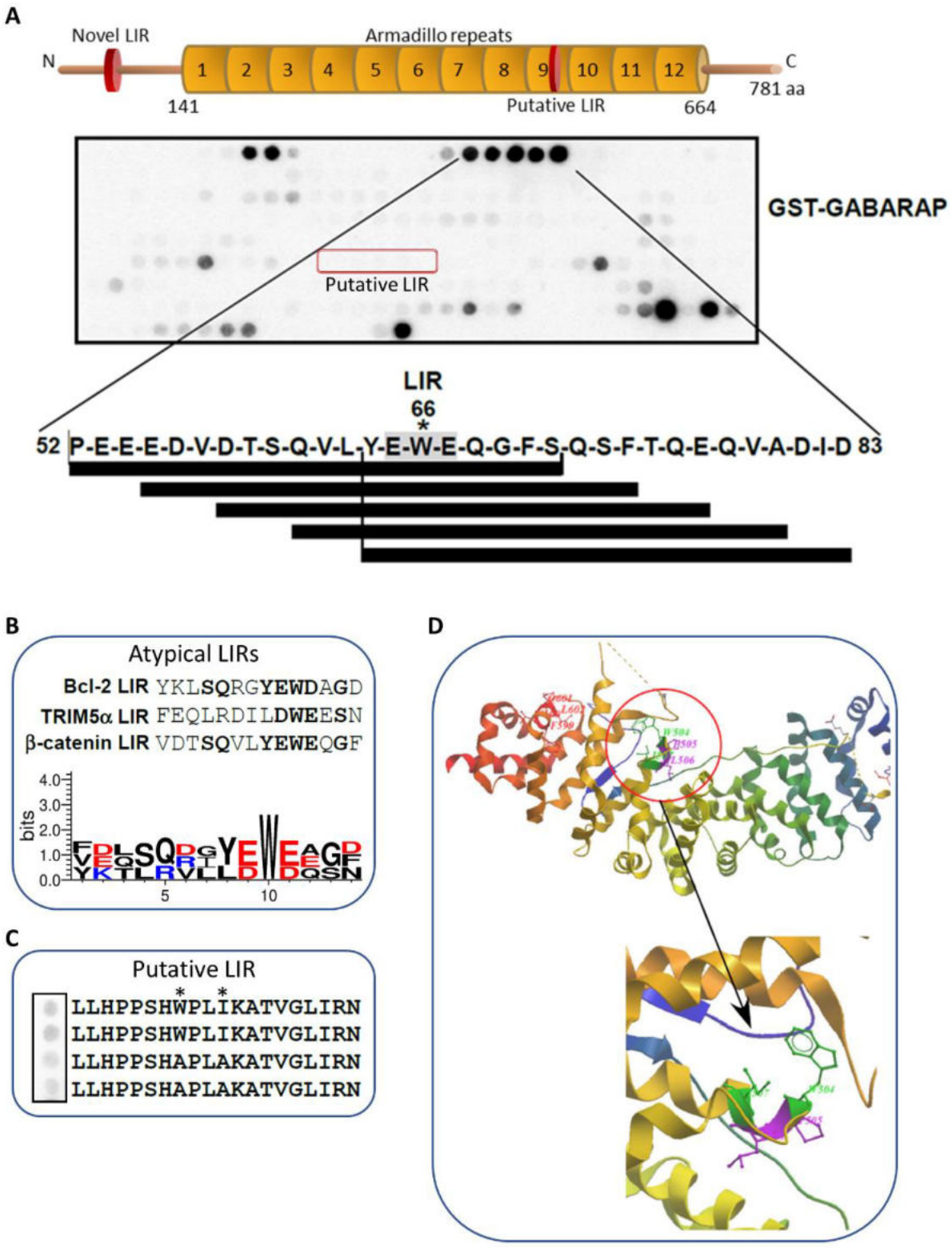

Figure 4.1 Identification of LIR motifs in β-catenin using peptide array. **(A)** A peptide array of 20-mer peptides covering full-length human β-catenin of 781 amino acids. Each peptide was shifted by three amino acids relative to the previous peptide. The array was probed with purified GST-GABARAP, and binding to GST-GABARAP was detected with an anti-GST antibody using chemiluminescence. The combined sequence of five consecutive GABARAP-interacting peptides is shown at the bottom, and the peptides comprising the LIR suggested by Petherick

et. al.,[112] are indicated in a red rectangle on the membrane. A schematic diagram of the domain organization of β-catenin is shown at the top with the novel (atypical) and previously reported (typical) putative LIR motifs. **(B)** WebLogo plot generated on the sequences of atypical LIR motifs from Bcl-2, TRIM5α, and β-catenin[132, 133]. Acidic amino acids are colored in red, and basic amino acids are in blue. **(C)** A peptide array performed as in A but with the 20-mer harboring the previously reported putative LIR motif[112] with or without the core Trp (W) and Ile (I) residues mutated to Ala (A) in duplicate. **(D)** Section of the β-catenin armadillo repeats with a previously reported putative LIR motif highlighted. Trp and Ile residues (green sticks) look inwards (PDB: 2Z6G).

On the other hand, Petherick and colleagues have previously identified a typical LIR motif that maps to the armadillo domain of β-catenin (aa 504-507) and therefore to a highly structured region[112]. However, the peptides corresponding to this typical LIR motif showed no binding to GST-GABARAP proteins in the peptide array assay (Fig 4.1A). In addition, an Ala substitution of the hydrophobic residues in the typical LIR peptides did not cause any change in the GST-GABARAP binding signal (Fig 4.1C). Furthermore, the crystal structure of a full-length zebrafish β-catenin shows that the hydrophobic residues in the putative LIR motif face inward (Fig 4.1D). This would make the motif inaccessible to LC3/GABARAP proteins unless the armadillo domain is locally de-stabilised in some way. However, there is no precedent for this, and combined with the lack of GST-GABARAP binding in the peptide array, this points to a likely non-functional motif.

Additional consecutive peptides showing binding in the peptide array assay are represented in appendix Figure 3. These putative peptides may also have a potential to facilitate an interaction between LC3/GABARAP and β-catenin proteins. However, in this study, I focused on the validation of the atypical LIR motif in the β-catenin N-terminus.

4.1.1. β-catenin binds to LC3/GABARAP proteins

To determine whether β-catenin can bind to LC3/GABARAP proteins, GST-pulldown assays were used. All six isoforms of LC3/GABARAP proteins were produced in bacteria with a GST-tag, and subsequently purified using Sepharose resin. Subsequent incubation of the resin with HEK293 cell lysate as a source of β-catenin protein showed that β-catenin could be pulled down with all isoforms of LC3/GABARAP proteins (Fig 4.2A). GABARAP proteins showed stronger binding than LC3 proteins (Fig 4.2A). GST alone showed no binding, which confirms LC3/GABARAP specific binding to β-catenin. In addition, pulldown of the p62 protein was used as a positive control, with a stronger binding to LC3 proteins (Fig 4.2A). Bcl-2 protein with a β-catenin-like atypical LIR motif also showed stronger binding to GABARAP proteins

(Fig 4.2A). As negative binding control, there was no actin pulldown with any of the bait proteins (Fig 4.2A).

On the other hand, there might be adaptor proteins in the HEK293 cell lysate facilitating the interaction between LC3/GABARAP and β-catenin proteins, such as p62 (with an ability to bind ubiquitin and LC3/GABARAP proteins simultaneously[32]). Direct binding to LC3/GABARAP resins (either agarose or sepharose) was shown using recombinant β-catenin (Fig 4.2B). With an increased amount of agarose-GABARAP and -LC3A resin, levels of precipitated β-catenin also increased (Fig 4.2B). However, similar gradual increase was not observed with GST-GABARAP resin, which is possibly due to saturating amount of bait protein on the resin. In summary, these assays confirmed direct interaction between β-catenin and LC3/GABARAP proteins.

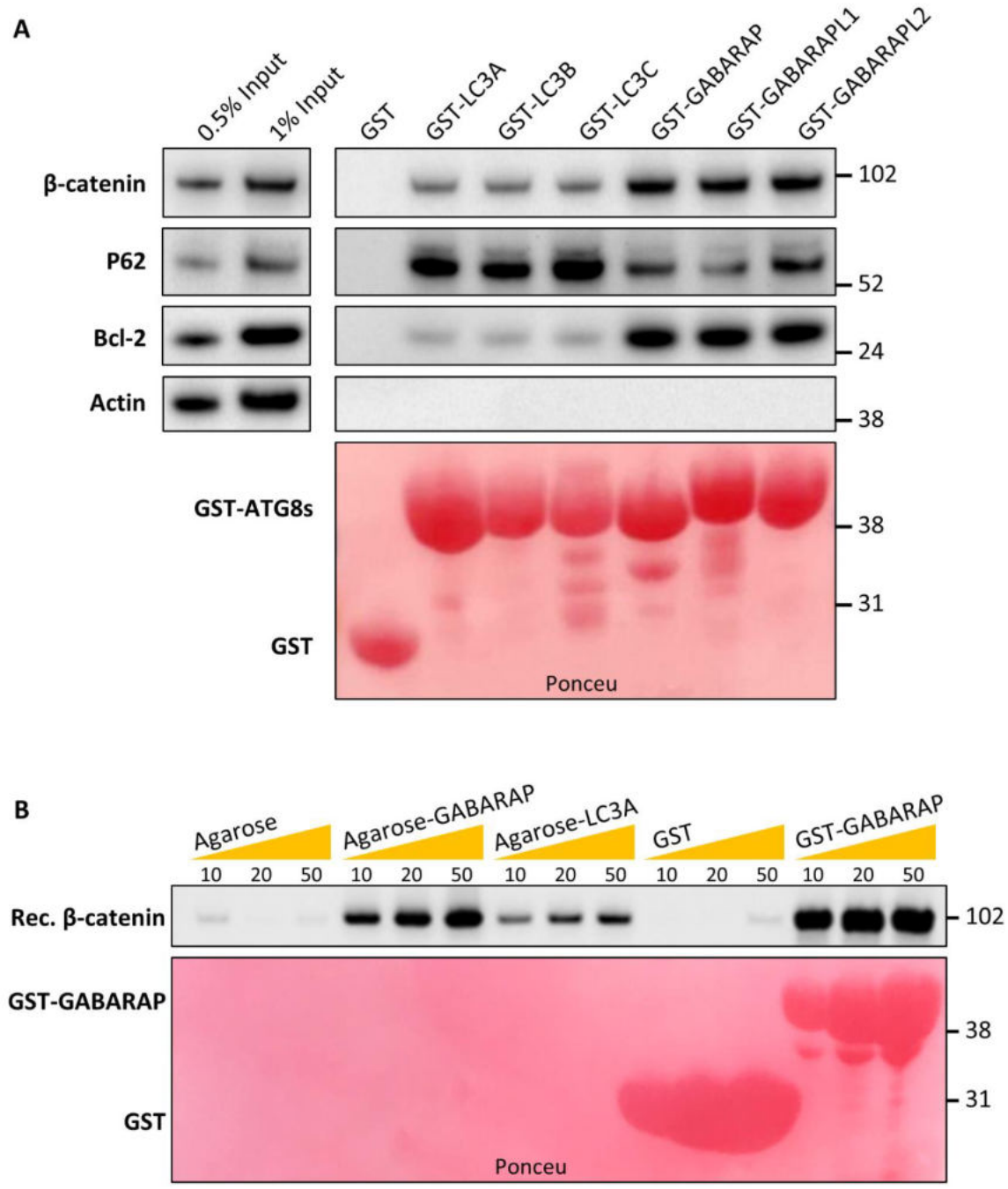

Figure 4.2 β-catenin interacts with mammalian ATG8 proteins LC3/GABARAPs. ***(A)*** GST-pulldown assay of endogenous β-catenin, p62, and Bcl-2 in the lysate of human HEK293 cells incubated with recombinant GST or GST-LC3/GABARAP proteins immobilized on glutathione-sepharose resin. The precipitated proteins and 1-2% of the input lysate were analyzed by Western blotting using anti-β-catenin, anti-Bcl-2, and anti-p62 antibodies. Actin was used as a loading control in immunoblot analysis. GST or GST fusion proteins were visualized by Ponceau S staining (lower panel). **(B)** GST-pulldown assay of recombinant β-catenin protein incubated with varying amounts (10-50 µl) of LC3A- or GABARAP-coupled agarose resin, or GST-GABARAP bound glutathione-sepharose resin. Uncoupled agarose beads or GST-coupled glutathione-sepharose resin were used as negative binding controls. GST or GST-GABARAP proteins were visualized by Ponceau S staining (lower panel). Of

note, there is no GABARAP or LC3A Ponceau staining from agarose resin, as these proteins were covalently linked to the beads.

4.1.2. The LIR motif as a binding determinant

Having shown the interaction between β-catenin and LC3/GABARAP proteins, the nature of the binding was interrogated. For this purpose, the functional sites in the GABARAP proteins including LDS and UDS sites were mutated. Double Ala substitution in the LDS site or triple Ala substitution in the UDS site affected solubility (and thereby likely the folding) of GABARAP protein dramatically (Appendix Fig 4A and 4B). Therefore, the production and purification of these mutant proteins were not successful (Appendix Fig 4A and 4B). On the other hand, single Ala substitution in the LDS site appeared to be better tolerated; these mutant variants were therefore used in the GST-pulldown assays (Fig 4.3A). Pulldown with the HEK293 cell lysate showed that binding of both p62 and β-catenin to GST-GABARAP protein was reduced by the mutation in the LDS site (Fig 4.3A). This suggests a LIR-mediated interaction between these proteins. Similar results were also observed with recombinant β-catenin (Fig 4.3B).

To gain structural insight into the interaction between the identified atypical LIR motif and GABARAP, the LIR peptide:GABARAP complex was predicted using AlphaFold. The analysis was performed by Dr Stephane Mouilleron, Francis Crick Institute, London. The resulting model predicted that that $W66^{\beta\text{-catenin}}$ binds to the HP1 of GABARAP (Fig 4.3C). In addition, hydrogen bounds formed between the LIR side chains (YEWE) and GABARAP (Fig 4.3C). Furthermore, $L63^{\beta\text{-catenin}}$ was predicted to partially occupy the HP2, which resembles canonical LIR binding (Fig 4.3C). However, canonical LIR motifs contain a hydrophobic residue (L/I/V) two amino acid C-terminal to the aromatic residues (F/W/Y)[34]. Conversely, in the β-catenin LIR, the hydrophobic residue (Leu) precedes the aromatic residue (W). Moreover, the canonical LIR motif of p62 (WxxL) presents as a β-strand forming an intermolecular parallel β-sheet with the β2 strand of LC3B[104], whilst the putative LIR peptide is extended and binds to GABARAP in the opposite orientation relative to canonical LIR motif. Intriguing as this may be, the AlphaFold model will require further validation.

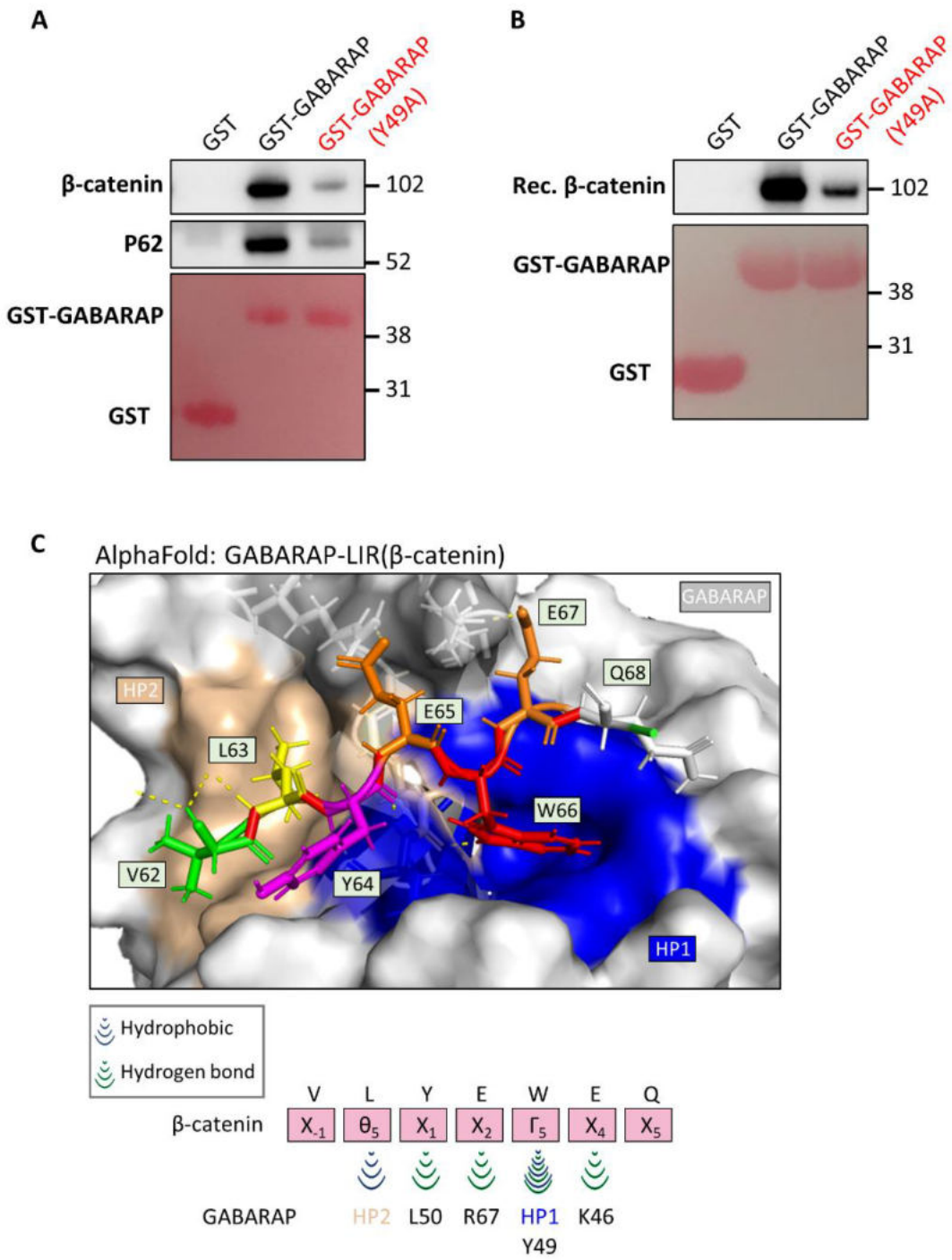

Figure 4.3 β-catenin binds to the LDS pocket of GABARAP via the novel typical LIR. (A-B) GST-pulldown assay of endogenous β-catenin (A) and p62 (A) from lysate of human HEK293 cells, and recombinant β-catenin proteins (B) incubated with recombinant GST, GST-GABARAP or LDS-mutant GST-GABARAP (Y49A) proteins immobilized on glutathione-sepharose resin. The precipitated proteins were analyzed by Western blotting using anti-β-catenin and anti-p62 antibodies. GST or GST fusion proteins were visualized by Ponceau S staining (lower panel). **(C)** AlphaFold prediction of the structure of the β-catenin LIR domain (aa 52–83) bound to GABARAP. The β-catenin LIR sequence is shown as sticks. GABARAP is displayed in white cartoon with HP1 and HP2 coloured in blue and light brown surfaces,

respectively. The yellow dashed lines indicate hydrogen bonds. The lower panel represents a schematic overview of the interactions observed in the structure of the GABARAP bound to the β-catenin LIR domain. Blue lines indicate hydrophobic contacts with HP1 and HP2, and green lines indicate hydrogen bonds. The figure is made using PyMOL 2.5.

To identify residues essential for the binding of LC3/GABARAP *in vitro*, amino acid residues within the LIR motif of β-catenin were mutated to Ala in the context of the full-length protein. Mutant and WT HA-β-catenin constructs were overexpressed in HEK293 cells and used in pulldown assays. Mutation of $W66^{\beta\text{-catenin}}$ decreased the binding of GABARAP (Fig 4.4B and C). However, $L63^{\beta\text{-catenin}}$ mutations did not bring any further decrease in the binding of GABARAP. Complete substitution of the atypical LIR motif to Ala (YEWE/AAAA) resulted in the biggest decrease in β-catenin binding (Fig 4.4B and C). Moreover, mutating the previously identified typical LIR motif to Ala (W504A/I507A) did not show any abrogation in the binding of β-catenin to GABARAP (Fig 4.4B and C). However, effects of the mutations introduced in the atypical LIR motif was less effective on decreasing LC3B binding than GABARAP (Fig 4.4.D). Surprisingly, mutating the previously identified typical LIR motif to Ala (W504A/I507A) showed a decrease in the LC3B binding at a similar level to YEWE/AAAA substation. This may suggest that the typical LIR is only effective in LC3B binding. On the other hand, Y64 in the LIR motif was published to be phosphorylated by the kinase protein tyrosine kinase 6 (PTK6)[341]. Therefore, its independent contribution to the GABARAP binding was also studied. However, neither Ala nor Phe substitutions changed binding of GFP-β-catenin proteins to the GABARAP proteins (Appendix Fig 4C). These results suggest that $W66^{\beta\text{-catenin}}$ is the main driver of the LIR-mediated binding of GABARAP; however, the flanking acidic residues (E65 and E67) and Y64 also strongly contribute to the binding. Nevertheless, the binding of β-catenin to GABARAP was not lost even with the YEWE/AAAA substitutions (Fig 4.4B), which might suggest several partially redundant interaction sites within β-catenin.

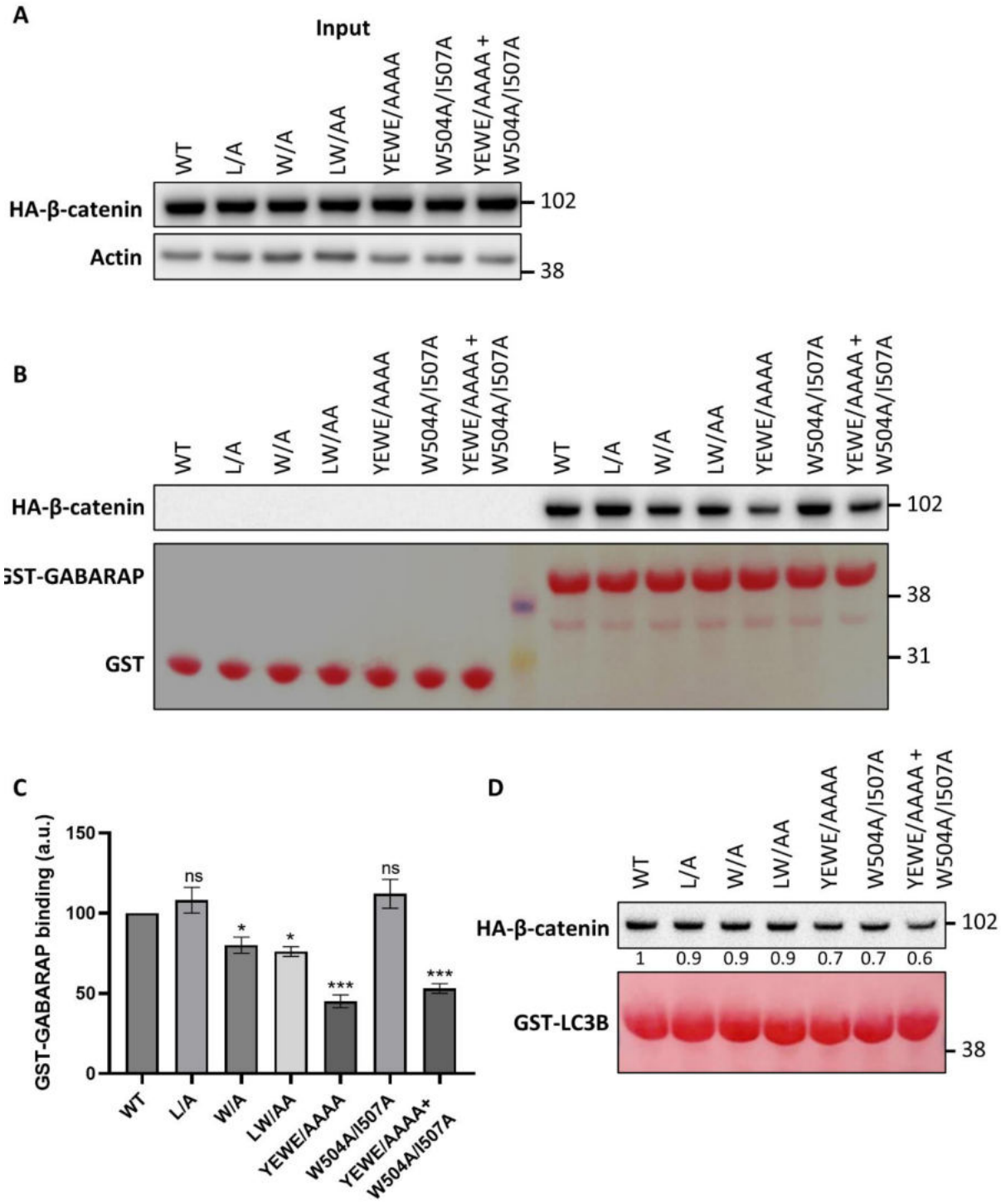

Figure 4.4 Mutations in the LIR motif disrupts β-catenin binding to GABARAP. ***(A)*** The WT and mutant HA-β-catenin proteins expressed in HEK293 cells for 24 h, and the lysates were used in the GST-GABARAP pulldown assay. The input lysate was analyzed by Western blotting using an anti-HA antibody. Actin was used as a loading control. **(B)** GST-pulldown assay of WT and mutant HA-β-catenin incubated with recombinant GST or GST-GABARAP proteins immobilized on glutathione-sepharose resin. **(C)** The bar graph represents the amount of HA-β-catenin proteins precipitated with GST-GABARAP resin. The band intensities in the pulldown assay were determined using ImageJ. Data are mean ± SD from n=3 independent experiments. Statistical significance was assessed using paired Student's t-test (*p<0.05, and

***p < 0.001 as compared to WT HA-β-catenin). **(D)** GST-pulldown assay (n=1) of WT and mutant HA-β-catenin incubated with recombinant GST-LC3B proteins immobilized on glutathione-sepharose resin. The band intensities in the pulldown assay were determined using ImageJ and shown at the bottom of the immunoblot.

To better understand the interaction sites, β-catenin domains were investigated for their binding to LC3/GABARAP. β-catenin comprises an N-terminal unstructured region (NT, aa 1–141), a central region harbouring armadillo repeats (Arm, aa 141–664), and an unstructured C-terminal domain (CT, aa 664–781). To interrogate the binding of β-catenin domains to LC3/GABARAP proteins, full length (FL) and truncated Strep-tagged β-catenin proteins were produced and purified from insect cells (Fig 4.5A and 4.5B). Their binding to GST-LC3B and GST-GABARAP proteins was studied using pulldown assays. Deletion of NT (ΔNT and Arm) significantly disrupted β-catenin binding to GABARAP (Fig 4.5C). In contrast, a less profound reduction in GABARAP binding was observed upon deletion of the C-terminus (ΔCT) (Fig 4.5C). These results suggest that the N-terminus of the β-catenin is the main GABARAP binding determinant. Moreover, LIR-mutant (ΔLIR, YEWE/AAAA) β-catenin proteins significantly showed a significantly decreased binding to GABARAP (Fig 4.5C). This is compatible with a LIR-mediated interaction of GABARAP with the N-terminus of β-catenin. On the other hand, binding of the full length and truncated β-catenin proteins to LC3B was dramatically lower than that to GABARAP. Nevertheless, the high exposure images of the western blots showed that neither truncations nor ΔLIR mutation abrogated LC3B binding (Appendix Fig 5). These results once again emphasize the GABARAP specificity of the β-catenin binding.

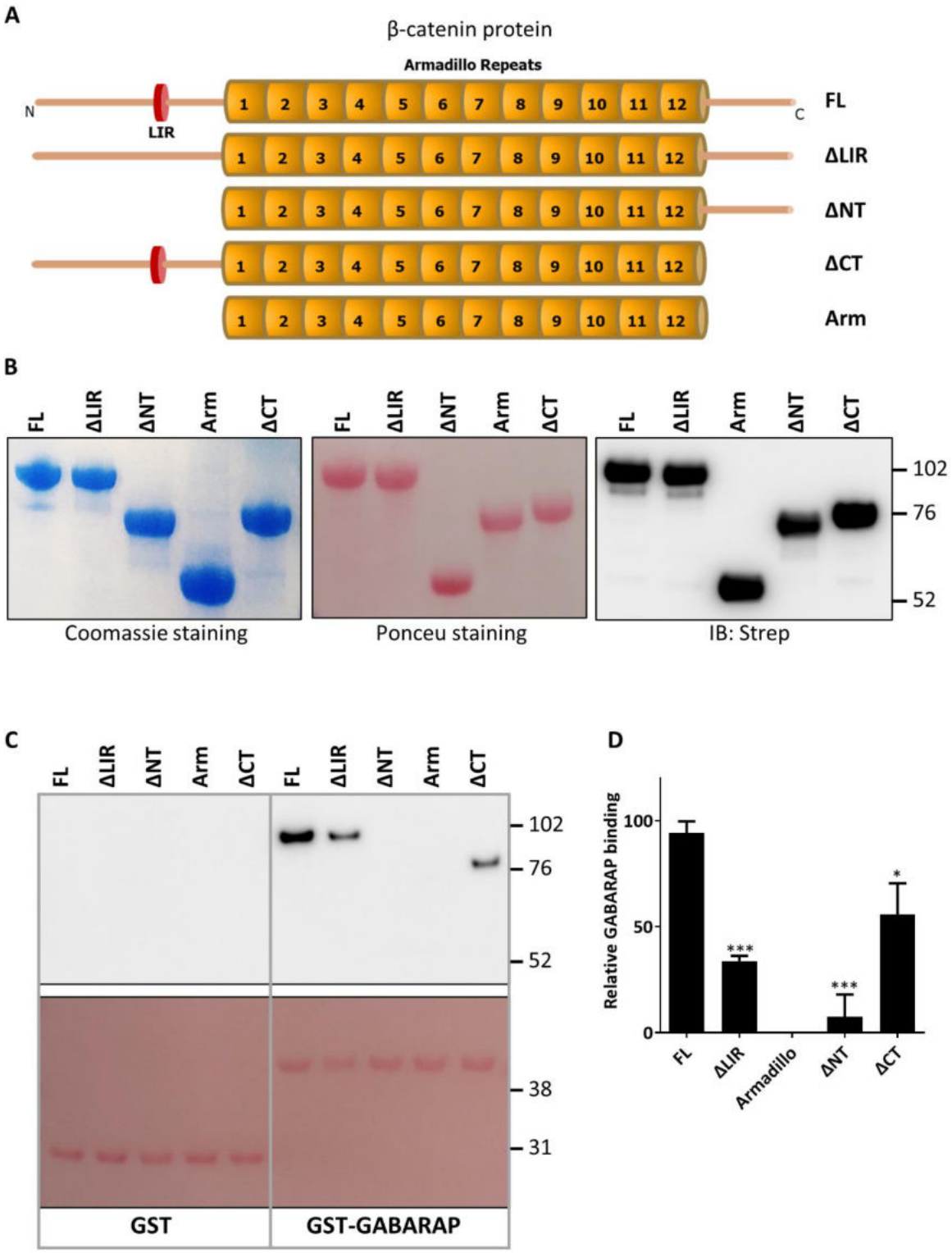

Figure 4.5 LIR-mediated binding of recombinant β-catenin to GABARAP. ***(A)*** Schematic diagram of double Strep-tagged (N-terminus, not shown) β-catenin proteins produced and purified from insect cells. FL: Full-length aa 1-781, ΔLIR:YEWE/AAAA mutation, ΔNT: aa 141-781, ΔCT: aa 1-664, Arm: aa 141-664. **(B)** 1 µg of the purified protein was visualized by Coomassie (left) and Ponceau (middle) staining to represent the input amounts of bait protein used in the GST pulldown assays in C. Also, 1 ng protein was visualized by Western blotting

(right) using an anti-Strep antibody. **(C)** GST-pulldown assay with 1 µg recombinant β-catenin. Precipitated proteins were visualized by an anti-Strep antibody. GST or GST-GABARAP proteins used in the pulldown assay were visualized by Ponceau S staining (lower panel). **(D)** Quantifications of the binding of recombinant β-catenin proteins to the GST-GABARAP proteins presented as band intensities calculated using ImageJ. The bars represent the mean values with standard deviations of three independent experiments. Statistical significance was assessed using paired Student's t-test (*$p<0.05$, and ***$p < 0.001$ as compared to FL β-catenin binding.

To gain functional insight into the role of $W66^{\beta\text{-catenin}}$ in the LC3B/GABARAP binding, fluorescently labelled 18-mer β-catenin LIR peptides were designed (Fig 4.6A). The WT and W/A mutant LIR peptides were incubated with GST-LC3B and GST-GABARAP resin, and their binding was assessed by fluorescence microscopy. The results suggested that W/A substitution fully abolished binding of LIR peptides to both GST-LC3B and GST-GABARAP resin (Fig 4.6B and 4.6C). Moreover, fluorescently labelled 14-mer Bcl-2 LIR peptides were also tested under the same conditions. Bcl-2 peptides showed lower binding to GST-LC3B and GST-GABARAP resin compared to β-catenin LIR peptides.

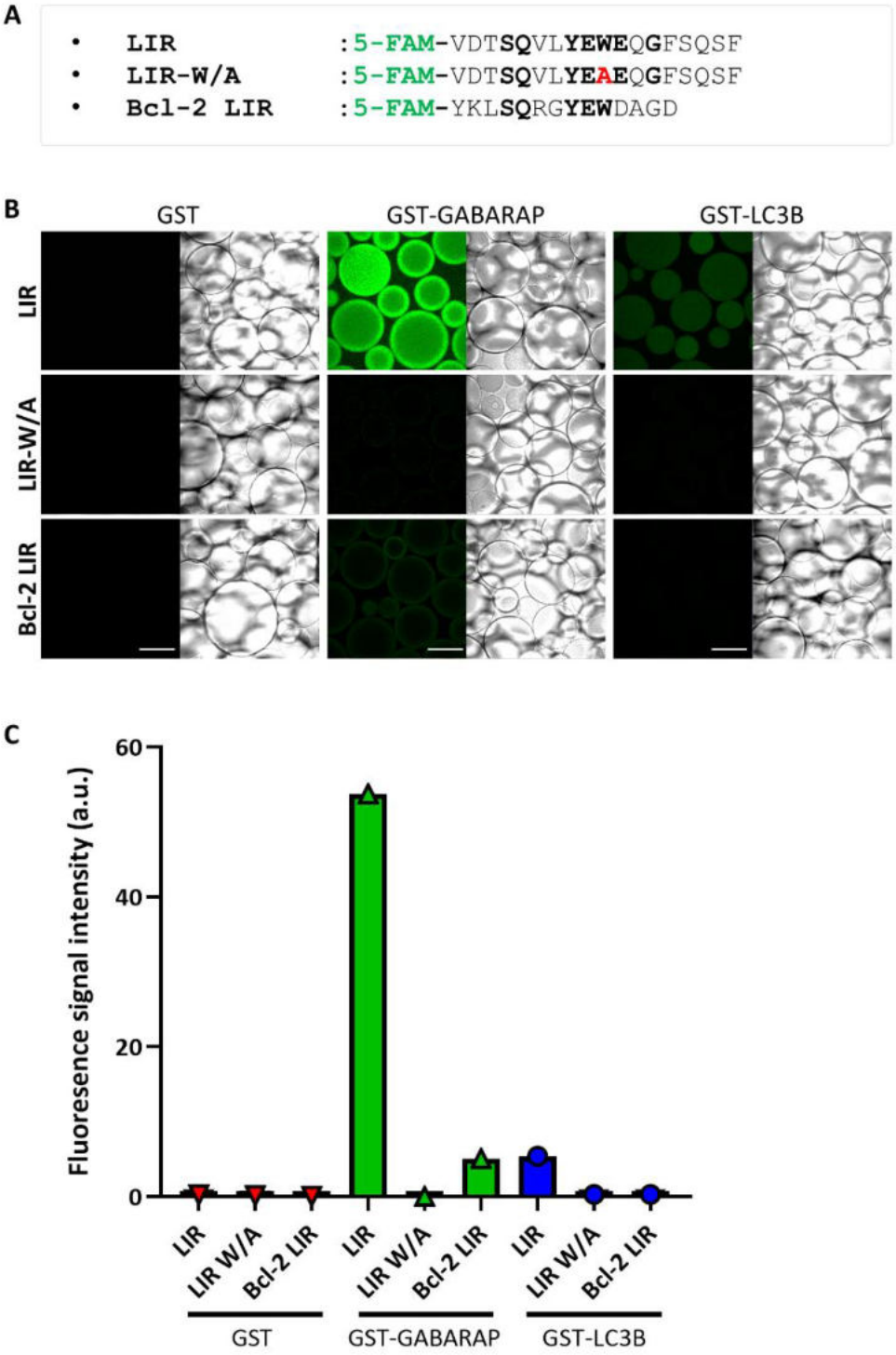

Figure 4.6 GST-pulldown assay with β-catenin LIR peptides. (A) AA sequences of the fluorescently (5-FAM)-labelled WT or mutant β-catenin and WT Bcl-2 LIR peptides are shown. **(B)** GST pulldown assays with the LIR peptides. Glutathione-sepharose resin with bound GST, GST-GABARAP, or GST-LC3B were incubated with 1 µg of the fluorescently labelled peptides, and their binding (green signal) was visualized under fluorescent microscopy. The beads were also visualized under visible light (right panel in each image). Scale bar = 100 µm. **(C)** Quantification of the fluorescence signal from each image taken (represents >10 images per condition) using ImageJ.

The fluorescently labelled peptides were also used to quantitatively assess direct LC3/GABARAP interactions. For that purpose, a fluorescence polarization (FP) assay was conducted (Fig 4.7A). This assay measures the binding of a fluorescently labelled smaller molecule to a bigger molecule by means of the change in polarization (ΔFP). In this assay, peptide concentrations should be kept as low as reasonably possible in order to exclude the peptide concentration from K_d calculations. Also, ΔFP readings should be independent from peptide concentrations. ΔFP readings between 6.25 and 50 nM were approximately constant for β-catenin and Bcl-2 peptides (Appendix Fig 6B and 6C). A peptide concentration of 12.5 nM was chosen for the protein titration experiments. Next, recombinant LC3B and GABARAP proteins were prepared (Appendix Fig 6A). ΔFP readings from the mixture of peptide and LC3B or GABARAP titrations in solution were used to calculate K_d values of interactions. β-catenin LIR peptides showed low μM (K_d: 4.9 μM) binding to GABARAP protein (Fig 4.7B). The W/A substitution in the LIR peptide increased Kd to 37.6 μM (~8-fold lower affinity). These results suggest that Trp is an important binding determinant of the β-catenin LIR:GABARAP interaction. Moreover, higher K_d values were calculated for LC3B binding which is consistent with the fluorescence microscopy assay (Fig 4.6B and 4.7C). Nevertheless, the W/A substitution effectively reduced LC3B binding. On the other hand, the Bcl-2 LIR peptide showed lower affinity to both LC3B and GABARAP proteins compared to β-catenin peptides (Fig 4.7B and 4.7C). This might provide an interesting insight into the binding mode of atypical LIR motifs to LC3/GABARAP proteins.

In summary, these results indicate that β-catenin can directly interact with LC3/GABARAP proteins, and that its affinity against GABARAP is higher than LC3 proteins. The interaction is mainly driven by the atypical LIR motif which uses a Trp residue to potentially occupy the HP1 of GABARAP.

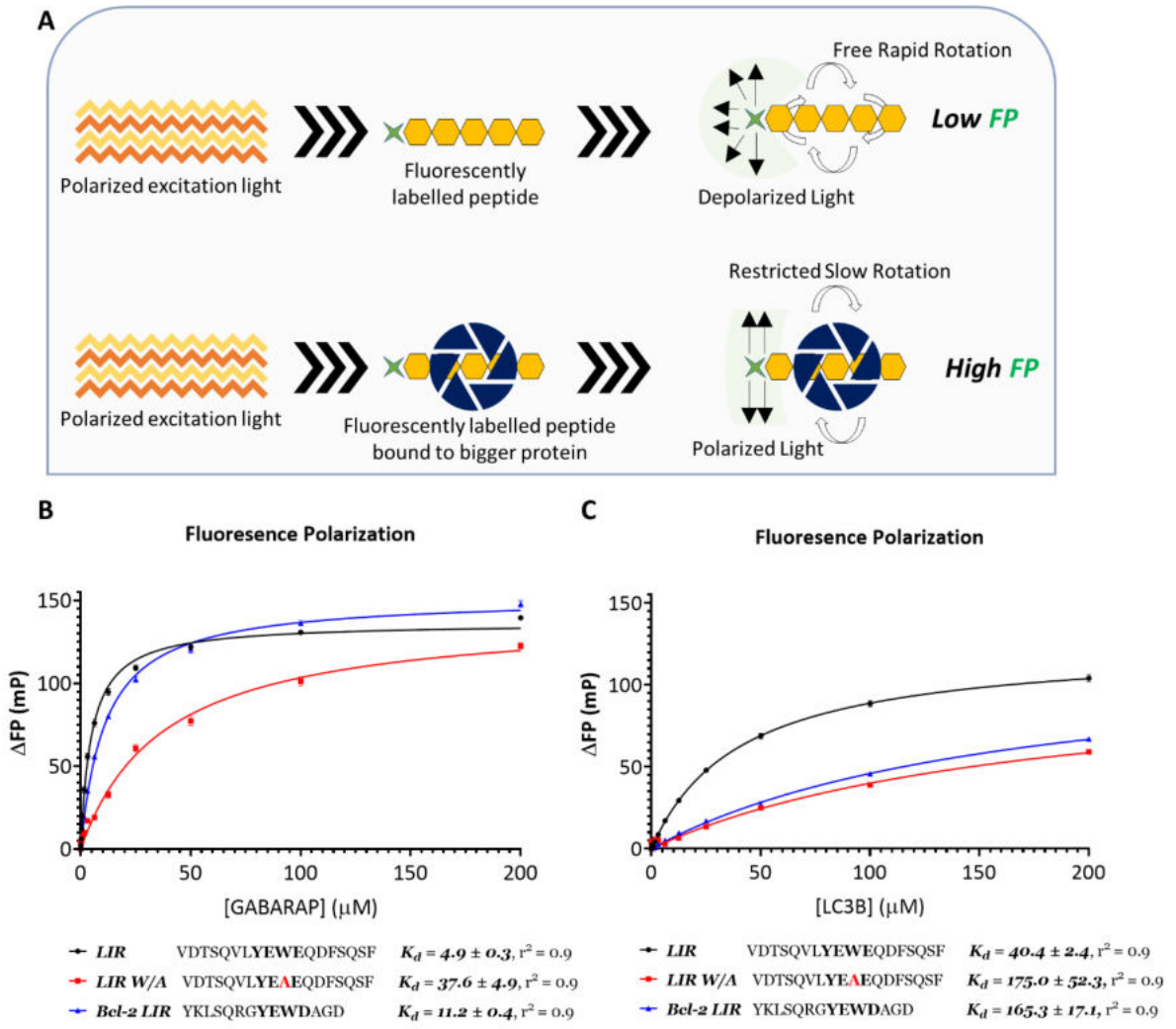

Figure 4.7 Assessing LC3B/GABARAP-LIR peptide interactions by fluorescence polarization. ***(A)*** Schematic depicting the basic principle of a fluorescence polarization assay. When a peptide (yellow hexagons) with a fluorescent label (green star) is excited by polarized light at the excitation wavelength of the fluorophore, it emits largely depolarized light due to molecular tumbling. If the peptide binds to a bigger molecule (protein), it tumbles much slower, and the emitted light retains its polarization. The polarization difference (ΔFP) between the peptide's bound and unbound states allows to calculate interaction affinity to the partner molecule. **(B-C)** ΔFP curves of FP binding assays for the LIR peptides (12.5 nM) from β-catenin (WT and mutant) and Bcl-2 at the concentrations between 0-200 μM . Calculated affinities of the peptides for GABARAP (B) and LC3B (C) are indicated. n = 3 separate experiments; error bars, SEM.

4.2. Studying β-catenin as a target of autophagic degradation

LC3/GABARAP proteins are known to bind cargo molecules targeted for selective degradation in autolysosmes[31]. Having shown that β-catenin contains a functional (albeit atypical) LIR motif, one could hypothesize that β-catenin might be selectively degraded via the formation of β-catenin-LC3/GABARAP complex through autophagic clearance. Indeed, previous publications suggested this possibility[112, 390]. Understanding of non-proteasomal regulation of Wnt/β-catenin signalling could reveal a key cellular integration point linking cell proliferation with autophagy by attenuating β-catenin/TCF-driven transcription. Thus, I examined β-catenin as a target of autophagic degradation.

To determine whether β-catenin's abundance is regulated by autophagic degradation, autophagy was activated in HeLa cells by amino acid starvation (EBSS) or Torin1 (mTOR inhibitor) treatments for several time intervals from 30 minutes to 4 h (Fig 4.8A and 4.8B). Autophagy activation was confirmed by the ongoing degradation of p62 protein. β-catenin protein level showed a slight decrease after 4 h of EBSS but not with Torin1 treatment (Fig 4.8A and 4.8B). These data might be suggestive of autophagic clearance of β-catenin under starvation in HeLa cells. However, this observation could not be confirmed using microscopy. Neither EBSS- nor Torin1-mediated autophagy activation caused a detectable change in the β-catenin staining in HeLa cells (Fig 4.8C). Moreover, confluency of the cells was proposed to be affecting β-catenin's cellular localization[391]. Regarding that, the effect of autophagy activation on confluent and sub-confluent cells were tested (data not shown), but both conditions resulted in the same way as shown in Figure 4.8C.

Wnt/β-catenin signalling is wild-type in HeLa cells, as β-catenin level is highly regulated by the UPS in these cells. To reveal the true potential of autophagy in the regulation of β-catenin protein abundance, several cell lines bearing different mutations were tested (Fig 4.8D). These mutations stabilize β-catenin levels in the cytoplasm by interfering with its proteasomal degradation. In these cells, Western blot analysis of β-catenin protein level did not show a major change in response to 4 h of EBSS or Torin1 treatment (Fig 4.8D). Only Ls174T and HCT116 cells showed a slight decrease in β-catenin levels upon EBSS treatment (Fig 4.8D). Similar to HeLa cells, HCT116 and Ls174T cells showed a stronger decrease in β-catenin levels after 4 h of EBSS treatment (Appendix Fig 7A). However, once again, the same decrease could not be observed using microscopy for Ls174T and HCT116 cells (Appendix Fig 7B).

Moreover, Torin1 treatment did not change β-catenin levels in any of the cell lines tested (Fig 4.8D).

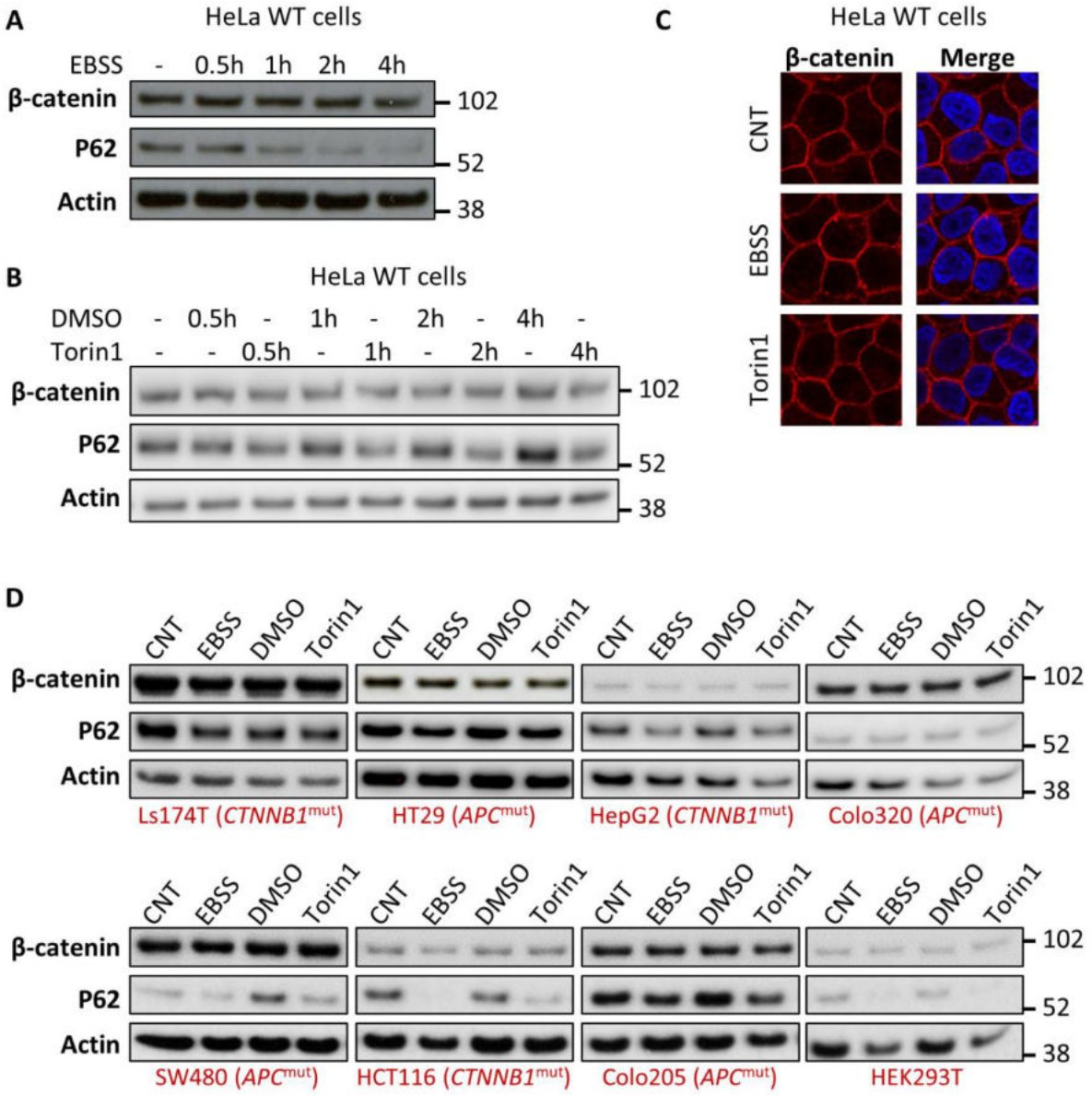

Figure 4.8 Study of possible regulation of β-catenin protein abundance by autophagy. (A) Total protein levels of β-catenin and p62 under normal (CNT) and starved (EBSS for 0-4 h) conditions in HeLa cells. **(B)** Protein levels of β-catenin and p62 upon DMSO and 250 nM Torin1 (prepared in DMSO) treatment for 0-4 h in HeLa cells. **(C)** Immunofluorescence analysis of endogenous β-catenin (red) in HeLa cells treated with EBSS or Torin1 for 4 h. DAPI staining was used to mark the nuclei (blue), scale bar = 10 μm. **(D)** Total protein levels of β-catenin and p62 under EBSS and Torin1 treatments for 4 h in various cell lines. The cells bearing a mutation in APC or CTNNB1 genes are indicated. Actin was used as a loading control in immunoblot analysis. Results are representative of n=2 independent experiments.

To better understand possible effects of autophagy on the regulation of β-catenin, Baf A_1 and CQ treatments were used to block autophagic degradation in the cells (Fig 4.9A). As a

result of autophagy blockage, the lipid-bound LC3B (LC3B-II, lower band) and TAX1BP1 (i.e., aggrephagy receptor) accumulated in the cells. However, autophagy inhibition did not cause any accumulation of β-catenin (Fig 4.9A). Moreover, the EBSS-induced decrease in β-catenin levels was observed even in the presence of Baf A_1 treatment. In addition, β-catenin proteins have previously been shown to form aggregates (i.e., insoluble proteins) in HEK293 cells[392]. Therefore, the level of insoluble β-catenin was checked in response to autophagy blockade (Fig 4.9A). As expected, LC3B and TAX1BP1 proteins aggregated in the cells upon autophagy inhibition (Fig 4.9A). However, blocking of autophagy by Baf A_1 or CQ did not cause an accumulation in the insoluble β-catenin level. These results suggest that β-catenin may not be degraded by autophagy, and EBSS might decrease β-catenin levels independently from autophagy.

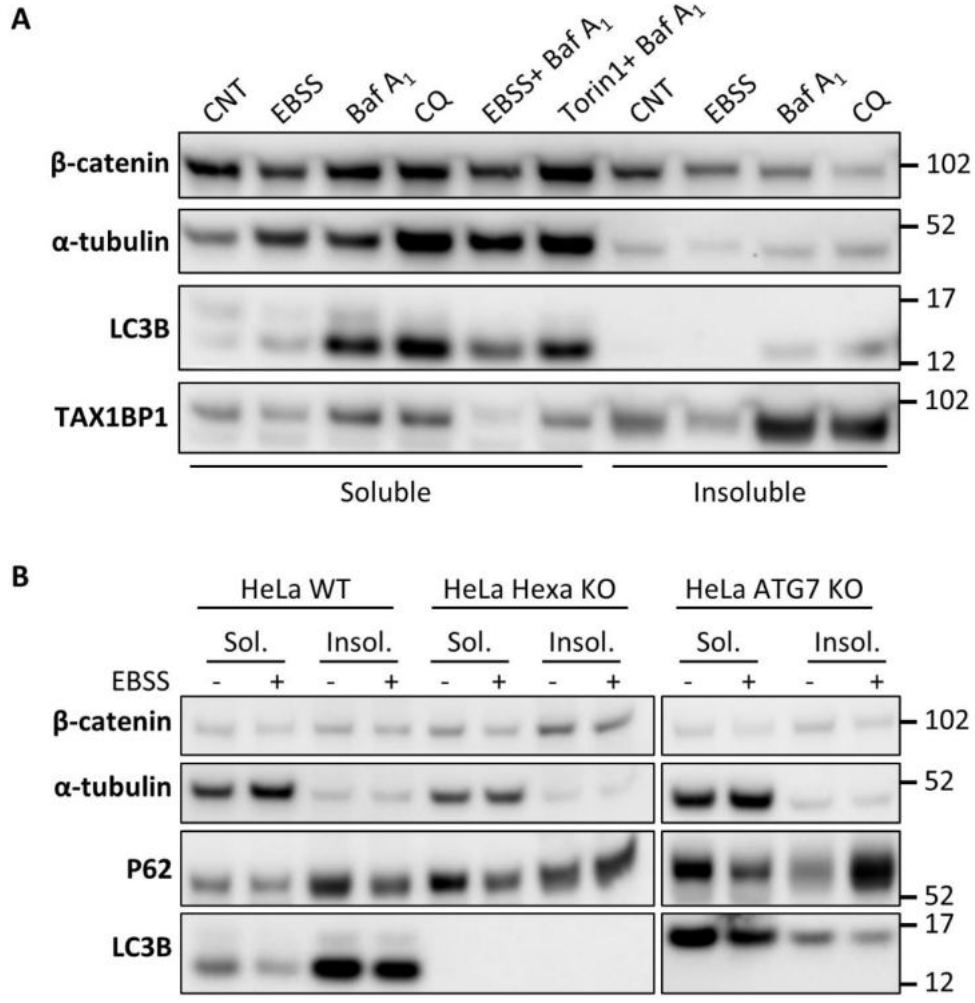

Figure 4.9 Study of possible regulation of β-catenin protein levels by autophagy inhibition. ***(A)*** Western blotting of soluble and insoluble β-catenin, TAX1BP1, and LC3B proteins following EBSS, 200 nM Baf A_1, 10 μM CQ, and/or 250 nM Torin1 treatment for 4 h in HeLa cells. CNT represents DMSO treatment for 4 h **(B)** Western blotting of soluble and insoluble β-catenin, p62, and LC3B proteins following 4 h of EBSS treatment in WT and autophagy-

incompetent (Hexa KO: *LC3A/B/C*, *GABARAP/L1/L2* KO, and *ATG7* KO) HeLa cells. Insoluble proteins were obtained by boiling the cell pellet after soluble protein extraction with cell lysis buffer. α-tubulin was used as a loading control of soluble protein fractions. Results are representative of n=2 independent experiments.

Notably, Baf A_1 treatment did not block EBSS-mediated degradation of soluble LC3B and TAX1BP1 proteins (Fig 4.9A). Therefore, I decided to observe soluble and insoluble β-catenin levels in a setting with more robust autophagy inhibition. For that purpose, β-catenin protein levels in autophagy competent HeLa cells were compared with autophagy-incompetent HeLa *Hexa* KO and *ATG7* KO cells (Fig 4.9B). Autophagy incompetence of the KO cells was confirmed by the absence of LC3B in the Hexa KO cells and presence of only unlipidated LC3B (LC3B-I, upper band) in the *ATG7* KO cells. Moreover, p62 was not degraded by autophagy in the *ATG7* KO and *Hexa* KO cells; thus, its level was increased (Fig 4.9B). However, neither soluble nor insoluble β-catenin levels increased in the KO cells. EBSS treatment decreased both soluble and insoluble p62 levels in HeLa WT cells, whilst increasing insoluble p62 level and decreasing soluble p62 in KO cells (Fig 4.9B). This suggested that EBSS treatment causes p62 to accumulate within protein aggregates, but these aggregates could not be degraded in the KO cells. In contrast to p62, β-catenin showed no accumulation in the insoluble fraction upon EBSS treatment (Fig 4.9B). Overall, these results suggest autophagy-independent regulation of β-catenin abundance by EBSS.

Under basal conditions, β-catenin is ubiquitinated and degraded by the UPS[325]. Moreover, the majority of the β-catenin found on the cell membrane contributes to cell junctions, whereas autophagy occurs only in the cytoplasm (Fig 4.8C). β-catenin might therefore be subjected to autophagic degradation when its cytoplasmic level is increased. To prevent proteasomal degradation of β-catenin, HeLa cells were treated with Velcade (*i.e.,* proteasome inhibitor) for 4 h. Unlike Baf A_1, Velcade treatment increased cytoplasmic and nuclear β-catenin level independent of the autophagy status of the cells (Fig 4.10A). Moreover, EBSS treatment decreased β-catenin levels even in the presence of Velcade treatment (Fig 4.10A). This suggests a proteosome-independent regulation of the β-catenin level by EBSS. Similar decrease was also observed in the presence of Baf A_1 or in the autophagy-incompetent cells (Fig 4.10A). Besides that, there was no substantial Torin1-mediated change in the β-catenin levels in either WT or KO cells with/without Velcade co-treatment (Fig 4.10B). These results indicated that EBSS regulates β-catenin abundance independently of autophagy and proteasome-mediated degradations.

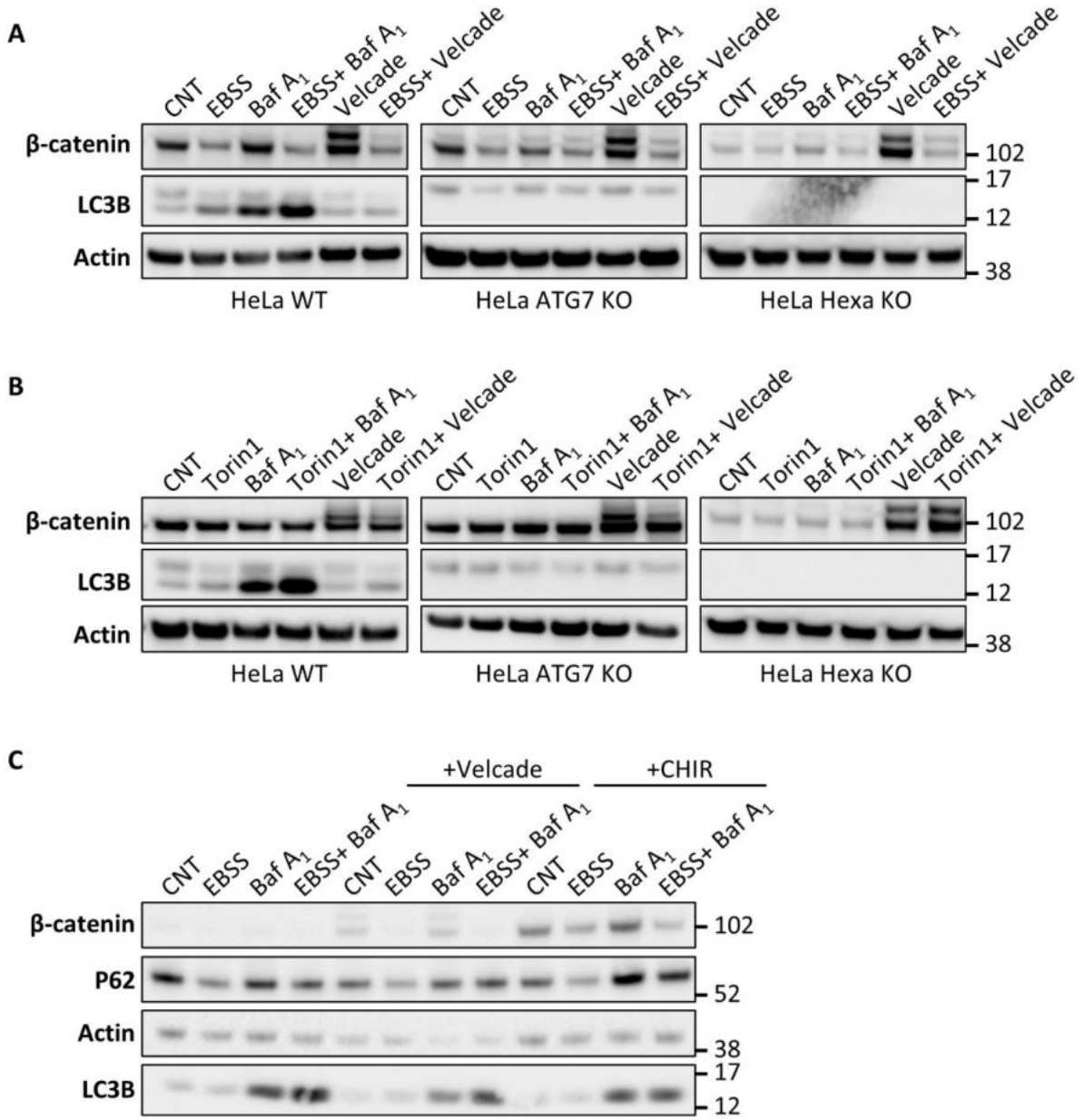

Figure 4.10 Study of possible regulation of β-catenin protein levels by autophagy under proteasome inhibition. (A-B) Western blotting of β-catenin and LC3B proteins following EBSS(A), 250 nM Torin1 (B), 200 nM Baf A_1, and/or 100 nM Velcade treatments for 4 h in HeLa WT, *ATG7* KO and *Hexa* KO cells. **(C)** Western blotting of β-catenin, p62, and LC3B proteins following EBSS, 200 nM Baf A_1, 100 nM Velcade and/or 5 μM CHIR treatments for 4 h in HeLa WT cells. Actin was used as a loading control.

To facilitate a more specific inhibition of β-catenin degradation, cells were treated with a GSK-3β inhibitor (CHIR-99021, in short CHIR). Inhibition of GSK-3β prevents phosphorylation and subsequent ubiquitination of β-catenin. 4 h of 5 μM CHIR was found to increase β-catenin at a similar level in the HeLa WT and *ATG7* KO cells (Appendix Fig 8A). CHIR treatment increased cytosolic β-catenin even more than Velcade treatment in WT and

KO cells at a similar level (Appendix Fig 8B). However, EBSS decreased β-catenin level even in the presence of CHIR (Fig 4.10C) in HeLa WT cells. Moreover, Baf A_1 co-treatment in addition to Velcade or CHIR did not prevent the EBSS-mediated reduction in the β-catenin level (Fig 4.10C). This confirms autophagy and proteasome independent activity of EBSS on β-catenin. Additionally, similar decreases were observed in the phospho- and non-phospho-β-catenin pools (Appendix Fig 9). EBSS treatment decreased their level similar to total β-catenin. This suggests that EBSS treatment does not interfere with the phosphodegron regulation of β-catenin. Furthermore, β-catenin staining showed that the Velcade-induced increase in the cytoplasmic and nuclear β-catenin was suppressed after EBSS treatment, but not after Torin1 treatment (Fig 4.11). Similar observations were also made in HCT116 cells: β-catenin accumulated in the cytoplasm in response to Velcade treatment but not with Baf A_1 treatment (Appendix Fig 10A); EBSS but not Torin1 treatment reduced β-catenin level in the presence of Baf A_1, Velcade or CHIR (Appendix Fig 10B). These results confirmed that EBSS modulates β-catenin levels independently of autophagy and proteasome degradation.

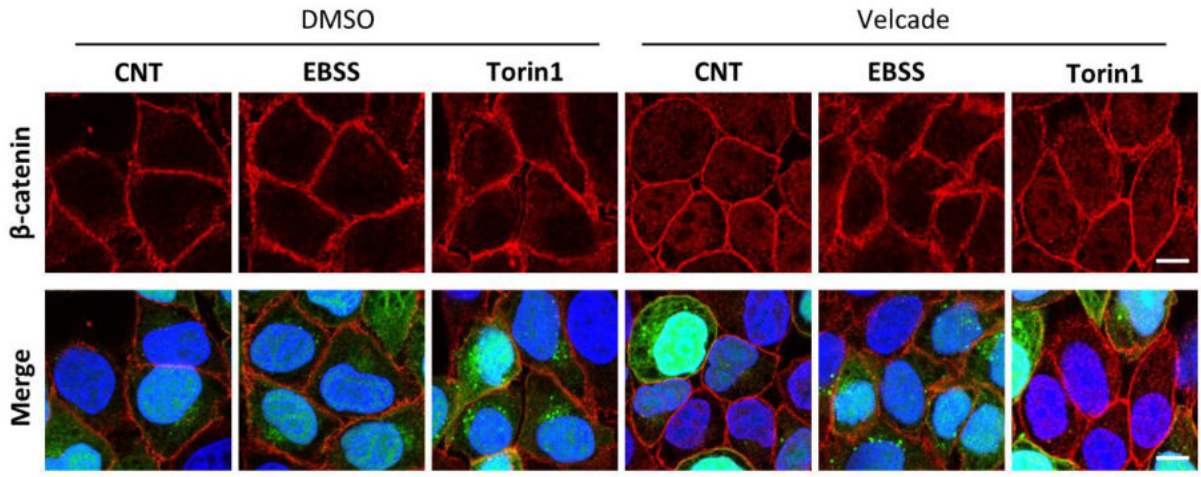

Figure 4.11 Modulation of cytosolic ß-catenin levels by EBSS treatment. Immunofluorescence analysis of endogenous β-catenin (red) in HeLa cells treated with EBSS and 250 nM Torin1 for 4 h in the presence or absence of 100 nM Velcade co-treatment. Merge represents β-catenin, LC3B (green) and DAPI (blue) staining. Scale bar = 10 μm.

To further interrogate the effect of autophagy on the β-catenin protein level, autophagy was reactivated in autophagy-incompetent cells. *ATG7* KO HeLa cells were transfected with WT human ATG7 or active-site mutant ATG7(CS) (Fig 4.12A). Even though re-expression of either ATG7 variants rescued autophagy in HeLa *ATG7* KO cells, β-catenin levels were not changed (Fig 4.12A). In fact, comparison of different isogenic cell line pairs with intact or lost *ATG7* KO showed no differences in β-catenin levels in any of the cell line pairs tested

(Appendix Fig 11A). Indeed, inhibiting autophagy by CRISPR/Cas9-mediated KO of key autophagy genes other than *ATG7* in U2OS cells also showed no change in the β-catenin levels (Appendix Fig 11B). These results indicate that β-catenin levels are insensitive to genetic activation or inhibition of autophagy.

It is a possibility that CRISPR/Cas9-mediated KO cells might have adapted to the lack of autophagy over the time. In addition, in the previously shown data, 4 h of Baf A_1 and CQ treatments might have been insufficient for a robust autophagy inhibition and subsequent β-catenin regulation (Fig 4.9A). Conversely, longer exposure of the cells to Baf A_1 and CQ have also been found to toxic (data not shown), which could affect β-catenin levels in an autophagy-independent manner. Therefore, an inducible autophagy inhibition system was established in HeLa cells. Doxycycline-inducible expression of EGFP tagged ATG4B-dominant negative mutant ($ATG4B^{DN}$) was shown to inactivate autophagy in two different clones, while expression of EGFP alone did not affect cellular autophagy (Fig 4.12B). However, β-catenin levels did not change even after 24 or 48 h of EGFP-ATG4BDN expression in these cells. Moreover, $ATG4B^{DN}$-mediated inhibition of autophagy changed neither levels nor cellular localization of β-catenin (Fig 4.12B). Similar observations were also made in MiaPaca cells (data not shown). These results suggest that β-catenin levels are also independent of the duration of autophagy inhibition.

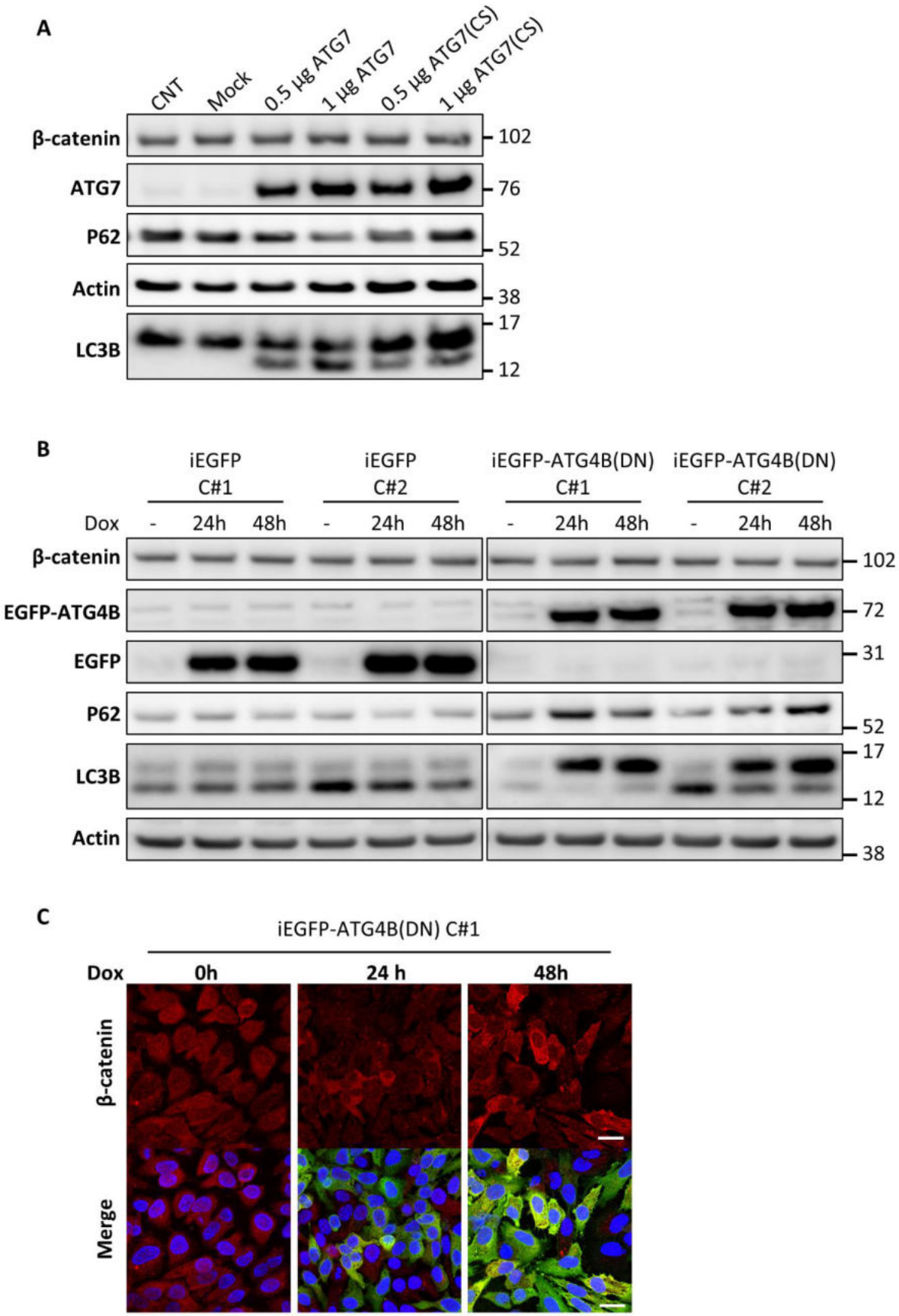

Figure 4.12 Genetic blockage of autophagy does not affect β-catenin levels. ***(A)*** Western blotting of β-catenin, ATG7, LC3B, and p62 following reactivation of autophagy in HeLa

ATG7 KO cells 24 h after transfection with of 0.5-1 μg of WT ATG7 or active-site mutant ATG7(CS). Mock represents transfection with empty plasmid. **(B)** Western blotting of β-catenin, EGFP-ATG4B^{DN} (anti-GFP), EGFP, p62, and LC3B following inhibition of autophagy by Dox-mediated ATG4B-DN expression (Dox treatment for 0-48 h). Two different clones (C#1 and C#2) of HeLa cells are shown for each condition. **(C)** Immunofluorescence analysis of endogenous β-catenin (red) in HeLa cells treated with Dox for 0-48 h. Merge represents β-catenin, EGFP-ATG4B^{DN} (green) and DAPI (blue) staining. Scale bar = 20 μm.

4.3. Exploring a role of LC3/GABARAP in regulation of Wnt/β-catenin signalling

Having shown that β-catenin is not a target of autophagic degradation, I hypothesized that LC3/GABARAP binding might exert another regulatory role in Wnt/β-catenin signalling. To begin with, the intracellular interaction of β-catenin with GFP-LC3B proteins was shown using HeLa cells stably expressing GFP-LC3B (Fig 4.13A). Endogenous β-catenin proteins were immunoprecipitated together with GFP-LC3B proteins (Fig 4.13A). This suggests an intracellular interaction between these two proteins. Moreover, colocalization of β-catenin with endogenous LC3B (data not shown) and GABARAP (Fig 4.13B) proteins was examined under autophagy- and proteasome-inhibited conditions. β-catenin mostly colocalized with GABARAP proteins in the cytoplasm and nucleus when the proteasome was inhibited using Velcade, or when β-catenin phosphorylation/degradation was inhibited by CHIR treatment (Fig 4.13B). Consistent with previous results suggesting that β-catenin is not a target of autophagic degradation, there was no specific colocalization between autophagosome puncta (green dots) and β-catenin staining (Fig 4.13B). Under basal conditions, β-catenin showed only a modest cytoplasmic and nuclear colocalization with GABARAP proteins (Fig 4.13B).

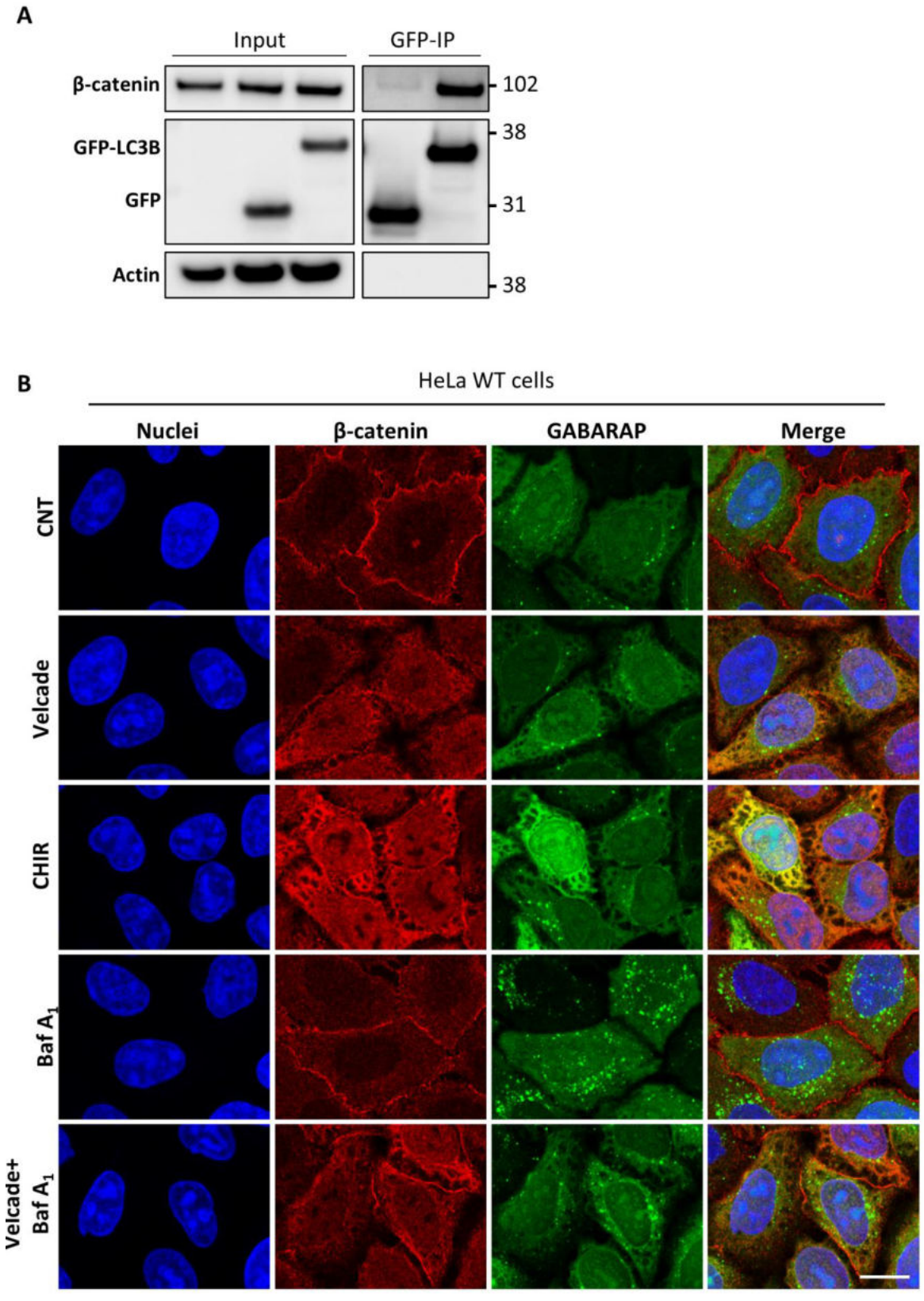

Figure 4.13 Endogenous β-catenin interacts with LC3B and GABARAP proteins. (A) Co-immunoprecipitation of β-catenin with GFP-LC3B. GFP-IP was done using cell lysates from HeLa cells stably expressing GFP-LC3B (input shown right-hand lane) and HeLa cells transfected with GFP (input shown in middle lane). WT HeLa cells were also shown in the

input. Immunoprecipitation of GFP–LC3B or negative control GFP were shown (GFP-IP) using an anti-GFP ab. **(B)** Confocal immunofluorescence microscopy analysis of endogenous β-catenin (red) and LC3B (green) in HeLa WT cells treated with 100 nM Velcade, 5 μM CHIR and/or 200 nM Baf A_1 for 4 h. DAPI used to stain nuclei (blue). Scale bar = 10 μm.

To examine the effect of LC3/GABARAP proteins on β-catenin protein abundance, GFP-LC3B and GFP-GABARAP proteins were expressed in HeLa cells at various amounts (Fig 4.14A). However, no change was detected in β-catenin protein level 24 h upon the transfections. Additionally, to prevent proteasomal degradation of β-catenin, HEK293, HCT116, HeLa WT, and HeLa Hexa KO cells were treated with Velcade or Wnt3a-conditioned medium (Appendix Fig 12). Wnt3a induces the accumulation of β-catenin by stimulating Wnt/β-catenin signalling axis, which leads to release of β-catenin from the destruction complex and its stabilization in the cytosol and the nucleus[325]. However, LC3B/GABARAP expression did not change β-catenin abundance in any of the cell lines tested (Appendix Fig 12). Nor was Velcade- and Wnt3a-mediated accumulation of β-catenin affected by LC3B/GABARAP expression in these cells after the transfections. These results suggest that LC3/GABARAP proteins are not likely to regulate β-catenin abundance in the cells.

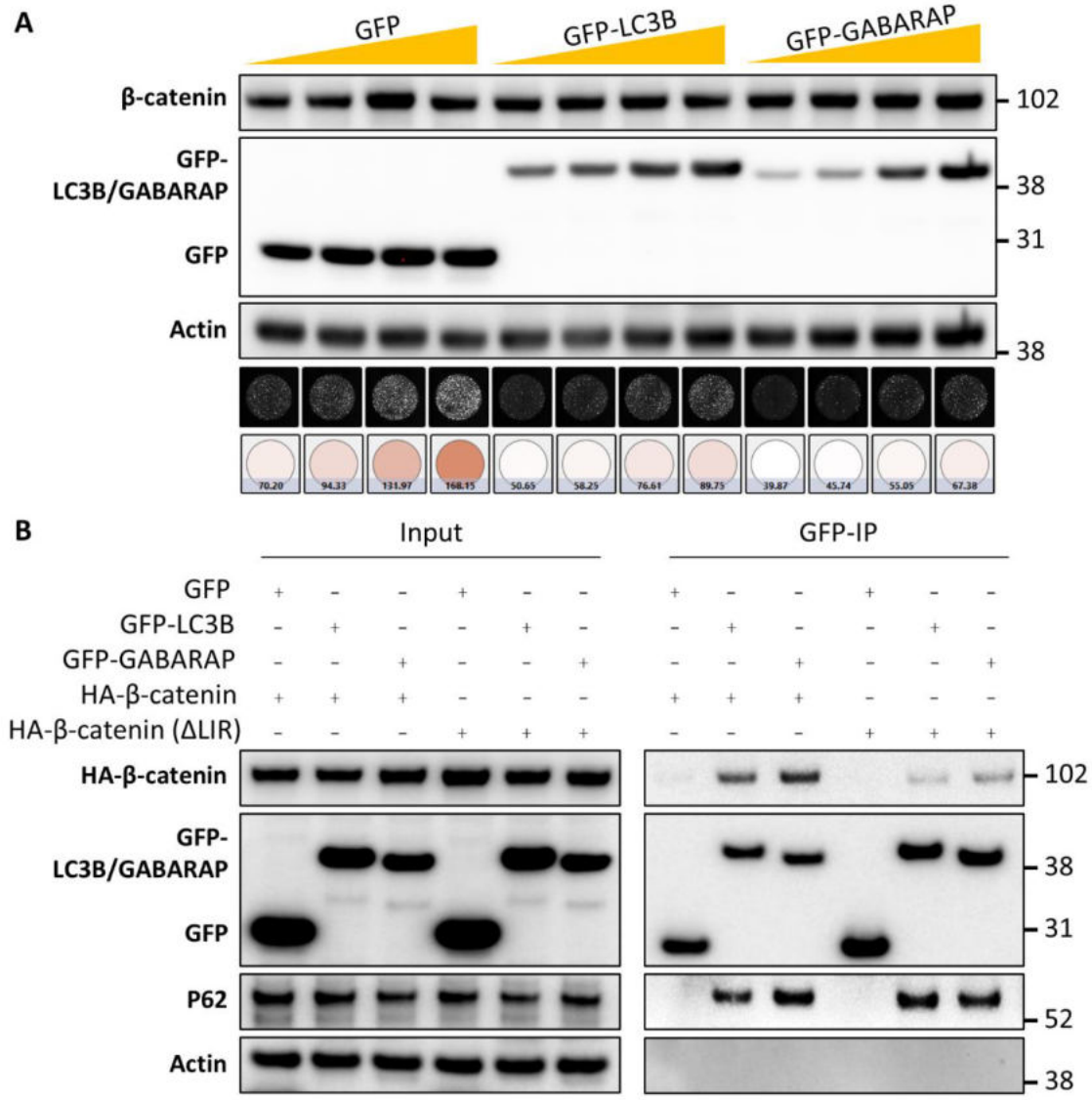

Figure 4.14 Study of possible regulation of β-catenin protein levels by LC3/GABARAP in HeLa cells. ***(A)*** Varying amounts (0.5-2 μg) of GFP-LC3B, GFP-GABARAP, and free GFP were expressed in HeLa WT cells for 24 h, and cell lysates were immunoblotted with anti-GFP and anti-β-catenin antibodies. In the bottom panel, the GFP signal and mean signal intensity from the transfected cells are shown. **(B)** Co-immunoprecipitation of GFP, GFP–LC3B, and GFP-GABARAP in HeLa WT cells. 1 μg HA-β-catenin or 0.4 μg HA-β-catenin(ΔLIR) and 0.5 μg GFP/LC3B/GABARAP were co-expressed in HeLa cells for 24 h. Binding of HA-β-catenin and HA-β-catenin(ΔLIR) to GFP, GFP-LC3B and GFP-GABARAP was probed using anti-HA antibody. Actin was used as a loading control.

Next, intracellular functionality of the β-catenin LIR motif was examined. For that purpose, WT and LIR-mutant β-catenin variants were overexpressed in HEK293 cells. Surprisingly, the same amount of DNA transfections produced different amount of β-catenin in the cells (Appendix Fig 13A). cDNA encoding LIR-mutant β-catenin resulted in more protein than that encoding WT β-catenin for the same amount of DNA used for transfection. A similar difference was observed in *ATG7* KO HEK293 cells and when the cells were treated

with CHIR or Velcade after 24 h of transfection (Appendix Fig 13B). This suggested that higher expression of the LIR-mutant β-catenin is independent from autophagy- or proteasome-dependent turnover. It is concluded that these plasmids needed to be transfected with a 5:2 ratio to achieve equal amount of β-catenin protein in the cells (data not shown).

After adjusting their transfection ratio, a co-IP experiment was performed to determine whether β-catenin associates with GFP-LC3B/GABARAP proteins through its LIR motif (Fig 4.14B). Results showed that more β-catenin immunoprecipitated with GFP-GABARAP compared to GFP-LC3B, and that the interaction was reduced by the LIR mutation (Fig 4.14B). Taken together, these findings support the data obtained with GST pulldown assays (Fig 4.4).

Furthermore, effects of the LIR mutation on the β-catenin phosphorylation and its binding to Wnt signalling proteins were examined with a co-IP experiment (Fig 4.15). There was no dramatic difference in the phosphorylation status of immunoprecipitated WT and LIR-mutant β-catenin proteins. Velcade and CHIR treatments also similarly affected the phosphorylation status of WT and LIR-mutant β-catenin (Fig 4.15). On the other hand, LIR-mutant β-catenin was found to bind more GSK3β than WT β-catenin, whereas there was no difference in the AXIN1/2 binding (Fig 4.15). This effect was lost after CHIR treatment, which suggests that the kinase activity of GSK3β is important for this difference. Nevertheless, it is hard to associate more GSK3β binding with LC3/GABARAP proteins as there was no LC3B or GABARAP co-precipitated with β-catenin proteins (Fig 4.15). Detection of LC3B and GABARAP binding to β-catenin proteins might have been compromised by involvement of β-catenin proteins in other intracellular complexes bound to β-catenin with a higher affinity than LC3/GABARAP proteins.

Taken together, these data show that β-catenin interacts with intracellular LC3/GABARAP proteins through its LIR motif. However, this interaction does not regulate β-catenin abundance or phosphorylation.

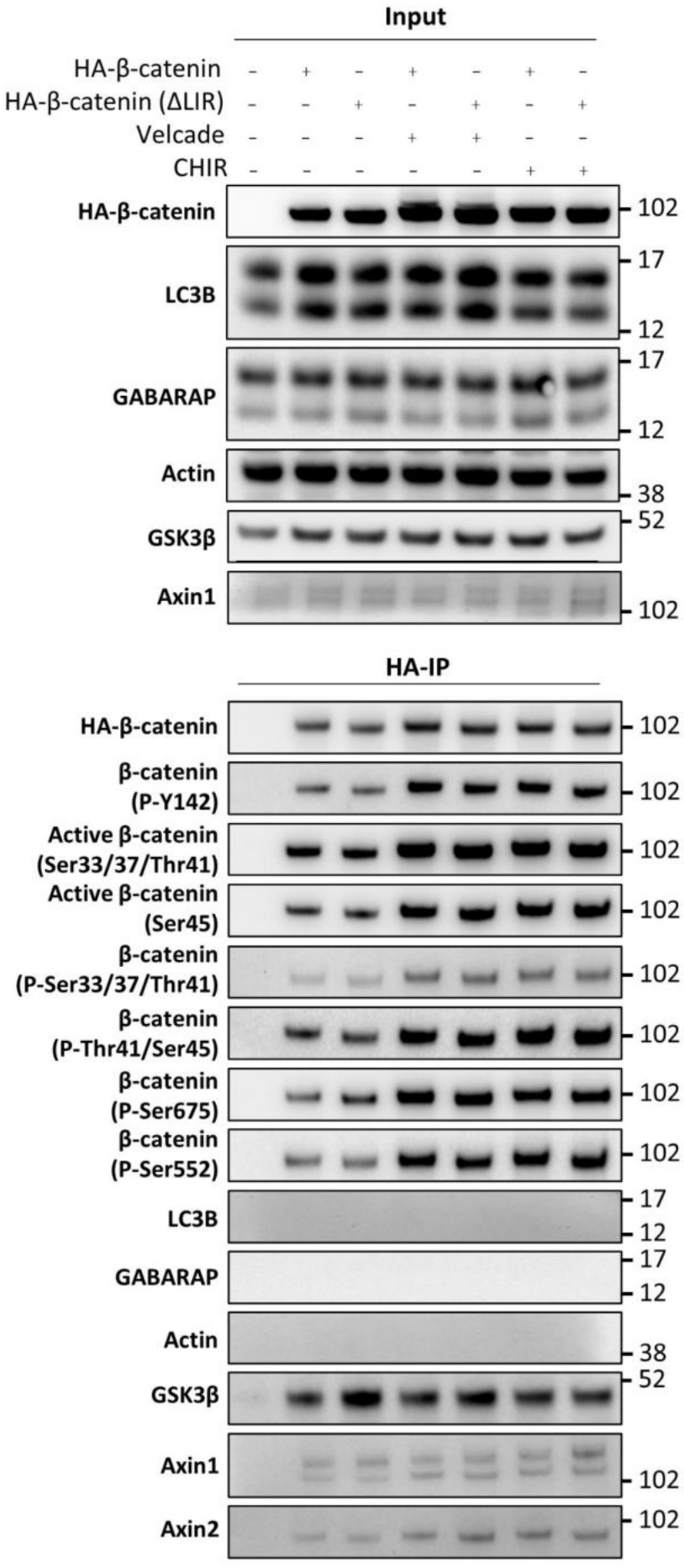
Input
HA-β-catenin - + - + - + -
HA-β-catenin (ΔLIR) - - + - + - +
Velcade - - - + + - -
CHIR - - - - - + +
HA-β-catenin
LC3B
GABARAP
Actin
GSK3β
Axin1
102
17
12
17
12
38
52
102
HA-IP
HA-β-catenin
β-catenin (P-Y142)
Active β-catenin (Ser33/37/Thr41)
Active β-catenin (Ser45)
β-catenin (P-Ser33/37/Thr41)
β-catenin (P-Thr41/Ser45)
β-catenin (P-Ser675)
β-catenin (P-Ser552)
LC3B
GABARAP
Actin
GSK3β
Axin1
Axin2
102
102
102
102
102
102
102
102
17
12
17
12
38
52
102
102

Figure 4.15 Study of regulation of β-catenin phosphorylation and interactions by the LIR mutation in HeLa WT cells. Co-IP of HA-β-catenin and HA-β-catenin(ΔLIR) in HeLa cells treated with 100 nM Velcade or 5 μM CHIR for 4 h as indicated. HeLa cells were transfected with 1 μg of HA-β-catenin and 0.4 μg of HA-β-catenin(ΔLIR), and cells analyzed 24 h after transfection. Immunoblotting with the indicated antibodies demonstrates β-catenin phosphorylation and its binding to AXIN1/2 and GSK3β.

4.4. Studying the role of LC3/GABARAP in β-catenin transcriptional activity

Previous reports indicated that autophagy, by degrading β-catenin, may regulate its transcriptional activity[112, 393]. For example, Petherick and colleagues used the TopFlash luciferase reporter system to assess the transcriptional activity of β-catenin[112]. They showed that induction of autophagy by nutrient deprivation reduced the transcriptional output of β-catenin signalling in HT29 cells. Likewise, I could show that the luciferase activity in HEK293 cells transfected with the TopFlash reporter vectors was reduced by EBSS treatment (Appendix Fig 14A). However, TopFlash activity was also reduced by EBSS in *ATG7* KO HEK293 cells, which suggests an autophagy-independent effect (Appendix Fig 14A). More surprisingly, Torin1 and Baf A_1 treatments also decreased TopFlash activity (Appendix Fig 14A). This may suggest downregulation of the transcriptional output of the Wnt/β-catenin pathway in response to cellular stress.

To investigate the role of the novel LIR motif in β-catenin transcriptional activity, WT and LIR-mutant forms of β-catenin were co-expressed with TopFlash reporter vectors in HEK293 cells. The luciferase activity induced by the WT and LIR mutant β-catenin proteins strongly correlated with the expression of these proteins in HEK293 cells (Fig 4.16A-C). Similar levels of proteins generated similar luciferase activities.

To address the effect of LC3/GABARAP proteins on the β-catenin luciferase activity, GFP, GFP-LC3B, or GFP-GABARAP were co-expressed with TopFlash reporter vectors in HEK293 cells (Fig 4.16D and 16E). These transfections did not affect β-catenin levels (Fig 4.16D). Nevertheless, GFP-LC3B and GFP-GABARAP expressions increased luciferase activity under basal, CHIR- and Wnt3a-treated conditions compared to the transfection with GFP alone (Fig 4.16F). These results suggest that LC3/GABARAP proteins might regulate β-catenin transcription activity.

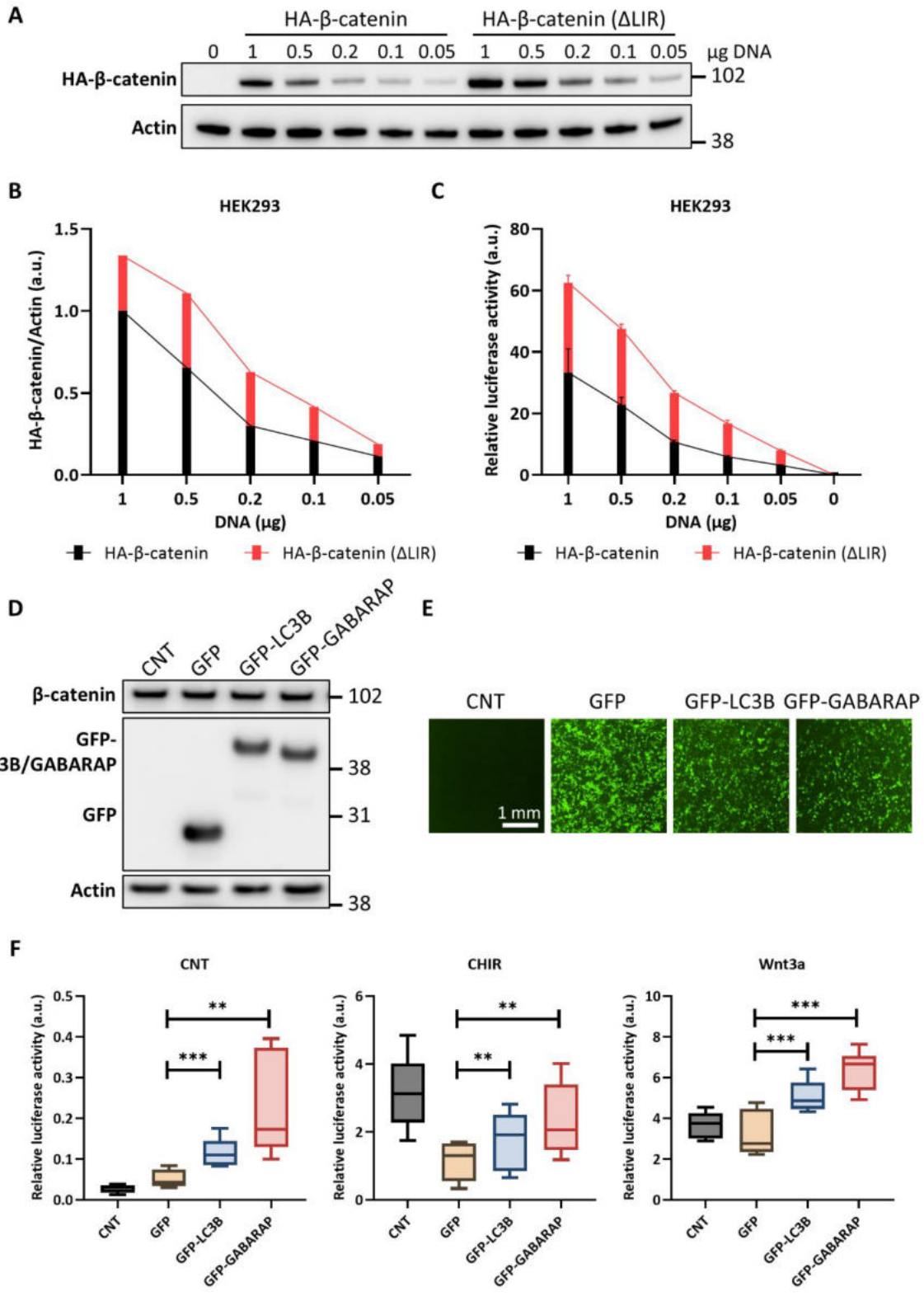

Figure 4.16 Effect of LC3/GABARAP interaction on β-catenin transcription activity in the TopFlash luciferase assay. ***(A)*** Varying amounts (0.05-1 µg) of HA-β-catenin and HA-β-catenin(ΔLIR) were expressed in HEK293 cells along with TopFlash reporter vectors for 24 h, and the cell lysate were immunoblotted with anti-HA antibody. **(B)** Quantification by densitometry of the HA-β-catenin/actin ratio in HEK293 cells. **(C)** Luciferase activity produced by HA-β-catenin and HA-β-catenin(ΔLIR) expression in TopFlash assay (see

methods). The bars represent the mean values with standard deviations of three independent experiments. **(D)** HEK293 cells were transfected with the same amount of GFP, GFP-LC3B and GFP-GABARAP, and cells were analyzed 24 h after transfection using anti-GFP antibody. Endogenous β-catenin levels were determined by anti-β-catenin immunoblotting. **(E)** Expression of the proteins was observed by fluorescence microscopy. **(F)** Top/Flash Luciferase activity upon expression of GFP, GFP-LC3B, and GFP-GABARAP. 24 h upon transfection, HEK293 cells were treated with 5 μM CHIR for 4 h after 24 h of the transfections, or transfections were performed in Wnt3a-conditioned media. The bars represent the mean values with standard deviations of three independent experiments. Statistical significance was assessed using paired Student's t-test (**p<0.01, and ***p < 0.001). a.u., arbitrary units

To further probe whether LC3/GABARAP proteins stimulate β-catenin transcription activity, a GFP reporter system was tested. This system represents a unique tool for live cell analysis and helps the formulation of a high-resolution understanding of the events that affect β-catenin transcription activity. It works on the same principle as the TopFlash system, and instead of chemiluminescence produced by the luciferase, it induces GFP protein expression as an output of β-catenin transcription activity. To this end, HEK293 cells stably expressing GFP reporter vectors were generated (see methods). 30% of these cells produced GFP in response to 24 h treatment with Wnt3a-conditioned media (Fig 4.17). Surprisingly, overexpression of mCherry-LC3B or mCherry-GABARAP did not cause any further increase in the GFP-positive cell pool under basal or Wnt3a-treated conditions (Fig 4.17). Nevertheless, the ratio of GFP-positive cells within the mCherry-positive pool (LC3B: 29.7/46.1, GABARAP: 28.4/48.0) was higher than in the cells lacking mCherry-LC3/GABARAP expression at the basal condition (30.0/68.1). Similar observations were made in HEK293 *ATG7* KO cells (Appendix Fig 14B). These results should be taken with caution as the effect of mock transfection (mCherry alone) was not tested. On the other hand, EBSS treatment did not reduce the Wnt3a-induced GFP signal, although it was shown to decrease β-catenin level effectively (Appendix Fig 14C). This suggests that the GFP reporter system may not be as sensitive as the TopFlash luciferase systems (Fig 16F). Other treatments regulating autophagy (Torin1, Baf A_1 and CQ) did not cause any change in the GFP-positive pool either under basal condition or after the treatment with Wnt3a-conditioned media (Appendix Fig 14C).

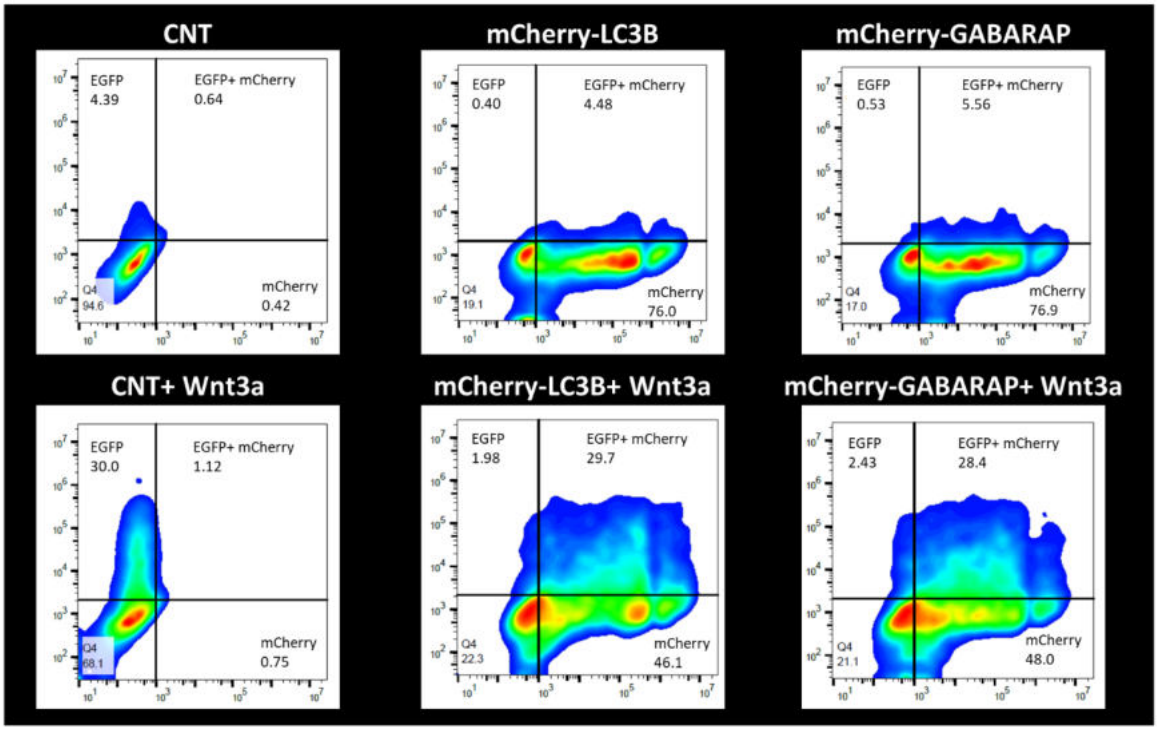

Figure 4.17 Effect of LC3/GABARAP interaction on β-catenin transcription activity as assessed by the GFP reporter assay. The GFP-reporter assay produces a GFP signal in response to β-catenin activity. β-catenin transcriptional activity upon expression of mCherry-LC3B and mCherry-GABARAP in HEK293 was determined using the GFP reporter assay (see methods). The LC3/GABARAP transfections were performed either in control media (*i.e.,* L-cell media without Wnt3a) or in Wnt3a-conditioned media. The GFP/mCherry-positive cells were detected by flow cytometry.

4.5. Studying the role of β-catenin on autophagy

In the cell nucleus, β-catenin associates with transcriptional factors from the TCF/Lef family and drives transcription of Wnt-responsive genes responsible for the control of cell fate decisions in many cells and tissues[325]. Therefore, expression of many genes is activated or repressed by β-catenin activity. Recently, Wnt/βcatenin was reported to supresses autophagy and p62 expression[112]. To address the effect of β-catenin on autophagy, β-catenin expression was silenced in HeLa cells using siRNAs (Fig 4.18A). Western blotting confirmed decreased levels of p62 following β-catenin silencing. Besides, silencing β-catenin did not exert a major shift in LC3B proteins under control or Baf A_1 treatment conditions, suggesting no regulation of autophagy by β-catenin (Fig 4.18A). Similar results were observed in HEK293 cells (Appendix Fig 15). Surprisingly, reduced p62 levels were not observed when β-catenin was silenced in parallel with Baf A_1-mediated blockage of autophagy; this was the case in both HeLa and HEK293 cells (Fig 4.18A and Appendix Fig 15). These data may suggest that β-

catenin silencing makes p62 more prone to degradation by basal autophagy. On the other hand, p62 and LC3B levels were not affected by WT or LIR mutant β-catenin expression in HeLa cells (Fig 4.19B).

To further interrogate the effect of β-catenin on autophagy, β-catenin was knocked out in HAP1 cells using the CRISPR/Cas9 system (Fig 4.18C). Interestingly, deletion of β-catenin increased p62 levels and the LC3B-II/I ratio compared to WT cells (Fig 4.18C). In addition, more GFP-LC3B puncta were observed in the β-catenin KO clones than WT HAP1 cells (Fig 4.18D). These results suggest that deletion of β-catenin blocks autophagic degradation in HAP1 cells. Nevertheless, these assays should be repeated in the same cell lines in a systemic comparison to understand the potentially cell-specific roles of β-catenin. For now, these preliminary data suggest a role for β-catenin in the regulation of autophagy in HAP1 cells but not in HeLa and HEK293 cells.

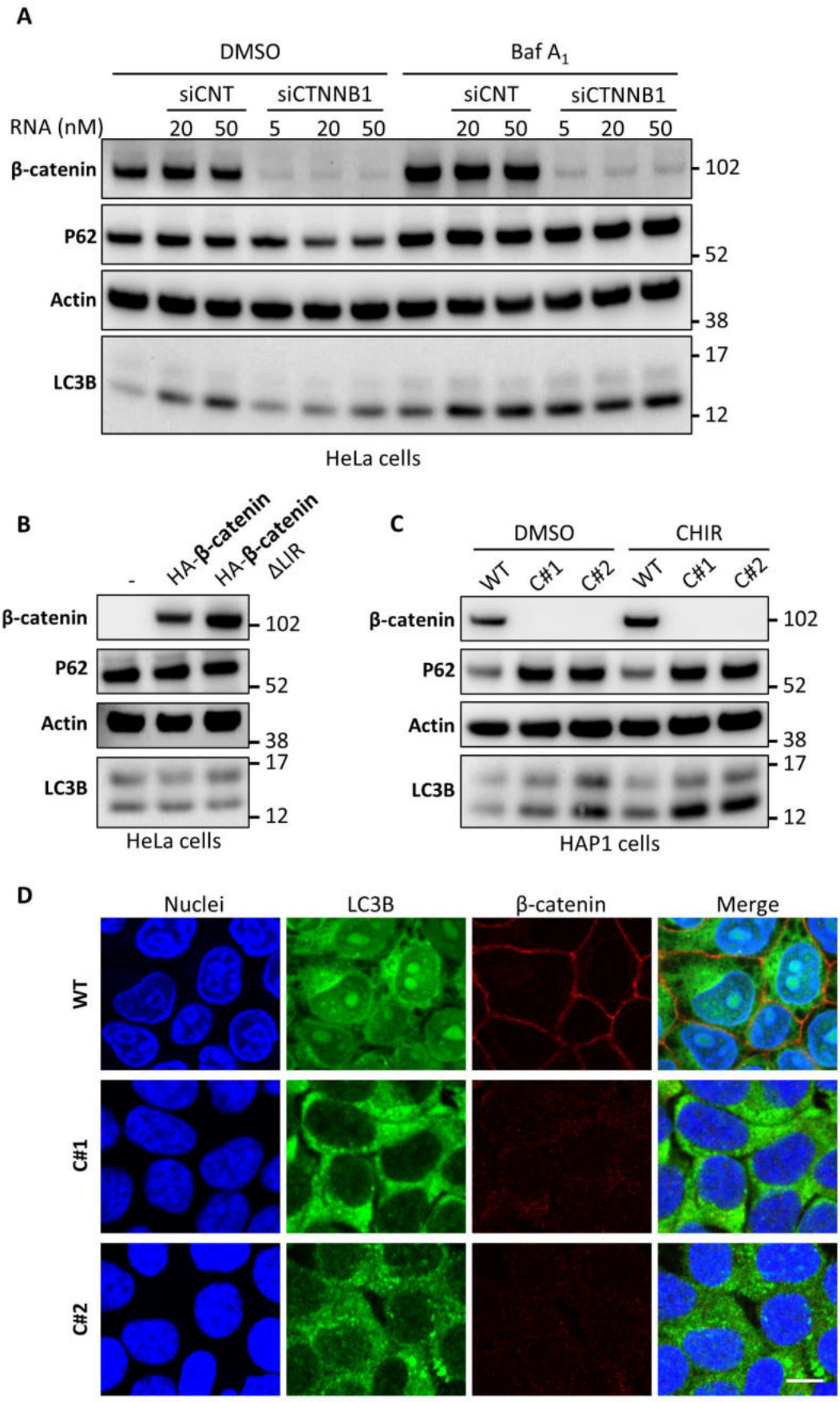
A
DMSO
Baf A1
siCNT
siCTNNB1
siCNT
siCTNNB1
RNA (nM)
20 50 5 20 50
20 50 5 20 50
β-catenin
P62
Actin
LC3B
102
52
38
17
12
HeLa cells
B
-
HA-β-catenin
HA-β-catenin ΔLIR
β-catenin
P62
Actin
LC3B
102
52
38
17
12
HeLa cells
C
DMSO
CHIR
WT C#1 C#2 WT C#1 C#2
β-catenin
P62
Actin
LC3B
102
52
38
17
12
HAP1 cells
D
Nuclei
LC3B
β-catenin
Merge
WT
C#1
C#2

Figure 4.18 Effect of β-catenin on autophagy. (A) HeLa cells were transfected with various amounts of (5-50 nM) non-targeting (siCNT) or β-catenin targeting (siCTNNB1) siRNAs for 24 h in the presence or absence of 200 nM Baf A_1. Immunoblotting confirmed siCTNNB1-mediated silencing of endogenous β-catenin. **(B)** HA-β-catenin and HA-β-catenin(ΔLIR) were overexpressed in HeLa cells for 24 h, which confirmed using an anti-HA antibody. **(C)** CRISPR-mediated deletion of β-catenin in two separate clones (C#1 and C#2) of HAP1 cells are shown in the presence and absence of 5 μM CHIR treatment for 4 h. **(D)** Deletion of β-catenin (red) in HAP1 cells was shown by confocal microscopy along with LC3B staining (green). DAPI was used to mark nuclei.

5. Results Summary

The data provided in this thesis presents a framework of identifying and studying autophagosome-associated proteins and will help in describing cellular mechanisms controlling the biogenesis and cargo preference of autophagosomes. While addressing the aims of the study, the main discoveries are as follows:

Aim 1: To create the basis for understanding functions of autophagy through studying the composition of autophagosomes isolated from tumour cells (Chapter I)

- Comparison of more than one autophagy-incompetent cell line with WT cells provides a better image of autophagy substrates through whole-cell proteomics analysis.
- A combinatorial autophagosome isolation protocol was established and shown to be more efficient than the singular applications of immune isolation and fractionation approaches.
- Analysis of purified autophagosomes revealed many novel potential autophagy substrates.
- EAAT1 is defined as a novel target of autophagic degradation.

Aim 2: To study the interplay between autophagy and Wnt/β-catenin signalling (Chapter II)

- An atypical LIR motif in the β-catenin protein structure was identified.
- β-catenin was shown not to be a target of autophagic degradation.
- Amino acid starvation downregulates β-catenin levels independently from autophagy and proteasome.
- LC3/GABARAP proteins (up)regulate transcriptional activity of β-catenin.
- β-catenin regulates autophagy in a cell-type specific manner.

6. Discussion

Autophagy as a cellular process has been known for more than 50 years. Yoshinori Ohsumi's paradigm-shifting research performed in the 1990s brought to light autophagy's fundamental significance in physiology and medicine. For his discoveries, he was awarded the Nobel Prize in Physiology or Medicine. To date, defective autophagy has been linked to Parkinson's disease, type-2 diabetes, and other age-related illnesses. Mutations in autophagy genes were shown to underlie several genetic diseases. Disturbances in autophagic activity have also been observed in many human cancers. The recurring theme from autophagy research is that autophagy maintains cellular homeostasis by regulating cellular stresses (e.g., oxidative stress), DNA damage response mechanism, proliferative signals (e.g., Nrf-2 and Wnt/β-catenin), and inflammation[394]. Although intensive research has been carried out to date, it still requires significant effort to decipher the mechanism of autophagy and to fully understand its physiological roles. Therefore, in this thesis, I aimed to create the basis for understanding the functions of autophagy by studying cargo targeted by autophagy and the interconnection between autophagy and the proliferative Wnt/β-catenin signalling.

Employing proteomics-based studies to examine proteins targeted by autophagy has been embraced by many autophagy researchers. The findings in this thesis show the use of proteomics at high efficiency and accuracy in identifying proteins targeted by autophagy. In the review of autophagy literature, proteomics is mainly used to analyse changes in the entire cellular proteome in the context of genetic or pharmacological autophagy modification[160, 161]. However, whole-cell proteomics studies have shown to be bringing lots of false-positive hits along with a comprehensive list of autophagy substrates. The findings of this study suggest a way to reduce the number of non-specific hits in the whole-cell autophagy proteomics studies by clustering out the proteins whose levels changed by some autophagy-independent roles of each ATG protein.

This thesis has also aimed to increase the efficiency and accuracy of proteomics by focusing the scope of analysis on purified autophagosomes instead of whole-cell lysate. Therefore, having a robust technique for purifying autophagosomes was key to the success of this project. A number of protocols for the isolation of autophagosomes have been published (Table 2). They typically involve the use of density gradients or, alternatively, immunoprecipitations using GFP-LC3 anchored in the autophagic membranes. Only a few of

them employed proteomics analysis of their autophagosome preparations. A comparison revealed low overlap between the proteins identified in these studies, suggesting an unmet need for autophagosome purification and proteome analysis methods. This thesis established a new methodology combining fractionation and immune isolation methods to purify intact autophagosomes from the cells. Subsequent proteomic analysis of the purified autophagosomes has revealed many known and novel potential autophagy substrates (e.g., EAAT1). I was also able to show that many of the proteins identified in this study were commonly shared by other proteomics studies that analysed autophagosome proteins. The method developed, and proteins identified in this study can pave the way for many other studies to attain a role for autophagy in the various cell signalling or disease settings. For example, analysis of autophagosomes purified under certain conditions, such as treatments inducing mitophagy (FCCP[395]) or aggrephagy (Velcade[396]), could help researchers to comparatively study and explore mechanisms behind the selective autophagy. Moreover, the purification methodology developed in this thesis can be used to explore lipid composition and membrane sources of autophagosomes, as well as to study the lysosomal fusion mechanism by setting up in vitro fusion assays with purified autophagosomes and lysosomes.

This thesis has also analysed the interplay between autophagy and Wnt/β-catenin signalling. Both autophagy and Wnt signalling have been shown to play essential roles in development, tissue homeostasis, and tumorigenesis[393]. In addition, both pathways have been found commonly (up)regulated in various types of cancer (e.g., hepatocellular carcinoma, breast, lung cancer, and colorectal cancer) and associated with therapy resistance[393]. As mentioned in the review of literature, many studies suggested crosstalk between the Wnt/β-catenin pathway and autophagy at various stages. However, the mechanisms regulating the interplay between these pathways still need to be elucidated. This may reveal new mechanisms to overcome therapy resistance and limit the progression of certain types of cancer.

Work presented in this thesis has focused on the link between β-catenin and LC3/GABARAP proteins. The LC3/GABARAP protein interaction network is involved in regulating an increasing number of cellular processes, of which autophagy is the best studied[31]. Besides that, LC3/GABARAP proteins regulate non-autophagic processes by interacting with different classes of proteins such as kinases, RABGAPs, ubiquitin-ligases, etc[31]. All of these interactions require the presence of a functional LIR motif for the LC3/GABARAP interaction partners. In this thesis, I was able to identify an atypical LIR motif in the β-catenin protein sequence, which facilitates its binding to LC3/GABARAP with a stronger avidity to the

GABARAP family. In contrast to the two hydrophobic residues containing canonical LIR motifs (F/W/YxxL/I/V), the β-catenin's atypical-LIR motif contains only one central hydrophobic residue (W) surrounded by two acidic residues (E). This motif also shares high sequence similarity with two others previously published atypical LIR motifs from Bcl-2[132] and Trim5α[133]. To date, the number of the atypical LIR motif identified is limited[32]. The non-canonical mode of interaction presented in this thesis can open a new field to explore autophagy regulation as well as new LC3/GABARAP interactors. In addition, a comprehensive understanding of the LIR-mediated interactions can contribute to the efforts to design potent autophagy modulators.

In this study, I was also able to show that neither β-catenin protein abundance nor its transcriptional activity is regulated by autophagy but (down)regulated by amino acid starvation (EBSS) independently from autophagy. Moreover, LC3/GABARAP proteins are shown to (up)regulate β-catenin's transcriptional activity, where the contribution of the LIR motif still needs to be elucidated. These results may suggest an integration point to overcome Wnt/β-catenin signalling-mediated tumour proliferation and drug resistance mechanisms using amino acid starvation and targeting LC3/GABARAP interaction of β-catenin.

In conclusion, this study made an important contribution to the autophagy literature by *i.* establishing an efficient method for analysing autophagy-related proteins *ii.* revealing many potential new autophagy substrates, *iii*. identifying a link and a new binding mode between LC3/GABARAP and β-catenin proteins, *iv.* showing autophagy-independent regulation but amino acid starvation- and LC3/GABARAP-mediated regulation of β-catenin's transcriptional activity.

Further experimental details and findings will be discussed in the following sections.

6.1. Whole-cell proteome of autophagy-competent and -incompetent cells

In order to create a comparative basis for the analysis of purified autophagosomes, a whole-cell proteomics analysis was done (Fig 3.2). Comparison of HeLa WT cells with its autophagy-incompetent *ATG* gene KO counterparts revealed many proteins upregulated in the KO cells. It was expected that nearly all the proteins upregulated in the KO cells compared to WT cells would be traced back to the lack of autophagic activity. However, clustering of the

hits using a k-means algorithm has shown that it's not quite true (Fig 3.2B). This analysis exposed clusters referring to a collection of data points aggregated together because of certain similarities[397]. Analysis of 3 separate *ATG* KO cell lines along with one WT cell line revealed that each KO cell line has their own set of upregulated proteins (Fig 3.2B, cluster 1: *ATG7* KO specific, cluster 2: *Hexa* KO specific and cluster 4: *ATG4A/B* KO specific). This might be explained by autophagy-independent roles of each of the ATG protein (Table 3). The absence of each *ATG* gene might have affected a pathway other than autophagy. This clustering might also suggest one of the main reasons why comparative whole-cell proteomics studies result in many non-specific hits. Because, in many of those studies, one WT or untreated cell line was compared with another cell line in which autophagy is stimulated genetically or pharmacologically[160, 161]. The autophagy-independent roles of ATG proteins or absence of autophagy-specific modulators could be the main challenges in the autophagy-proteomics studies.

As a way to tackle this issue, comparison of more than one type of *ATG* KO cell line as in Figure 3.2 allowed to cluster proteins commonly increased in all of the *ATG* KO cells (cluster 5, Fig 3.2C). This cluster contained 5/6 well-known SARs except OPTN. Therefore, it can be suggested that cluster 5 is a better representative of autophagy target proteins compared to other clusters. OPTN is a well-studied aggrephagy and mitophagy receptor. The reason why OPTN was not commonly upregulated in ATG KO cells as other SARs is unclear. The data analysed in this study represents only one biological replicate. With additional replicates, OPTN might also move into the cluster 5. On the other hand, OPTN needs to be phosphorylated by TBK1 in order to bind LC3/GABARAP[107]. Perhaps, its role as SAR is inhibited or not activated in some cell lines.

Another notable finding of the whole-cell proteome analysis was that GABARAPL2 was increased in *ATG4A/B* KO and *ATG7* KO HeLa cells, while the levels of other ATG8 paralogs were either not changed or decreased (Fig 3.2E). A similar observation was made by Mancias *et. al.*,[65] in which GABARAPL2 was the most increased ATG8 paralog in their whole-cell proteome analysis of CQ-mediated autophagy-inhibited pancreatic cancer cells. There could be two reasons for that. First, ATG8 paralogs are indispensable for the elongation of the phagophore membrane, whereas the GABARAPL2 was found to act late in autophagosome maturation by promoting either sealing of autophagosomes or their fusion with lysosomes in HeLa cells[398]. Moreover, the presence of uncomplete autophagosomes was confirmed in

various *ATG* gene KO cells[203-205]. Thus, GABARAPL2 might be accumulated on incomplete autophagosomal membranes in *ATG* KO cells for the purpose of enabling their sealing and fusion with lysosome. The second reason for GABARAPL2 enrichment in the *ATG* KO cells might be the small size and high sequence similarity of the ATG8 paralogs (over 80%). This might compromise the detection of unique peptides for each ATG8 proteins in the MS analysis.

In autophagy proteomics studies, ATG proteins appear to be of low abundance, and their level is not largely affected by autophagy stimulation[172]. The same observation was made in this study. The levels of autophagy regulators (ATG proteins, Fig 3.2E) in autophagy-incompetent cells were not different from WT cells, except for ATG4C, which is increased in all the autophagy-incompetent cells for an unknown reason. This confirms the notion that core autophagy regulators are not subjected to autophagic degradation but may be recycled back to cytoplasm to contribute to the formation of new autophagosomes[16]. This analysis might also refer to that whole-cell proteomics analysis is not effective for detecting autophagy regulators.

6.2. Establishing an autophagosome isolation method and a proteomics analysis of constituents of isolated autophagosomes

Analysis of bulk cytoplasmic autophagy has contributed significantly to our understanding of the autophagy process. Nevertheless, little is known about how specific cargo molecules, such as organelles, proteins, or intracellular pathogens, are targeted for selective autophagy. I aimed to employ quantitative proteomics to identify a cohort of novel and known autophagosome-enriched proteins, including cargo receptors. Having a robust technique for purifying autophagosomes is key to the success of this project. A number of protocols for isolation of autophagosomes have been published (Table 2). They typically involve use of density gradients or alternatively immunoprecipitations using GFP-LC3 anchored in the autophagic membranes. Use of special treatments, such as CQ or vinblastine to block microtubular movement and thus fusion between the autophagosomes and the lysosomes, provides an additional modification to the protocols aiming to enrich the autophagosomal fraction. However, analysis of three previous studies examining proteins in purified autophagosomal preparations showed low overlap in the proteins identified between these studies. For example, three studies purifying autophagosomes using density gradients and catalogue autophagosomal proteins using quantitative proteomics showed only one protein (PRDX6) in common[65, 166, 172]. Therefore, it suggests that there is still need for improvement in

autophagosome purification and proteome analysis methods. For that purpose, I established a distinctive method to purify autophagosomes from cancer cell lines.

To begin with, an immune isolation approach was employed to obtain an enriched autophagosomal fraction from cancer cells. The immune isolation protocol used in this study was adapted mainly from two studies that purified autophagosomes from GFP-LC3B mouse tissues using μMACS magnetic anti-GFP beads[187, 188]. These studies employed EM to confirm the success of the purification protocol. However, EM images presented in these papers included intact autophagosomes along with broken autophagosomal membranes as well as unidentified membrane particles. More strikingly, immunoblots of the isolated autophagosomes showed strong presence of LC3-I (non-lipidated, membrane-free LC3). This suggests involvement of the cytoplasmic LC3 interactome in addition to autophagosomes in these purifications[187, 188]. Nevertheless, these studies did not aim to analyse proteome content of autophagosomes but used them only for biochemical analysis, such as examining the presence of visual transduction proteins on the autophagosomes[187]. Therefore, I included additional washing steps before obtaining post-nuclear organellar fraction to remove all residual membrane-free LC3 proteins (see Methods). Even though the analysis of the purified autophagosomes from HCT116 GFP-LC3B cells did not involve any LC3-I proteins (Fig 3.4C), the protease protection assay showed no protection of the LC3 and p62 proteins from protease degradation (Fig 3.4E). There might be several possible explanations for such a result. First, the autophagosomes might have been disrupted during the immune isolation procedure. Another possible, and more likely, explanation for this might be that the GFP-LC3B proteins on the autophagosome membrane could be removed by the activity of ATG4 proteins in the cells once the autophagosomes were fully sealed. Therefore, it is possible that the intact autophagosomes in the organelle fraction might have no or much reduced amount of GFP-LC3B on their surface, which compromises their capturing by GFP-magnetic beads. Moreover, the GFP-LC3B and p62 proteins captured with magnetic beads might be coming from growing autophagosome membranes (not sealed yet), which are supposed to be rich in GFP-LC3B to complete the expansion and sealing of the autophagosome. In this regard, I decided to increase the amount of GFP-LC3B protein on the surface of intact autophagosomes by limiting ATG4 activity in the cells.

Activity of ATG4B in autophagy and LC3/GABARAP processing in HeLa cells were revealed by Robin Kettler's group[373] and briefly shown in Fig 3.5A,B,C. Therefore, *ATG4B*

KO HeLa cells expressing a pre-cleaved GFP-LC3B were used for immune isolation of autophagosomes. Evaluation of the isolated autophagosomes from HeLa G120 cells with the protease protection assay identified a degree of protection of GFP-LC3B and p62 proteins. However, the EM analysis showed many broken membranes in the isolates (Fig 3.6) like in the previous studies[187, 188]. One reason for capturing broken autophagosome membranes could be their disruption caused during homogenization of the cells. Thus, I decided to design a pre-purification step to immune isolation using a density gradient separation method.

Density-gradient separation method (also known as a membrane flotation assay) is used to separate particles (in our case: organelles) according to their size and density under a high centrifugal force. In the literature, the protocols established to fractionate autophagosomes mainly differ in the separation matrix (e.g., Metrazamide, Iodixanol, Percoll or Sucrose, listed in Table 2). These protocols require overnight centrifugation of the cell lysate inside of the gradient of one of these matrices. The most detailed, but also label-intensive, fractionation protocol was published by Seglen's group[173]. This protocol includes sequential multi-step long centrifugations of the cell homogenate into four different matrices including sucrose, Nycodenz, Percoll and Iodixanol. The most practical (time-wise) protocol was established by Mizushima's group[189] in which a discontinuous Optiprep (also known as Iodixanol) gradient matrix was used to fractionate autophagosomes with 3 hours of ultracentrifugation. They used the purified autophagosomes for a biochemical analysis but not for an MS analysis of their content. I decided to use this protocol to fractionate autophagosomes. The fractionation profile of the organelles in this thesis (Fig 3.8) is quite similar to the profile shown in Mizushima's paper. Also, analysis of the autophagosomes enriched fractions with the protease protection assay and the EM analysis confirmed presence of multiple intact autophagosomes in these fractions (Fig 3.7D and 3.8B). However, there were still some impurities, which is formulated to be removed with an additional immune isolation step as described in this thesis.

Previous studies used fractionation and immune isolation techniques separately to isolate autophagosomes (listed in Table 2). However, most of these studies did not evaluate the integrity of the isolated autophagosomes, and only a few of them employed an MS analysis to study the content of autophagosomes. There is only one study used a combinatorial approach (fractionation + immune isolation) to isolate and analyse the content of autophagosomes[184]. However, their methodology resulted in containing nonspecific membrane contaminants and broken membranes. In addition, the number of proteins (19) associated with autophagosomes

was very limited and none shared with my result. It is possibly due to that the author's mainly focused on the Hepatitis C Virus-induced autophagy in their study[184]. In my thesis, the purity and integrity of the isolated autophagosomes were shown by EM analysis (Fig 3.9F) and protease protection assays (Fig 3.9B). In the EM images, many autophagosomes with double membranes were detected. However, there was also a good deal of single-membraned vesicles in the autophagosome preparations. Nevertheless, every single vesicle was surrounded by GFP-magnetic beads, which suggests the presence of GFP-LC3B on the surface of these vesicle, also a strong proof for their being part of an autophagosome. The presence of single-membraned vesicles might be ascribed to the lysosomal fusion. Firstly, the lysosomal marker LAMP2 showed a shift in the lighter fractions together with GFP-LC3B and p62 proteins in response to Baf A_1 treatment (Fig 3.8A). Secondly, the short-term Baf A_1 treatment was shown not to block the lysosomal fusion of the autophagosomes[29]. Regarding these observations, the identified morphological heterogeneity in autophagosome preparation (Fig 3.9F) might be due to the loss of the inner membrane of autophagosomes after the lysosomal fusion. Therefore, the observed single-membrane vesicles might represent autolysosomes. On the other hand, the conjugation of LC3/GABARAP proteins to endolysosomal single membranes has been recently characterized[192]. This might also be considered as an alternative explanation to the single-membraned vesicle in the isolation.

The proteomics analysis of the isolated autophagosomes revealed many proteins involved in the formation of autophagosomes. With this approach, a total of 2460 autophagosomal candidate proteins were identified. In the hit list, abundance of almost every single protein was increased in Baf A_1 + Tor preparations compared to DMSO preparations. This might reflect that the Baf A_1 + Tor treatment affected quantity but not quality of the isolated autophagosomes. Besides, the average amount of total peptides detected in the DMSO samples was half of the average amount of peptides detected in the Baf A_1 + Tor samples (Fig 3.10B). This shows that more autophagosomes in the Baf A_1 + Tor samples were subjected to the MS analysis compared to the DMSO samples. Therefore, to create a more stringent list of autophagy proteins, the data was normalized against the average peptide count (Fig 3.10B). The data suggests that 47 proteins were significantly increased in the Baf A_1 + Tor samples. These proteins involved 8 known autophagy proteins including GABARAPL2, LC3B, and SARs, 8 lysosomal proteins, and 7 late endosomal proteins. The presence of lysosomal and late endosomal proteins suggests the occurrence of autolysosomes and amphisomes in the analysed autophagosome preparations. Moreover, previous studies have proposed that the ER,

mitochondria, the Golgi complex, and the plasma membrane may be the source of the autophagosomal membrane[399]. In addition, intracellular organelles are natural targets of selective autophagy[32]. These might help to explain presence of the proteins annotated to other organelles (Fig 3.10C).

The proteins identified in this study were compared with the most comprehensive three other studies that employed a proteomics analysis of autophagosomes. The number of proteins shared with these studies was determined: 127 shared with Mancias *et. al.,*[65] 27 shared with Dangiel *et. al.,*[172] and 14 shared with proteins identified in Christian Behrend's close-proximity labelling study. Also, all shared proteins were increased in the Baf A_1 +Tor samples (Fig 3.11A). The higher overlap with the Mancias's study might be explained by the use of similar approaches to purify autophagosomes; both of us subjected the autophagosomes to MS analysis, that are obtained after an immune isolation step. In Dangiel's study, a density gradient separation protocol was used to purify autophagosomes. Close-proximity labelling is by far the most distinguished method and showing the least overlap with my analysis. This concludes that the choice of the method for purification of autophagosomes can dramatically affect the outcome the MS analysis. On the other hand, the only ATG protein (except ATG8s) identified in my approach and that by Macias *et. al.,* was ATG9A which is the only transmembrane protein involved in autophagosome formation. However, Dangiel *et. al.,*[172] identified ATG3 and ATG4B in addition to ATG9A, and their close-proximity labelling study did not identify any ATG proteins except for ATG8s. These results might suggest that autophagy pathway proteins are mostly excluded from the autophagosome preparations.

Proteins significantly increased in the Baf A_1 + Tor preparations were also compared with those enriched in each *ATG* KO cells in the whole-cell analysis shown in figure 2 (Fig 3.11B). This comparison showed that 30 out of 47 proteins were not increased in any of the *ATG* KO cells. Moreover, 13 of the remaining 17 proteins were increased commonly in the *ATG* KO cells. Four SARs (TAX1BP1, p62, NDP52, and NBR1) and GABARAPL2 were among the commonly shared proteins. This may suggest the shared proteins as autophagy substrates. On the other hand, non-shared proteins might play a role in the autophagy regulation and reside on the outer surface of the autophagosome membrane, thus co-purified with the autophagosomes. They may be escaping the lysosomal degradation, thereby showing no accumulation in *ATG* KO cells. In this respect, the non-shared proteins might be implicated in the lysosomal/endosomal fusion, autophagosome trafficking, recycling of autophagy proteins,

or signalling for autophagosome formation. Thus, identification of the autophagy regulators may be an advantage of my protocol.

As the final validation, involvement of the proteins in the autophagy pathway was evaluated using immunoblotting and immunofluorescence microscopy. The results revealed many proteins colocalizing with autophagosomes and their increased level in the cells upon Baf A_1 treatment (Fig 3.12 and 3.13). However, another group of Baf A_1-responsive proteins was identified (Fig 3.12C). The level of these proteins was increased with Baf A_1 treatment in both HeLa G120 and HeLa G120A cells, which may suggest their involvement in lysosomal biogenesis. Two of these proteins IFITM3[387] and LITAF[383] were previously shown to localize on autophagosomes and lysosomes, and regulate autophagy. This suggests that this group of proteins might be implicated in the regulation of autophagy machinery or lysosomal fusion. Nonetheless, additional work is required to reveal the nature of their presence on the purified autophagosomes and the Baf A_1 sensitivity. This also shows us that the autophagosome isolation protocol might benefit from a more specific way to accumulate autophagosomes in the cells such as STX17 overexpression. Overexpression of the Qa-SNARE STX17 lacking the N-terminal domain or N-terminally tagged GFP-STX17 causes accumulation of undigested autophagosomes[189].

As one of the most significantly increased protein in the autophagosome preparation, EAAT1 was chosen to further interrogate its involvement in autophagy. EAAT1, the excitatory amino acid transporter 1, is a member of the high-affinity glutamate transporter family primarily expressed in the cerebellum and cerebral neocortex and is required for glutamate transport in astrocytes[400]. Both EAAT1 expression and autophagy are essential for astrocyte differentiation[401, 402] and progression of certain type of cancers[260, 403]. I showed that EAAT1 colocalizes with autophagosomes and accumulates in the cells upon Baf A_1 treatment (Fig 3.13 and 3.14). Moreover, amino acid starvation decreases its level in autophagy-competent cells while increasing its glycosylation in autophagy-incompetent cells (Fig 3.14B). This data sets the ground for EAAT1 as a target of autophagic degradation. On the other hand, EAAT1 overexpression resulted in p62 accumulation and LC3-I reduction, which might suggest an autophagy-regulating role for EAAT1 (Appendix Fig 1A). Moreover, silencing EAAT1 did not affect the level of p62 and LC3B (Appendix Fig 1B) but caused accumulation of bigger GFP-LC3B dots (Appendix Fig 1C) compared to WT cells. This may suggest that EAAT1 silencing might enhance protein aggregation or deregulate their degradation. Finally, the effect of

glutamate transporter activity of EAAT1 on autophagy regulation was questioned by treating the cells with a non-substrate inhibitor of EAAT1, UCPH 101. However, it did not affect autophagic flux in the cells (data not shown).

Finally, evaluation of the applicability of the combinatorial approach to tissue samples was attempted using autophagy reporter *KPC* mice in this study (Fig 3.15). However, fractionation of autophagosomes in various tissues resulted in a profile different from the fractionation performed with the cell lines. This might have been caused by the high level of lipids and other stromal factors like collagen in the tissue samples subjected to fractionation analysis. This might have compromised the enrichment of autophagosomes in certain fractions. On the other hand, to mimic the accumulation of autophagosomes in the cell lines with Baf A_1 treatment, mice were treated with 100 mg/kg CQ (*i.e.,* lysosomal alkalizer) for various time intervals, and tissues were collected and subjected to density gradient separation. However, the CQ treatment showed no further accumulation of the autophagosomes in any of the tissues (data not shown). The time and the dose of the CQ treatment needed to be optimized for these mice. Nevertheless, fraction 6 contained an mCherry-EGFP-LC3B signal in each tissue, subjected to immune isolation of autophagosomes. However, the GFP-magnetic beads could not capture any autophagosomes (data not shown). To get over drawbacks of the tissue samples, primary PDAC tumour cells isolated from *KPC* autophagy reporter mice were used for isolation of autophagosomes. However, mCherry-GFP-LC3B proteins in the autophagosome preparation were not protected from protease K degradation. This may suggest necessity of ATG4 silencing for the success of the combinatorial autophagosome isolation protocol under the mouse tissue setting.

6.3. The role of autophagy in Wnt/β-catenin signalling

In this study, I demonstrated a potential integration point between autophagy and Wnt/β-catenin signalling, which may coordinate proliferative signalling in cells. The data in this study indicate that LC3/GABARAP proteins bind to β-catenin through a novel LIR:LDS interaction dependent manner. However, this interaction does not lead β-catenin to autophagic degradation. Instead, it might be contributing to either transcriptional roles of Wnt/β-catenin signalling or, conversely, regulate autophagy. Furthermore, the atypical LIR motif characterized in this study represents a new paradigm for the interaction mode of LIR:LDS.

The findings may create a groundwork for studying reciprocal regulation of Wnt/β-catenin signalling and autophagy in the context of various disease settings or metabolic stresses.

6.3.1. LIR motif in the β-catenin protein sequence

In this work, I provide data in support of GABARAP representing a novel interactor of β-catenin. Following the discovery of LIR peptide in Terje Johansen's laboratory (Fig 4.1), I applied pulldown and immunoprecipitation techniques to verify the significance of the β-catenin LIR motif in the LC3/GABARAP interaction.

As outlined previously, ligands of LC3/GABARAP often contain the sequence motif of a canonical LIR motif as an essential binding determinant. The results of the present study suggest that, in addition to hydrophobic side chains (W66) occupying the HP1, GABARAP-ligand interactions are stabilized by electrostatic forces (Fig 4.3C), thus rationalizing the frequent occurrence of acidic residues (E65 and E67) in the LIR motif. Indeed, the hydrophobic surface of GABARAP is coated in part by basic amino acids, which are most likely to take part in salt bridges with the side chains of the ligands. This may also help to explain the higher affinity of binding between the β-catenin LIR peptide and GABARAP than LC3 proteins.

The functionality of the LIR motif previously identified by Petherick *et. al.,* was also questioned in this study. The peptide array showed no signal for peptides covering the previously discovered LIR position, and mutational analysis implicated in Petherick's paper (W540A/I507A) did not abrogate the binding of GABARAP to β-catenin (Fig 4.1). One possible explanation for that could be that the functionality of the typical LIR motif (503-WxxI-508) was only tested for LC3B binding in Petherick's study. My data also confirms that mutations in the typical LIR motif causes a subtle decrease in LC3B binding. However, in this study, I showed that β-catenin has a stronger binding to GABARAP than to LC3 proteins. Therefore, the LIR interactions were tested for GABARAP binding. It might be that Petherick's LIR motif is only functional for LC3B binding but not for GABARAP binding. Additional mutations in the Petherick's LIR motif did not bring any further decrease to the GABARAP binding of atypical LIR mutant β-catenin. Also, Petherick's LIR motif seems to be embedded in a highly rigid Armadillo repeat domain, where hydrophobic residues line up inward (Fig 4.1D). This may suggest that it is positioned in a way which makes it difficult to be reached by

LC3/GABARAP proteins. To conclude, this study showed that the atypical LIR motif may be the main binding determinant between LC3/GABARAP and β-catenin proteins.

The atypical LIR motif in the β-catenin structure resembles two other atypical motifs: in Bcl-2 and Trim5α. Further comparative analysis of these atypical LIR motifs can open new fields for exploration of autophagy regulation and new LC3/GABARAP interactors. It is also important to fully understand the kinetics of LIR:LDS interaction in terms of developing rational drug design approaches, such as LIR-targeted therapy agents.

6.3.2. β-catenin as a target of autophagic degradation

The question of whether β-catenin is a target of autophagic degradation was answered properly in this study. In the literature, several studies interrogated the interplay between autophagy and Wnt/β-catenin signalling[393]. The most important findings implied that autophagy negatively regulates Wnt signalling by promoting Dishevelled and β-catenin degradation through their LIR-mediated recognition by LC3/GABARAP proteins[111, 404]. In my study, I focused on the β-catenin-autophagy interplay due to the identified LIR motif in β-catenin.

Defining a protein as a target of autophagic degradation requires a diligent work for two reasons. First, none of the current autophagy modulating chemical compounds are specific to the autophagy pathway. They show activity on many other pathways in parallel to autophagy. The second reason is that autophagy proteins are involved in other cellular functions, such as LANDO and LAP pathways. Therefore, it is wise to question involvement of a protein in the autophagic degradation with more than one stimulus and/or genetic modification in the autophagy pathway. In many studies, regulation of the Wnt/β-catenin by autophagy was interrogated using only one autophagy stimulator. For example, starvation-mediated decrease in the β-catenin protein level was explained by its autophagic degradation[367, 390]. However, in another contradicting study starvation was shown to increase β-catenin level in the cells[367]. It is important to note that starvation affects a broad range of cellular signalling from proliferative signalling to mitochondrial biogenesis. Therefore, starvation mediated changes in the cellular signalling does not necessarily associate with autophagic activity. Furthermore, in Petherick's paper[112], β-catenin was asserted to be degraded by autophagy. They showed that β-catenin level accumulated in cells upon pharmacological and genetic inhibition

of autophagy. They used Baf A_1 and CQ to inhibit autophagy, but only CQ facilitated β-catenin accumulation in the cells. This suggests that the observed effect might have been derived from autophagy-independent activities of CQ (explained previously in the Introduction). In addition, siRNA-mediated silencing of ATG7 also caused accumulation of β-catenin. However, they also showed that siATG7 treatment caused 40% cell death, which must be taken into consideration while evaluating the changes in a proliferative signal. A similar issue was observed in a study supressing autophagy with three autophagy inhibitors including CQ, 3-MA, and LiCl for 24 h[405]. Long exposure of the cells to these compounds led to increased cell death, but still the rise in the β-catenin level was associated with autophagy suppression.

In my study, I interrogated whether β-catenin is a subject of autophagic degradation by the following assays:

- Autophagy induction by EBSS or Torin1 treatments
- Blocking autophagy by Baf A_1 or CQ treatments
- Autophagy inhibition by knocking out several *ATG* genes (e.g., *ATG7*, *ATG9A*, *ATG14* etc.)
- GFP-LC3B/GABARAP colocalization assay
- Autophagy rescue assay (by rescuing ATG7 expression in *ATG7* KO cells)
- Inducibly blocking of autophagy using dominant negative ATG4B expression
- Repeating these assays more than in one cell line

In these assays, the protein level of β-catenin and autophagy substrate p62 were observed simultaneously. β-catenin was found to be irresponsive to changes in the autophagic activity of the cells, while p62 was responding to all autophagy stimuli. β-catenin levels were only found to be decreased by amino acid starvation (EBSS treatment) independent of autophagy (Fig 4.10). EBSS treatment led to decreased β-catenin levels even when its proteasomal degradation was inhibited by Velcade or CHIR treatment (Fig 4.10). This may suggest that EBSS regulates β-catenin at the transcriptional level. Starvation-mediated decrease in the β-catenin abundance was confirmed by many other studies[393]. Moreover, starvation found to decrease β-catenin transcriptional activity in the TOP/Flash assay in many studies, which was linked to autophagic degradation of β-catenin[112, 406]. The findings in this study confirms the starvation-mediated repression of the transcription activity of β-catenin. However, it is not linked to autophagic degradation, as the same observations were made in autophagy-

incompetent *ATG7* KO cells (Appendix Fig 14A). Overall, these results lead to the conclusion that β-catenin may not be a target of autophagic degradation.

LIR mutation (YEWE/AAAA) in the β-catenin was found to increase its protein level in the cells. However, this effect was independent of autophagy as *ATG7* KO cells showed the same. It might be associated with the proximity of the LIR motif to the phosphodegron motif of β-catenin. However, phosphorylation of the β-catenin was shown to be not affected by the LIR mutation. Moreover, Velcade or CHIR treatment did not change this differential expression caused by the LIR mutation. The expressional difference can also be explained in part by the phosphorylation of Y64 in the LIR motif. Y64 is phosphorylated by Janus kinase 3 (JAK3) and PTK6 kinases, which regulates β-catenin interaction at the cell membrane with α-catenin[341, 407]. It might be speculated that Y64A substitution in the course of LIR mutation might have affected its cellular localization and increased its level at the cell membrane. This might have resulted in a pool of β-catenin with a higher stability. Further studies of how LIR mutations may affect β-catenin stability would need to be undertaken.

6.4. Role of LC3/GABARAP on Wnt/β-catenin signalling

A proportion of LC3/GABARAP-binding proteins are known to be autophagy substrates[31]. However, proteins with LIR motifs capable of escaping from the autophagic degradation were exemplified in the previous sections of this thesis (see the section: 1.2.2.2. LIR-LDS interaction). Hence, it could be hypothesized that LC3/GABARAP binding might regulate other functions of β-catenin instead of directing it to autophagic degradation. First of all, the intracellular binding of LC3/GABARAP to β-catenin was confirmed by a Co-IP experiment (Fig 4.13 and 4.14). β-catenin was co-purified with the GFP-LC3B and GFP-GABARAP proteins from HEK293 cell extracts, and this interaction was reduced by the LIR mutation (YEWE/AAAA). However, contrary to expectations, β-catenin immunoprecipitation did not bring any endogenous LC3B or GABARAP protein (Fig 4.15). Also, immunostaining of β-catenin and LC3B showed weak co-staining in the cytoplasm, which is increased by proteosome inhibition by Velcade and GSK3β inhibition by CHIR treatments (Fig 4.13). These results suggest that under basal conditions, only a small amount of β-catenin interacts with endogenous LC3/GABARAPs. It seems likely that β-catenin has stronger interactors than LC3/GABARAP under basal conditions, such as AXIN1/2, APC, and E-cadherin. Therefore,

the main role of LC3/GABARAP interactions might be observed under some stress conditions, such as hypoxia (*i.e.,* increasing LC3/GABARAP and β-catenin levels simultaneously[408, 409]).

Possible involvement of LC3/GABARAP proteins in the regulation of β-catenin transcriptional activity was studied using the well-established Top/Flash assay by overexpressing LC3B and GABARAP proteins in cells. The results showed that LC3B and GABARAP overexpression upregulated β-catenin transcriptional activity (Fig 4.16F). This result was not previously described and could be due to the shuttling activity of LC3/GABARAP proteins between the cytoplasm and the nucleus. It has previously been shown that Sirt1-mediated acetylation-deacetylation cycle of LC3 proteins facilitates their shuttling between the cytoplasm and the nucleus[410]. Hence, it can be hypothesized that the observed increase in the β-catenin transcriptional activity might be derived from transfer of β-catenin to the nucleus by the overexpressed LC3B and GABARAP proteins. This finding, while preliminary, may suggest a role for LC3/GABARAP proteins in the regulation of transcription of some genes, e.g. involved in regulating autophagy. It needs to be elucidated with further studies.

6.5. Role of β-catenin in autophagy

Wnt/βcatenin itself was reported to supresses autophagy and p62 expression[112]. β-catenin and TCF4 binds to the *p62/SQSTM1* gene promoter, where they behave as a transcriptional co-repressor[112]. Here, I studied the effect of β-catenin on the autophagy regulation. First of all, overexpression of β-catenin did not affect the levels of autophagy proteins (LC3B and p62). β-catenin silencing, on the other hand, slightly decreased p62 level in HeLa and HEK293 cells, which might be attributed to its autophagic degradation as it is reversed by Baf A_1 treatment. Complete deletion of β-catenin expression from HAP1 cells, showed a blocked autophagy; p62 and LC3-II levels were increased and more GFP-LC3B puncta were observed in the β-catenin KO clones than WT HAP1 cells. The contradicting results between siRNA-mediated silencing and CRISPR/Cas9-mediated KO of β-catenin could be attributed to two factors. First, different cells respond differently to the β-catenin repression. Second, siRNA-mediated silencing does not completely remove all the β-catenin from cells. Therefore, it might be possible that reduced β-catenin levels might decrease proliferative signals yet activating autophagy. However, complete deletion of β-catenin in HAP1 cells might have failed to activate autophagy in the nucleus. Either way, these findings contradict with the

studies proposing a negative feedback loop between autophagy and Wnt/β-catenin signalling[112]. Regarding accumulation of autophagosomes and p62 proteins in the β-catenin KO HAP1 cells, I tend to speculate that Wnt/β-catenin signalling may be required for the regulation of late-stage autophagy. It needs to be clarified with further studies. Moreover, deletion of β-catenin in HAP1 cells resulted in reduced staining in the nucleus for LC3B. Nuclear LC3 is known to be required for the initiation of starvation induced autophagy[410]. This might represent a unique role for β-catenin in the regulation of autophagy through nuclear transport of LC3 proteins. This point needs to be further elucidated.

7. References

1. Martinez-Jimenez F, Muinos F, Sentis I, Deu-Pons J, Reyes-Salazar I, Arnedo-Pac C, et al. A compendium of mutational cancer driver genes. Nat Rev Cancer 2020; 20:555-72.

2. Yao Y, Dai W. Genomic Instability and Cancer. J Carcinog Mutagen 2014; 5.

3. Liu B, Hu FF, Zhang Q, Hu H, Ye Z, Tang Q, et al. Genomic landscape and mutational impacts of recurrently mutated genes in cancers. Mol Genet Genomic Med 2018; 6:910-23.

4. Brancolini C, Iuliano L. Proteotoxic Stress and Cell Death in Cancer Cells. Cancers (Basel) 2020; 12.

5. Kanapathipillai M. Treating p53 Mutant Aggregation-Associated Cancer. Cancers (Basel) 2018; 10.

6. Guang MHZ, Kavanagh EL, Dunne LP, Dowling P, Zhang L, Lindsay S, et al. Targeting Proteotoxic Stress in Cancer: A Review of the Role that Protein Quality Control Pathways Play in Oncogenesis. Cancers (Basel) 2019; 11.

7. Adams CJ, Kopp MC, Larburu N, Nowak PR, Ali MMU. Structure and Molecular Mechanism of ER Stress Signaling by the Unfolded Protein Response Signal Activator IRE1. Front Mol Biosci 2019; 6:11.

8. Lianos GD, Alexiou GA, Mangano A, Mangano A, Rausei S, Boni L, et al. The role of heat shock proteins in cancer. Cancer Lett 2015; 360:114-8.

9. Clarke R, Cook KL. Unfolding the Role of Stress Response Signaling in Endocrine Resistant Breast Cancers. Front Oncol 2015; 5:140.

10. Wang M, Kaufman RJ. The impact of the endoplasmic reticulum protein-folding environment on cancer development. Nat Rev Cancer 2014; 14:581-97.

11. Manasanch EE, Orlowski RZ. Proteasome inhibitors in cancer therapy. Nat Rev Clin Oncol 2017; 14:417-33.

12. Gandolfi S, Laubach JP, Hideshima T, Chauhan D, Anderson KC, Richardson PG. The proteasome and proteasome inhibitors in multiple myeloma. Cancer Metastasis Rev 2017; 36:561-84.

13. Kawaguchi Y, Kovacs JJ, McLaurin A, Vance JM, Ito A, Yao TP. The deacetylase HDAC6 regulates aggresome formation and cell viability in response to misfolded protein stress. Cell 2003; 115:727-38.

14. Kirkin V, Lamark T, Johansen T, Dikic I. NBR1 cooperates with p62 in selective autophagy of ubiquitinated targets. Autophagy 2009; 5:732-3.

15. Guo JY, Karsli-Uzunbas G, Mathew R, Aisner SC, Kamphorst JJ, Strohecker AM, et al. Autophagy suppresses progression of K-ras-induced lung tumors to oncocytomas and maintains lipid homeostasis. Genes Dev 2013; 27:1447-61.

16. Cao W, Li J, Yang K, Cao D. An overview of autophagy: Mechanism, regulation and research progress. Bull Cancer 2021; 108:304-22.

17. Yang Z, Klionsky DJ. An overview of the molecular mechanism of autophagy. Curr Top Microbiol Immunol 2009; 335:1-32.

18. Levine B, Kroemer G. Autophagy in the pathogenesis of disease. Cell 2008; 132:27-42.

19. Yu L, Chen Y, Tooze SA. Autophagy pathway: Cellular and molecular mechanisms. Autophagy 2018; 14:207-15.

20. Zachari M, Ganley IG. The mammalian ULK1 complex and autophagy initiation. Essays Biochem 2017; 61:585-96.

21. Graef M. Membrane tethering by the autophagy ATG2A-WIPI4 complex. Proc Natl Acad Sci U S A 2018; 115:10540-1.

22. Klionsky DJ, Abdel-Aziz AK, Abdelfatah S, Abdellatif M, Abdoli A, Abel S, et al. Guidelines for the use and interpretation of assays for monitoring autophagy (4th edition). Autophagy 2021:1-382.

23. Nakatogawa H. Two ubiquitin-like conjugation systems that mediate membrane formation during autophagy. Essays Biochem 2013; 55:39-50.

24. Yamamoto H, Kakuta S, Watanabe TM, Kitamura A, Sekito T, Kondo-Kakuta C, et al. Atg9 vesicles are an important membrane source during early steps of autophagosome formation. J Cell Biol 2012; 198:219-33.

25. Tsuboyama K, Koyama-Honda I, Sakamaki Y, Koike M, Morishita H, Mizushima N. The ATG conjugation systems are important for degradation of the inner autophagosomal membrane. Science 2016; 354:1036-41.

26. Lorincz P, Juhasz G. Autophagosome-Lysosome Fusion. J Mol Biol 2020; 432:2462-82.

27. Kawai A, Uchiyama H, Takano S, Nakamura N, Ohkuma S. Autophagosome-lysosome fusion depends on the pH in acidic compartments in CHO cells. Autophagy 2007; 3:154-7.

28. Mauthe M, Orhon I, Rocchi C, Zhou X, Luhr M, Hijlkema KJ, et al. Chloroquine inhibits autophagic flux by decreasing autophagosome-lysosome fusion. Autophagy 2018; 14:1435-55.

29. Klionsky DJ, Elazar Z, Seglen PO, Rubinsztein DC. Does bafilomycin A1 block the fusion of autophagosomes with lysosomes? Autophagy 2008; 4:849-50.

30. Mauvezin C, Nagy P, Juhasz G, Neufeld TP. Autophagosome-lysosome fusion is independent of V-ATPase-mediated acidification. Nat Commun 2015; 6:7007.

31. Kirkin V. History of the Selective Autophagy Research: How Did It Begin and Where Does It Stand Today? J Mol Biol 2019.

32. Kirkin V, Rogov VV. A Diversity of Selective Autophagy Receptors Determines the Specificity of the Autophagy Pathway. Mol Cell 2019.

33. Ochaba J, Lukacsovich T, Csikos G, Zheng S, Margulis J, Salazar L, et al. Potential function for the Huntingtin protein as a scaffold for selective autophagy. Proc Natl Acad Sci U S A 2014; 111:16889-94.

34. Birgisdottir AB, Lamark T, Johansen T. The LIR motif - crucial for selective autophagy. J Cell Sci 2013; 126:3237-47.

35. Khaminets A, Behl C, Dikic I. Ubiquitin-Dependent And Independent Signals In Selective Autophagy. Trends Cell Biol 2016; 26:6-16.

36. Bjorkoy G, Lamark T, Brech A, Outzen H, Perander M, Overvatn A, et al. p62/SQSTM1 forms protein aggregates degraded by autophagy and has a protective effect on huntingtin-induced cell death. J Cell Biol 2005; 171:603-14.

37. Pankiv S, Clausen TH, Lamark T, Brech A, Bruun JA, Outzen H, et al. p62/SQSTM1 binds directly to Atg8/LC3 to facilitate degradation of ubiquitinated protein aggregates by autophagy. J Biol Chem 2007; 282:24131-45.

38. Kirkin V, Lamark T, Sou YS, Bjorkoy G, Nunn JL, Bruun JA, et al. A role for NBR1 in autophagosomal degradation of ubiquitinated substrates. Mol Cell 2009; 33:505-16.

39. Korac J, Schaeffer V, Kovacevic I, Clement AM, Jungblut B, Behl C, et al. Ubiquitin-independent function of optineurin in autophagic clearance of protein aggregates. J Cell Sci 2013; 126:580-92.

40. Heo JM, Ordureau A, Paulo JA, Rinehart J, Harper JW. The PINK1-PARKIN Mitochondrial Ubiquitylation Pathway Drives a Program of OPTN/NDP52 Recruitment and TBK1 Activation to Promote Mitophagy. Mol Cell 2015; 60:7-20.

41. Lazarou M, Sliter DA, Kane LA, Sarraf SA, Wang C, Burman JL, et al. The ubiquitin kinase PINK1 recruits autophagy receptors to induce mitophagy. Nature 2015; 524:309-14.

42. Wong YC, Holzbaur EL. Optineurin is an autophagy receptor for damaged mitochondria in parkin-mediated mitophagy that is disrupted by an ALS-linked mutation. Proc Natl Acad Sci U S A 2014; 111:E4439-48.

43. Strappazzon F, Nazio F, Corrado M, Cianfanelli V, Romagnoli A, Fimia GM, et al. AMBRA1 is able to induce mitophagy via LC3 binding, regardless of PARKIN and p62/SQSTM1. Cell Death Differ 2015; 22:419-32.

44. Novak I, Kirkin V, McEwan DG, Zhang J, Wild P, Rozenknop A, et al. Nix is a selective autophagy receptor for mitochondrial clearance. EMBO Rep 2010; 11:45-51.

45. Bhujabal Z, Birgisdottir AB, Sjottem E, Brenne HB, Overvatn A, Habisov S, et al. FKBP8 recruits LC3A to mediate Parkin-independent mitophagy. EMBO Rep 2017; 18:947-61.

46. Chu CT, Ji J, Dagda RK, Jiang JF, Tyurina YY, Kapralov AA, et al. Cardiolipin externalization to the outer mitochondrial membrane acts as an elimination signal for mitophagy in neuronal cells. Nat Cell Biol 2013; 15:1197-205.

47. Sentelle RD, Senkal CE, Jiang W, Ponnusamy S, Gencer S, Selvam SP, et al. Ceramide targets autophagosomes to mitochondria and induces lethal mitophagy. Nat Chem Biol 2012; 8:831-8.

48. Hanna RA, Quinsay MN, Orogo AM, Giang K, Rikka S, Gustafsson AB. Microtubule-associated protein 1 light chain 3 (LC3) interacts with Bnip3 protein to selectively remove endoplasmic reticulum and mitochondria via autophagy. J Biol Chem 2012; 287:19094-104.

49. Liu L, Feng D, Chen G, Chen M, Zheng Q, Song P, et al. Mitochondrial outer-membrane protein FUNDC1 mediates hypoxia-induced mitophagy in mammalian cells. Nat Cell Biol 2012; 14:177-85.

50. Wei Y, Chiang WC, Sumpter R, Jr., Mishra P, Levine B. Prohibitin 2 Is an Inner Mitochondrial Membrane Mitophagy Receptor. Cell 2017; 168:224-38 e10.

51. Zhang Y, Yao Y, Qiu X, Wang G, Hu Z, Chen S, et al. Listeria hijacks host mitophagy through a novel mitophagy receptor to evade killing. Nat Immunol 2019; 20:433-46.

52. Deosaran E, Larsen KB, Hua R, Sargent G, Wang Y, Kim S, et al. NBR1 acts as an autophagy receptor for peroxisomes. J Cell Sci 2013; 126:939-52.

53. Zhang J, Tripathi DN, Jing J, Alexander A, Kim J, Powell RT, et al. ATM functions at the peroxisome to induce pexophagy in response to ROS. Nat Cell Biol 2015; 17:1259-69.

54. Li X, Han H, Zhou MT, Yang B, Ta AP, Li N, et al. Proteomic Analysis of the Human Tankyrase Protein Interaction Network Reveals Its Role in Pexophagy. Cell Rep 2017; 20:737-49.

55. Maejima I, Takahashi A, Omori H, Kimura T, Takabatake Y, Saitoh T, et al. Autophagy sequesters damaged lysosomes to control lysosomal biogenesis and kidney injury. EMBO J 2013; 32:2336-47.

56. Chauhan S, Kumar S, Jain A, Ponpuak M, Mudd MH, Kimura T, et al. TRIMs and Galectins Globally Cooperate and TRIM16 and Galectin-3 Co-direct Autophagy in Endomembrane Damage Homeostasis. Dev Cell 2016; 39:13-27.

57. Eapen VV, Swarup S, Hoyer MJ, Paulo JA, Harper JW. Quantitative proteomics reveals the selectivity of ubiquitin-binding autophagy receptors in the turnover of damaged lysosomes by lysophagy. Elife 2021; 10.

58. Grasso D, Ropolo A, Lo Re A, Boggio V, Molejon MI, Iovanna JL, et al. Zymophagy, a novel selective autophagy pathway mediated by VMP1-USP9x-p62, prevents pancreatic cell death. J Biol Chem 2011; 286:8308-24.

59. Smith MD, Harley ME, Kemp AJ, Wills J, Lee M, Arends M, et al. CCPG1 Is a Non-canonical Autophagy Cargo Receptor Essential for ER-Phagy and Pancreatic ER Proteostasis. Dev Cell 2018; 44:217-32 e11.

60. Fumagalli F, Noack J, Bergmann TJ, Cebollero E, Pisoni GB, Fasana E, et al. Translocon component Sec62 acts in endoplasmic reticulum turnover during stress recovery. Nat Cell Biol 2016; 18:1173-84.

61. Grumati P, Morozzi G, Holper S, Mari M, Harwardt MI, Yan R, et al. Full length RTN3 regulates turnover of tubular endoplasmic reticulum via selective autophagy. Elife 2017; 6.

62. Khaminets A, Heinrich T, Mari M, Grumati P, Huebner AK, Akutsu M, et al. Regulation of endoplasmic reticulum turnover by selective autophagy. Nature 2015; 522:354-8.

63. Chen Q, Xiao Y, Chai P, Zheng P, Teng J, Chen J. ATL3 Is a Tubular ER-Phagy Receptor for GABARAP-Mediated Selective Autophagy. Curr Biol 2019; 29:846-55 e6.

64. An H, Ordureau A, Paulo JA, Shoemaker CJ, Denic V, Harper JW. TEX264 Is an Endoplasmic Reticulum-Resident ATG8-Interacting Protein Critical for ER Remodeling during Nutrient Stress. Mol Cell 2019; 74:891-908 e10.

65. Mancias JD, Wang X, Gygi SP, Harper JW, Kimmelman AC. Quantitative proteomics identifies NCOA4 as the cargo receptor mediating ferritinophagy. Nature 2014; 509:105-9.

66. Jiang S, Wells CD, Roach PJ. Starch-binding domain-containing protein 1 (Stbd1) and glycogen metabolism: Identification of the Atg8 family interacting motif (AIM) in Stbd1 required for interaction with GABARAPL1. Biochem Biophys Res Commun 2011; 413:420-5.

67. Dou Z, Xu C, Donahue G, Shimi T, Pan JA, Zhu J, et al. Autophagy mediates degradation of nuclear lamina. Nature 2015; 527:105-9.

68. Tumbarello DA, Manna PT, Allen M, Bycroft M, Arden SD, Kendrick-Jones J, et al. The Autophagy Receptor TAX1BP1 and the Molecular Motor Myosin VI Are Required for Clearance of Salmonella Typhimurium by Autophagy. PLoS Pathog 2015; 11:e1005174.

69. Wild P, Farhan H, McEwan DG, Wagner S, Rogov VV, Brady NR, et al. Phosphorylation of the autophagy receptor optineurin restricts Salmonella growth. Science 2011; 333:228-33.

70. Thurston TL, Ryzhakov G, Bloor S, von Muhlinen N, Randow F. The TBK1 adaptor and autophagy receptor NDP52 restricts the proliferation of ubiquitin-coated bacteria. Nat Immunol 2009; 10:1215-21.

71. Zheng YT, Shahnazari S, Brech A, Lamark T, Johansen T, Brumell JH. The adaptor protein p62/SQSTM1 targets invading bacteria to the autophagy pathway. J Immunol 2009; 183:5909-16.

72. Mandell MA, Kimura T, Jain A, Johansen T, Deretic V. TRIM proteins regulate autophagy: TRIM5 is a selective autophagy receptor mediating HIV-1 restriction. Autophagy 2014; 10:2387-8.

73. Orvedahl A, MacPherson S, Sumpter R, Jr., Talloczy Z, Zou Z, Levine B. Autophagy protects against Sindbis virus infection of the central nervous system. Cell Host Microbe 2010; 7:115-27.

74. Wyant GA, Abu-Remaileh M, Frenkel EM, Laqtom NN, Dharamdasani V, Lewis CA, et al. NUFIP1 is a ribosome receptor for starvation-induced ribophagy. Science 2018; 360:751-8.

75. Mandell MA, Jain A, Kumar S, Castleman MJ, Anwar T, Eskelinen EL, et al. TRIM17 contributes to autophagy of midbodies while actively sparing other targets from degradation. J Cell Sci 2016; 129:3562-73.

76. Isakson P, Lystad AH, Breen K, Koster G, Stenmark H, Simonsen A. TRAF6 mediates ubiquitination of KIF23/MKLP1 and is required for midbody ring degradation by selective autophagy. Autophagy 2013; 9:1955-64.

77. Pohl C, Jentsch S. Midbody ring disposal by autophagy is a post-abscission event of cytokinesis. Nat Cell Biol 2009; 11:65-70.

78. Liu WJ, Ye L, Huang WF, Guo LJ, Xu ZG, Wu HL, et al. p62 links the autophagy pathway and the ubiqutin-proteasome system upon ubiquitinated protein degradation. Cell Mol Biol Lett 2016; 21:29.

79. Turco E, Witt M, Abert C, Bock-Bierbaum T, Su MY, Trapannone R, et al. FIP200 Claw Domain Binding to p62 Promotes Autophagosome Formation at Ubiquitin Condensates. Mol Cell 2019; 74:330-46 e11.

80. von Muhlinen N, Akutsu M, Ravenhill BJ, Foeglein A, Bloor S, Rutherford TJ, et al. LC3C, bound selectively by a noncanonical LIR motif in NDP52, is required for antibacterial autophagy. Mol Cell 2012; 48:329-42.

81. Boyle KB, Thurston TL, Randow F. TBK1 directs WIPI2 against Salmonella. Autophagy 2016; 12:2508-9.

82. Osawa T, Mizuno Y, Fujita Y, Takatama M, Nakazato Y, Okamoto K. Optineurin in neurodegenerative diseases. Neuropathology 2011; 31:569-74.

83. Yin Z, Popelka H, Lei Y, Yang Y, Klionsky DJ. The Roles of Ubiquitin in Mediating Autophagy. Cells 2020; 9.

84. Kim JH, Seo D, Kim SJ, Choi DW, Park JS, Ha J, et al. The deubiquitinating enzyme USP20 stabilizes ULK1 and promotes autophagy initiation. EMBO Rep 2018; 19.

85. Raimondi M, Cesselli D, Di Loreto C, La Marra F, Schneider C, Demarchi F. USP1 (ubiquitin specific peptidase 1) targets ULK1 and regulates its cellular compartmentalization and autophagy. Autophagy 2019; 15:613-30.

86. Chen YH, Huang TY, Lin YT, Lin SY, Li WH, Hsiao HJ, et al. VPS34 K29/K48 branched ubiquitination governed by UBE3C and TRABID regulates autophagy, proteostasis and liver metabolism. Nat Commun 2021; 12:1322.

87. Matsumoto G, Wada K, Okuno M, Kurosawa M, Nukina N. Serine 403 phosphorylation of p62/SQSTM1 regulates selective autophagic clearance of ubiquitinated proteins. Mol Cell 2011; 44:279-89.

88. Rogov VV, Suzuki H, Marinkovic M, Lang V, Kato R, Kawasaki M, et al. Phosphorylation of the mitochondrial autophagy receptor Nix enhances its interaction with LC3 proteins. Sci Rep 2017; 7:1131.

89. Jiang X, Wang X, Ding X, Du M, Li B, Weng X, et al. FAM134B oligomerization drives endoplasmic reticulum membrane scission for ER-phagy. EMBO J 2020; 39:e102608.

90. You Z, Jiang WX, Qin LY, Gong Z, Wan W, Li J, et al. Requirement for p62 acetylation in the aggregation of ubiquitylated proteins under nutrient stress. Nat Commun 2019; 10:5792.

91. Sheehan BK, Orefice NS, Peng Y, Shapiro SL, Puglielli L. ATG9A regulates proteostasis through reticulophagy receptors FAM134B and SEC62 and folding chaperones CALR and HSPB1. iScience 2021; 24:102315.

92. Johansen T, Lamark T. Selective Autophagy: ATG8 Family Proteins, LIR Motifs and Cargo Receptors. J Mol Biol 2019.

93. Ichimura Y, Kumanomidou T, Sou YS, Mizushima T, Ezaki J, Ueno T, et al. Structural basis for sorting mechanism of p62 in selective autophagy. J Biol Chem 2008; 283:22847-57.

94. Rozenknop A, Rogov VV, Rogova NY, Lohr F, Guntert P, Dikic I, et al. Characterization of the interaction of GABARAPL-1 with the LIR motif of NBR1. J Mol Biol 2011; 410:477-87.

95. Wild P, McEwan DG, Dikic I. The LC3 interactome at a glance. J Cell Sci 2014; 127:3-9.

96. Holdgaard SG, Cianfanelli V, Pupo E, Lambrughi M, Lubas M, Nielsen JC, et al. Selective autophagy maintains centrosome integrity and accurate mitosis by turnover of centriolar satellites. Nat Commun 2019; 10:4176.

97. Alemu EA, Lamark T, Torgersen KM, Birgisdottir AB, Larsen KB, Jain A, et al. ATG8 family proteins act as scaffolds for assembly of the ULK complex: sequence requirements for LC3-interacting region (LIR) motifs. J Biol Chem 2012; 287:39275-90.

98. Birgisdottir AB, Mouilleron S, Bhujabal Z, Wirth M, Sjottem E, Evjen G, et al. Members of the autophagy class III phosphatidylinositol 3-kinase complex I interact with GABARAP and GABARAPL1 via LIR motifs. Autophagy 2019; 15:1333-55.

99. Habisov S, Huber J, Ichimura Y, Akutsu M, Rogova N, Loehr F, et al. Structural and Functional Analysis of a Novel Interaction Motif within UFM1-activating Enzyme 5 (UBA5) Required for Binding to Ubiquitin-like Proteins and Ufmylation. J Biol Chem 2016; 291:9025-41.

100. Olsvik HL, Lamark T, Takagi K, Larsen KB, Evjen G, Overvatn A, et al. FYCO1 Contains a C-terminally Extended, LC3A/B-preferring LC3-interacting Region (LIR) Motif Required for Efficient Maturation of Autophagosomes during Basal Autophagy. J Biol Chem 2015; 290:29361-74.

101. Genau HM, Huber J, Baschieri F, Akutsu M, Dotsch V, Farhan H, et al. CUL3-KBTBD6/KBTBD7 ubiquitin ligase cooperates with GABARAP proteins to spatially restrict TIAM1-RAC1 signaling. Mol Cell 2015; 57:995-1010.

102. Lystad AH, Ichimura Y, Takagi K, Yang Y, Pankiv S, Kanegae Y, et al. Structural determinants in GABARAP required for the selective binding and recruitment of ALFY to LC3B-positive structures. EMBO Rep 2014; 15:557-65.

103. Rogov VV, Stolz A, Ravichandran AC, Rios-Szwed DO, Suzuki H, Kniss A, et al. Structural and functional analysis of the GABARAP interaction motif (GIM). EMBO Rep 2017; 18:1382-96.

104. Wirth M, Zhang W, Razi M, Nyoni L, Joshi D, O'Reilly N, et al. Molecular determinants regulating selective binding of autophagy adapters and receptors to ATG8 proteins. Nat Commun 2019; 10:2055.

105. Johansen T, Birgisdottir AB, Huber J, Kniss A, Dotsch V, Kirkin V, et al. Methods for Studying Interactions Between Atg8/LC3/GABARAP and LIR-Containing Proteins. Methods Enzymol 2017; 587:143-69.

106. Wurzer B, Zaffagnini G, Fracchiolla D, Turco E, Abert C, Romanov J, et al. Oligomerization of p62 allows for selection of ubiquitinated cargo and isolation membrane during selective autophagy. Elife 2015; 4:e08941.

107. Richter B, Sliter DA, Herhaus L, Stolz A, Wang C, Beli P, et al. Phosphorylation of OPTN by TBK1 enhances its binding to Ub chains and promotes selective autophagy of damaged mitochondria. Proc Natl Acad Sci U S A 2016; 113:4039-44.

108. Kuang Y, Ma K, Zhou C, Ding P, Zhu Y, Chen Q, et al. Structural basis for the phosphorylation of FUNDC1 LIR as a molecular switch of mitophagy. Autophagy 2016; 12:2363-73.

109. Zhu Y, Massen S, Terenzio M, Lang V, Chen-Lindner S, Eils R, et al. Modulation of serines 17 and 24 in the LC3-interacting region of Bnip3 determines pro-survival mitophagy versus apoptosis. J Biol Chem 2013; 288:1099-113.

110. Cherra SJ, 3rd, Kulich SM, Uechi G, Balasubramani M, Mountzouris J, Day BW, et al. Regulation of the autophagy protein LC3 by phosphorylation. J Cell Biol 2010; 190:533-9.

111. Gao C, Cao W, Bao L, Zuo W, Xie G, Cai T, et al. Autophagy negatively regulates Wnt signalling by promoting Dishevelled degradation. Nat Cell Biol 2010; 12:781-90.

112. Petherick KJ, Williams AC, Lane JD, Ordonez-Moran P, Huelsken J, Collard TJ, et al. Autolysosomal beta-catenin degradation regulates Wnt-autophagy-p62 crosstalk. EMBO J 2013; 32:1903-16.

113. Shpilka T, Welter E, Borovsky N, Amar N, Shimron F, Peleg Y, et al. Fatty acid synthase is preferentially degraded by autophagy upon nitrogen starvation in yeast. Proc Natl Acad Sci U S A 2015; 112:1434-9.

114. Sharifi MN, Mowers EE, Macleod KF. Autophagic degradation of focal adhesions underlies metastatic cancer dissemination. Mol Cell Oncol 2017; 4:e1198299.

115. Liu D, Wu H, Wang C, Li Y, Tian H, Siraj S, et al. STING directly activates autophagy to tune the innate immune response. Cell Death Differ 2019; 26:1735-49.

116. Toledo M, Batista-Gonzalez A, Merheb E, Aoun ML, Tarabra E, Feng D, et al. Autophagy Regulates the Liver Clock and Glucose Metabolism by Degrading CRY1. Cell Metab 2018; 28:268-81 e4.

117. Saito T, Kuma A, Sugiura Y, Ichimura Y, Obata M, Kitamura H, et al. Autophagy regulates lipid metabolism through selective turnover of NCoR1. Nat Commun 2019; 10:1567.

118. Nowak J, Archange C, Tardivel-Lacombe J, Pontarotti P, Pebusque MJ, Vaccaro MI, et al. The TP53INP2 protein is required for autophagy in mammalian cells. Mol Biol Cell 2009; 20:870-81.

119. Pankiv S, Alemu EA, Brech A, Bruun JA, Lamark T, Overvatn A, et al. FYCO1 is a Rab7 effector that binds to LC3 and PI3P to mediate microtubule plus end-directed vesicle transport. J Cell Biol 2010; 188:253-69.

120. Popovic D, Akutsu M, Novak I, Harper JW, Behrends C, Dikic I. Rab GTPase-activating proteins in autophagy: regulation of endocytic and autophagy pathways by direct binding to human ATG8 modifiers. Mol Cell Biol 2012; 32:1733-44.

121. Itoh T, Kanno E, Uemura T, Waguri S, Fukuda M. OATL1, a novel autophagosome-resident Rab33B-GAP, regulates autophagosomal maturation. J Cell Biol 2011; 192:839-53.

122. Stadel D, Millarte V, Tillmann KD, Huber J, Tamin-Yecheskel BC, Akutsu M, et al. TECPR2 Cooperates with LC3C to Regulate COPII-Dependent ER Export. Mol Cell 2015; 60:89-104.

123. McEwan DG, Popovic D, Gubas A, Terawaki S, Suzuki H, Stadel D, et al. PLEKHM1 regulates autophagosome-lysosome fusion through HOPS complex and LC3/GABARAP proteins. Mol Cell 2015; 57:39-54.

124. Tseng WC, Jenkins PM, Tanaka M, Mooney R, Bennett V. Giant ankyrin-G stabilizes somatodendritic GABAergic synapses through opposing endocytosis of GABAA receptors. Proc Natl Acad Sci U S A 2015; 112:1214-9.

125. Joachim J, Razi M, Judith D, Wirth M, Calamita E, Encheva V, et al. Centriolar Satellites Control GABARAP Ubiquitination and GABARAP-Mediated Autophagy. Curr Biol 2017; 27:2123-36 e7.

126. Ebner P, Poetsch I, Deszcz L, Hoffmann T, Zuber J, Ikeda F. The IAP family member BRUCE regulates autophagosome-lysosome fusion. Nat Commun 2018; 9:599.

127. Schaaf MB, Keulers TG, Vooijs MA, Rouschop KM. LC3/GABARAP family proteins: autophagy-(un)related functions. FASEB J 2016; 30:3961-78.

128. Ye J, Zou G, Zhu R, Kong C, Miao C, Zhang M, et al. Structural basis of GABARAP-mediated GABAA receptor trafficking and functions on GABAergic synaptic transmission. Nat Commun 2021; 12:297.

129. Cook JL, Re RN, deHaro DL, Abadie JM, Peters M, Alam J. The trafficking protein GABARAP binds to and enhances plasma membrane expression and function of the angiotensin II type 1 receptor. Circ Res 2008; 102:1539-47.

130. Chen C, Li JG, Chen Y, Huang P, Wang Y, Liu-Chen LY. GEC1 interacts with the kappa opioid receptor and enhances expression of the receptor. J Biol Chem 2006; 281:7983-93.

131. Lainez S, Valente P, Ontoria-Oviedo I, Estevez-Herrera J, Camprubi-Robles M, Ferrer-Montiel A, et al. GABAA receptor associated protein (GABARAP) modulates TRPV1 expression and channel function and desensitization. FASEB J 2010; 24:1958-70.

132. Ma P, Schwarten M, Schneider L, Boeske A, Henke N, Lisak D, et al. Interaction of Bcl-2 with the autophagy-related GABAA receptor-associated protein (GABARAP): biophysical characterization and functional implications. J Biol Chem 2013; 288:37204-15.

133. Keown JR, Black MM, Ferron A, Yap M, Barnett MJ, Pearce FG, et al. A helical LC3-interacting region mediates the interaction between the retroviral restriction factor Trim5alpha and mammalian autophagy-related ATG8 proteins. J Biol Chem 2018; 293:18378-86.

134. Huber J, Obata M, Gruber J, Akutsu M, Lohr F, Rogova N, et al. An atypical LIR motif within UBA5 (ubiquitin like modifier activating enzyme 5) interacts with GABARAP proteins and mediates membrane localization of UBA5. Autophagy 2020; 16:256-70.

135. Lei Y, Klionsky DJ. UIM-UDS: a new interface between ATG8 and its interactors. Cell Res 2019; 29:507-8.

136. Marshall RS, Hua Z, Mali S, McLoughlin F, Vierstra RD. ATG8-Binding UIM Proteins Define a New Class of Autophagy Adaptors and Receptors. Cell 2019; 177:766-81 e24.

137. Ravenhill BJ, Boyle KB, von Muhlinen N, Ellison CJ, Masson GR, Otten EG, et al. The Cargo Receptor NDP52 Initiates Selective Autophagy by Recruiting the ULK Complex to Cytosol-Invading Bacteria. Mol Cell 2019; 74:320-9 e6.

138. Zhou Z, Liu J, Fu T, Wu P, Peng C, Gong X, et al. Phosphorylation regulates the binding of autophagy receptors to FIP200 Claw domain for selective autophagy initiation. Nat Commun 2021; 12:1570.

139. Gammoh N, Florey O, Overholtzer M, Jiang X. Interaction between FIP200 and ATG16L1 distinguishes ULK1 complex-dependent and -independent autophagy. Nat Struct Mol Biol 2013; 20:144-9.

140. Fu T, Zhang M, Zhou Z, Wu P, Peng C, Wang Y, et al. Structural and biochemical advances on the recruitment of the autophagy-initiating ULK and TBK1 complexes by autophagy receptor NDP52. Sci Adv 2021; 7.

141. Popelka H, Klionsky DJ. The RB1CC1 Claw-binding motif: a new piece in the puzzle of autophagy regulation. Autophagy 2022; 18:237-9.

142. Torggler R, Papinski D, Kraft C. Assays to Monitor Autophagy in Saccharomyces cerevisiae. Cells 2017; 6.

143. Chan EY, Kir S, Tooze SA. siRNA screening of the kinome identifies ULK1 as a multidomain modulator of autophagy. J Biol Chem 2007; 282:25464-74.

144. Hasson SA, Kane LA, Yamano K, Huang CH, Sliter DA, Buehler E, et al. High-content genome-wide RNAi screens identify regulators of parkin upstream of mitophagy. Nature 2013; 504:291-5.

145. Lipinski MM, Hoffman G, Ng A, Zhou W, Py BF, Hsu E, et al. A genome-wide siRNA screen reveals multiple mTORC1 independent signaling pathways regulating autophagy under normal nutritional conditions. Dev Cell 2010; 18:1041-52.

146. Orvedahl A, Sumpter R, Jr., Xiao G, Ng A, Zou Z, Tang Y, et al. Image-based genome-wide siRNA screen identifies selective autophagy factors. Nature 2011; 480:113-7.

147. Strohecker AM, Joshi S, Possemato R, Abraham RT, Sabatini DM, White E. Identification of 6-phosphofructo-2-kinase/fructose-2,6-bisphosphatase as a novel autophagy regulator by high content shRNA screening. Oncogene 2015; 34:5662-76.

148. Evers B, Jastrzebski K, Heijmans JP, Grernrum W, Beijersbergen RL, Bernards R. CRISPR knockout screening outperforms shRNA and CRISPRi in identifying essential genes. Nat Biotechnol 2016; 34:631-3.

149. DeJesus R, Moretti F, McAllister G, Wang Z, Bergman P, Liu S, et al. Functional CRISPR screening identifies the ufmylation pathway as a regulator of SQSTM1/p62. Elife 2016; 5.

150. Potting C, Crochemore C, Moretti F, Nigsch F, Schmidt I, Manneville C, et al. Genome-wide CRISPR screen for PARKIN regulators reveals transcriptional repression as a determinant of mitophagy. Proc Natl Acad Sci U S A 2018; 115:E180-E9.

151. Shoemaker CJ, Huang TQ, Weir NR, Polyakov NJ, Schultz SW, Denic V. CRISPR screening using an expanded toolkit of autophagy reporters identifies TMEM41B as a novel autophagy factor. PLoS Biol 2019; 17:e2007044.

152. Mizushima N, Murphy LO. Autophagy Assays for Biological Discovery and Therapeutic Development. Trends Biochem Sci 2020; 45:1080-93.

153. Panda PK, Fahrner A, Vats S, Seranova E, Sharma V, Chipara M, et al. Chemical Screening Approaches Enabling Drug Discovery of Autophagy Modulators for Biomedical Applications in Human Diseases. Front Cell Dev Biol 2019; 7:38.

154. Sun N, Malide D, Liu J, Rovira, II, Combs CA, Finkel T. A fluorescence-based imaging method to measure in vitro and in vivo mitophagy using mt-Keima. Nat Protoc 2017; 12:1576-87.

155. McWilliams TG, Prescott AR, Allen GF, Tamjar J, Munson MJ, Thomson C, et al. mito-QC illuminates mitophagy and mitochondrial architecture in vivo. J Cell Biol 2016; 214:333-45.

156. Jacomin AC, Samavedam S, Promponas V, Nezis IP. iLIR database: A web resource for LIR motif-containing proteins in eukaryotes. Autophagy 2016; 12:1945-53.

157. Kittanakom S, Chuk M, Wong V, Snyder J, Edmonds D, Lydakis A, et al. Analysis of membrane protein complexes using the split-ubiquitin membrane yeast two-hybrid (MYTH) system. Methods Mol Biol 2009; 548:247-71.

158. Seguin-Py S, Lucchi G, Croizier S, Chakrama FZ, Despouy G, Le Grand JN, et al. Identification of HSP90 as a new GABARAPL1 (GEC1)-interacting protein. Biochimie 2012; 94:748-58.

159. Rasmussen MS, Birgisdottir AB, Johansen T. Use of Peptide Arrays for Identification and Characterization of LIR Motifs. Methods Mol Biol 2019; 1880:149-61.

160. Cudjoe EK, Jr., Saleh T, Hawkridge AM, Gewirtz DA. Proteomics Insights into Autophagy. Proteomics 2017; 17.

161. Wong YK, Zhang J, Hua ZC, Lin Q, Shen HM, Wang J. Recent advances in quantitative and chemical proteomics for autophagy studies. Autophagy 2017; 13:1472-86.

162. Kristensen AR, Schandorff S, Hoyer-Hansen M, Nielsen MO, Jaattela M, Dengjel J, et al. Ordered organelle degradation during starvation-induced autophagy. Mol Cell Proteomics 2008; 7:2419-28.

163. Zhuo C, Ji Y, Chen Z, Kitazato K, Xiang Y, Zhong M, et al. Proteomics analysis of autophagy-deficient Atg7-/- MEFs reveals a close relationship between F-actin and autophagy. Biochem Biophys Res Commun 2013; 437:482-8.

164. Behrends C, Sowa ME, Gygi SP, Harper JW. Network organization of the human autophagy system. Nature 2010; 466:68-76.

165. Negrete-Hurtado A, Overhoff M, Bera S, De Bruyckere E, Schatzmuller K, Kye MJ, et al. Autophagy lipidation machinery regulates axonal microtubule dynamics but is dispensable for survival of mammalian neurons. Nat Commun 2020; 11:1535.

166. Le Guerroue F, Eck F, Jung J, Starzetz T, Mittelbronn M, Kaulich M, et al. Autophagosomal Content Profiling Reveals an LC3C-Dependent Piecemeal Mitophagy Pathway. Mol Cell 2017; 68:786-96 e6.

167. Zellner S, Schifferer M, Behrends C. Systematically defining selective autophagy receptor-specific cargo using autophagosome content profiling. Mol Cell 2021.

168. Tu YXI, Sydor AM, Coyaud E, Laurent EMN, Dyer D, Mellouk N, et al. Global Proximity Interactome of the Human Macroautophagy Pathway. Autophagy 2022; 18:1174-86.

169. Heo JM, Harper NJ, Paulo JA, Li M, Xu Q, Coughlin M, et al. Integrated proteogenetic analysis reveals the landscape of a mitochondrial-autophagosome synapse during PARK2-dependent mitophagy. Sci Adv 2019; 5:eaay4624.

170. Lamb CA, Nuhlen S, Judith D, Frith D, Snijders AP, Behrends C, et al. TBC1D14 regulates autophagy via the TRAPP complex and ATG9 traffic. EMBO J 2016; 35:281-301.

171. Sanwald JL, Poschmann G, Stuhler K, Behrends C, Hoffmann S, Willbold D. The GABARAP Co-Secretome Identified by APEX2-GABARAP Proximity Labelling of Extracellular Vesicles. Cells 2020; 9.

172. Dengjel J, Hoyer-Hansen M, Nielsen MO, Eisenberg T, Harder LM, Schandorff S, et al. Identification of autophagosome-associated proteins and regulators by quantitative proteomic analysis and genetic screens. Mol Cell Proteomics 2012; 11:M111 014035.

173. Stromhaug PE, Berg TO, Fengsrud M, Seglen PO. Purification and characterization of autophagosomes from rat hepatocytes. Biochem J 1998; 335 (Pt 2):217-24.

174. Gao W, Kang JH, Liao Y, Ding WX, Gambotto AA, Watkins SC, et al. Biochemical isolation and characterization of the tubulovesicular LC3-positive autophagosomal compartment. J Biol Chem 2010; 285:1371-83.

175. Seglen PO, Brinchmann MF. Purification of autophagosomes from rat hepatocytes. Autophagy 2010; 6:542-7.

176. Marzella L, Ahlberg J, Glaumann H. Isolation of autophagic vacuoles from rat liver: morphological and biochemical characterization. J Cell Biol 1982; 93:144-54.

177. Berg TO, Fengsrud M, Stromhaug PE, Berg T, Seglen PO. Isolation and characterization of rat liver amphisomes. Evidence for fusion of autophagosomes with both early and late endosomes. J Biol Chem 1998; 273:21883-92.

178. Rothenberg C, Srinivasan D, Mah L, Kaushik S, Peterhoff CM, Ugolino J, et al. Ubiquilin functions in autophagy and is degraded by chaperone-mediated autophagy. Hum Mol Genet 2010; 19:3219-32.

179. Gnanadhas DP, Dash PK, Sillman B, Bade AN, Lin Z, Palandri DL, et al. Autophagy facilitates macrophage depots of sustained-release nanoformulated antiretroviral drugs. J Clin Invest 2017; 127:857-73.

180. Chen X, Li LJ, Zheng XY, Shen HQ, Shang SQ. Isolation of autophagosome subpopulations after induction of autophagy by calcium. Biochem Cell Biol 2015; 93:180-4.

181. Koga H, Kaushik S, Cuervo AM. Altered lipid content inhibits autophagic vesicular fusion. FASEB J 2010; 24:3052-65.

182. Li Y, Wang LX, Yang G, Hao F, Urba WJ, Hu HM. Efficient cross-presentation depends on autophagy in tumor cells. Cancer Res 2008; 68:6889-95.

183. Overbye A, Fengsrud M, Seglen PO. Proteomic analysis of membrane-associated proteins from rat liver autophagosomes. Autophagy 2007; 3:300-22.

184. Kim JY, Wang L, Lee J, Ou JJ. Hepatitis C Virus Induces the Localization of Lipid Rafts to Autophagosomes for Its RNA Replication. J Virol 2017; 91.

185. Filimonenko M, Isakson P, Finley KD, Anderson M, Jeong H, Melia TJ, et al. The selective macroautophagic degradation of aggregated proteins requires the PI3P-binding protein Alfy. Mol Cell 2010; 38:265-79.

186. Suzuki K, Nakamura S, Morimoto M, Fujii K, Noda NN, Inagaki F, et al. Proteomic profiling of autophagosome cargo in Saccharomyces cerevisiae. PLoS One 2014; 9:e91651.

187. Yao J, Jia L, Feathers K, Lin C, Khan NW, Klionsky DJ, et al. Autophagy-mediated catabolism of visual transduction proteins prevents retinal degeneration. Autophagy 2016; 12:2439-50.

188. Yao J, Qiu Y, Jia L, Zacks DN. Autophagosome immunoisolation from GFP-LC3B mouse tissue. Autophagy 2019; 15:341-6.

189. Uematsu M, Nishimura T, Sakamaki Y, Yamamoto H, Mizushima N. Accumulation of undegraded autophagosomes by expression of dominant-negative STX17 (syntaxin 17) mutants. Autophagy 2017; 13:1452-64.

190. Zhang T, Shen S, Qu J, Ghaemmaghami S. Global Analysis of Cellular Protein Flux Quantifies the Selectivity of Basal Autophagy. Cell Rep 2016; 14:2426-39.

191. Ryzhikov M, Ehlers A, Steinberg D, Xie W, Oberlander E, Brown S, et al. Diurnal Rhythms Spatially and Temporally Organize Autophagy. Cell Rep 2019; 26:1880-92 e6.

192. Urbanska K, Orzechowski A. The Secrets of Alternative Autophagy. Cells 2021; 10.

193. Cheong H, Lindsten T, Wu J, Lu C, Thompson CB. Ammonia-induced autophagy is independent of ULK1/ULK2 kinases. Proc Natl Acad Sci U S A 2011; 108:11121-6.

194. Feng Y, Kang HH, Wong PM, Gao M, Wang P, Jiang X. Unc-51-like kinase (ULK) complex-independent autophagy induced by hypoxia. Protein Cell 2019; 10:376-81.

195. Corona Velazquez A, Corona AK, Klein KA, Jackson WT. Poliovirus induces autophagic signaling independent of the ULK1 complex. Autophagy 2018; 14:1201-13.

196. Mohamud Y, Shi J, Tang H, Xiang P, Xue YC, Liu H, et al. Coxsackievirus infection induces a non-canonical autophagy independent of the ULK and PI3K complexes. Sci Rep 2020; 10:19068.

197. Scarlatti F, Maffei R, Beau I, Codogno P, Ghidoni R. Role of non-canonical Beclin 1-independent autophagy in cell death induced by resveratrol in human breast cancer cells. Cell Death Differ 2008; 15:1318-29.

198. Tian S, Lin J, Jun Zhou J, Wang X, Li Y, Ren X, et al. Beclin 1-independent autophagy induced by a Bcl-XL/Bcl-2 targeting compound, Z18. Autophagy 2010; 6:1032-41.

199. Grishchuk Y, Ginet V, Truttmann AC, Clarke PG, Puyal J. Beclin 1-independent autophagy contributes to apoptosis in cortical neurons. Autophagy 2011; 7:1115-31.

200. Zhou X, Wang L, Hasegawa H, Amin P, Han BX, Kaneko S, et al. Deletion of PIK3C3/Vps34 in sensory neurons causes rapid neurodegeneration by disrupting the endosomal but not the autophagic pathway. Proc Natl Acad Sci U S A 2010; 107:9424-9.

201. Boukhalfa A, Nascimbeni AC, Ramel D, Dupont N, Hirsch E, Gayral S, et al. PI3KC2alpha-dependent and VPS34-independent generation of PI3P controls primary cilium-mediated autophagy in response to shear stress. Nat Commun 2020; 11:294.

202. Nguyen TN, Padman BS, Usher J, Oorschot V, Ramm G, Lazarou M. Atg8 family LC3/GABARAP proteins are crucial for autophagosome-lysosome fusion but not autophagosome formation during PINK1/Parkin mitophagy and starvation. J Cell Biol 2016; 215:857-74.

203. Uemura T, Yamamoto M, Kametaka A, Sou YS, Yabashi A, Yamada A, et al. A cluster of thin tubular structures mediates transformation of the endoplasmic reticulum to autophagic isolation membrane. Mol Cell Biol 2014; 34:1695-706.

204. Ohnstad AE, Delgado JM, North BJ, Nasa I, Kettenbach AN, Schultz SW, et al. Receptor-mediated clustering of FIP200 bypasses the role of LC3 lipidation in autophagy. EMBO J 2020; 39:e104948.

205. Nagata M, Arakawa S, Yamaguchi H, Torii S, Endo H, Tsujioka M, et al. Dram1 regulates DNA damage-induced alternative autophagy. Cell Stress 2018; 2:55-65.

206. Nishida Y, Arakawa S, Fujitani K, Yamaguchi H, Mizuta T, Kanaseki T, et al. Discovery of Atg5/Atg7-independent alternative macroautophagy. Nature 2009; 461:654-8.

207. Yamaguchi H, Arakawa S, Kanaseki T, Miyatsuka T, Fujitani Y, Watada H, et al. Golgi membrane-associated degradation pathway in yeast and mammals. EMBO J 2016; 35:1991-2007.

208. Yamaguchi H, Honda S, Torii S, Shimizu K, Katoh K, Miyake K, et al. Wipi3 is essential for alternative autophagy and its loss causes neurodegeneration. Nat Commun 2020; 11:5311.

209. Qiu W, Zhang AL, Tian Y. Tetrandrine triggers an alternative autophagy in DU145 cells. Oncol Lett 2017; 13:3734-8.

210. Wang J, Fang Y, Yan L, Yuan N, Zhang S, Xu L, et al. Erythroleukemia cells acquire an alternative mitophagy capability. Sci Rep 2016; 6:24641.

211. Zhang P, Ling L, Zheng Z, Zhang Y, Wang R, Wu M, et al. ATG7-dependent and independent autophagy determine the type of treatment in lung cancer. Pharmacol Res 2021; 163:105324.

212. Julg J, Strohm L, Behrends C. Canonical and non-canonical autophagy pathways in microglia. Mol Cell Biol 2020.

213. Subramani S, Malhotra V. Non-autophagic roles of autophagy-related proteins. EMBO Rep 2013; 14:143-51.

214. Baisamy L, Cavin S, Jurisch N, Diviani D. The ubiquitin-like protein LC3 regulates the Rho-GEF activity of AKAP-Lbc. J Biol Chem 2009; 284:28232-42.

215. Shroff A, Nazarko TY. The Molecular Interplay between Human Coronaviruses and Autophagy. Cells 2021; 10.

216. Monastyrska I, Ulasli M, Rottier PJ, Guan JL, Reggiori F, de Haan CA. An autophagy-independent role for LC3 in equine arteritis virus replication. Autophagy 2013; 9:164-74.

217. Heckmann BL, Green DR. LC3-associated phagocytosis at a glance. J Cell Sci 2019; 132.

218. Heckmann BL, Teubner BJW, Tummers B, Boada-Romero E, Harris L, Yang M, et al. LC3-Associated Endocytosis Facilitates beta-Amyloid Clearance and Mitigates Neurodegeneration in Murine Alzheimer's Disease. Cell 2019; 178:536-51 e14.

219. Romao S, Gasser N, Becker AC, Guhl B, Bajagic M, Vanoaica D, et al. Autophagy proteins stabilize pathogen-containing phagosomes for prolonged MHC II antigen processing. J Cell Biol 2013; 203:757-66.

220. Martinez J, Cunha LD, Park S, Yang M, Lu Q, Orchard R, et al. Noncanonical autophagy inhibits the autoinflammatory, lupus-like response to dying cells. Nature 2016; 533:115-9.

221. Ma J, Becker C, Lowell CA, Underhill DM. Dectin-1-triggered recruitment of light chain 3 protein to phagosomes facilitates major histocompatibility complex class II presentation of fungal-derived antigens. J Biol Chem 2012; 287:34149-56.

222. Ponpuak M, Mandell MA, Kimura T, Chauhan S, Cleyrat C, Deretic V. Secretory autophagy. Curr Opin Cell Biol 2015; 35:106-16.

223. Rabouille C. Pathways of Unconventional Protein Secretion. Trends Cell Biol 2017; 27:230-40.

224. Zhang M, Kenny SJ, Ge L, Xu K, Schekman R. Translocation of interleukin-1beta into a vesicle intermediate in autophagy-mediated secretion. Elife 2015; 4.

225. Dupont N, Jiang S, Pilli M, Ornatowski W, Bhattacharya D, Deretic V. Autophagy-based unconventional secretory pathway for extracellular delivery of IL-1beta. EMBO J 2011; 30:4701-11.

226. Kraya AA, Piao S, Xu X, Zhang G, Herlyn M, Gimotty P, et al. Identification of secreted proteins that reflect autophagy dynamics within tumor cells. Autophagy 2015; 11:60-74.

227. Ejlerskov P, Rasmussen I, Nielsen TT, Bergstrom AL, Tohyama Y, Jensen PH, et al. Tubulin polymerization-promoting protein (TPPP/p25alpha) promotes unconventional secretion of alpha-synuclein through exophagy by impairing autophagosome-lysosome fusion. J Biol Chem 2013; 288:17313-35.

228. Sousa CM, Biancur DE, Wang X, Halbrook CJ, Sherman MH, Zhang L, et al. Pancreatic stellate cells support tumour metabolism through autophagic alanine secretion. Nature 2016; 536:479-83.

229. Lee JG, Takahama S, Zhang G, Tomarev SI, Ye Y. Unconventional secretion of misfolded proteins promotes adaptation to proteasome dysfunction in mammalian cells. Nat Cell Biol 2016; 18:765-76.

230. Chua CE, Gan BQ, Tang BL. Involvement of members of the Rab family and related small GTPases in autophagosome formation and maturation. Cell Mol Life Sci 2011; 68:3349-58.

231. Longatti A, Lamb CA, Razi M, Yoshimura S, Barr FA, Tooze SA. TBC1D14 regulates autophagosome formation via Rab11- and ULK1-positive recycling endosomes. J Cell Biol 2012; 197:659-75.

232. Takeshita F, Kobiyama K, Miyawaki A, Jounai N, Okuda K. The non-canonical role of Atg family members as suppressors of innate antiviral immune signaling. Autophagy 2008; 4:67-9.

233. Jounai N, Takeshita F, Kobiyama K, Sawano A, Miyawaki A, Xin KQ, et al. The Atg5 Atg12 conjugate associates with innate antiviral immune responses. Proc Natl Acad Sci U S A 2007; 104:14050-5.

234. Ishibashi K, Uemura T, Waguri S, Fukuda M. Atg16L1, an essential factor for canonical autophagy, participates in hormone secretion from PC12 cells independently of autophagic activity. Mol Biol Cell 2012; 23:3193-202.

235. Cadwell K, Liu JY, Brown SL, Miyoshi H, Loh J, Lennerz JK, et al. A key role for autophagy and the autophagy gene Atg16l1 in mouse and human intestinal Paneth cells. Nature 2008; 456:259-63.

236. Cadwell K, Patel KK, Komatsu M, Virgin HWt, Stappenbeck TS. A common role for Atg16L1, Atg5 and Atg7 in small intestinal Paneth cells and Crohn disease. Autophagy 2009; 5:250-2.

237. DeSelm CJ, Miller BC, Zou W, Beatty WL, van Meel E, Takahata Y, et al. Autophagy proteins regulate the secretory component of osteoclastic bone resorption. Dev Cell 2011; 21:966-74.

238. Betin VM, Lane JD. Caspase cleavage of Atg4D stimulates GABARAP-L1 processing and triggers mitochondrial targeting and apoptosis. J Cell Sci 2009; 122:2554-66.

239. Wirawan E, Vande Walle L, Kersse K, Cornelis S, Claerhout S, Vanoverberghe I, et al. Caspase-mediated cleavage of Beclin-1 inactivates Beclin-1-induced autophagy and enhances apoptosis by promoting the release of proapoptotic factors from mitochondria. Cell Death Dis 2010; 1:e18.

240. Zhu Y, Zhao L, Liu L, Gao P, Tian W, Wang X, et al. Beclin 1 cleavage by caspase-3 inactivates autophagy and promotes apoptosis. Protein Cell 2010; 1:468-77.

241. Benjamin D, Colombi M, Moroni C, Hall MN. Rapamycin passes the torch: a new generation of mTOR inhibitors. Nat Rev Drug Discov 2011; 10:868-80.

242. Sun F, Xu X, Wang X, Zhang B. Regulation of autophagy by Ca(2). Tumour Biol 2016.

243. Martens S, Nakamura S, Yoshimori T. Phospholipids in Autophagosome Formation and Fusion. J Mol Biol 2016.

244. Motoi Y, Shimada K, Ishiguro K, Hattori N. Lithium and autophagy. ACS Chem Neurosci 2014; 5:434-42.

245. Sarkar S, Floto RA, Berger Z, Imarisio S, Cordenier A, Pasco M, et al. Lithium induces autophagy by inhibiting inositol monophosphatase. J Cell Biol 2005; 170:1101-11.

246. Perez-Hernandez M, Arias A, Martinez-Garcia D, Perez-Tomas R, Quesada R, Soto-Cerrato V. Targeting Autophagy for Cancer Treatment and Tumor Chemosensitization. Cancers (Basel) 2019; 11.

247. Vakifahmetoglu-Norberg H, Xia HG, Yuan J. Pharmacologic agents targeting autophagy. J Clin Invest 2015; 125:5-13.

248. Ding ZB, Hui B, Shi YH, Zhou J, Peng YF, Gu CY, et al. Autophagy activation in hepatocellular carcinoma contributes to the tolerance of oxaliplatin via reactive oxygen species modulation. Clin Cancer Res 2011; 17:6229-38.

249. Verbaanderd C, Maes H, Schaaf MB, Sukhatme VP, Pantziarka P, Sukhatme V, et al. Repurposing Drugs in Oncology (ReDO)-chloroquine and hydroxychloroquine as anti-cancer agents. Ecancermedicalscience 2017; 11:781.

250. Boya P, Gonzalez-Polo RA, Poncet D, Andreau K, Vieira HL, Roumier T, et al. Mitochondrial membrane permeabilization is a critical step of lysosome-initiated apoptosis induced by hydroxychloroquine. Oncogene 2003; 22:3927-36.

251. Jacquin E, Leclerc-Mercier S, Judon C, Blanchard E, Fraitag S, Florey O. Pharmacological modulators of autophagy activate a parallel noncanonical pathway driving unconventional LC3 lipidation. Autophagy 2017; 13:854-67.

252. Eng CH, Wang Z, Tkach D, Toral-Barza L, Ugwonali S, Liu S, et al. Macroautophagy is dispensable for growth of KRAS mutant tumors and chloroquine efficacy. Proc Natl Acad Sci U S A 2016; 113:182-7.

253. King MA, Ganley IG, Flemington V. Inhibition of cholesterol metabolism underlies synergy between mTOR pathway inhibition and chloroquine in bladder cancer cells. Oncogene 2016; 35:4518-28.

254. Maycotte P, Aryal S, Cummings CT, Thorburn J, Morgan MJ, Thorburn A. Chloroquine sensitizes breast cancer cells to chemotherapy independent of autophagy. Autophagy 2012; 8:200-12.

255. Carew JS, Espitia CM, Zhao W, Han Y, Visconte V, Phillips J, et al. Disruption of Autophagic Degradation with ROC-325 Antagonizes Renal Cell Carcinoma Pathogenesis. Clin Cancer Res 2017; 23:2869-79.

256. Choi HS, Jeong EH, Lee TG, Kim SY, Kim HR, Kim CH. Autophagy Inhibition with Monensin Enhances Cell Cycle Arrest and Apoptosis Induced by mTOR or Epidermal Growth Factor Receptor Inhibitors in Lung Cancer Cells. Tuberc Respir Dis (Seoul) 2013; 75:9-17.

257. Renna M, Schaffner C, Brown K, Shang S, Tamayo MH, Hegyi K, et al. Azithromycin blocks autophagy and may predispose cystic fibrosis patients to mycobacterial infection. J Clin Invest 2011; 121:3554-63.

258. Yamamoto A, Tagawa Y, Yoshimori T, Moriyama Y, Masaki R, Tashiro Y. Bafilomycin A1 prevents maturation of autophagic vacuoles by inhibiting fusion between autophagosomes and lysosomes in rat hepatoma cell line, H-4-II-E cells. Cell Struct Funct 1998; 23:33-42.

259. Yang YP, Hu LF, Zheng HF, Mao CJ, Hu WD, Xiong KP, et al. Application and interpretation of current autophagy inhibitors and activators. Acta Pharmacol Sin 2013; 34:625-35.

260. Kocak M, Ezazi Erdi S, Jorba G, Maestro I, Farres J, Kirkin V, et al. Targeting autophagy in disease: established and new strategies. Autophagy 2022; 18:473-95.

261. Li J, Zhu R, Chen K, Zheng H, Zhao H, Yuan C, et al. Potent and specific Atg8-targeting autophagy inhibitory peptides from giant ankyrins. Nat Chem Biol 2018; 14:778-87.

262. Fassi EMA, Garofalo M, Sgrignani J, Dei Cas M, Mori M, Roda G, et al. Focused Design of Novel Cyclic Peptides Endowed with GABARAP-Inhibiting Activity. Int J Mol Sci 2022; 23.

263. Gray JP, Uddin MN, Chaudhari R, Sutton MN, Yang H, Rask P, et al. Directed evolution of cyclic peptides for inhibition of autophagy. Chem Sci 2021; 12:3526-43.

264. Brown H, Chung M, Uffing A, Batistatou N, Tsang T, Doskocil S, et al. Structure-Based Design of Stapled Peptides That Bind GABARAP and Inhibit Autophagy. J Am Chem Soc 2022; 144:14687-97.

265. Vargas JNS, Wang C, Bunker E, Hao L, Maric D, Schiavo G, et al. Spatiotemporal Control of ULK1 Activation by NDP52 and TBK1 during Selective Autophagy. Mol Cell 2019; 74:347-62 e6.

266. Zhao L, Zhao J, Zhong K, Tong A, Jia D. Targeted protein degradation: mechanisms, strategies and application. Signal Transduct Target Ther 2022; 7:113.

267. Bekes M, Langley DR, Crews CM. PROTAC targeted protein degraders: the past is prologue. Nat Rev Drug Discov 2022; 21:181-200.

268. Takahashi D, Moriyama J, Nakamura T, Miki E, Takahashi E, Sato A, et al. AUTACs: Cargo-Specific Degraders Using Selective Autophagy. Mol Cell 2019; 76:797-810 e10.

269. Takahashi D, Arimoto H. Targeting selective autophagy by AUTAC degraders. Autophagy 2020; 16:765-6.

270. Li Z, Zhu C, Ding Y, Fei Y, Lu B. ATTEC: a potential new approach to target proteinopathies. Autophagy 2020; 16:185-7.

271. Schneider JL, Cuervo AM. Autophagy and human disease: emerging themes. Curr Opin Genet Dev 2014; 26:16-23.

272. Thellung S, Corsaro A, Nizzari M, Barbieri F, Florio T. Autophagy Activator Drugs: A New Opportunity in Neuroprotection from Misfolded Protein Toxicity. Int J Mol Sci 2019; 20.

273. Mainz L, Rosenfeldt MT. Autophagy and cancer - insights from mouse models. FEBS J 2018; 285:792-808.

274. Amaravadi R, Kimmelman AC, White E. Recent insights into the function of autophagy in cancer. Genes Dev 2016; 30:1913-30.

275. Mathew R, Karantza-Wadsworth V, White E. Role of autophagy in cancer. Nat Rev Cancer 2007; 7:961-7.

276. Rouschop KM, van den Beucken T, Dubois L, Niessen H, Bussink J, Savelkouls K, et al. The unfolded protein response protects human tumor cells during hypoxia through regulation of the autophagy genes MAP1LC3B and ATG5. J Clin Invest 2010; 120:127-41.

277. Lebovitz CB, Robertson AG, Goya R, Jones SJ, Morin RD, Marra MA, et al. Cross-cancer profiling of molecular alterations within the human autophagy interaction network. Autophagy 2015; 11:1668-87.

278. Qu X, Yu J, Bhagat G, Furuya N, Hibshoosh H, Troxel A, et al. Promotion of tumorigenesis by heterozygous disruption of the beclin 1 autophagy gene. J Clin Invest 2003; 112:1809-20.

279. Kimkong I, Kunanopparat A. Autophagy related protein 9A increase in hepatitis B virus-associated hepatocellular carcinoma and the role in apoptosis. World J Hepatol 2020; 12:1367-71.

280. Cuomo F, Altucci L, Cobellis G. Autophagy Function and Dysfunction: Potential Drugs as Anti-Cancer Therapy. Cancers (Basel) 2019; 11.

281. Coppola D, Khalil F, Eschrich SA, Boulware D, Yeatman T, Wang HG. Down-regulation of Bax-interacting factor-1 in colorectal adenocarcinoma. Cancer 2008; 113:2665-70.

282. Kang MR, Kim MS, Oh JE, Kim YR, Song SY, Kim SS, et al. Frameshift mutations of autophagy-related genes ATG2B, ATG5, ATG9B and ATG12 in gastric and colorectal cancers with microsatellite instability. J Pathol 2009; 217:702-6.

283. Wible DJ, Chao HP, Tang DG, Bratton SB. ATG5 cancer mutations and alternative mRNA splicing reveal a conjugation switch that regulates ATG12-ATG5-ATG16L1 complex assembly and autophagy. Cell Discov 2019; 5:42.

284. Kuma A, Hatano M, Matsui M, Yamamoto A, Nakaya H, Yoshimori T, et al. The role of autophagy during the early neonatal starvation period. Nature 2004; 432:1032-6.

285. Komatsu M, Waguri S, Ueno T, Iwata J, Murata S, Tanida I, et al. Impairment of starvation-induced and constitutive autophagy in Atg7-deficient mice. J Cell Biol 2005; 169:425-34.

286. Yoshii SR, Kuma A, Akashi T, Hara T, Yamamoto A, Kurikawa Y, et al. Systemic Analysis of Atg5-Null Mice Rescued from Neonatal Lethality by Transgenic ATG5 Expression in Neurons. Dev Cell 2016; 39:116-30.

287. Saito T, Ichimura Y, Taguchi K, Suzuki T, Mizushima T, Takagi K, et al. p62/Sqstm1 promotes malignancy of HCV-positive hepatocellular carcinoma through Nrf2-dependent metabolic reprogramming. Nat Commun 2016; 7:12030.

288. Xiang X, Qin HG, You XM, Wang YY, Qi LN, Ma L, et al. Expression of P62 in hepatocellular carcinoma involving hepatitis B virus infection and aflatoxin B1 exposure. Cancer Med 2017; 6:2357-69.

289. Takamura A, Komatsu M, Hara T, Sakamoto A, Kishi C, Waguri S, et al. Autophagy-deficient mice develop multiple liver tumors. Genes Dev 2011; 25:795-800.

290. Yang A, Rajeshkumar NV, Wang X, Yabuuchi S, Alexander BM, Chu GC, et al. Autophagy is critical for pancreatic tumor growth and progression in tumors with p53 alterations. Cancer Discov 2014; 4:905-13.

291. Strohecker AM, Guo JY, Karsli-Uzunbas G, Price SM, Chen GJ, Mathew R, et al. Autophagy sustains mitochondrial glutamine metabolism and growth of BrafV600E-driven lung tumors. Cancer Discov 2013; 3:1272-85.

292. Cassidy LD, Young AR, Perez-Mancera PA, Nimmervoll B, Jaulim A, Chen HC, et al. A novel Atg5-shRNA mouse model enables temporal control of Autophagy in vivo. Autophagy 2018; 14:1256-66.

293. Cassidy LD, Young ARJ, Young CNJ, Soilleux EJ, Fielder E, Weigand BM, et al. Temporal inhibition of autophagy reveals segmental reversal of ageing with increased cancer risk. Nat Commun 2020; 11:307.

294. Seton-Rogers S. Eliminating protective autophagy in KRAS-mutant cancers. Nat Rev Cancer 2019; 19:247.

295. Karsli-Uzunbas G, Guo JY, Price S, Teng X, Laddha SV, Khor S, et al. Autophagy is required for glucose homeostasis and lung tumor maintenance. Cancer Discov 2014; 4:914-27.

296. Rao S, Tortola L, Perlot T, Wirnsberger G, Novatchkova M, Nitsch R, et al. A dual role for autophagy in a murine model of lung cancer. Nat Commun 2014; 5:3056.

297. Rosenfeldt MT, O'Prey J, Morton JP, Nixon C, MacKay G, Mrowinska A, et al. p53 status determines the role of autophagy in pancreatic tumour development. Nature 2013; 504:296-300.

298. Yang A, Herter-Sprie G, Zhang H, Lin EY, Biancur D, Wang X, et al. Autophagy Sustains Pancreatic Cancer Growth through Both Cell-Autonomous and Nonautonomous Mechanisms. Cancer Discov 2018; 8:276-87.

299. Xie X, Koh JY, Price S, White E, Mehnert JM. Atg7 Overcomes Senescence and Promotes Growth of BrafV600E-Driven Melanoma. Cancer Discov 2015; 5:410-23.

300. Garcia-Fernandez M, Karras P, Checinska A, Canon E, Calvo GT, Gomez-Lopez G, et al. Metastatic risk and resistance to BRAF inhibitors in melanoma defined by selective allelic loss of ATG5. Autophagy 2016; 12:1776-90.

301. Santanam U, Banach-Petrosky W, Abate-Shen C, Shen MM, White E, DiPaola RS. Atg7 cooperates with Pten loss to drive prostate cancer tumor growth. Genes Dev 2016; 30:399-407.

302. Huo Y, Cai H, Teplova I, Bowman-Colin C, Chen G, Price S, et al. Autophagy opposes p53-mediated tumor barrier to facilitate tumorigenesis in a model of PALB2-associated hereditary breast cancer. Cancer Discov 2013; 3:894-907.

303. Armaghany T, Wilson JD, Chu Q, Mills G. Genetic alterations in colorectal cancer. Gastrointest Cancer Res 2012; 5:19-27.

304. Devenport SN, Shah YM. Functions and Implications of Autophagy in Colon Cancer. Cells 2019; 8.

305. Chen Z, Li Y, Zhang C, Yi H, Wu C, Wang J, et al. Downregulation of Beclin 1 and impairment of autophagy in a small population of colorectal cancer. Dig Dis Sci 2013; 58:2887-94.

306. Zheng HY, Zhang XY, Wang XF, Sun BC. Autophagy enhances the aggressiveness of human colorectal cancer cells and their ability to adapt to apoptotic stimulus. Cancer Biol Med 2012; 9:105-10.

307. Levy J, Cacheux W, Bara MA, L'Hermitte A, Lepage P, Fraudeau M, et al. Intestinal inhibition of Atg7 prevents tumour initiation through a microbiome-influenced immune response and suppresses tumour growth. Nat Cell Biol 2015; 17:1062-73.

308. Wei H, Wei S, Gan B, Peng X, Zou W, Guan JL. Suppression of autophagy by FIP200 deletion inhibits mammary tumorigenesis. Genes Dev 2011; 25:1510-27.

309. Gammoh N, Fraser J, Puente C, Syred HM, Kang H, Ozawa T, et al. Suppression of autophagy impedes glioblastoma development and induces senescence. Autophagy 2016; 12:1431-9.

310. Barbosa MC, Grosso RA, Fader CM. Hallmarks of Aging: An Autophagic Perspective. Front Endocrinol (Lausanne) 2018; 9:790.

311. Mei Y, Thompson MD, Cohen RA, Tong X. Autophagy and oxidative stress in cardiovascular diseases. Biochim Biophys Acta 2015; 1852:243-51.

312. Corti O, Blomgren K, Poletti A, Beart PM. Autophagy in neurodegeneration: New insights underpinning therapy for neurological diseases. J Neurochem 2020; 154:354-71.

313. Conway O, Akpinar HA, Rogov VV, Kirkin V. Selective Autophagy Receptors in Neuronal Health and Disease. J Mol Biol 2020; 432:2483-509.

314. Crews L, Spencer B, Desplats P, Patrick C, Paulino A, Rockenstein E, et al. Selective molecular alterations in the autophagy pathway in patients with Lewy body disease and in models of alpha-synucleinopathy. PLoS One 2010; 5:e9313.

315. Pickford F, Masliah E, Britschgi M, Lucin K, Narasimhan R, Jaeger PA, et al. The autophagy-related protein beclin 1 shows reduced expression in early Alzheimer disease and regulates amyloid beta accumulation in mice. J Clin Invest 2008; 118:2190-9.

316. Moscat J, Karin M, Diaz-Meco MT. p62 in Cancer: Signaling Adaptor Beyond Autophagy. Cell 2016; 167:606-9.

317. Monkkonen T, Debnath J. Inflammatory signaling cascades and autophagy in cancer. Autophagy 2018; 14:190-8.

318. Nakahira K, Haspel JA, Rathinam VA, Lee SJ, Dolinay T, Lam HC, et al. Autophagy proteins regulate innate immune responses by inhibiting the release of mitochondrial DNA mediated by the NALP3 inflammasome. Nat Immunol 2011; 12:222-30.

319. Wileman T. Autophagy as a defence against intracellular pathogens. Essays Biochem 2013; 55:153-63.

320. Bauckman KA, Owusu-Boaitey N, Mysorekar IU. Selective autophagy: xenophagy. Methods 2015; 75:120-7.

321. Migneault F, Hebert MJ. Autophagy, tissue repair, and fibrosis: a delicate balance. Matrix Biol 2021.

322. Moulis M, Vindis C. Autophagy in Metabolic Age-Related Human Diseases. Cells 2018; 7.

323. Meng T, Lin S, Zhuang H, Huang H, He Z, Hu Y, et al. Recent progress in the role of autophagy in neurological diseases. Cell Stress 2019; 3:141-61.

324. Ren L, Han W, Yang H, Sun F, Xu S, Hu S, et al. Autophagy stimulated proliferation of porcine PSCs might be regulated by the canonical Wnt signaling pathway. Biochem Biophys Res Commun 2016; 479:537-43.

325. Liu J, Xiao Q, Xiao J, Niu C, Li Y, Zhang X, et al. Wnt/beta-catenin signalling: function, biological mechanisms, and therapeutic opportunities. Signal Transduct Target Ther 2022; 7:3.

326. Mah AT, Yan KS, Kuo CJ. Wnt pathway regulation of intestinal stem cells. J Physiol 2016; 594:4837-47.

327. Zhang Y, Wang X. Targeting the Wnt/beta-catenin signaling pathway in cancer. J Hematol Oncol 2020; 13:165.

328. Koni M, Pinnaro V, Brizzi MF. The Wnt Signalling Pathway: A Tailored Target in Cancer. Int J Mol Sci 2020; 21.

329. MacDonald BT, Tamai K, He X. Wnt/beta-catenin signaling: components, mechanisms, and diseases. Dev Cell 2009; 17:9-26.

330. Zhan T, Rindtorff N, Boutros M. Wnt signaling in cancer. Oncogene 2017; 36:1461-73.

331. Krishnamurthy N, Kurzrock R. Targeting the Wnt/beta-catenin pathway in cancer: Update on effectors and inhibitors. Cancer Treat Rev 2018; 62:50-60.

332. Libro R, Bramanti P, Mazzon E. The role of the Wnt canonical signaling in neurodegenerative diseases. Life Sci 2016; 158:78-88.

333. Palomer E, Buechler J, Salinas PC. Wnt Signaling Deregulation in the Aging and Alzheimer's Brain. Front Cell Neurosci 2019; 13:227.

334. Berwick DC, Harvey K. The importance of Wnt signalling for neurodegeneration in Parkinson's disease. Biochem Soc Trans 2012; 40:1123-8.

335. Shah K, Kazi JU. Phosphorylation-Dependent Regulation of WNT/Beta-Catenin Signaling. Front Oncol 2022; 12:858782.

336. Komiya Y, Habas R. Wnt signal transduction pathways. Organogenesis 2008; 4:68-75.

337. Grimson MJ, Coates JC, Reynolds JP, Shipman M, Blanton RL, Harwood AJ. Adherens junctions and beta-catenin-mediated cell signalling in a non-metazoan organism. Nature 2000; 408:727-31.

338. van der Wal T, van Amerongen R. Walking the tight wire between cell adhesion and WNT signalling: a balancing act for beta-catenin. Open Biol 2020; 10:200267.

339. Liu C, Li Y, Semenov M, Han C, Baeg GH, Tan Y, et al. Control of beta-catenin phosphorylation/degradation by a dual-kinase mechanism. Cell 2002; 108:837-47.

340. Yost C, Torres M, Miller JR, Huang E, Kimelman D, Moon RT. The axis-inducing activity, stability, and subcellular distribution of beta-catenin is regulated in Xenopus embryos by glycogen synthase kinase 3. Genes Dev 1996; 10:1443-54.

341. Palka-Hamblin HL, Gierut JJ, Bie W, Brauer PM, Zheng Y, Asara JM, et al. Identification of beta-catenin as a target of the intracellular tyrosine kinase PTK6. J Cell Sci 2010; 123:236-45.

342. Du C, Zhang C, Li Z, Biswas MH, Balaji KC. Beta-catenin phosphorylated at threonine 120 antagonizes generation of active beta-catenin by spatial localization in trans-Golgi network. PLoS One 2012; 7:e33830.

343. Weng J, Yu L, Chen Z, Su H, Yu S, Zhang Y, et al. beta-Catenin phosphorylation at Y654 and Y142 is crucial for high mobility group box-1 protein-induced pulmonary vascular hyperpermeability. J Mol Cell Cardiol 2019; 127:174-84.

344. Wu X, Tu X, Joeng KS, Hilton MJ, Williams DA, Long F. Rac1 activation controls nuclear localization of beta-catenin during canonical Wnt signaling. Cell 2008; 133:340-53.

345. Fang D, Hawke D, Zheng Y, Xia Y, Meisenhelder J, Nika H, et al. Phosphorylation of beta-catenin by AKT promotes beta-catenin transcriptional activity. J Biol Chem 2007; 282:11221-9.

346. Hino S, Tanji C, Nakayama KI, Kikuchi A. Phosphorylation of beta-catenin by cyclic AMP-dependent protein kinase stabilizes beta-catenin through inhibition of its ubiquitination. Mol Cell Biol 2005; 25:9063-72.

347. Liu C, Kato Y, Zhang Z, Do VM, Yankner BA, He X. beta-Trcp couples beta-catenin phosphorylation-degradation and regulates Xenopus axis formation. Proc Natl Acad Sci U S A 1999; 96:6273-8.

348. Hay-Koren A, Caspi M, Zilberberg A, Rosin-Arbesfeld R. The EDD E3 ubiquitin ligase ubiquitinates and up-regulates beta-catenin. Mol Biol Cell 2011; 22:399-411.

349. Shekhar MP, Gerard B, Pauley RJ, Williams BO, Tait L. Rad6B is a positive regulator of beta-catenin stabilization. Cancer Res 2008; 68:1741-50.

350. Dao KH, Rotelli MD, Petersen CL, Kaech S, Nelson WD, Yates JE, et al. FANCL ubiquitinates beta-catenin and enhances its nuclear function. Blood 2012; 120:323-34.

351. Chitalia VC, Foy RL, Bachschmid MM, Zeng L, Panchenko MV, Zhou MI, et al. Jade-1 inhibits Wnt signalling by ubiquitylating beta-catenin and mediates Wnt pathway inhibition by pVHL. Nat Cell Biol 2008; 10:1208-16.

352. Wolf D, Rodova M, Miska EA, Calvet JP, Kouzarides T. Acetylation of beta-catenin by CREB-binding protein (CBP). J Biol Chem 2002; 277:25562-7.

353. Levy L, Wei Y, Labalette C, Wu Y, Renard CA, Buendia MA, et al. Acetylation of beta-catenin by p300 regulates beta-catenin-Tcf4 interaction. Mol Cell Biol 2004; 24:3404-14.

354. Ge X, Jin Q, Zhang F, Yan T, Zhai Q. PCAF acetylates {beta}-catenin and improves its stability. Mol Biol Cell 2009; 20:419-27.

355. Ackers I, Malgor R. Interrelationship of canonical and non-canonical Wnt signalling pathways in chronic metabolic diseases. Diab Vasc Dis Res 2018; 15:3-13.

356. Fearnhead NS, Britton MP, Bodmer WF. The ABC of APC. Hum Mol Genet 2001; 10:721-33.

357. Tao H, Chen F, Liu H, Hu Y, Wang Y, Li H. Wnt/beta-catenin signaling pathway activation reverses gemcitabine resistance by attenuating Beclin1-mediated autophagy in the MG63 human osteosarcoma cell line. Mol Med Rep 2017; 16:1701-6.

358. Ryskalin L, Gaglione A, Limanaqi F, Biagioni F, Familiari P, Frati A, et al. The Autophagy Status of Cancer Stem Cells in Gliobastoma Multiforme: From Cancer Promotion to Therapeutic Strategies. Int J Mol Sci 2019; 20.

359. Nager M, Sallan MC, Visa A, Pushparaj C, Santacana M, Macia A, et al. Inhibition of WNT-CTNNB1 signaling upregulates SQSTM1 and sensitizes glioblastoma cells to autophagy blockers. Autophagy 2018; 14:619-36.

360. Jia Z, Wang J, Wang W, Tian Y, XiangWei W, Chen P, et al. Autophagy eliminates cytoplasmic beta-catenin and NICD to promote the cardiac differentiation of P19CL6 cells. Cell Signal 2014; 26:2299-305.

361. Colella B, Faienza F, Carinci M, D'Alessandro G, Catalano M, Santoro A, et al. Autophagy induction impairs Wnt/beta-catenin signalling through beta-catenin relocalisation in glioblastoma cells. Cell Signal 2019; 53:357-64.

362. Cheng M, Xue H, Cao W, Li W, Chen H, Liu B, et al. Receptor for Activated C Kinase 1 (RACK1) Promotes Dishevelled Protein Degradation via Autophagy and Antagonizes Wnt Signaling. J Biol Chem 2016; 291:12871-9.

363. Hwang SH, Bang S, Kang KS, Kang D, Chung J. ULK1 negatively regulates Wnt signaling by phosphorylating Dishevelled. Biochem Biophys Res Commun 2019; 508:308-13.

364. Choi JD, Ryu M, Ae Park M, Jeong G, Lee JS. FIP200 inhibits beta-catenin-mediated transcription by promoting APC-independent beta-catenin ubiquitination. Oncogene 2013; 32:2421-32.

365. Ndoye A, Budina-Kolomets A, Kugel CH, 3rd, Webster MR, Kaur A, Behera R, et al. ATG5 Mediates a Positive Feedback Loop between Wnt Signaling and Autophagy in Melanoma. Cancer Res 2017; 77:5873-85.

366. Rios JA, Godoy JA, Inestrosa NC. Wnt3a ligand facilitates autophagy in hippocampal neurons by modulating a novel GSK-3beta-AMPK axis. Cell Commun Signal 2018; 16:15.

367. Fan Q, Yang L, Zhang X, Ma Y, Li Y, Dong L, et al. Autophagy promotes metastasis and glycolysis by upregulating MCT1 expression and Wnt/beta-catenin signaling pathway activation in hepatocellular carcinoma cells. J Exp Clin Cancer Res 2018; 37:9.

368. Choi HK, Yuan H, Fang F, Wei X, Liu L, Li Q, et al. Tsc1 Regulates the Balance Between Osteoblast and Adipocyte Differentiation Through Autophagy/Notch1/beta-Catenin Cascade. J Bone Miner Res 2018; 33:2021-34.

369. Sanjana NE, Shalem O, Zhang F. Improved vectors and genome-wide libraries for CRISPR screening. Nat Methods 2014; 11:783-4.

370. Eskelinen EL, Illert AL, Tanaka Y, Schwarzmann G, Blanz J, Von Figura K, et al. Role of LAMP-2 in lysosome biogenesis and autophagy. Mol Biol Cell 2002; 13:3355-68.

371. Bieniossek C, Richmond TJ, Berger I. MultiBac: multigene baculovirus-based eukaryotic protein complex production. Curr Protoc Protein Sci 2008; Chapter 5:Unit 5 20.

372. Korolchuk VI, Mansilla A, Menzies FM, Rubinsztein DC. Autophagy inhibition compromises degradation of ubiquitin-proteasome pathway substrates. Mol Cell 2009; 33:517-27.

373. Agrotis A, Pengo N, Burden JJ, Ketteler R. Redundancy of human ATG4 protease isoforms in autophagy and LC3/GABARAP processing revealed in cells. Autophagy 2019; 15:976-97.

374. Gasser KW, DiDomenico J, Hopfer U. Separation of cell organelles in density gradients based on their permeability characteristics. Anal Biochem 1988; 171:41-6.

375. Boada-Romero E, Letek M, Fleischer A, Pallauf K, Ramon-Barros C, Pimentel-Muinos FX. TMEM59 defines a novel ATG16L1-binding motif that promotes local activation of LC3. EMBO J 2013; 32:566-82.

376. Zhou J, Yang J, Dong Y, Shi Y, Zhu E, Yuan H, et al. Oncostatin M receptor regulates osteoblast differentiation via extracellular signal-regulated kinase/autophagy signaling. Stem Cell Res Ther 2022; 13:278.

377. Takeda T, Komatsu M, Chiwaki F, Komatsuzaki R, Nakamura K, Tsuji K, et al. Upregulation of IGF2R evades lysosomal dysfunction-induced apoptosis of cervical cancer cells via transport of cathepsins. Cell Death Dis 2019; 10:876.

378. Chen X, Chen L, Tan J, Zhang L, Xia J, Cheng B, et al. Rspo1-LGR4 axis in BMSCs protects bone against radiation-induced injury through the mTOR-dependent autophagy pathway. J Cell Physiol 2021; 236:4273-89.

379. Zhan F, Deng Q, Chen Z, Xie C, Xiang S, Qiu S, et al. SAR1A regulates the RhoA/YAP and autophagy signaling pathways to influence osteosarcoma invasion and metastasis. Cancer Sci 2022.

380. Dortet L, Mostowy S, Samba-Louaka A, Gouin E, Nahori MA, Wiemer EA, et al. Recruitment of the major vault protein by InlK: a Listeria monocytogenes strategy to avoid autophagy. PLoS Pathog 2011; 7:e1002168.

381. Jing Z, He X, Jia Z, Sa Y, Yang B, Liu P. NCAPD2 inhibits autophagy by regulating Ca(2+)/CAMKK2/AMPK/mTORC1 pathway and PARP-1/SIRT1 axis to promote colorectal cancer. Cancer Lett 2021; 520:26-37.

382. Su BC, Hsu PL, Mo FE. CCN1 triggers adaptive autophagy in cardiomyocytes to curb its apoptotic activities. J Cell Commun Signal 2020; 14:93-100.

383. Bertolo C, Roa S, Sagardoy A, Mena-Varas M, Robles EF, Martinez-Ferrandis JI, et al. LITAF, a BCL6 target gene, regulates autophagy in mature B-cell lymphomas. Br J Haematol 2013; 162:621-30.

384. Zhang X, Wang Y. The Golgi stacking protein GORASP2/GRASP55 serves as an energy sensor to promote autophagosome maturation under glucose starvation. Autophagy 2018; 14:1649-51.

385. Talukdar S, Pradhan AK, Bhoopathi P, Shen XN, August LA, Windle JJ, et al. Regulation of protective autophagy in anoikis-resistant glioma stem cells by SDCBP/MDA-9/Syntenin. Autophagy 2018; 14:1845-6.

386. Yang RM, Tao J, Zhan M, Yuan H, Wang HH, Chen SJ, et al. TAMM41 is required for heart valve differentiation via regulation of PINK-PARK2 dependent mitophagy. Cell Death Differ 2019; 26:2430-46.

387. Jiang LQ, Xia T, Hu YH, Sun MS, Yan S, Lei CQ, et al. IFITM3 inhibits virus-triggered induction of type I interferon by mediating autophagosome-dependent degradation of IRF3. Cell Mol Immunol 2018; 15:858-67.

388. Hilverling A, Szego EM, Dinter E, Cozma D, Saridaki T, Falkenburger BH. Maturing Autophagosomes are Transported Towards the Cell Periphery. Cell Mol Neurobiol 2022; 42:155-71.

389. Bauer D, Haroutunian V, Meador-Woodruff JH, McCullumsmith RE. Abnormal glycosylation of EAAT1 and EAAT2 in prefrontal cortex of elderly patients with schizophrenia. Schizophr Res 2010; 117:92-8.

390. Wu H, Lu XX, Wang JR, Yang TY, Li XM, He XS, et al. TRAF6 inhibits colorectal cancer metastasis through regulating selective autophagic CTNNB1/beta-catenin degradation and is targeted for GSK3B/GSK3beta-mediated phosphorylation and degradation. Autophagy 2019; 15:1506-22.

391. Dietrich C, Scherwat J, Faust D, Oesch F. Subcellular localization of beta-catenin is regulated by cell density. Biochem Biophys Res Commun 2002; 292:195-9.

392. Jazi MS, Najafi SM. Beta-catenin Forms Protein Aggregation at High Concentrations in HEK293TCells. Iran J Med Sci 2017; 42:66-72.

393. Perez-Plasencia C, Lopez-Urrutia E, Garcia-Castillo V, Trujano-Camacho S, Lopez-Camarillo C, Campos-Parra AD. Interplay Between Autophagy and Wnt/beta-Catenin Signaling in Cancer: Therapeutic Potential Through Drug Repositioning. Front Oncol 2020; 10:1037.

394. Wang L, Ye X, Zhao T. The physiological roles of autophagy in the mammalian life cycle. Biol Rev Camb Philos Soc 2019; 94:503-16.

395. Berezhnov AV, Soutar MP, Fedotova EI, Frolova MS, Plun-Favreau H, Zinchenko VP, et al. Intracellular pH Modulates Autophagy and Mitophagy. J Biol Chem 2016; 291:8701-8.

396. Di Lernia G, Leone P, Solimando AG, Buonavoglia A, Saltarella I, Ria R, et al. Bortezomib Treatment Modulates Autophagy in Multiple Myeloma. J Clin Med 2020; 9.

397. Karimpour-Fard A, Epperson LE, Hunter LE. A survey of computational tools for downstream analysis of proteomic and other omic datasets. Hum Genomics 2015; 9:28.

398. Weidberg H, Shvets E, Shpilka T, Shimron F, Shinder V, Elazar Z. LC3 and GATE-16/GABARAP subfamilies are both essential yet act differently in autophagosome biogenesis. EMBO J 2010; 29:1792-802.

399. Wei Y, Liu M, Li X, Liu J, Li H. Origin of the Autophagosome Membrane in Mammals. Biomed Res Int 2018; 2018:1012789.

400. Roberts RC, Roche JK, McCullumsmith RE. Localization of excitatory amino acid transporters EAAT1 and EAAT2 in human postmortem cortex: a light and electron microscopic study. Neuroscience 2014; 277:522-40.

401. Todd AC, Hardingham GE. The Regulation of Astrocytic Glutamate Transporters in Health and Neurodegenerative Diseases. Int J Mol Sci 2020; 21.

402. Ha S, Jeong SH, Yi K, Chu JJ, Kim S, Kim EK, et al. Autophagy Mediates Astrogenesis in Adult Hippocampal Neural Stem Cells. Exp Neurobiol 2019; 28:229-46.

403. Xu L, Chen J, Jia L, Chen X, Awaleh Moumin F, Cai J. SLC1A3 promotes gastric cancer progression via the PI3K/AKT signalling pathway. J Cell Mol Med 2020; 24:14392-404.

404. Petherick KJ, Conway OJ, Mpamhanga C, Osborne SA, Kamal A, Saxty B, et al. Pharmacological inhibition of ULK1 kinase blocks mammalian target of rapamycin (mTOR)-dependent autophagy. J Biol Chem 2015; 290:11376-83.

405. Fan Y, Hou T, Dan W, Liu T, Luan J, Liu B, et al. Silibinin inhibits epithelial-mesenchymal transition of renal cell carcinoma through autophagy-dependent Wnt/beta-catenin signaling. Int J Mol Med 2020; 45:1341-50.

406. Zhang Y, Wang F, Han L, Wu Y, Li S, Yang X, et al. GABARAPL1 negatively regulates Wnt/beta-catenin signaling by mediating Dvl2 degradation through the autophagy pathway. Cell Physiol Biochem 2011; 27:503-12.

407. Mishra J, Das JK, Kumar N. Janus kinase 3 regulates adherens junctions and epithelial mesenchymal transition through beta-catenin. J Biol Chem 2017; 292:16406-19.

408. Xu W, Zhou W, Cheng M, Wang J, Liu Z, He S, et al. Hypoxia activates Wnt/beta-catenin signaling by regulating the expression of BCL9 in human hepatocellular carcinoma. Sci Rep 2017; 7:40446.

409. Mazure NM, Pouyssegur J. Hypoxia-induced autophagy: cell death or cell survival? Curr Opin Cell Biol 2010; 22:177-80.

410. Huang R, Xu Y, Wan W, Shou X, Qian J, You Z, et al. Deacetylation of nuclear LC3 drives autophagy initiation under starvation. Mol Cell 2015; 57:456-66.

411. Dosztanyi Z. Prediction of protein disorder based on IUPred. Protein Sci 2018; 27:331-40.

412. Jehl P, Manguy J, Shields DC, Higgins DG, Davey NE. ProViz-a web-based visualization tool to investigate the functional and evolutionary features of protein sequences. Nucleic Acids Res 2016; 44:W11-5.

8. APPENDIX

8.1. Appendix Tables

Appendix Table 1: Significant outliers in the whole-cell proteomics analysis (z-score)

Gene Symbol	*Log2FC*	*Z-score*	*Gene Symbol*	*Log2FC*	*Z-score*	*Gene Symbol*	*Log2FC*	*Z-score*	*Gene Symbol*	*Log2FC*	*Z-score*
MAT1A	6.10	6.57	ADA	3.29	3.46	DNM1	-3.18	-3.69	PSMB8	-4.84	-5.52
PAGE1	5.37	5.76	RYR3	3.28	3.45	CAMK1	-3.24	-3.75	MYL9	-4.85	-5.53
ANKRD2	4.74	5.07	STAT1	3.25	3.42	LAMA4	-3.25	-3.76	KCTD12	-4.86	-5.54
DCTD	4.74	5.07	MMP15	3.23	3.40	P4HA3	-3.26	-3.77	TGFB1I1	-4.86	-5.54
C4BPA	4.58	4.88	FBXO2	3.22	3.38	MICAL1	-3.28	-3.80	SUSD5	-4.95	-5.65
AGR2	4.53	4.83	GNB2	3.19	3.35	GBP2	-3.35	-3.88	S100A2	-4.99	-5.68
RTN4RL2	4.34	4.62	ABCC2	3.17	3.33	NNT	-3.38	-3.91	IQGAP2	-5.00	-5.70
RIMS1	4.33	4.60	MFI2	3.16	3.32	ALPL	-3.42	-3.95	TGM2	-5.01	-5.71
RPL22L1	4.32	4.59	SLC1A3	3.11	3.26	SLC22A3	-3.44	-3.98	AKR1C2	-5.01	-5.71
S100P	4.18	4.44	TRIM29	3.07	3.22	ITGB4	-3.58	-4.13	LEPREL2	-5.07	-5.77
CKMT1B	4.14	4.40	CDH10	3.06	3.21	NFATC4	-3.60	-4.16	CNN3	-5.08	-5.79
PRSS56	4.09	4.34	GNB4	3.04	3.18	EDIL3	-3.79	-4.36	BCAT1	-5.09	-5.80
MAGEB2	4.07	4.32	C1QTNF6	3.03	3.17	KHDRBS3	-3.80	-4.38	SCRN1	-5.37	-6.10
ALPPL2	3.97	4.21	GCA	3.03	3.17	SERPINB4	-3.84	-4.41	FHL1	-5.43	-6.17
ABCG2	3.95	4.19	FBXL16	3.02	3.17	ALDH3A1	-3.84	-4.42	TAGLN	-5.47	-6.21
PLLP	3.91	4.15	SLC25A35	3.00	3.14	PALM2	-3.85	-4.42	MYLK	-5.48	-6.23
TSPAN8	3.87	4.10	MYPN	2.99	3.13	CA2	-3.90	-4.48	CNTNAP1	-5.52	-6.27
ALPP	3.86	4.08	MYLK3	2.98	3.11	PTK7	-3.92	-4.51	ALDH2	-5.57	-6.33
GNB1	3.84	4.06	ECEL1	2.90	3.03	LPL	-4.02	-4.62	FADS2	-5.59	-6.35
LYPD3	3.77	3.99	RBKS	2.87	3.00	PRUNE2	-4.14	-4.74	FKBP11	-5.60	-6.36
GAGE2A	3.76	3.97	FOLR1	-2.58	-3.02	ARMCX2	-4.29	-4.92	MAP1B	-5.65	-6.42
APOBEC3C	3.75	3.97	ISG15	-2.59	-3.03	HLA-H	-4.32	-4.95	GSTM1	-5.68	-6.45
BRSK2	3.65	3.85	TPM1	-2.61	-3.06	TGFBI	-4.33	-4.95	COL7A1	-5.71	-6.49
PPM1H	3.61	3.81	HTRA1	-2.61	-3.06	AKAP12	-4.42	-5.06	CDH2	-5.76	-6.54
ISYNA1	3.59	3.79	HK1	-2.62	-3.06	COL14A1	-4.45	-5.09	HIST1H1D	-5.78	-6.56
PLA2G16	3.58	3.78	EBF2	-2.75	-3.22	HDGFRP3	-4.49	-5.13	GBP1	-5.79	-6.57
UBL5	3.46	3.65	SH3BGRL	-2.81	-3.28	FLNC	-4.57	-5.22	DPYSL3	-5.86	-6.65
CTAG1A	3.42	3.61	LGALS8	-2.88	-3.36	HNMT	-4.58	-5.23	AKR1C3	-5.88	-6.67
EGFL7	3.40	3.58	PCOLCE	-2.89	-3.37	HIST1H1A	-4.58	-5.24	ARMCX3	-5.99	-6.79
ACTL8	3.38	3.56	ANXA8	-2.95	-3.44	ALCAM	-4.61	-5.27	CRMP1	-6.14	-6.96
GDPD3	3.38	3.56	SERPINB9	-2.97	-3.45	GLIPR2	-4.63	-5.28	CDCP1	-6.36	-7.20
ASS1	3.37	3.55	CDKN2C	-3.01	-3.49	SCOC	-4.74	-5.41	STK39	-6.49	-7.35
SSX2B	3.37	3.55	EEF1A2	-3.07	-3.57	PCP4	-4.76	-5.43	MSRA	-6.55	-7.41
ACSF2	3.36	3.53	VASN	-3.10	-3.60	STAC2	-4.82	-5.50	ITGA11	-6.68	-7.55
SDR16C5	3.33	3.51	ANPEP	-3.10	-3.60	PSTPIP2	-4.83	-5.51	FABP5	-6.92	-7.82

Appendix Table 2: *Proteomics analysis of autophagosomes, significantly increased 46 proteins (LogFc>0.4 and p<0.05)*

Name	LogFC	pValue
GABARAPL2	1.400596	0.000702
MAP1LC3B	1.028956	0.023287
GORASP2	0.964257	0.001308
SQSTM1	0.922586	0.031963
EAAT1/SLC1A3	0.834901	0.006148
PRKAR1B	0.832412	0.003163
TAMM41	0.809014	0.021578
SDCBP	0.698229	0.030094
SLC39A14	0.624753	0.010869
SLC12A3	0.610108	0.001293
NCAPD2	0.585062	0.02
DNAH8	0.581226	0.016728
TMEM59	0.57028	0.00804
RNF149	0.566098	0.016783
CCN1	0.545594	0.015653
PRKAR1A	0.545152	0.006638
WBP2	0.543057	0.002454
LITAF	0.541949	1.08E-05
IGF2R	0.541841	0.015749
LGR4	0.52869	0.010094
GLG1	0.527622	0.011205
ITM2B	0.524964	0.014352
MAN2B2	0.509998	0.00579
NBR1	0.507233	0.034942
PRDX1	0.497277	0.004879
SAR1A	0.492935	0.004331
MVP	0.491868	0.038376
VLDLR	0.488094	0.024814
SLC38A2	0.485072	0.047257
TAX1BP1	0.480478	0.049738
NCOA4	0.476285	0.033803
NUDC	0.469046	7.72E-05

OSMR	0.463079	0.023256
PTTG1IP	0.460784	0.009015
FAM174A	0.4588	0.015322
SERINC3	0.45712	0.005166
SLC16A6	0.448744	0.015821
EEF1B2	0.423919	0.034156
EEF1D	0.418926	0.040634
C16orf72	0.417242	0.000722
PSMD9	0.414888	0.01722
EIF3J	0.410651	0.017141
IFNGR1	0.409655	0.017012
PPIA	0.401486	5.29E-05
LIFR	0.401216	0.022291

Appendix Table 3: *Fold Changes of the proteins have shown similar profile to p62 or Baf A_1 sensitivity in immunoblot analysis in Figure 3.12.*

Isolated autophagosomes			**Whole-cell analysis (Log2FC)**		
Name	**Log2FC**	**pValue**	**ATG7 KO**	**ATG4 A/B KO**	**Hexa KO**
SQSTM1	0.922586	0.031963	1.28513	1.335713	0.833672
EAAT1/SLC1A3	0.834901	0.006148	2.181518	3.081994	3.695597
PRKAR1B	0.832412	0.003163	0.93969	0.357677	0.760242
SDCBP/Syntenin1	0.698229	0.030094	1.310309	1.230326	1.232642
CCN1	0.545594	0.015653	n.d.	n.d.	n.d.
WBP2	0.543057	0.002454	0.796604	0.805174	0.755092
LITAF	0.541949	1.08E-05	n.d.	n.d.	n.d.
GLG1	0.527622	0.011205	1.482875	1.457812	1.225421

ITM2B	0.524964	0.014352	n.d.	n.d.	n.d.
PRDX1	0.497277	0.004879	n.d.	n.d.	n.d.
SAR1A	0.492935	0.004331	-0.2042	0.134144	-0.0561
FAM174A	0.4588	0.015322	n.d.	n.d.	n.d.
PPIA	0.401486	5.29E-05	-1.06659	-0.54908	-0.58794
BST2	0.357532	0.016088	-0.80576	-0.47468	-1.32061
RUVBL2	0.325284	0.00914	0.526762	0.287508	0.462559
PAICS	0.313047	0.008415	0.273749	0.01843	-0.06746
EPHA2	0.220853	0.133127	-0.59783	-0.25854	-0.24658
IFITM3	0.196397	0.128983	0.740995	0.347395	1.267511
ILK	0.093855	0.244964	-0.78777	-0.36841	-0.83074
HGS	-0.00177	0.903056	0.434477	0.540101	0.516873
DAB2	-0.01475	0.72056	-0.6524	-0.95592	-0.15429

8.2. Appendix Figures

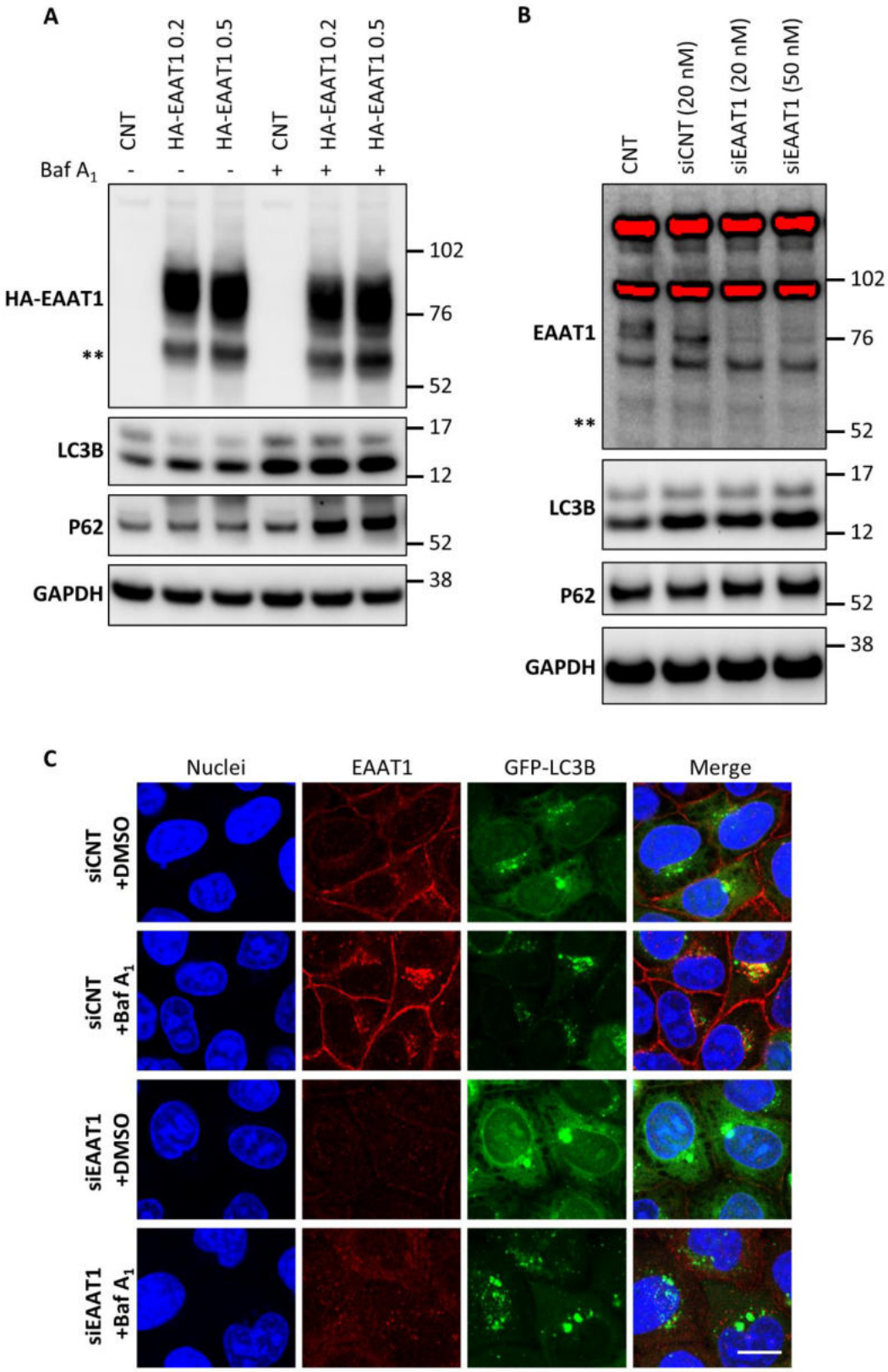

Appendix Figure 1. Effect of EAAT1 on autophagy regulation **(A)** Immunoblots for p62, HA-β-catenin (anti-HA ab), LC3B, and GAPDH (loading control) of cell extracts from HeLa WT

cells transfected with HA-EAAT1 (0.2 or 0.5 µg) for 24 h. **(B)** Immunoblots showing EAAT1 silencing after transfecting the HeLa WT cells with non-targeting (siCNT) or EAAT1 (siEAAT1) targeting siRNAs for 24 h. **(C)** Indirect immunofluorescence analysis of EAAT1 (red) in HeLa G120 cells transfected with siCNT (20 nM) or siEAAT1 (20 nM). The cells were also treated with 200 nM Baf A_1 or DMSO for 2h. DAPI staining was used to mark the nuclei (blue), scale bar = 10 µm

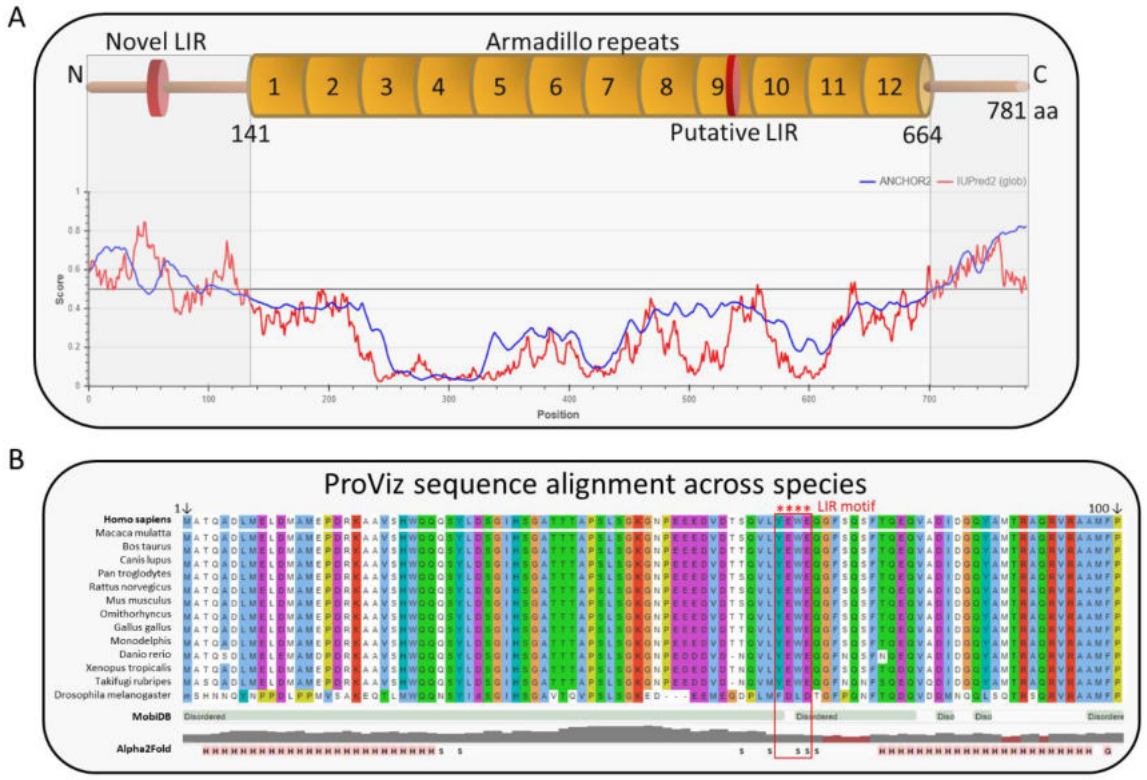

Appendix Figure 2. Structure and conservation of β-catenin protein sequence. **(A)** Prediction of protein disorder based on IUPred[411]. The N-terminus and C-terminus of β-catenin were predicted as disordered regions, while the armadillo repeats are highly structured. **(B)** Sequence alignment of the first 100 amino acids of β-catenin across species is shown. The atypical novel LIR motif is shown in a red box. The analysis was done using Proviz[412].

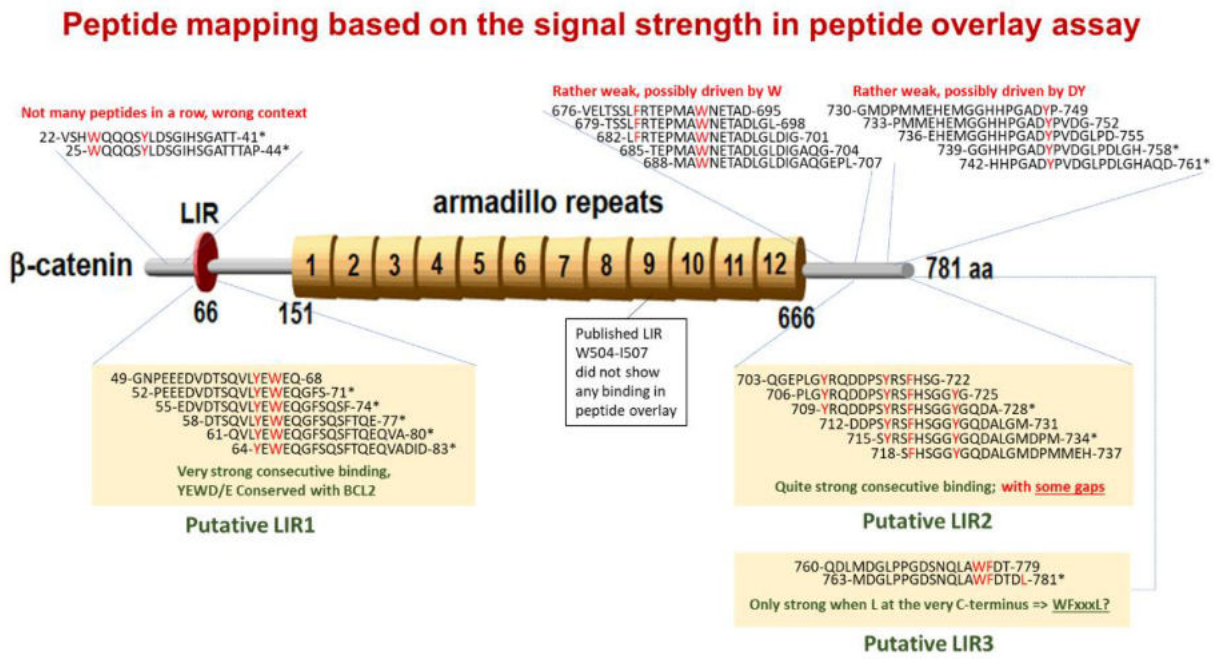

Appendix Figure 3. Peptide mapping based on the signal strength in the peptide array assay. Peptide sequences binding to GST-GABARAP are shown. Hydrophobic residues possibly driving the interaction are shown in red colour. Three putative LIR motifs were defined. This figure is prepared by Vladimir Kirkin.

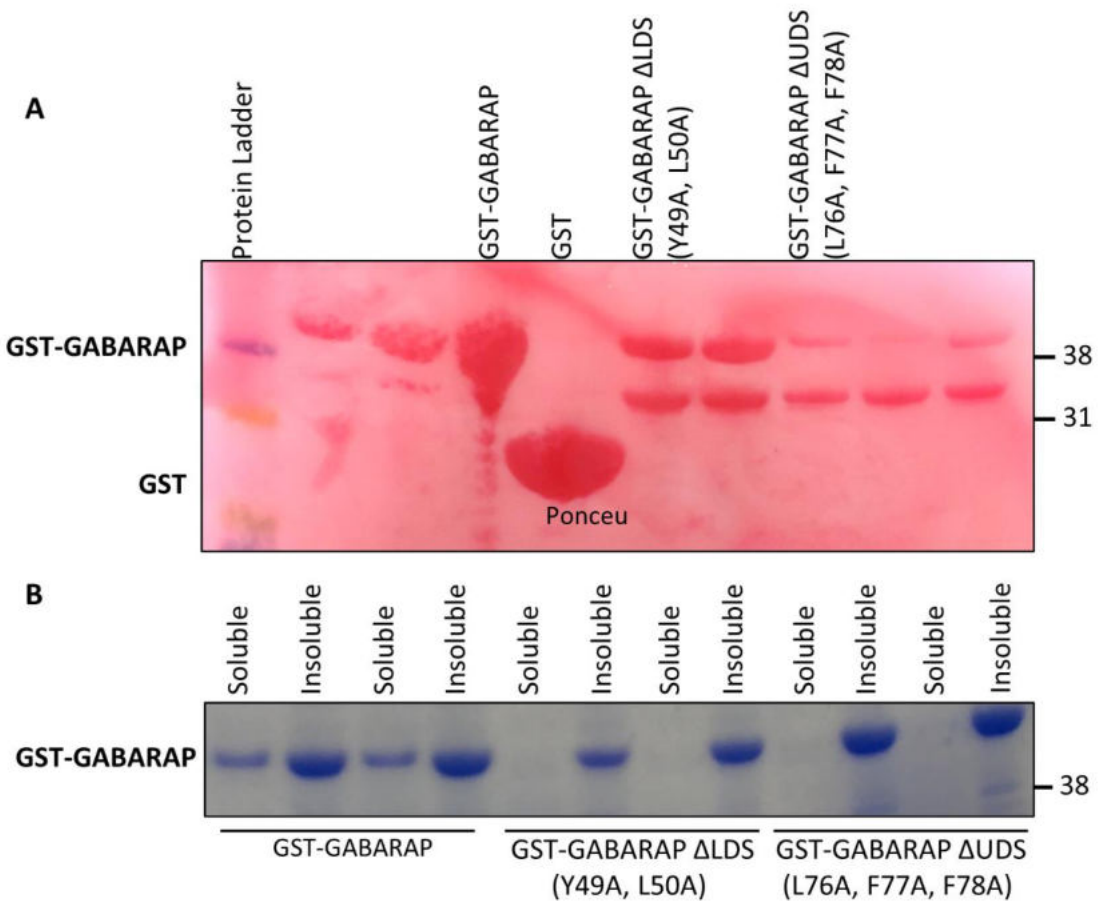
A
Protein Ladder
GST-GABARAP
GST
GST-GABARAP ΔLDS (Y49A, L50A)
GST-GABARAP ΔUDS (L76A, F77A, F78A)
GST-GABARAP
GST
Ponceu
38
31
B
Soluble
Insoluble
Soluble
Insoluble
Soluble
Insoluble
Soluble
Insoluble
Soluble
Insoluble
Soluble
Insoluble
GST-GABARAP
38
GST-GABARAP
GST-GABARAP ΔLDS (Y49A, L50A)
GST-GABARAP ΔUDS (L76A, F77A, F78A)

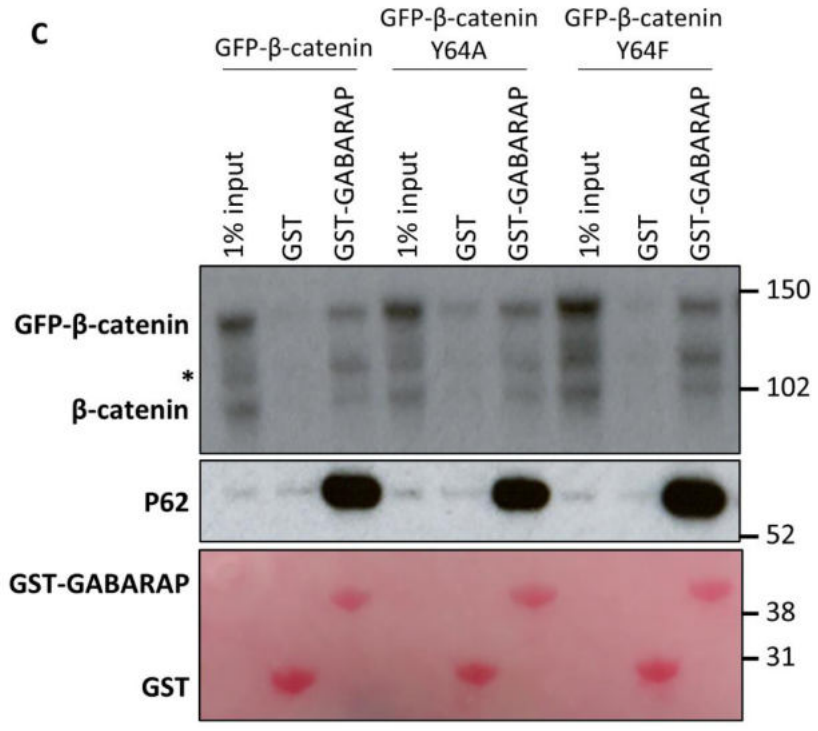
C
GFP-β-catenin
GFP-β-catenin Y64A
GFP-β-catenin Y64F
1% input
GST
GST-GABARAP
1% input
GST
GST-GABARAP
1% input
GST
GST-GABARAP
GFP-β-catenin
*
β-catenin
P62
GST-GABARAP
GST
150
102
52
38
31

Appendix Figure 4. Purification of mutant GST-GABARAP proteins from bacteria and GST pulldown with GFP-β-catenin constructs. (A) The amount of GST, GST-GABARAP, LDS-mutant GST-GABARAP (Y49A, L50A), and UDS-mutant GST-GABARAP (L76A, F77A, F78A) proteins purified from bacteria using glutathione-Sepharose beads, visualized by Ponceau S staining. The purification efficiency of mutant GST-GABARAP proteins was lower than WT GST and GST-GABARAP proteins. (B) Solubilization efficiency of WT and mutant GST-GABARAP proteins was shown by Coomassie staining in duplicates. Insoluble proteins were obtained by boiling the bacteria pellet after extracting the soluble proteins with the cell lysis buffer. (C) GST-pulldown assay of WT or mutant (Y64A, Y64F) GFP-β-catenin proteins expressed in human HEK293 cells. The precipitated proteins were analysed by Western blotting using anti-β-catenin and anti-p62 antibodies. GST or GST fusion proteins were visualized by Ponceau S staining (lower panel).

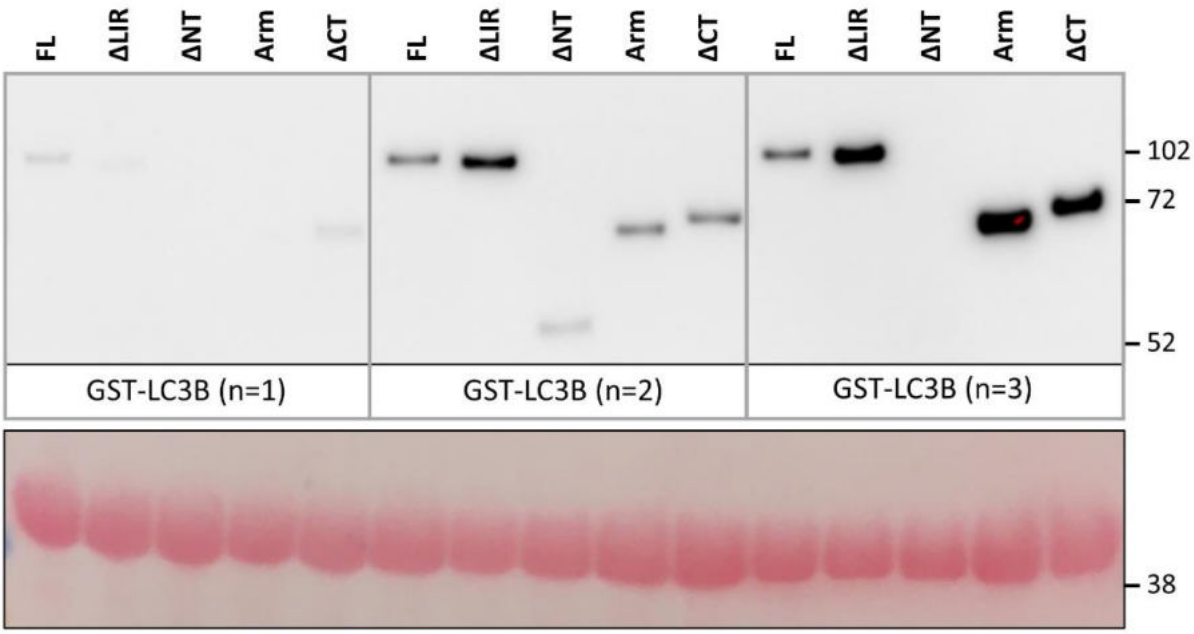

Appendix Figure 5. Recombinant β-catenin binding to GST-LC3B. *GST-pulldown assay with recombinant β-catenin proteins.* Three independent experiments are shown. The precipitated proteins were visualized by an anti-Strep antibody. GST-LC3B proteins used in the pulldown assay were visualized by Ponceau S staining (lower panel).

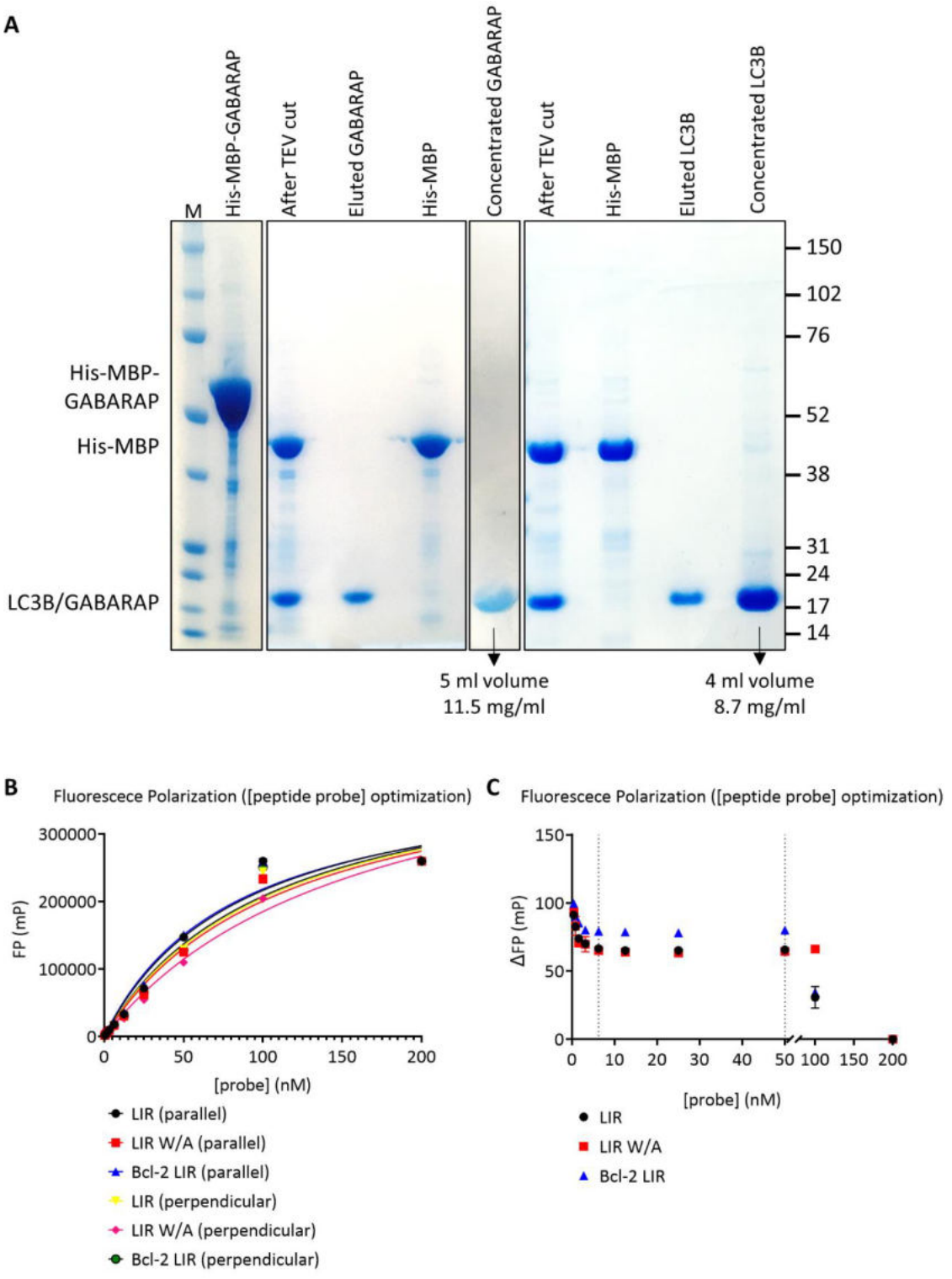

Appendix Figure 6. Production of LC3B/GABARAP proteins and probe optimization for FP binding assay. **(A)** Coomassie blue staining of the LC3B and GABARAP proteins purified from bacteria culture for use in the FP assay. His-MBP tagged LC3B and GABARAP proteins were separated from their tags by TEV protease cut. The concentrated amounts of proteins are

indicated. **(B-C)** Optimization of the peptide concentration for the FP binding assay. (B) Parallel and perpendicular FP readings for each peptide (0-200 nM) are indicated. (C) ΔFP values for each concentration of the peptides were calculated. The dashed vertical lines indicate the suitable peptide probe concentration range. 12.5 nM was chosen for the subsequent assays. n = 3 separate experiments; error bars, SEM.

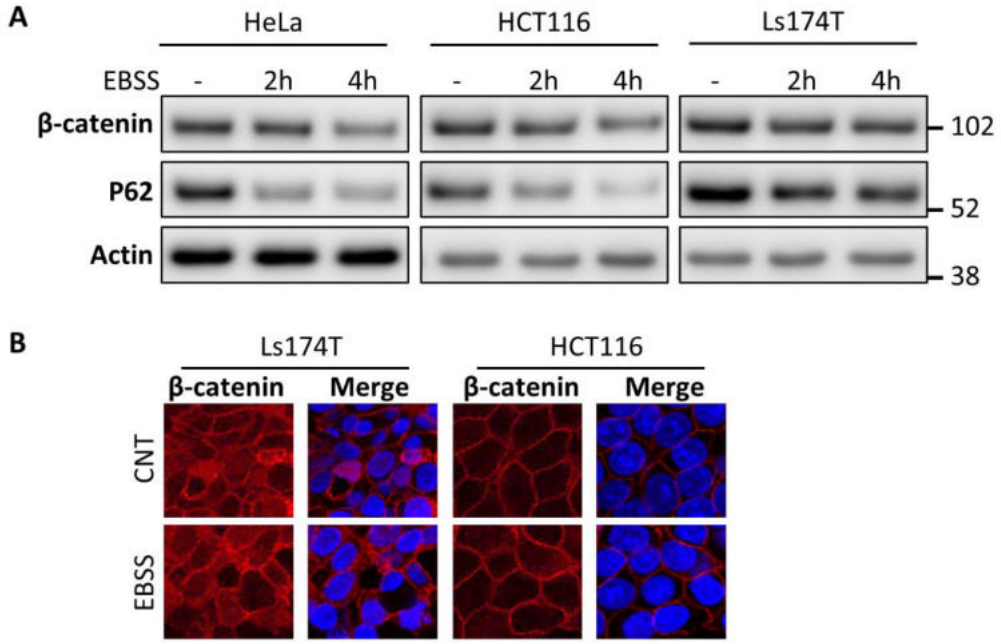

Appendix Figure 7. Regulation of β-catenin protein expression by starvation. **(A)** Protein expression of β-catenin and p62 under normal (CNT) and starved (EBSS for 0-4 h) conditions in HeLa, HCT116, and Ls174T cells. Actin was used as a loading control in immunoblot analysis. **(B)** Immunofluorescence analysis of endogenous β-catenin (Red) in Ls174T and HCT116 cells with/without 4 h EBSS treatment. DAPI staining was used to mark the nuclei (blue), scale bar = 10 μm.

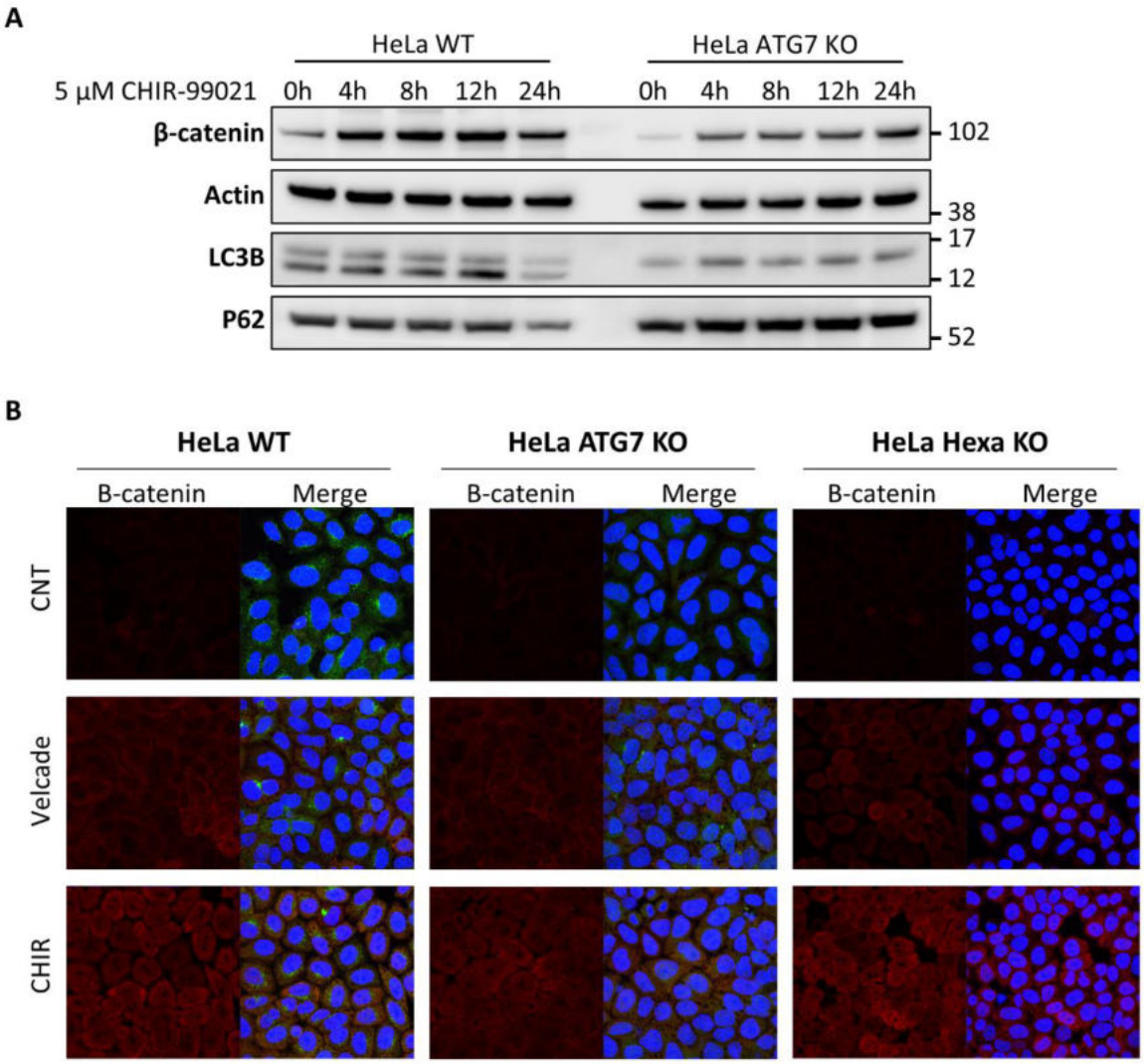

Appendix Figure 8. Accumulation of β-catenin in the cells upon proteasome inhibition. **(A)** Western blotting of β-catenin, LC3B, and p62 following 5 μM CHIR treatment for 0-24 h in HeLa WT and ATG7 KO cells. Actin was used as a loading control **(B)** Immunofluorescence analysis of endogenous β-catenin (Red) in HeLa cells treated with 100 nM Velcade or 5 μM CHIR for 4 h. Merge represents β-catenin, LC3B (Green) and DAPI (Blue) staining. CNT cells were treated with DMSO. Scale bar = 20 μm.

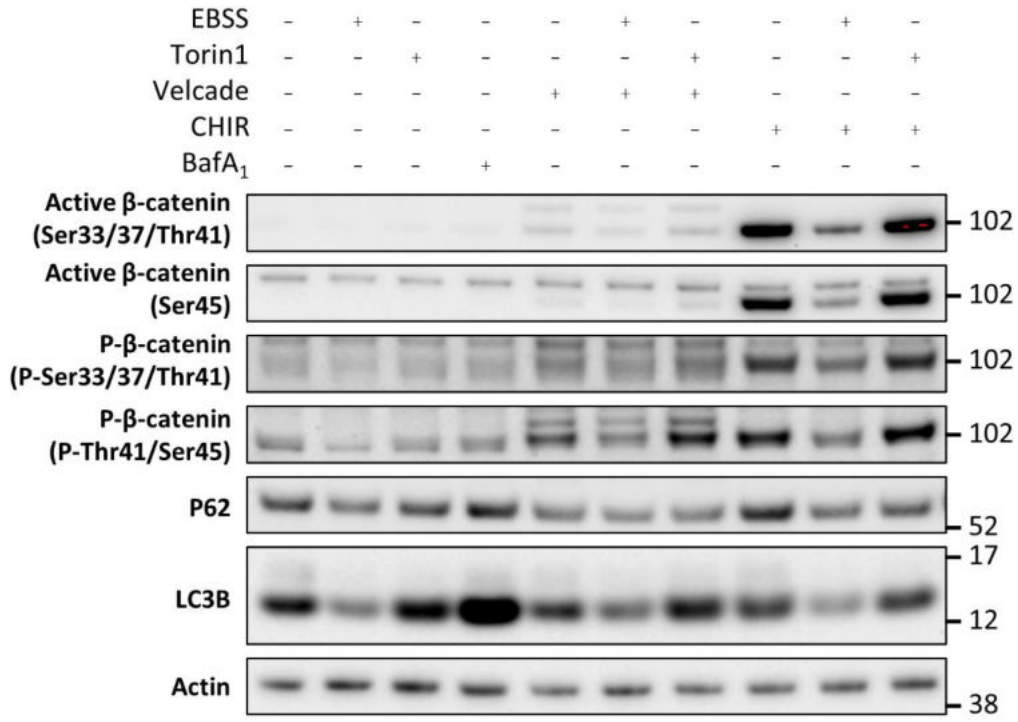

Appendix Figure 9. Regulation of β-catenin phosphorylation in response to autophagy induction. Western blotting of Active (non-phospho) and phospho (P) β-catenin, p62, and LC3B proteins following EBSS, 250 nM Torin1, 200 nM Baf A_1, 5 μM CHIR and/or 100 nM Velcade treatments for 4 h in HeLa WT cells. Actin was used as loading control.

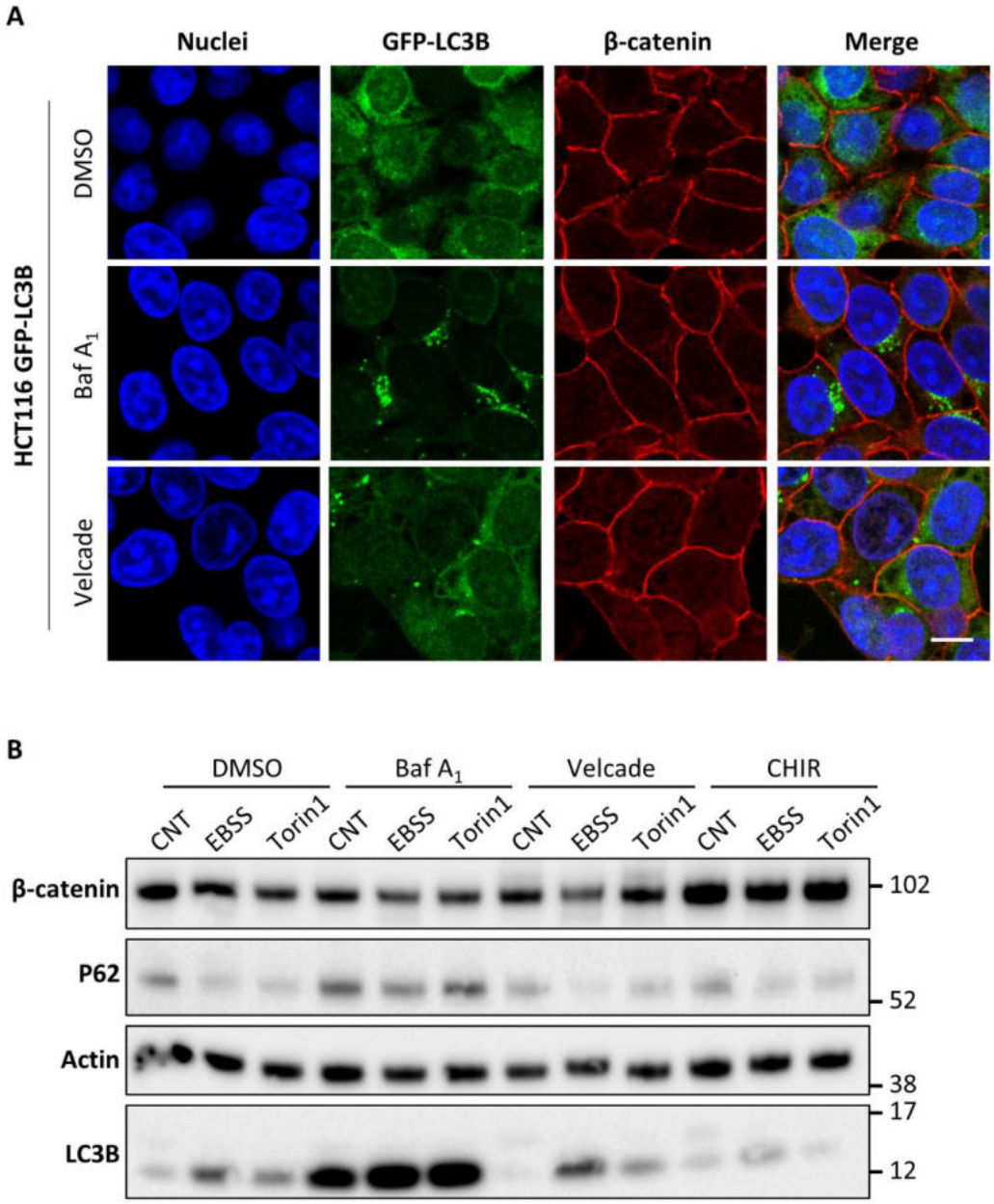

Appendix Figure 10. Regulation of cytosolic β-catenin. **(A)** Immunofluorescence analysis of endogenous β-catenin (Red) in HCT116 GFP-LC3B cells treated with 200 nM Baf A_1 or 100 nM Velcade for 4 h. Merge represents β-catenin, LC3B (Green) and DAPI (Blue) staining. Scale bar = 10 μm. **(B)** Western blotting of β-catenin, p62, and LC3B proteins following EBSS, 250 nM Torin1, 200 nM Baf A_1, 5 μM CHIR, and/or 100 nM Velcade treatments for 4 h in HCT116 WT cells. Actin was used as loading control.

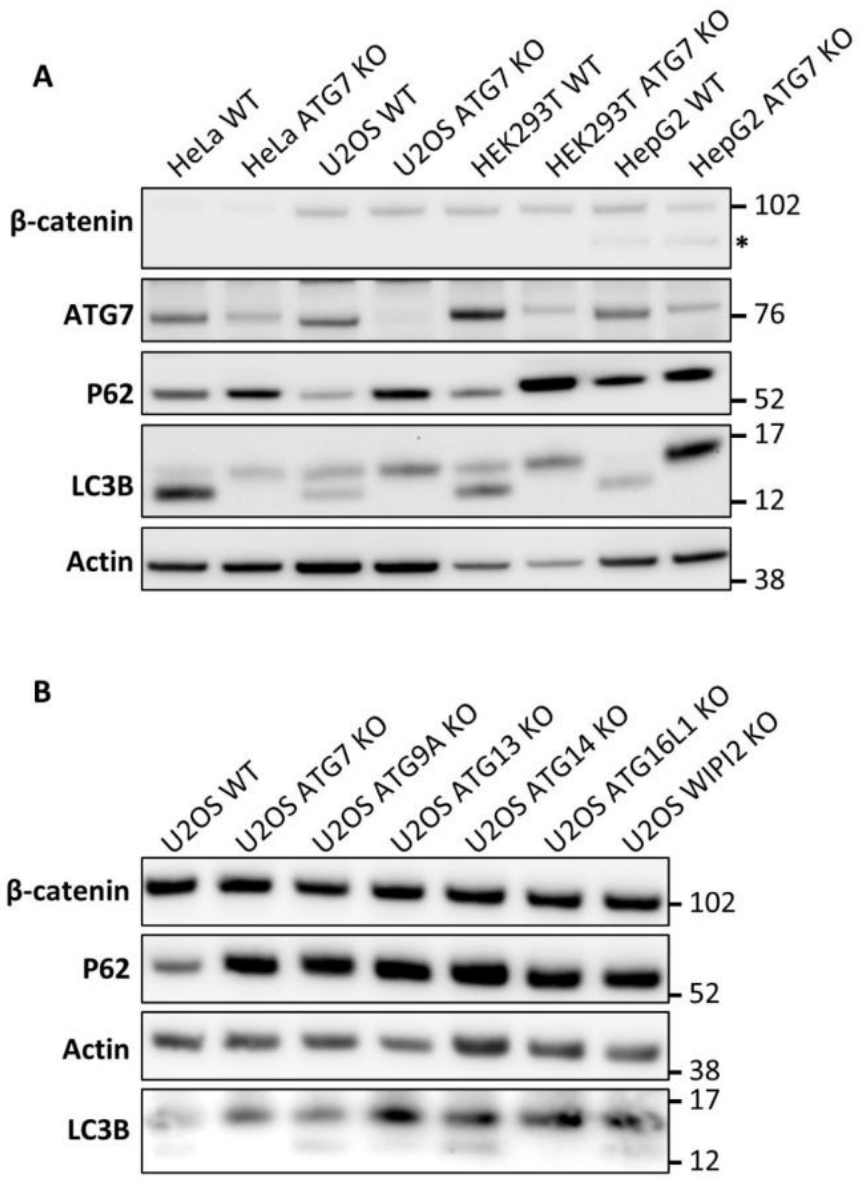

Appendix Figure 11. β-catenin is regulated independent of genetic autophagy inhibition. **(A)** Western blotting of β-catenin, ATG7, LC3B, and p62 in autophagy competent (WT) and incompetent (ATG7 KO) cells. **(B)** Comparison of U2OS WT cells with autophagy incompetent counterparts. Actin was used as a loading control in western blotting.

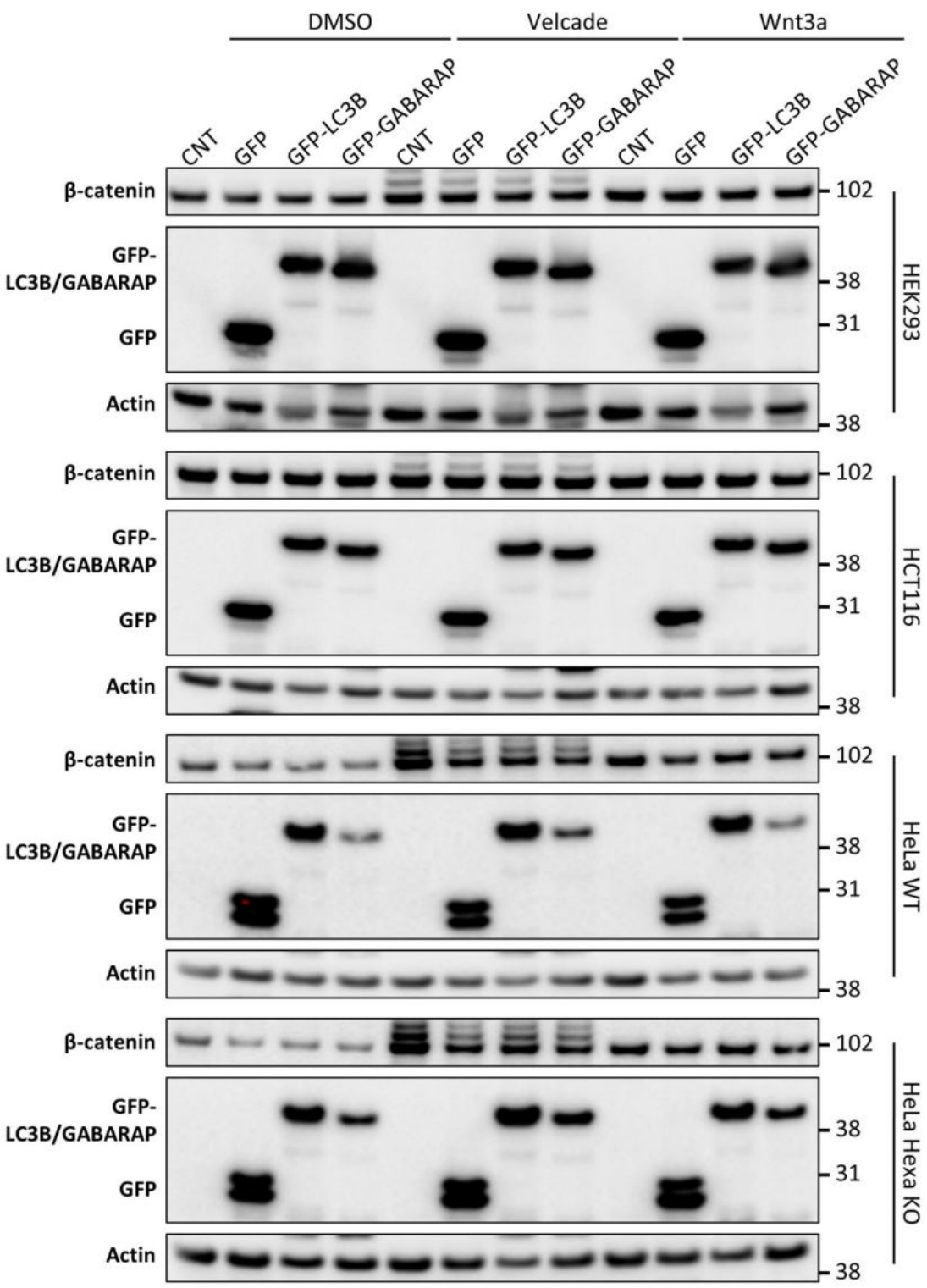

Appendix Figure 12. Regulation of β-catenin protein expression by LC3/GABARAP along with proteasome inhibition. The same amount (1 μg) of GFP-LC3B, GFP-GABARAP, and GFP was expressed in HEK293, HCT116, HeLa WT and HeLa Hexa KO cells for 24 h, and immunoblotted against anti-GFP and anti-β-catenin antibodies. These cells also treated with

DMSO and 100 nM Velcade for 4 h, or with Wnt3a conditioned media for 24 h. Actin was used as loading control.

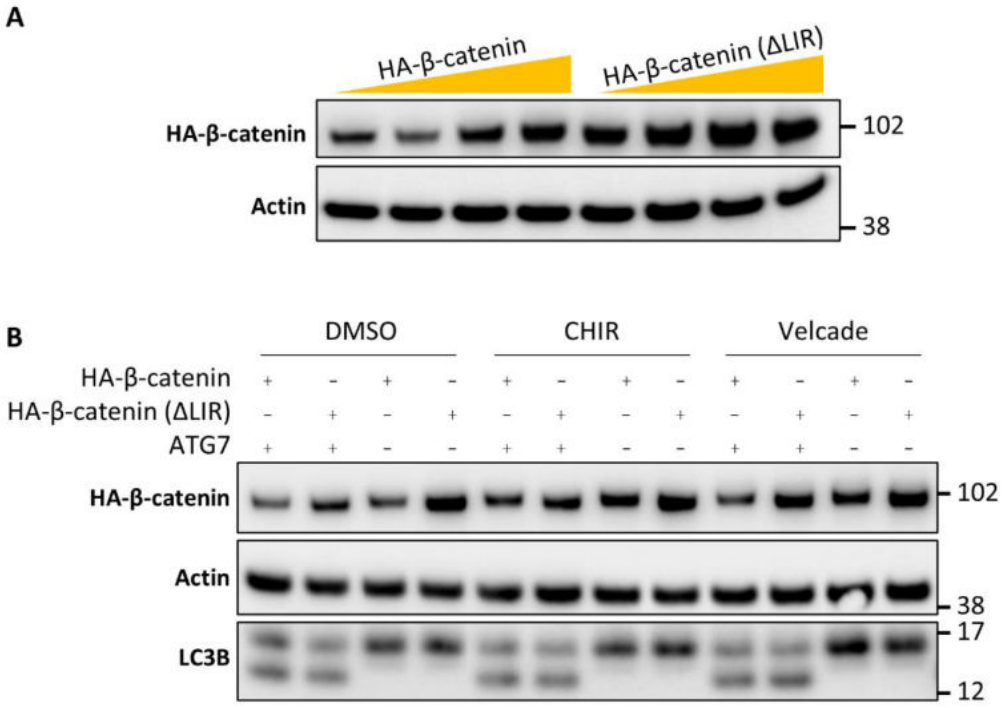

Appendix Figure 13. LIR mutation stabilizes β-catenin protein expression. **(A)** Various amounts (0.5-2 μg) of HA-β-catenin and HA-β-catenin(ΔLIR) were expressed in HeLa WT cells for 24 h and immunoblotted against anti-HA antibody. **(B)** The same amount of HA-β-catenin and HA-β-catenin(ΔLIR) was expressed in HeLa WT and HeLa *ATG7* KO cells for 24 h and treated with DMSO, 5 μM CHIR or 100 nM Velcade for 4 h. HA-β-catenin expression was detected using anti-HA antibody.

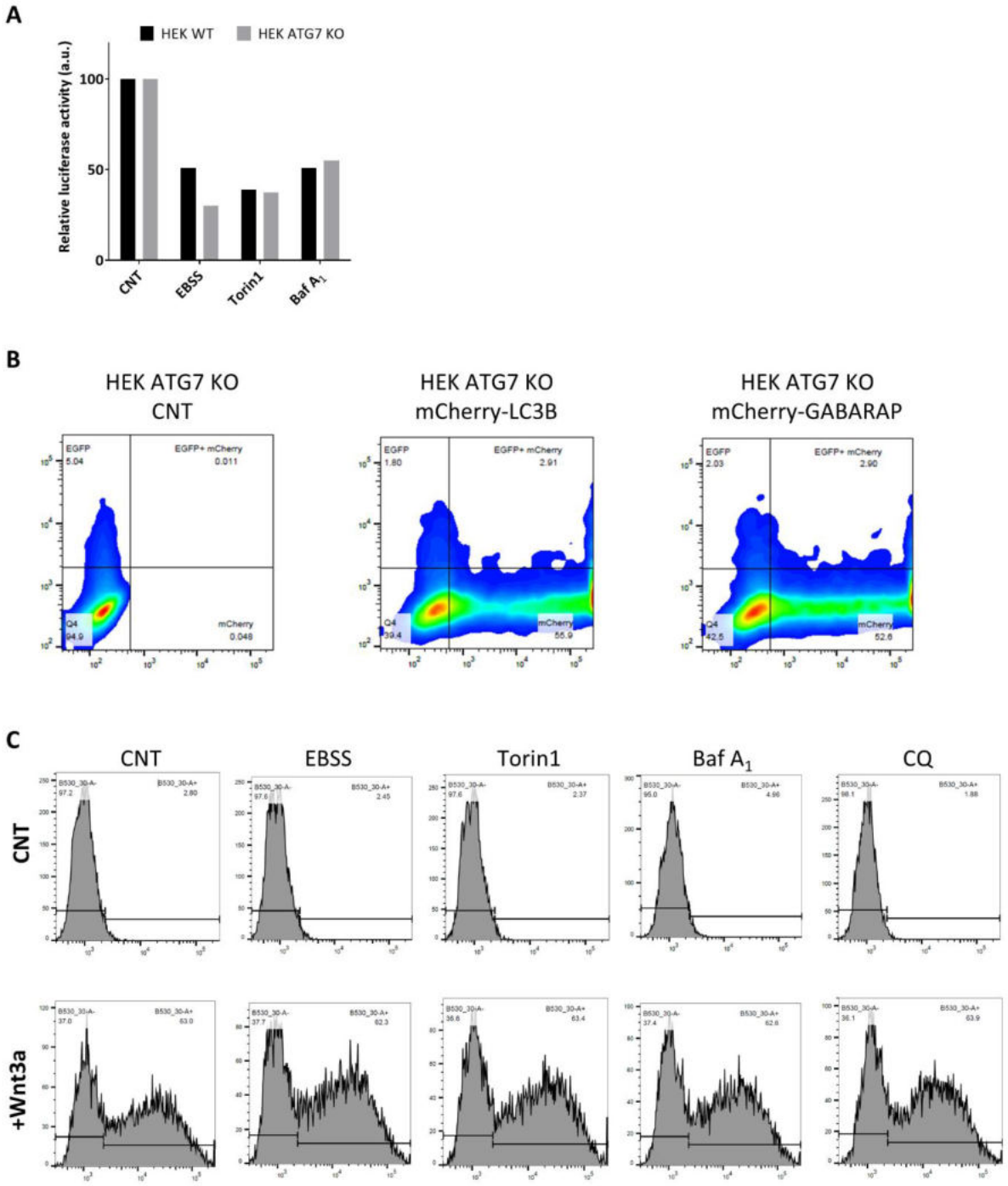

Appendix Figure 14. Effect of autophagy on β-catenin transcription activity **(A)** TopFlash luciferase activity in HEK293 WT and *ATG7* KO cells treated with EBSS, 250 nM Torin1 or 200 nM Baf A_1 for 4 h in the presence of 5 μM CHIR. The bars represent the mean values of two independent experiments. **(B)** β-catenin transcription activity produced by mCherry-LC3B and mCherry-GABARAP expression were determined in HEK293 ATG7 KO cells using the GFP-reporter assay. **(C)** β-catenin transcription activity produced by EBSS, 250 nM Torin1,

200 nM Baf A_1 and 10 μM CQ treatments for 4 h. In the bottom panel, these treatments were made after 24 h Wnt3a conditioned media treatment.

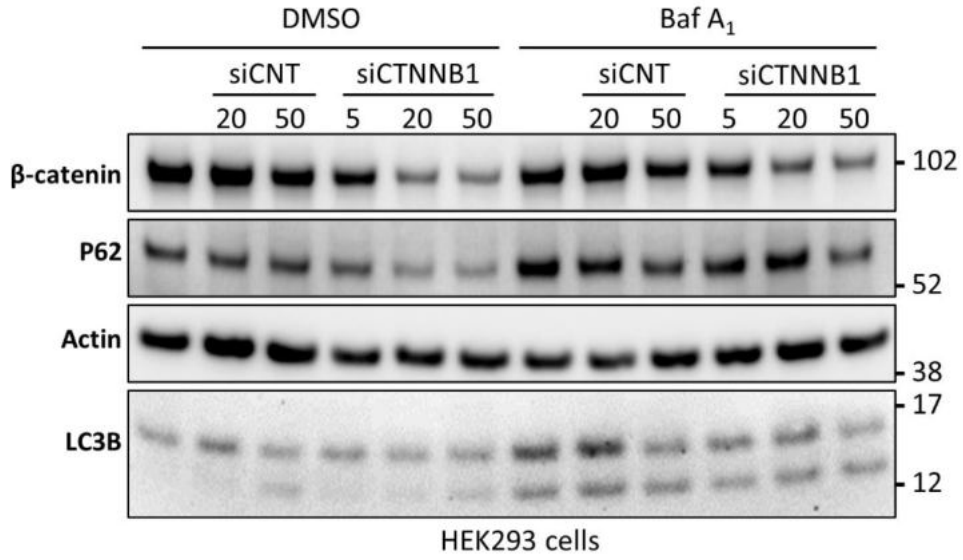

Appendix Figure 15. Effect of β-catenin on autophagy in HEK293 cells. HEK293 cells were transfected with various amounts of (5-50 nM) non-targeting (siCNT) or β-catenin targeting (siCTNNB1) siRNAs for 24 h in the presence or absence of 200 nM Baf A_1 treatment. Immunoblotting confirmed siCTNNB1-mediated silencing of endogenous β-catenin.